# Intensity, Frequency and Relaxation Time in the CH Stretch Overtones

**by**
**Brant E. Billinghurst**

B.Sc. (University of Manitoba) 1998

A thesis submitted in partial satisfaction of the requirements for the degree of

Doctor of Philosophy

in

Chemistry

in the

FACULTY OF GRADUATE STUDIES

of the

UNIVERSITY of MANITOBA

EXAMINING COMMITTEE

Dr. Kathleen M. Gough, Advisor

Dr. Anthony S. Secco

Dr. George Tabisz

EXTERNAL EXAMINER

Dr. Bryan R. Henry
Chemistry Department
University of Guelph

Chair: Dr. L.G. Goldsborough, Botany

# Intensity, Frequency and Relaxation time in The CH stretch overtones

BY

Brant E. Billinghurst

A Thesis/Practicum submitted to the Faculty of Graduate Studies of The University of Manitoba in partial fulfillment of the requirement of the degree

Of

DOCTOR OF PHILOSOPHY

Abstract

This thesis comprises three investigations, each into a different aspect of the CH stretch overtone vibrations.

The first project was to investigate the intensity of some overtone vibrations. Trimethyl amine was chosen for the subject of this study. Trimethyl amine is of particular interest because it exhibits the largest known difference in CH bond lengths within a methyl group. This is due to what is known as the lone pair *trans* effect. Dimethyl sulfide also exhibits the lone pair *trans* effect but to a far lesser extent making it ideal for comparison to trimethyl amine. In this part, the first through fourth overtone spectra of $N(CH_3)_3$,$N(CD_3)_3$, $N(CD_2H)(CD_3)_2$, $N(CH_3)(CD_3)_2$, $N(CD_3)(CH_3)_2$ and $S(CH_3)_2$ are reported. Tentative assignments are offered for all of the major bonds observed. The intensities of the observed bands are compared to predicted intensities calculated using the harmonically coupled anharmonic oscillator local mode (HCAO LM) model. Results of these experiments have shown good correlation between the experimental and predicted intensities. As well, some evidence that the lone pair produces increased coupling between methyl groups has been observed.

The second project investigated the energy of CH stretch overtone bands of metallocenes. The first through third overtone spectra of ferrocene, ruthenocene, nickelocene, cobaltocene, dicyclopentadienyl magnesium and sodium cyclopentadienyl are examined with particular attention to the CH stretching of the cyclopentadienyl. From semi-empirical correlations between CH bond length and CH stretching frequencies in each overtone region, it was determined that the type of metal atom within a metallocene complex has little effect on the CH bond length in the cyclopentadienyl. The only exception is cobal-

tocene where there is evidence that the Jahn-Teller effect results in several different CH bond lengths. Evidence that bis(cyclopentadienyl) magnesium is not ionic has been observed.

In the third project, a novel system based on photo acoustic spectroscopy was developed to measure the Vibrational-Translation relaxation rate of overtone vibrations. This is a subject of great interest as very little information exists on this process. The instrument developed here is termed Intra Cavity Laser Photo Acoustic Referenced Phase Shift (ICL-PARPS). This system relies on the tungsten wire within the cell to act as a reference so that accurate phase shifts can be measured. This allows for a Helmholtz resonator cell to be used to amplify the signal. This research serves as a feasibility study on the ICL-PARPS system. Some ambiguity still exists in the interpretation of the data collected and error in the values of the relaxation times found are still quite high. However, Vibrational-Translation relaxation times are reported for several overtone vibrations of trimethyl amine and an overtone vibration of methane. It is hoped that further development into this technique will lead to advances in overtone spectroscopy.

## List of Published Papers

1 A. V. Fedorov*, D. L. Snavely, K. M. Gough and B. Billinghurst "Vibrational Overtone Spectroscopy and Overtone Intensities of Cyclohexadiene Iron Tricarbonyl and 1,3-Cyclohexadiene" J. Phys. Chem. A, 105, (2001) 3459-3465.

2 Brant Billinghurst and K.M Gough, "Vibrational overtone spectra of Metallocenes: Effect of coordinating metal on CH bond lengths" J. Mol. Struct., 648, (2003) 139-149.

3 Brant Billinghurst*, K.M Gough, H. Kjaergaard and Geoff Low "A Study of the Overtone Spectra of Trimethyl Amine and Dimethyl Sulfide" J. Mol. Struct., 687, (2004) 87-99.

## List of Acronyms

PAS ..... Photoacoustic spectroscopy
ICL-PAS ..... Intra-Cavity Laser Photoacoustic spectroscopy
ICL-PARPS ..... Intra-Cavity Laser Photoacoustic Referenced Phase Shift
LM ..... Local Mode
L-L ..... Local-Local Combination
L-N ..... Local-Normal Combination
HCAO/LM ..... Harmonically Coupled Anharmonic Oscillator Local Mode Model
TMA ..... Trimethyl Amine
DMS ..... Dymethyl Sulfide
CHDIT ..... Cyclohexadiene Iron Tricarbonyl
Cp ..... cyclopentadienyl

# Acknowledgments

There are so many people that I would like to thank for their help and support throughout the years, that a complete list of them would rival this thesis in length. Therefore I shall only be able to mention a few. For those who are not mentioned, please accept my regrets and heart felt thanks.

First of all, I would like to thank my supervisor Dr. K. M. Gough for accepting me into the program and having faith in me all these years. It is rare in the Ph. D. program that one has as much freedom to explore their own lines of research as I was afforded. Also I would like to express my appreciation for the countless times that Dr. Gough proof read my papers and thesis, and for teaching me proper grammar along the way.

I would like to that the members of my committee: Dr. Secco, Dr. Wallace, Dr. Tabisz and Dr. Henry for all of the advice and support they provided me through the years, without which I could not have achieved the measure of success I have.

Of course my family (My Father Dr. M. W. Billinghurst, My Mother Darlene Billinghurst and My Sister Domanie Billinghurst) for their infinite love and support; one could not ask for a better family.

I have also been fortunate to be blessed with a vast number of very good friends; I fear that I will only be able to mention a few by name:

Nevin Stachiw who could have as easily been listed under family as I consider him the brother I don't have. He has been a constant source of support throughout my entire life.

Dr. Pamela Bromberg, who since the day we met, has been stead fast friend offering support, a laugh when needed and has listened and helped with every scientific and other problem that I have had since the day we met. There areno words to describe how much her friendship has meant to me over the years. All I can say is that if everyone was fortunate enough to have such a friend as she as been to me the world would be a better place.

Further to the above I would like to thank:

Robert Piche

Derek. Young

Marcus. Morrisey

Christina. O' Connor

And many many more.

I have also been blessed by working with a number of great graduate students; it would equally appropriate to list them as friends as they were all that as well:

Dr. Pamela Bromberg, who is of course mentioned above, but deserves to be mentioned twice.

Dr. Mark. McComb a great man who taught me the finer points of getting by in the dog eat dog world of science,

Dr. Angela Toms who was a good friend throughout the years and taught me a great deal,

Jason Hein whose generosity and winning of the "sucker of the year award" helped not only me but countless other graduate students,

Dr. Richard. Dawes who was always willing to help me in areas of theory in which his knowledge far exceeded my own,

and far too many others to mention hear but who all have a special place in my heart.

I would like to thank all of the Faculty and Staff at the University of Manitoba Chemistry Department, who have all been of great help. Truly anyone who has worked at the University of Manitoba Chemistry Department will be aware that what it lacks in size is more than made up for in the heart of the faculty and staff.

Of course, I wish to thank my collaborators without whom much of the work described in this thesis could not have been done:

Dr. H. Kjaergaard

Dr. G. Low

Dr. D. Snavely

Dr. A. Fedorov

Dr. T. Gough (no relation to my supervisor)

Their are also a number of companies I would like to ackownledge as thier service often went far beyond the call of duty:

National Instruments

Coherent

General Electric (who freely donated the tungsten wire I used)

If anyone reading this is looking for any of the products that are sold by the above listed companies (particularly the first two) I highly recommend them.

I would like to thank the University of Manitoba for granting me a University of Manitoba Graduate fellowship.

Thanks go to the University of Manitoba Chemistry department and Ernst and Ingrid Bock for the Ernst and Ingrid Bock award I was honored to receive.

Thanks go to The University of Manitoba and Medicure for the Medicure Graduate Scholarship that I was honored to receive.

Finally I would like to thank NSERC for providing funding for the research group I was a part of my research.

# Table of Contents

# List of Figures

# List of Tables

# 1 Introduction

## 1.1 General Introduction

This thesis comprises three investigations, each into a different aspect of the CH stretch overtone vibration:

1. The Intensity of the vibrational band
2. The Frequency of the vibrational band
3. The Vibrational-Translational relaxation rate of the vibration

The first study is an investigation into the intensities of the vibrational overtone bands of trimethyl amine and dimethyl sulfide, molecules that exhibit the lone pair *trans* effect. The lone pair trans effect causes a CH bond *trans* to a lone pair to be longer than those *gauche* to the lone pair. This study shows how experimental intensities along with *ab initio* calculations can yield valuable information about this effect and its impact on the vibrational overtone spectrum.

The second study deals with the frequency of CH vibrations of organometallics. In this study, the correlation between CH bond length and vibrational frequency is used to gain information on the effect of the coordinating metal on the CH bond length of the metallocenes.

In the third study, a novel instrument for the study of vibrational-translational relaxation of overtone vibrations was designed, and the feasibility of using such an instrument

effectively was investigated. Prior to this the vibrational-translation relaxation times of overtone bands had remained largely uninvestigated.

Before these projects are described individually an introduction to many of the concepts and techniques involved must be presented so that the reader will be familiar with the relevant issues.

## 1.2 Introduction to Overtone Spectroscopy

### 1.2.1 General

Vibrational spectroscopy has been studied for a very long time and for the most part has been well described with the normal mode model. Comprehensive descriptions of the normal mode model can be found in a number of texts such as Infrared and Raman Spectra by Herzberg[1], Molecular Vibrations by Wilson, Decius and Cross[2] and Modern Spectroscopy by Hollas[3]. These descriptions generally focus on what is commonly referred to as the fundamental region, which lies approximately between 500 and 4000 $cm^{-1}$. The normal mode model is based on the harmonic oscillator approximation, where normal modes of vibration have all the nuclei undergoing a simple harmonic motion with the same frequency and in phase with one another. Since the eigenvalues of a harmonic oscillator may be defined by:

**Equation 1-1.**

$$E_i = \frac{h}{2\pi}\omega\left(v_i + \frac{1}{2}\right)$$

where $v_i$ is the vibrational quantum number, $\omega$ is the harmonic frequency and h is Plank's constant, it follows that the total vibrational energy of the molecules would be the sum over all of the normal modes K:

**Equation 1-2.**

$$E = \sum_K \frac{h}{2\pi}\omega_K\left(v_K + \frac{1}{2}\right)$$

The application of this to what is observed in the infrared spectrum requires that certain selection rules be considered. First, for a mode to be infrared active, it must cause a change in the dipole moment of the molecule. This rule requires that symmetry concerns be addressed. A detailed account of symmetry and its implications will not be presented here; a good discussion of this may be found in a number of texts such as "Symmetry, Spectroscopy and Structure" by Kettle[4]. The requirement that there be a change in dipole moment of the harmonic oscillator approximation leads to the selection rule:

**Equation 1-3.**

$$\Delta v_i = \pm 1$$

This selection rule would eliminate the possibility of overtone bands appearing in absorption spectra. Therefore, from this it would be expected that the near infrared region would be free of vibrational absorption bands. However, this is not the case: high energy absorption bands were observed, even before the introduction of the normal mode model. Perhaps the first observation of high energy absorptions was that made by Pucciati [5] as reported in [6], who observed them in compounds which contained CH bonds. Following this observation, many researchers studied the near infrared region, compiling data on the spectra of a great many compounds. In 1929, Ellis published a paper detailing many of these

results[6]. The conclusions of this paper would foreshadow what would later appear as the local mode model. The overall conclusion that many of the outstanding features of the near infrared region could be associated with localized regions of the molecule was the most notable of these. Ellis also found that bands in the near infrared region could be grouped into series expressible by a simple anharmonic expression:

**Equation 1-4.**

$$\nu^n = \omega^0 n - bn^2$$

where $\omega^0$ and b are constants and n=1,2,3... With methods devised by Birge and Spöner[7] this series could be used to determine the energy of dissociation for the bond involved.

Many other papers were published on bands in the near infrared region, reinforcing the view that they could be attributed to localized regions of the molecule, particularly CH bonds[8][9][10][11]. Differences in the band position were attributed to the environment of the bond. *i.e.,* whether it was aryl, alkyl or other, the proximity to atoms with high electron affinities, the presence of hydrogen bonding etc. The advantage of studying this region even at this point was quite clear: information on specific types of bonds could be readily obtained.

In a series of papers published between 1935-1936, Mecke and co-workers devised a theory that closely resembles the Local mode model as it is known today [12][13][14][15]. Since this work so closely resembles the local mode model of today, which will be outlined later, details of this work are not presented. However, it should be noted that these scientists were true innovators in the study of overtone spectroscopy.

The limitations of the normal mode model were not a surprise, since the model rests on the assumption that the oscillations involved were infinitesimal and therefore only the

quadratic terms needed to be considered. This, however, is not the case, particularly when the overtones are the subject of interest. Since, if a displacement is large enough the potential energy will reach a value corresponding to the dissociation energy, higher powers of displacement must be involved. With quadratic and cubic terms added to the wave equation, the energy no longer reduces to the sum of independent normal vibrations, but contains cross terms containing the vibrational quanta of two or more normal modes[1]. In this case the vibrational energy can be written as:

**Equation 1-5.**

$$E = \sum_{K}\left(\nu_K + \frac{1}{2}\right)\frac{h}{2\pi}\omega_K + \sum\sum_{K \geq L}\left(\nu_K + \frac{1}{2}\right)\left(\nu_L + \frac{1}{2}\right)\frac{h}{2\pi}X_{KL} + \cdots$$

where $X_{KL}$ are the anharmonicity constants of the normal modes of vibration.

Recognizing the importance of CH-stretching overtone vibrations as receptors of energy in non-radiative transitions of the lowest triplet state of an aromatic hydrocarbon, Siebrand *et al.* studied them in a series of papers[16][17][18]. They noted the importance of anharmonicity and suggested the use of the more realistic Morse potential instead of the harmonic oscillator to account for anharmonicity.

Martin and Kalantar[19], noting the importance that Siebrand placed on anharmonicity in the competitive depopulation of the anharmonic triplet state, applied normal mode formalism to the overtones of benzene using an anharmonic expression. In this work, they noted that the overtone spectra arose because of couplings between CH stretching modes. They assigned the CH stretching overtones to the progression of the $\nu_{20}+n\nu_2$ combination. However, they noted that the normal mode description was inadequate when multiple

quanta excitation of the CH stretch were involved. They went on to suggest that it would be preferable to use an asymmetric potential function such as the Morse potential, and that a description in terms of local oscillators would be better. They also noted that the b constant in Equation 1-4, proposed by Ellis, corresponded to the anharmonicity.

In 1968, Henry and Siebrand[20] proposed that instead of deriving a model based on small amplitude vibrations (the normal mode model), a model should be derived based on large amplitude vibrations. They called this the local mode model. The motivation behind their effort was that rarely was there enough spectroscopic data to determine all of the $(^1/_2)N(N+1)$ anharmonicity constants that characterize a molecule with N normal modes. Since very large vibrational amplitudes correspond to dissociation and the physically important dissociation process is the dissociation of a single bond, a local mode description was considered preferable. Taking a Morse potential as an approximation to the vibrational potential, the relation between the anharmonicity constant and the dissociation energy is:

**Equation 1-6.**

$$X = \frac{-\omega^2}{4D}$$

Using this assumption, they were able to argue that even though local modes would be coupled both by harmonic and anharmonic interactions, the overall coupling for large amplitude vibrations would be much smaller than the coupling between normal modes.

The vibrational energy of a molecule in terms of the local mode model was given as:

**Equation 1-7.**

$$E = \sum_{i}\left(\nu_i + \frac{1}{2}\right)\frac{h}{2\pi}\omega_i + \sum\sum_{i>j} c_{ij}\frac{h}{2\pi}\omega_{ij} + \sum\sum_{i\geq j}\left(\nu_i + \frac{1}{2}\right)\left(\nu_j + \frac{1}{2}\right)\frac{h}{2\pi}X_{ij}$$

If this equation is compared to Equation 1-5, the only new term is the second summation, which incorporates the harmonic coupling terms into the model. For cases where there is only one set of equivalent local modes and the interaction between local modes is small, all the $\omega_i$ and all the $X_{ii}$ should be equivalent. Therefore, a number of simplifying relations between the $\omega_{ij}$ and between the $X_{ij}$ will exist. If there is a large enough set of equivalent local modes then the number of unknown $\omega_{ij}$ and $X_{ij}$ will be much smaller in the local mode representation than the number of knowns in normal mode representation. Because the local modes are directly associated with bonds it is easier to estimate the value of the $X_{ij}$ than it would be to estimate the $X_{KL}$ in the normal mode model. Henry and Siebrand[20] also showed that in the normal mode model, $|X_{KK}|<|X_{KL}|$, thus the matrix is not particularly diagonal. Whereas, using the local mode model, $|X_{ii}|>|X_{ij}|$, and the matrix is closer to diagonal than in the normal mode model. For benzene they found that $\omega_{ij}$ and $X_{ij}$ were very small in relation to $\omega_i$ and $X_{ii}$ and therefore could be neglected; the molecule could simply be considered a system of six uncoupled oscillators. Using this local mode model $X_{ii}$ was found from available spectroscopic data. The overall purpose of the paper was to show that the use of local modes could help derive the anharmonicity constants of the normal modes, which previously had been difficult to obtain. To accomplish this, combinations of local modes were formed that led to the same CH-stretching as specific combinations of normal modes. The anharmonicities of the normal modes could be solved for by equating energies of the combinations. Using the values they found for the anharmonicities of the normal

modes, they calculated the expected overtone frequencies and found that these agreed well with experimental results.

Henry *et al.* continued work using the local mode model to calculate normal mode anharmonicity constants: however they encountered difficulties. The diffulities that Hayward, Henry and Siebrand ran into were explained in a paper, published in 1973[21]. The problem arose because of the need to specify the phase designation of the normal modes in order to convert from local modes to normal mode anharmonicities. As the number of normal modes needed to equate with the local modes became larger than two, the phase designations became an increasingly inaccurate approximation. Henry *et al.* were able to correct this for benzene.

Hayward and Henry then applied the local mode model to the relatively simple molecules: ammonia and methane[22]. They found that the local mode model described these molecules well, but if the normal mode anharmonicities were calculated as previously and the normal mode model was applied after the third overtone, the normal mode model broke down and was unable to account for the experimental observations. Consistently, the normal mode model predicted a larger number of allowed states than were observed experimentally, whereas the local mode model predicted only a relatively small number of states that agreed with those observed. In 1975, Hayward and Henry extended their study to dichloromethane and once again showed that the local mode model gave predictions that were closer to the experimentally observed spectra than the normal mode model[23]. The anharmonic normal mode model led to band shapes that were broad and complex, however the experimentally observed bandshapes were relatively narrow. This observation agreed well with the local mode model predictions.

Hayward and Henry extended the local mode model to include the effects of non-equivalent XH groups in a molecule [24]. In this paper they revisited acetylene, hydrogen cyanide, chloroform and dichloromethane, and extended their study to substituted benzenes that contained non-equivalent CH bonds. The spectra of *o*-xylene, *p*-xylene, *m*-xylene and toluene all exhibited two intense peaks in the overtone regions, one which roughly correlated with the peak observed in methane and ethane and one that correlated to benzene. This observation showed that the local mode model could be extended to molecules with non-equivalent XH bonds. Differences between the spectra were not discussed, but would be addressed in papers that will be discussed later. Also noted was the increase in complexity of the spectra of lower overtones. This increase in complexity was attributed to convergence to normal-mode pattern.

Henry and Hayward also noted that the separation between the aromatic and aliphatic CH peaks in the xylenes decreased as progressively lower overtones were observed. The decrease in seperation was expected as a consequence of the differences in the anharmonicities of the different CH bonds.

It is important to keep in mind that both the local and the normal mode treatments are models and there is no specific point where one is appropriate and the other is not; the choice of model is made on the basis of which leads to the most diagonal matrix for the spectrum in question. This thesis is primarily a discussion of local-modes and as such, spectra will be discussed in terms of local modes. However, at times the terms local mode character or normal mode character will be used. These terms are meant to point out that there could be aspects of the spectra that could be better described by one or the other model. For example in the first overtone some peaks may not be assigned due to the fact that the region

still shows "normal mode character", meaning that the peaks would be better described using a normal mode formalism that is outside of the scope of this thesis.

It must be noted that there are several types of combination bands that are also observed with the overtone regions. The first type is the local-local combination. Which occur when the energy is not localized in a single oscillator, but is divided among several oscilators. This can be conveniently described using the $|x_1,x_2>$ notation, where $x_i$ is the number of quanta of energy located in an oscillator. For example, the third overtone of water |2,0> refers to the pure local mode of OH stretching, with both quanta in a single oscillator, whereas, |1,1> refers to local-local combination with one quantum in each oscillator. This notation can be expanded to cases where there are several non-equivalent oscillators by adding positions for each oscillator and grouping equivalent oscillators, $|x_1,x_2,...>|x_3,x_4...>$...etc. The other combination is the local-normal combination where energy is divided between a local mode and a normal mode. Examples of both of these are described by Henry[25].

The first theoretical support for the local mode model was provided by Wallace in 1975[26]. He shows that the spectral characteristics of the local mode model could be explained analytically using a model where bond stretching coordinates were described by a Morse potential and bending was described by a harmonic potential. The examples provided in his paper were water and benzene; both showed excellent agreement with experimental observations. The calculations show that the most intense bands were attributed to the pure local modes. The model Wallace presented was clearly superior to the harmonic since, unlike the harmonic model, it could describe anharmonicity. However, as Wallace pointed out, it was unreasonable to compare this model to variants of the harmonic model

that could account for anharmonicity, as they were highly refined by comparison containing many more parameters than the two parameter model that he presented. Considering the two parameter nature of the Wallace model, the results were remarkable, showing the validity of the local mode model, and particularly the use of the Morse potential in the description of XH stretching. Later Wallace developed approximate eigenfunctions of the Morse oscillator, expressed in terms of Laguerre polynomials. The approximation responded to the errors in the boundary conditions that Morse had assumed, which led the energy levels of the Morse hamiltonian to be approximate. These new expressions were shown to be approximately orthogonal and analytical expressions for the matrix elements of common operators were obtained[27].

In 1976, Albrecht *et al.* [28] used thermal lensing spectroscopy to study the fifth overtone of benzene, methyl substituted derivatives of benzene, naphthalene and anthracene. They found that the local mode model worked very well in describing these spectra. They found that as they substituted methyl groups for the hydrogens on benzenes, the peak associated with the aryl hydrogens decreased as the peak associated with the methyl hydrogens increased, as would be expected. They also found that, even though the number of allowed modes increased with quantum number, only the most anharmonic (*i.e.*,. the mode with all quanta in a single bond) was active. They also noted that the model could be improved by allowing for intermode coupling.

Observations made by Henry *et al.* [25] show how systematic the overtone spectra can be within the local mode interpretation. They studied the overtone spectra up to the fifth overtone of normal alkanes from methane to heptane, as well as some branched species. What they observed agreed perfectly with the local mode model predictions. Differences in

the harmonic frequency of the CH oscillators were clearly evident. The harmonic frequency decreased by ~50 $cm^{-1}$ as the number of hydrogens bonded to the carbon declined (four hydrogens for methane, three hydrogens in ethane and so on). In molecules such as pentane, $CH_3$ and $CH_2$ were clearly resolved. This observation was very important as it showed that the different "types" of CH bonds could easily be resolved in the overtone spectra. This point will be of great importance for the study described in Chapter 3. The intensities of the lower energy $CH_2$ relative to the $CH_3$ peak increased in a regular way from ethane to heptane. Due to the difference in anharmonicities, the spacing between the peaks increased at higher overtones, as the local mode model predicts.

The effect of steric hindrance on the local mode parameters was first suggested by Henry and Greenlay in 1978 [29] when they noticed that the anharmonicity constants were lower in 3-methylpentane, 2-methylbutane and isobutane than in the straight chain hydrocarbons. They attributed this to intramolecular steric hindrances that presented a barrier to large amplitude vibrations in these molecules, leading the oscillator to behave in a more harmonic fashion. To further investigate this theory, Henry and Miller [31] studied 2,2,3,3-tetramethyl butane, 2,2-dimethyl butane and 2,3-dimethyl butane and found that the results were in keeping with the previous theory; anharmonicity decreased as the steric crowding increased. This study was later expanded by Henry, Mohammadi and Thomson [30] to include many more substituted pentanes. The general trend of decreased anharmonicity with increased steric hindrance was found to continue throughout, save for a few outliers where the methyl was in the 3 position; the reason for this is unknown.

In 1978, Greenlay and Henry[32] showed that the anharmonicity is dependent on the environment of the molecule. In their study, they measured the anharmonicity of the

methyl CH oscillator of 3-methyl pentane in both the solid and liquid state. They found that the anharmonicity was significantly lower in the solid state than in the liquid state. This observation shows that the vibrational potential can be effected by the surrounding environment, and that these affects can be probed by studying overtone spectra. The dependence of both the harmonic frequency and anharmonicity on environment is a topic that is of great interest, however a complete discussion of this topic will be deferred to Chapter 3.

In 1979, Mϕller and Mortensen [33] calculated the vibrational states of water using both the normal and local mode models. The results of their paper clearly showed that the states were purer in the local mode model than in the normal mode model. They also introduced the concept of symmetry for the pseudo-resonant interactions. The interactions that were considered were between states that were permutationally related (*i.e.*, |2,0> and |0,2>, different but equivalent oscillators). This led to a symmetrization of the wavefunctions. These mixings in the local mode picture could be attributed to either kinetic energy or non-local potential energy couplings. Following this Mortensen, Henry and Mohammadi[34] reexamined a previous paper on the overtones of difluoro-, dichloro-, dibromo- and di-iodomethane, by Henry and Hung[35], taking symmetry into account. They found that even small coupling terms for initially degenerate states led to a splitting and the formation of new symmetrized states,

**Equation 1-8.**

$$|\nu, 0\rangle_{\pm} = \frac{1}{\sqrt{2}}(|\nu, 0\rangle \pm |0, \nu\rangle)$$

These results gave a much better explanation of the observed spectral features.

Since 1978 to the present, many researchers have continued to develop and use the local mode model, sconsider the following are but examples: Henry, Wong, Moore, Snavely, Kjaergaard, Quack and Gough. However, this work will not be discussed now; instead it will be referred to in later chapters when appropriate to research being discussed.

### 1.2.2 Local-Normal combinations

Combination bands are a common feature in the fundamental region. In the overtone regions combination bands are also an issue. As stated previously, both local and normal modes are models, either of which may be used. The choice often rests on their ability to describe the observed vibrations clearly and simply. In the case of combination bands, both models are used simultaneously, because combinations sometimes occur between high energy vibrations that are best described using the local mode model, and low energy vibrations that are best described using the normal mode model. We refer to these as local-normal (L-N) combinations.

In their paper on dichloromethane, Hayward and Henry [23] did observe combination bands that fell off in intensity rapidly relative to the pure local modes. However, the combination of a pure local mode with the CH bending normal mode was still observable at the third overtone. In later work on dichloromethane [24], they observed three separate combination bands falling on the high energy side of the third overtone of the CH stretching vibration. These corresponded to combinations of the pure local mode with CCl stretch, CH bend and $CH_2$ twist. The characterization of these local-normal combinations was confirmed by later work on dihalomethanes [35] in which the position of the combination bands relative to the local mode shifted with changing halogens in a manner consistent with the changes in the fundamental region observed for the normal modes involved. They found that the splitting observed between the pure local mode and the combination band could be related to the fundamental frequencies of the relevant normal-modes and their off diagonal coupling constants by:

**Equation 1-9.**

$$E(3, 1_j) - E(3, 0) = \nu_j + \nu X_{ij}$$

where v is the vibrational quantum number, $\nu_j$ is the fundamental frequency of the normal-mode and $X_{ij}$ is the off-diagonal coupling. Furthermore, it was found that the coupling between the normal modes and the pure local-mode decreased on going from dichloro- to dibromo- to diiodo-methanes due to mass effects.

Fang and Swofford also studied halomethanes [36] and identified a number of combination bands in the second through sixth overtones, including combinations of the CH stretching overtones with 2 quanta of CH bend. This is of particular interest because, along with earlier work by Henry *et al.* [24], it shows that local-normal combinations may have more than one quanta of normal mode vibration. In most cases, the energies of the combinations agreed well with the additive energy relationship expected for two simultaneously excited but essentially non interacting oscillators. The only notable exception was observed for $CHX_3$ where X is a halogen, and the combination involved XCH bend. They pointed out that these cases could be treated as two coupled anharmonic oscillators as shown by Herzberg [1]:

**Equation 1-10.**

$$\Delta E(\nu_1, \nu_2, 0) = \nu_1(A_1 + B_1\nu_1) + \nu_2(A_2 + B_2\nu_2) + B_{12}\nu_1\nu_2$$

where $\nu_1$ and $\nu_2$ are the quantum numbers, $B_{12}$ is the coefficient of anharmonic coupling between the two oscillators and the A's are the mechanical frequencies and the B's anharmonicities. Fang and Swofford [36] showed that the significant coupling could be viewed

as a result of physical coupling of the individual oscillators. They also found that steric crowding was not a dominant factor in the interaction. This was evident from the fact that the coupling was not stronger in trichloromethane than in the tribromomethane as would be expected if steric crowding was in fact a dominant factor. The importance of Fermi resonance was also noted. However further discussion of this will be reserved for the next section.

In a study of normal, branched and cyclo-alkanes, Fang and Swofford [37] found combinations of CH stretching pure local modes and one quantum of the CH bending normal mode were very important even in the higher overtones of the alkanes. A band consistently appeared at approximately 1200 $cm^{-1}$ above the pure local mode band and decreased in intensity with higher overtones more slowly than the local-local combinations for both the primary and secondary CH oscillators. The energies observed were significantly different than what would be predicted for two simultaneously excited but non interacting oscillators. They were able to calculate a value for the anharmonic coupling coefficient of -33.15 $cm^{-1}$ between the local mode and the CH bending modes. They were unable to obtain the harmonic frequency and the anharmonicity of the bending modes, but the values of the sum of the two agreed well with the fundamental frequency.

In 1981 Mortensen, Henry and Mohammadi [34] revisited the combination of the CH stretching pure local mode with CH bending in halomethanes. They took into account that, since the overtones involve progressively larger displacements, they would have a progressively larger effect on the effective CH bond length. This in turn, would have a progressively larger effect on the effective mass for the CH bending mode, which is dependant on the second inverse power of the bond length. Considering this, they were able to predict

the frequencies of the combinations with the pure local mode. The agreement between observed and calculated frequencies was good, though there was a tendency for the observed frequencies to decrease more quickly with increased overtone than had been predicted. The tendency was attributed to potential energy coupling which had been neglected in the calculations. They also noted that no corrections for the effects of Fermi resonance had been applied.

Combinations between the pure local modes and two quanta of CH bend, similar to those observed in the dihalomethanes, were observed by Henry and Mohammadi in the penta and tetra haloethanes [38]. They found that the energies of the combinations corresponded to:

**Equation 1-11.**

$$E(v_{CH}, 2) = E(v_{CH}) + 2\upsilon_i + 2v_{CH}X_{ii}$$

where $v_{CH}$ is the quantum number of the CH stretching overtone, $\upsilon_i$ is the fundamental frequency of the CH bending vibration. and $X_{ii}$ is the anharmonic coupling constant. Values between -15 and -22 $cm^{-1}$ were found for the $X_{ii.}$

From the proceeding, it is evident that any study of overtone vibrations must take into account local-normal combination. However, some simplifying assumptions can be made. The importance of these assumptions will become evident in the second chapter, which deals with the intensity of overtone vibrations. The study of overtone intensities would be very difficult if we had to consider every possible local-normal combination band. However, any combinations of a pure local mode with a normal mode such as CH bending, will likely be well removed from the local-mode, typically by 1000 $cm^{-1}$or more.

An example of the speration between the combinations described above and the pure local modes can be seen in the spectrum of trimethyl amine for example. The peaks associated with combinations of the local modes and one quanta of normal mode are clearly visible between, but well removed from, the first and second overtones, Figure 1-1.

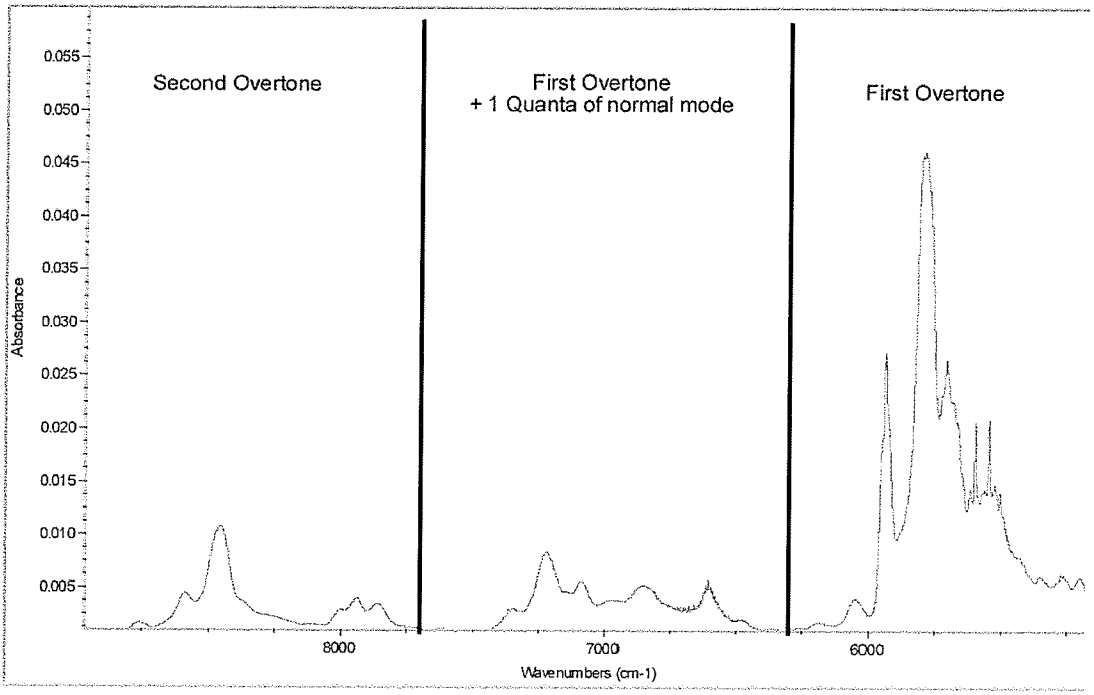


**Figure 1-1.** First overtone, combinations with one quantum of fundamental vibrations and second overtone of trimethyl amine. 128 co-added scans collected on a Bio-Rad FTS-40 spectrometer using a 1 meter nominal path length at ~ 300 torr.

Though the combination bands observed in the center rectangle of Figure 1-1 have not been formally assigned, it is interesting to note the similarity of this region to the preceding and following regions, suggesting that combinations between a local modes and one quanta of a normal mode such as CH bend dominate. However this region is not of interest to this thesis and will not be discussed further. The combination bands that are of interest are those where 2 quanta of either the same normal mode or 1 quanta of two separate normal modes combine with a local mode. This situation may lead the combination band to fall

within the region of the next higher overtone. Generally these combinations will have low intensity and therefore can often be considered negligible. However, if they have similar energy, *i.e.*, are accidentally degenerate to a local mode vibration, Fermi resonance interactions may cause considerable complications for the analysis of the spectrum.

### 1.2.3 Fermi Resonances

The mathematical formulation for Fermi resonance has been explained very well by Herzberg [1]. It will be briefly presented here since, even though it will not be formally used in this thesis, it provides the basis for the consideration of Fermi resonance interactions.

The magnitude of the energy shift that the vibrations involved in the Fermi resonance will display may be determined using first order-perturbation theory [39]. Considering the secular determinant we find:

**Equation 1-12.**

$$\begin{bmatrix} E_n^0 - E & W_{ni} \\ W_{in} & E_i^0 - E \end{bmatrix} = 0$$

where $E_n^0$ and $E_i^0$ are the unperturbed energies, E is the perturbed energy, $W_{ni}$ and $W_{ni}$ are the corresponding matrix elements of the perturbation function W. Since $W_{ni} = W_{ni}^*$ one obtains:

**Equation 1-13.**

$$E = \bar{E}_{ni} \pm \frac{1}{2}\sqrt{4|W_{ni}|^2 + \delta^2}$$

where

**Equation 1-14.**

$$\bar{E}_{ni} = \frac{1}{2}(E_i^0 + E_n^0)$$

and $\delta = E_n^0 - E_i^0$ is the separation between the two unperturbed energy levels. Equation 1-13 can be applied to instances where $\delta$ is small; in cases where $\delta$ is large compared to $2|W_{ni}|$, the equation expands to:

**Equation 1-15.**

$$E = \bar{E}_{ni} \pm \left( \frac{\delta}{2} + \frac{|W_{ni}|^2}{\delta} \right)$$

The eigenfunctions of the two resulting states $\psi_i$ and $\psi_n$ are mixtures of the zero order approximation eigenfunctions of the two vibrational energy levels involved in the Fermi resonance interaction $\psi_i^0$ and $\psi_n^0$:

**Equation 1-16.**

$$\psi_n = a\psi_n^0 - b\psi_i^0$$

**Equation 1-17.**

$$\psi_i = b\psi_n^0 + a\psi_i^0$$

where

**Equation 1-18.**

$$a = \left( \frac{\sqrt{4|W_{ni}|^2 + \delta^2} + \delta}{2\sqrt{4|W_{ni}|^2 + \delta^2}} \right)^{\frac{1}{2}}$$

and

**Equation 1-19.**

The matrix elements $W_{ni}$ are can be found using:

$$b = \left( \frac{\sqrt{4|W_{ni}|^2 + \delta^2} - \delta}{2\sqrt{4|W_{ni}|^2 + \delta^2}} \right)^{\frac{1}{2}}$$

**Equation 1-20.**

$$W_{ni} = \int \psi_n^0 W \psi_i^0 \, d\tau$$

Solution of equations 1-12 through 1-20 is not a simple task. This will not be undertaken here since, to solve for the matrix elements, the wavefunctions of the combination bands would have to be known and typically there is not enough data available in this work to reliably find the anharmonic constants for the coupling between the local and normal modes. Moreover, in the work presented here, an exact solution for the Fermi resonance is not required, since it is not the Fermi resonances themselves that are of interest. Rather, they are a complication in the analysis, that can be dealt with using simpler approximations. However, equations 1-12 through 1-19 do offer valuable insight into the assignment of the bands involved in the Fermi resonance. In most cases, the resonances considered will be between a pure local mode and a combination of a pure local mode with 2 quanta of normal modes. The unperturbed intensity of the pure local mode will be much more intense than the combination. Therefore, if the relative intensity of the two observed bands does not favor the pure local mode by a very large amount, insight as to the energy difference between the unperturbed energy levels may be gained. By considering the wavefunction mixing described by equations 1-16 through 1-19, we can often obtain a qualitative esti-

mate of the difference in energy of the unperturbed energy levels. For example, if the two peaks had equal intensity, one could assume that the energy difference was zero. Further more, the greater the difference in intensity, the larger the energy difference can be assumed to be. From equations 1-13 through 1-15, it is clear that the change in energy between the unperturbed and perturbed states is applied to each of the unperturbed states in an equal but opposite manner. Therefore, if one of the unperturbed states can be estimated, then the energy of the other unperturbed state can be estimated from the energy of the perturbed band. Using the same equations, it can be seen that the magnitude of the energy change is inversely proportional to the difference between the unperturbed energy levels. All of these observations allow for more reliable assignments of Fermi resonant bands. The application of this will be seen extensively in Chapter 2. It should be noted that, in Chapter 2, Fermi polyads are often involved; typically three vibrations are involved in the Fermi resonant interaction. This does complicate the considerations somewhat. In Chapter 2, a method for handling this situation in an qualitative fashion is described. This method is an extension of the above description. However, a more quantitative method for handling Fermi polyads can be found in the work of Quack *et al.* [40][41].

Fang and Swofford observed that the overtone spectra of both $CHCl_3$ and $CHBr_3$ exhibited Fermi resonance [36]. Their observations demonstrated the expected relationships described above very elegantly, as well as another phenomenon often referred to as Fermi tuning. Fermi tuning occurs because of the difference in the anharmonicities of the pure local mode and the combination band. The anharmonicity of the pure local mode will generally be higher than the anharmonicity of the combination band. Therefore, at successively higher overtones, a combination band that appeared much lower in energy than the

pure local mode at lower overtones will appear much closer in energy to the pure local mode at higher overtones. At some point the combination band will appear at higher energy than the pure local mode. As a result, a weak Fermi resonant interaction at lower overtones will become increasingly stronger at increasingly higher overtones, until the combination band is found at higher energy than the pure local mode at which point the trend will be reversed. The combination band will appear to increase in intensity in relation to the intensity of the pure local mode at increasingly higher overtones. This is the opposite of what would be expected if Fermi resonance was not involved. In Fang and Swofford's paper, they observed that the $\Delta\nu_{CH}(2)$+2CH bend combination appeared with very low intensity relative to the pure $\Delta\nu_{CH}(2)$, approximately 500 $cm^{-1}$ to the low energy side. Looking at the higher overtones, they found that the $\Delta\nu_{CH}(n)$+2CH combination appeared progressively closer to the $\Delta\nu_{CH}(n+1)$ band and with progressively higher relative intensity. By the sixth overtone, the combination band had nearly the same intensity as the local mode.

In a paper on ethylene and its fully deuterated counterpart [42], Duncan and Ferguson found that three major Fermi resonance interactions had to be accounted for, in order to get an acceptable characterization of the CH stretching manifold. The modes involved were: the $CH_2$ scissoring, $CH_2$ rocking and C-C stretching. They found that treatment of these interactions could be accomplished using either a local mode or a normal mode basis. However, even for the relatively simple ethylene molecule, the vibrational matrix had a dimension of 133. The details of the treatment will not be presented here. However, it should be noted that this type of calculation is possible.

Duncan applied this type of calculation to methyl bromide [43]. In this paper, he points out that any calculation must account for Fermi and Darling-Dennison interactions,

if it is to provide an accurate representation of all the vibrational levels. He notes that it is necessary to account for two Fermi-type interactions, both involving methyl deformation. Again the details of the treatment will not be presented here. One notable result is that the assumption that the combination band gained all of its intensity from the pure local mode could lead to unreliable results. In the case of methyl bromide, there was a significant over-estimation of the coupling parameters.

### 1.2.4 Intensities

Thus far, most of what has been presented has focused primarily on the energy of the overtone vibrations. The intensities of these bands are also of interest. There have been a number of theories as to the origin of intensity in the overtone region. Several are discussed briefly here. A more detailed discussion is reserved for Chapter 2.

The number of local mode states increases greatly with quantum number. It is therefore quite remarkable that the Full Width at Half Height (FWHH) does not change considerably with the increase of quanta. This indicates that there is little coupling between LM states. Benzene has historically been one of the first molecules researched in reference to the local mode model. Benzene was the subject of a 1979 paper by Burberry and Albrecht, in which they compared oscillator strengths determined empirically from experimental data to those determined from *ab initio* methods [44]. Before details of their calculations are reviewed, an important point made in the paper should be stressed. The local mode view requires that oscillator strengths for any given oscillator must be invariant to the total number of oscillators that exist in the molecule. This will be very important to the discussions in Chapter 2, where deuteration is used extensively. It is important to note because of the preceding point about the local mode model, that regardless of isotopic substitution, the pattern seen in the overtone spectra should remain a collection of localized uncoupled, vibrational modes.

In the paper by Burberry and Albrecht, the oscillator strength of the 0 to v transition in the ground electronic state $|g\rangle$ in the adiabatic approximation (which assumes that energy cannot be transferred between modes) was written as:

**Equation 1-21.**

$$f(\nu) = 4.702 \times 10^{-4} \bar{\nu}_{\nu 0} |\langle 0|(g|\mu|g)|\nu\rangle|^2$$

where

$$\bar{\nu}_{\nu 0} = E_\nu + E_0$$

and $\mu$ is the complete dipole moment operator. In order to determine the oscillator strength, the vibrational wavefunction $|\nu>$ and the nuclear coordinate dependence of the electronic dipole moment in the ground state $(g|\mu|g)$ have to be known. The vibrational wavefunctions used for the experimental fit were determined from the Morse potential written in the form:

**Equation 1-22.**

$$\nu(x) = D_e(1 - e^{-\beta x})^2$$

where

$$D_e = \frac{(A+B)^2}{4B}$$

with A and B being the Birge-Spöner parameters, and $\beta = 7.202\mu^{1/2}|B|^{1/2}$. The wavefunctions $|\nu>$ are the solutions of the Schrodinger equation. They also did the calculations by expanding the potential energy as a power series in the displacement coordinates:

**Equation 1-23.**

$$\nu(x) = \sum_{i=2} \chi_i x^i$$

with the $\chi_i$'s determined by a best fit of the eigen energies to the observed spectrum. The wavefunction was found by writing the Hamiltonian in a finite harmonic basis set and diagonalizing this matrix.

The dipole moment operator used was a power series expansion:

**Equation 1-24.**

$$M(x) = \sum_k M_k x^k$$

where x is the nuclear displacement and $M_k$'s represent the coefficients. For the empirical approach, the $M_k$'s were chosen to achieve the best fit to the observed oscillator strength. Only the first two terms in the power series were used. This still allowed for a good fit.

For comparison to the empirical treatment, a theoretical treatment was presented. CNDO/S methods were used to calculate dipole moments for various displacements of a single CH bond from the equilibrium configuration. These were then fitted to a power series. The results of this fit did not agree with the empirical results. This was not surprising as various inconsistencies in the empirical results had been noted. For example the $M_1$ and $M_2$ values should have been invariant irrespective of deuteration. This however was not observed. If this invariance was insisted upon in the calculations, then the calculated intensities for the CD overtones were found to be weaker than those observed. Both this and the deviation between the empirical and theoretical results were attributed to neglect of the higher order terms.

Further work on intensities was done by Schek, Jortner and Sage, in a study on napthalene[45]. They too used the Morse oscillator to describe the CH bonds. However, the dipole moment operator they used was of the form:

**Equation 1-25.**

$$\mu(R) = kR\exp(-R/R')$$

where k was the proportionality constant, R was the nuclear coordinate and R′ represented the position with the maximum μ(R). They found that the conventional linear approxima-

tion often used for low energy vibrations, with $R' = -\infty$, was insufficient. For naphthalene $R'/R_0 = 0.79$ gave the best agreement with experimental data.

The effect of local-local combinations was not considered in any of the papers that have been described above. This was the focus of a 1979 paper by Burberry and Albrecht [46]. In order to take these transitions into account, changes to the dipole operator were needed. The new dipole moment operator had to include excitations of more than one oscillator. The dipole moment operator then becomes:

**Equation 1-26.**

$$\mu = M_0 + \sum M_k q_k + \frac{1}{2}\sum_k \sum_l M_{kl} q_k q_l + \sum_k \sum_l \sum_m M_{klm} q_k q_l q_m + \ldots$$

where $M_0$ is the molecular dipole moment at the equilibrium geometry, the $q_i$'s are the local mode displacement coordinates for the k,l,m... oscillators and the coefficients are the dipole derivatives, which are treated as empirical parameters and fitted to the spectroscopic data. Then, assuming only binary combinations and writing $(M_{kl})^2$ as a semi-empirical parameter $\sigma_{kl}^2$, the integrated intensity of a binary combination becomes:

**Equation 1-27.**

$$\int \alpha(\bar{\nu}) d\bar{\nu} = \frac{(\pi \bar{\nu}_{\nu^K, \nu^L})}{3c\nu_0} g \sigma_{KL}^2 \left|\langle \nu^K | q_K | 0 \rangle\right|^2 \left|\langle \nu^L | q_L | 0 \rangle\right|^2$$

Though good agreement for general trends was observed, shortcomings were evident. The combination intensity decreased more rapidly with quantum number than was observed and the |1,1> combination was 4 times larger than the total observed first overtone intensity.

They then turned their attention to the Hamiltonian, which they found was not separable in local mode space as had previously been assumed. To deal with this they applied a first order correction:

**Equation 1-28.**

$$\hat{H} = \hat{H}^0 + \hat{H}^1$$

where the terms are the pure local mode Hamiltonian and a Hamiltonian including all the local-local mode mixing terms both kinetic and potential, respectively. This gave greatly improved results. Hence, they concluded that the separability of the Hamiltonian was more important than that of the dipole moment operator.

A complete presentation of the calculation of overtone intensities was done on water by Stannard *et al.* [47]. The methods used were similar to those already described. However, they noted that the zero order picture will break down when the density of states becomes very high.

Tamagake *et al.* made an interesting observation for benzene while fitting overtone intensities for a series of molecules to the first and second order terms of the one dimensional dipole moment functions [48]. They noticed that the first overtone was much weaker than would be expected by extrapolation from the other overtones. This observation allowed them to find better values for the ratio of the coefficients of the dipole moment function, $M_2/M_1$, since they found that accidental cancellation of the mechanical and electrical anharmonicities could occur at certain values of $M_2/M_1$. This cancellation was determined to be the reason for the low intensity of the first overtone. Therefore they were able to determine the sign and value of $M_2/M_1$, by choosing them to be such that the accidental cancellation could be recreated in the calculations. It is more important perhaps to note that

the ability of the model to "recreate" this unusually low intensity of the first overtone of benzene lends credibility. In later papers they used the process successfully on chlororform [49] and on 1,1 dichloroethene [50] using a two dimensional dipole moment function.

In 1985, Mortensen *et al.* used a model without any adjustable parameters [51]. The dipole moments were calculated from molecular orbital calculations at the STO-3G level of theory, or with semi empirical open shell INDO or CNDO/2 molecular orbital methods. They found that the CNDO/2 gave the best results. The dipole derivatives were taken to the cubic terms, which proved to have a significant contribution to the overtone intensities. They treated local-local coupling with a harmonic coupling model. The results showed good qualitative agreement with the observed spectra. Quantitative inconsistencies were attributed to several factors. The overlap of peaks in the experimental spectra made it difficult to get reliable experimental intensities. They also suggested that the Morse potential may not have been the best choice for the calculation of wavefunctions. However, it should be noted that at the time, and even now, the Morse potential function is the preferred potential function since it can be solved analytically. Finally they felt that some of the error may have come from the level of theory that was used in the calculations. In a later paper, they repeated these calculations using higher levels of theory and obtained reasonably quantitative results [52]. This would eventually lead to the harmonically coupled anharmonic oscillator local mode model (HCAO/LM) which will be discussed in Chapter 2.

Finally, some interesting observations by Lehmann and Smith indicated that the overtone intensity may in fact be influenced greatly by the slope of the inner wall of the potential function [53]. The influence of the inner wall of the potential suggests that a more general potential function than the Morse potential might be beneficial. Also, overtone

bands might be instrumental in gaining a better understanding of the inner wall of the CH stretching vibrations.

The preceding is a quick summary of the early work on the intensities of overtone vibrations. The work referenced above set the stage for future advances that would come in later years. Its was these papers that showed the importance of local-local combinations and the dipole moment function to the intensity. Later work would build on this work and lead to better models, most notably for this thesis the HCAO-LM model, developed by Kjaergaard and co-workers. These latter papers will be discussed as they become relevant.

# 2 CH- Stretch Overtone Study of Trimethyl Amine and Dimethyl Sulfide

## 2.1 Introduction

Trimethyl amine (TMA) has been the subject of many studies and much of the interest arises from the unusual difference in the C-H bond lengths, the largest known within a single methyl group [54]. This difference is attributed to the effect of the lone pair of electrons *trans* to the longer C-H bond. Though most pronounced in TMA, this effect can be observed in many molecules possessing the arrangement M-X-H, where X is a heavy atom such as carbon and M is an atom bearing a lone pair. Dimethyl sulfide (DMS) is studied in this project for comparison to TMA, because DMS exhibits a weak lone pair *trans* effect compared to TMA. In this project, the effect of the lone pair *trans* effect on the intensity of overtone absorptions is studied. It was of particular interest to see if the HCAO/LM model could predict the intensities accurately. Also of interest is the possibility of couplings that may appear between methyl groups due to the presence of the lone pair. Herein, the hydrogens will be referred to as *gauche* or *trans* based on their relation to the lone pair (see Figure 2-1).

The lone pair *trans* effect leads to the appearance of symmetric stretching vibrations in the fundamental region at lower energies than typically expected. Examples of this in methoxyl groups were first reported as early as 1957 by Henbert *et al.* [55]. They found that

the energy of the symmetric $CH_3$ stretching of the OMe group was lowered by 50 $cm^{-1}$ compared to methyl groups that were not connected to oxygens. Cases where the methyl group was bonded to a nitrogen were studied by Braunholtz *et al.* [56].

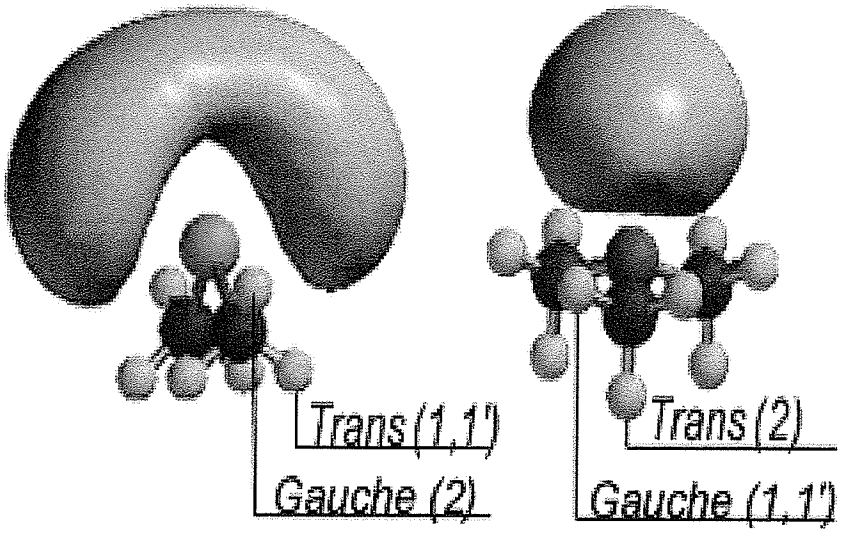


**Figure 2-1.** Structure of DMS and TMA, calculated using Spartan 5.0 at the HF/6-31G* level.

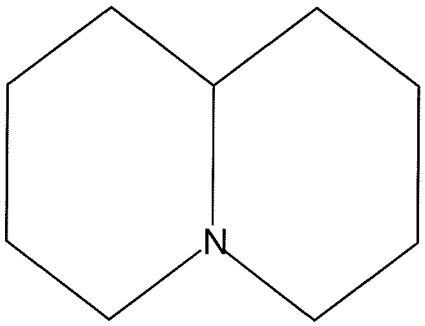


**Figure 2-2.** Structure of Quinolizidine

They also found that the low energy vibration was not observed in molecules where the lone pair of the nitrogen was no longer present, such as in salts and quaternary complexes. These observations clearly show the connection between the low energy bands and the lone pair. Similar observations were also made by Hill and Meakins [57].

Hamlow and Okuda examined this question using NMR techniques. The focus of their study was quinolizidine [58] (Figure 2-2). They found that there was a large shift between the axial and equatorial hydrogens bonded to the carbons adjacent to the nitrogen. They proposed that, in quinolizidine, the lone pair partially participated in an anti-bonding interaction with the axial CH bond. This interaction gave the axial CH bond some double bond character and increased electron density. The equatorial CH bond however could not engage in such an interaction as it lay in the plane perpendicular to the lone pair.

Further elaboration on the lone pair *trans* effect was presented by Pople [59]. In his paper on molecular orbital studies of conformation he noted that, using the 4-31G level of theory, fluoromethylamine had far greater stability with the fluorine in the position *trans* to the lone pair. This was found to be due to what they termed "back donation" [59] from the lone pair to the CF bond. This type of interaction was most favored when the CF bond occupied the position *trans* to the lone pair. Though not exactly the same as the lone pair *trans* effect seen in trimethyl amine, the molecular interactions involved are analogous.

The first unequivocal proof of the non-equivalence of CH bonds in the methyl groups came from a series of studies by McKean *et al.* [60][61] These papers focused on dimethyl ethers and methyl amines. What makes these studies of particular interest is the use of deuteration to help with the assignment of the peaks. The most interesting observation made for dimethyl ether was in the spectrum of $O(CD_3)(CD_2H)$. Since the CH stretching in this molecule is essentially decoupled from the CD stretches, information about the CH bond in various positions can easily be obtained. In the spectrum of $O(CD_3)(CD_2H)$, two bands are observed in the CH stretching region with a roughly 2/1 intensity ratio [60]. This is exactly what would be expected for a situation where the *trans* and *gauche* are non

equivalent, as there are two *gauche* positions for each *trans* position. Later, similar observations were made for a number of compounds, most notably $N(CD_3)_2(CD_2H)$ [61]. The importance of the lone pair *trans* effect became clear when McKean *et al.* compared the CH stretching frequencies of a large number of molecules, including trimethyl amine and dimethyl ether, to the CH bond lengths and dissociation energies. They found very good correlation between both the bond length and the dissociation energies, and the CH stretching frequency [62]. Specifically, for the lone pair *trans* effect, the CH bond *trans* to the lone pair is longer and weaker than that of the CH bond *gauche* to the lone pair. Bellamy and Mayo reviewed relevant data on the lone pair *trans* effect and described it as a weakening of the *trans* C-H bond arising from delocalization of lone pair electrons into an anti-bonding methyl orbital [63]. Though this interpretation has gained general acceptance, the factors that determine the strength of this effect are not completely understood. *Ab initio* calculations can be used to predict the lone pair *trans* effect with a fair degree of accuracy in that the difference in bond lengths is well approximated, however the intrinsic factors governing its magnitude are not well understood.

In Chapter 1, it was explained that CH-stretching overtone vibrations are known to provide bond-specific information, due to their local mode (LM) nature. Therefore, overtone spectroscopy may be instrumental in the study of non-equivalent CH bonds such as those caused by the lone pair *trans* effect. Both the LM parameters and the band intensities should exhibit differences that reflect the lone pair *trans* effect. Differences in the local mode parameters of non-equivalent CH oscillators have been documented in a variety of papers. For example, Gough and Henry found marked differences in the anharmonicities of the CH oscillators in fluorinated benzenes [64]. In that study, the CH bond lengths were-

calculated through *ab initio* geometry optimizations, with the STO-3G and 4-21G basis sets. When the results from these calculations are compared with the experimentally determined anharmonicities of the CH oscillators, it is found that the longer bonds are generally more anharmonic.

The origin of the intensities of LM peaks, as well as local-local mode (L-L) combination and local-normal mode (L-N) combinations, is complicated. However, referring back to the discussion in Chapter 1, the sources for the intensity may be summarized as: i) the anharmonic character of the LM oscillator (pure LM intensity), ii) the non-linear terms in the dipole moment operator (both pure LM and L-L mode combination intensities), iii) the mixing of states due to non-separable components in the vibrational Hamiltonian (intensity in the LM-combination modes), iv) off diagonal terms in the dipole moment operator (intensity in the L-L and L-N combination modes). Considering point i), it is clear that, unless other differences are involved, the more anharmonic oscillator should be more intense. Therefore, we would expect to observe differences in intensity for non-equivalent oscillators.

Of course, in studying intensities, it is beneficial to have a theoretical model for the intensities for comparison to experiment. Section 1.2.4 described much of the early work on overtone intensities. That work led to the HCAO/LM model, which will be used here. The mathematical details of the model will be described in Section 2.2.3. The HCAO/LM model has been used with success on many systems: propane [65], dimethyl ether, acetone [66] and cyclopropylamine [67] to name a few. In all cases, relatively good agreement between observed and calculated intensities was found. The HCAO/LM model calculations

presented here were done by H. G. Kjaergaard and G. R. Low, as part of a collaborative study with our group[69].

There have been two previous studies of the overtone spectra of trimethyl amine. Fang and Swofford reported the first through fifth pure LM peak positions for trimethyl amine and dimethyl sulfide as well as many other molecules with non-equivalent bonds [68]. It should be noted that the sixth overtone of the *trans* band of trimethyl amine was reported, but the sixth overtone of the *gauche* CH was not. This is presumably because it fell outside of the tuning range of their dye laser. Manzanares *et al.* also reported the position of the first through fifth overtones of trimethyl amine, as well as those of several other pyramidal molecules [70]. They were able to report on the *gauche* CH, but the *trans* was out of the ranges they scanned. In both of these papers, little attention was paid to the intensities or to the assignments of the L-L mode combinations.

In order to make assignments of the observed peaks, it is important to be aware of the possibility of methyl rotation, as this could have significant influence on the spectra. Barriers to internal rotation of the methyl groups of trimethyl amine have been reported to be 18.41 kJ/mol, as measured by computer aided microwave experiments [71]. The barrier to internal rotation for dimethyl sulfide has been reported to be 7.91 kJ/mol [72]. Both barrier heights are high enough to effectively decouple the CH stretching motion from the internal methyl rotation. The decoupling of the methyl rotation and the CH stretching at high rotational barriers has been demonstrated by Anastasakos and Wildman, in a paper on toluene and xylenes [73]. In molecules such as toluene, with low rotational barriers, the spectra were found to be that of an essentially free rotor, while in molecules with high rotational barriers, such as *o*-xylene, only two bands associated with the non-equivalent CH

bonds, locked in the minimum energy conformation, were observed. This was also shown for a wider range of molecules by Rong, Howard and Kjaergaard [74].

McKean, Murphy *et al.* discussed the *trans* lone pair effect in a study of the fundamental infrared spectra of trimethyl amine-$d_0$ and several deuterated isotopomers: $N(CD_3)_3$, $N(CD_2H)(CD_3)_2$, $N(CH_3)(CD_3)_2$, and $N(CD_3)(CH_3)_2$ [54]. The latter were used for the simplification of the fundamental CH-stretch region, since the deuteration eliminates the Fermi resonant coupling between the C-H stretching and bending modes. A detailed assignment of the fundamental spectra of these trimethyl amines was completed.

Overtone excitation also achieves this isolation of the C-H vibrations. In the higher overtones, the vibrations become increasingly less coupled and hence are best described by the LM model. While higher overtones might obviate the need for deuterated compounds, deuterated compounds can be instrumental in the proper assignment of peaks where, even in the overtones, the bands are often not completely resolved. As well, even in some of the higher overtones, combination bands and Fermi resonances may be observed, and may more easily be identified by comparison with the spectra of isotopomers. Finally, deuterium isolation can provide information on intra- and inter-group coupling. In this project, the $d_0$, $d_3$,$d_6$, $d_8$ and $d_9$ isotopomers of trimethyl amine are examined.

The study of the intensities can be difficult due to the number of overlapping peaks in the overtone region, and curve fitting is often required to estimate the intensity of individual bands. This leads to some ambiguity in the assignments of the peaks and their intensity. Curve fitting was required in this study; however, the relative simplicity of the molecules limited the amount of uncertainty in the assignments.

In this work, the first through fourth overtone spectra of the gas phase CH-stretching in TMA and its deuterated counterparts are presented. The experimental results are compared with *ab initio* calculations for the estimation of intensities through the HCAO/LM model. For comparison, the same overtone series for dimethyl sulfide (DMS), in which the *trans* lone pair effect is found to be very weak, is recorded.

The overall goal of this study was to improve our understanding of the overtone spectra of trimethyl amine and dimethyl sulfide within the context of the LM model. Previously unassigned peaks are tentatively identified through reference to the spectra of the deuterated compounds. HCAO/LM intensity predictions are compared to experimental results. Finally, the frequencies and intensities of the TMA and DMS spectra are analyzed in an attempt to gain more insight into the factors determining the origin and magnitude of the lone pair *trans* effect.

## 2.2 Experimental

### 2.2.1 Samples

Samples of TMA-$d_0$ (Matheson of Canada Limited), DMS (Sigma-Aldrich Limited 99+% pure) and TMA $d_8$ (Cambridge Isotopes 98% pure) were used without further purification. TMA $d_3$, $d_6$ and $d_9$ (MSD Isotopes) [76] had residual gases that were removed through repeated freeze-pump-thaw cycles of the sample on a vac-line. If necessary, samples were dried over KOH pellets.

### 2.2.2 Spectra

All FT-IR spectra were taken in single beam mode and a separate empty cell spectrum was recorded in each case, for calculation of an absorbance spectrum. Spectra of the fundamental region were obtained using a Bio-Rad FTS-60 Spectrometer with a WilMad glass long path mini-cell with a nominal path length of 1m, at pressures between 6 and 10 torr. The spectra of the first and second overtones were collected using a Bio-Rad FTS-40 with the same long path gas cell. The pressures used were between 200 and 500 torr. In the fundamental region, 128 scans were co-added and 2048 scans were co-added in the first and second overtone regions.

The third and fourth overtone spectra were obtained using a Nicolet 10 m multi-pass gas cell in a Nicolet Nexus 870 spectrometer equipped with a quartz beam splitter and a silicon detector. Pressures between 300 and 600 torr were used and 16384 scans were co-added. In the fourth overtone region some anomalies were observed, in the form of two sinusoidal curves in the baseline. For example, see the uncorrected spectra of the fourth overtone shown in Figure 2-3.

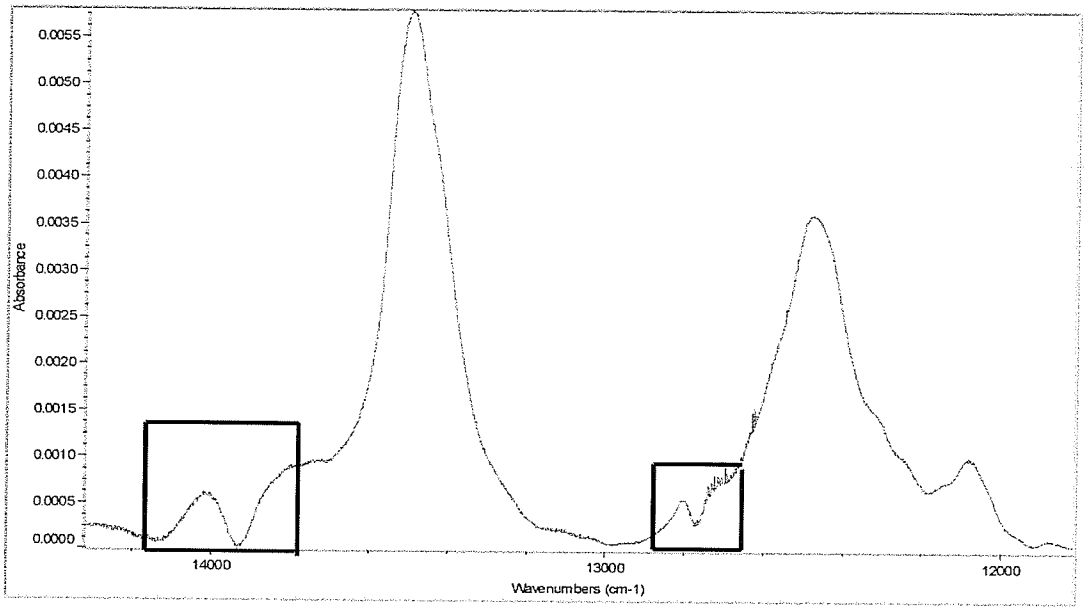


**Figure 2-3.** The uncorrected spectrum of the fourth overtone of trimethyl amine. The anomalies are within the boxes.

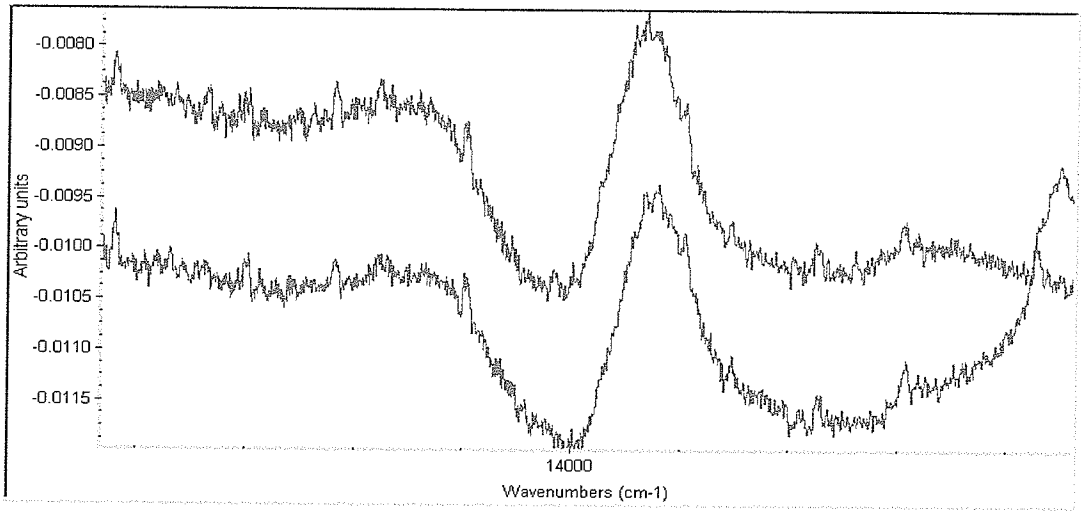


**Figure 2-4.** Derivative spectra of the 10 meter gas cell empty (top) and filled with trimethyl amine (bottom).

To determine the source of these anomalies, both the single beam spectra of the samples and the empty cell were studied. Features at approximately the same position as the anomalies were found in both the empty cell and the sample spectra. The features are

too weak to see in the transmission spectra, but are clearly visible in the derivative (see Figure 2-4). These features could be due to OH impurities in the silica windows. However, on further inspection it was noticed that, though very similar, the features observed in the empty cell were at a slightly different frequency than in the sample spectra. Therefore, it was postulated that the anomalies in the absorbance spectra were due to the ratioing of these features in the background and the sample spectra. It was determined that the easiest and most reliable way to correct for this was to construct an absorbance spectrum from a background and the same background shifted by the same amount as the feature in the sample spectrum; this will be called the anomaly spectrum for the purposes of the rest of the discussion (see Figure 2-5).

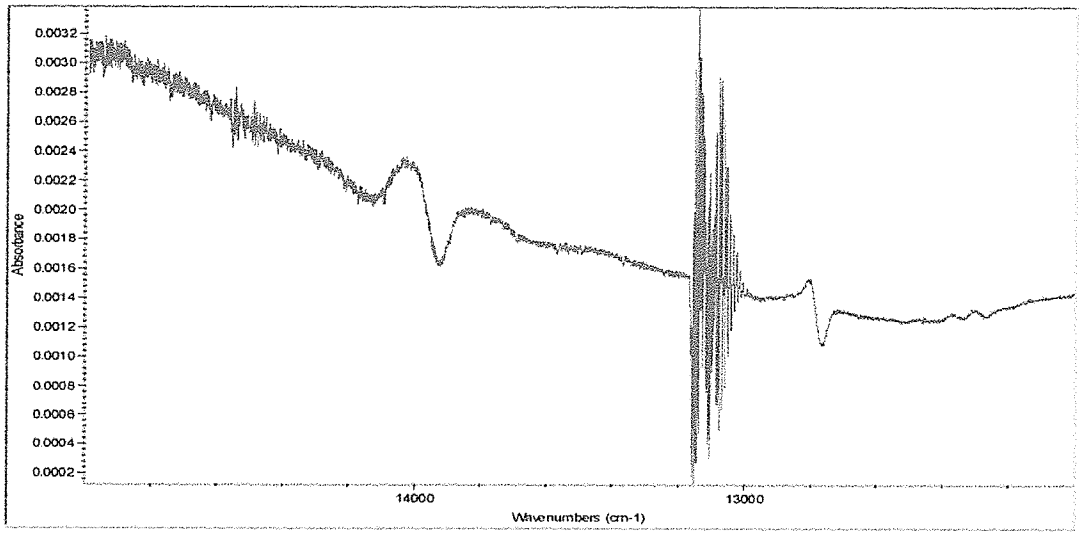


**Figure 2-5.** "Absorbance spectrum" of the background ratioed against itself, shifted by 7 $cm^{-1}$.

The strong features in the center of this spectrum are due to a mismatch of carbon dioxide peaks caused by the shift. The "carbon dioxide feature" of course could not be subtracted from the spectrum so it had to be removed. A further complication was that this feature made it very difficult to perform a reasonable baseline correction. To alleviate this

problem, a new file was created where everything except the carbon dioxide was replaced by straight lines; this will be called the carbon dioxide correction. The carbon dioxide correction was subtracted from the anomaly spectrum, after which the baseline could be corrected. Since the purpose was to remove the anomalies, everything but the sections where the anomalies appeared was replaced with a straight line. The result (see Figure 2-6) was then subtracted from the absorbance spectrum of the sample. The fact that a spectrum constructed entirely from the background could be used to subtract out the "anomalies" supports the theory that they in fact are not related to the sample.

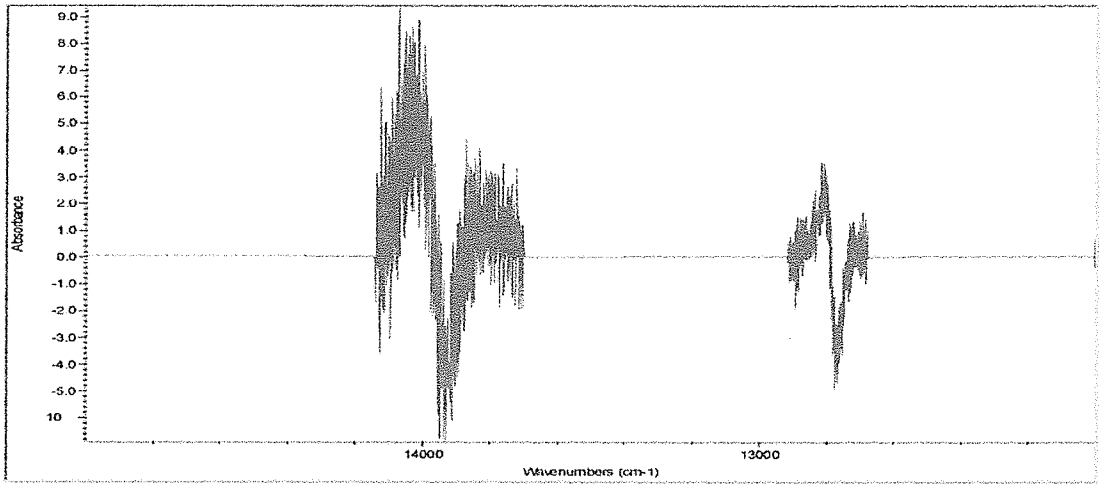


**Figure 2-6.** Example of the "correction spectrum" subtracted from the fourth overtones.

The 5th and 6th overtones were collected using an Intra-Cavity Laser Photo Acoustic spectroscopy system (ICL-PAS) that had been constructed prior to the start of this research; details are described elsewhere [77]. A diagram and photograph of the ICL-PAS system are shown in Figure 2-7 and Figure 2-8 respectively. The laser was a Coherent 599 dye laser pumped by a Coherent Innova 200 argon laser.

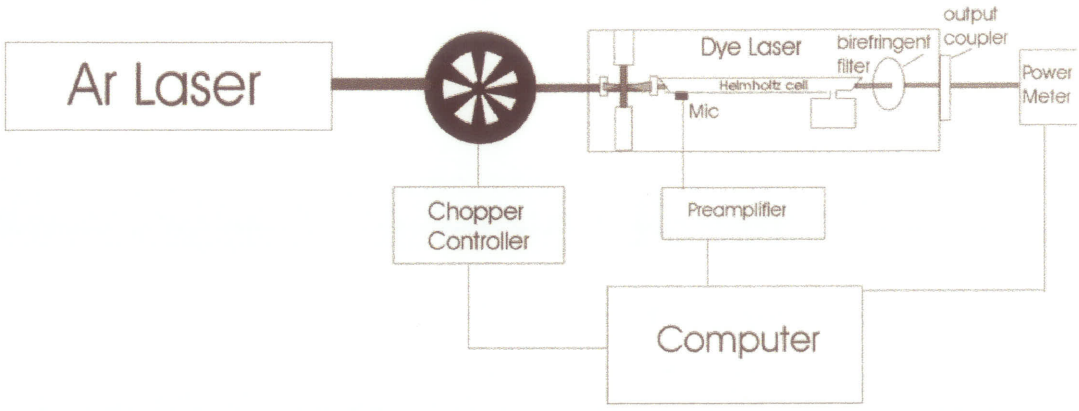


**Figure 2-7.** Diagram of the ICL-PAS system.

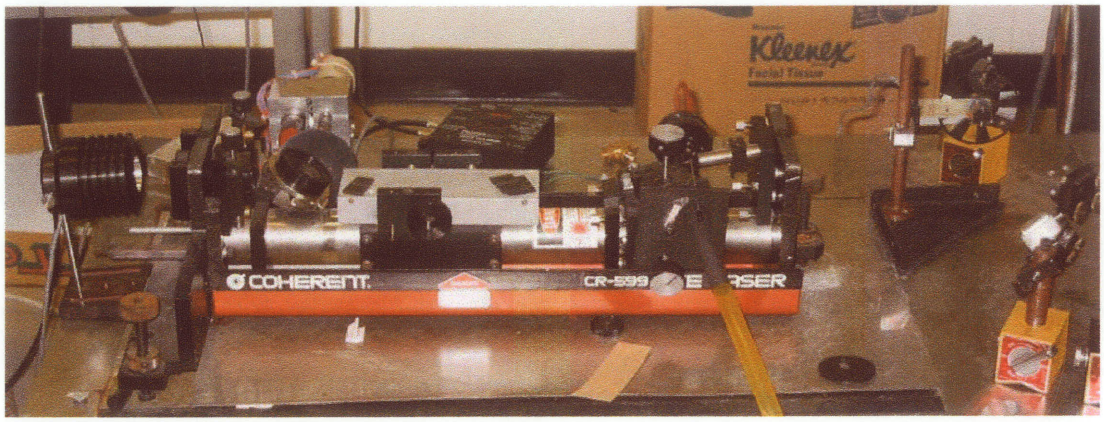


**Figure 2-8.** Picture of ICL-PAS system, cell and pump laser not shown.

The cell used for these experiments was a resonance cell constructed in our lab. The design of the cell has been described previously [78]. A photograph of the cell can be seen in Figure 2-9.

The equation reported earlier [78] for the calculation of the resonant frequency of the cell, though accurate for the specific cell used at that time, is not entirely correct for the general case. On further examination, we have found that the cavity of the cell does not approximate an open end perfectly and therefore the resonant cell likely operates as a

Helmholtz cell. Since the nature of the resonance is of far greater importance to the work presented in Chapter 4, the discussion of it will be presented in chapter 4. A Monolight Instruments chopping device is used to chop the pump beam at the resonant frequency of the cell. By pulsing the laser at the cell's resonant frequency, a constructive interference is created that increases the amplitude of the resonant frequency while destructive interference eliminates the non resonant frequencies. In this way, the signal to noise ratio is improved by a factor of 100, compared to non-resonance conditions.

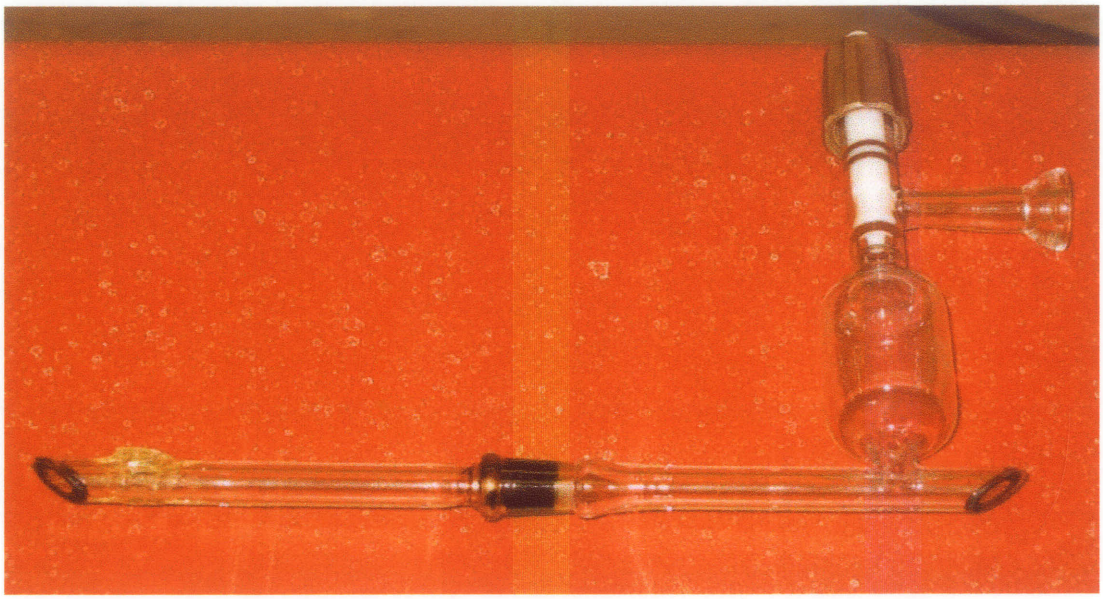

**Figure 2-9.** Picture of resonance cell.

The dye laser frequency is selected in the standard way, by the rotation of the three plate birefringent filter.

The dye laser frequency was calibrated in two stages. First, for any given dye, a fraction of the extra-cavity laser beam is directed to a SPEX 14018 double monochromator, equipped with a photomultiplier detector interfaced to a computer. The monochromator is used to measure the frequency of the laser at several points throughout the tunable range of

the birefringent filter. A polynomial function was created to relate the micrometer arm to the laser frequency. The coefficients of the polynomial are entered as parameters in the program that controls the equipment. After the spectra are recorded, a second calibration refinement is made by comparing the position of the rotational lines of water to a standard water spectrum. Small deviations can be adjusted by changing the start and end points of the recorded spectrum.

A power meter was used to record power fluctuation during the scan. The spectra were then normalized to intracavity power using [79]:

**Equation 2-1.**

$$P_i = P_e\left(\frac{2 - T(\lambda)}{T(\lambda)}\right)$$

where $P_i$ is the intracavity power, $P_e$ is the extra cavity power and $T(\lambda)$ is the wave length dependence of the output coupler transmission. Several different laser dyes were used to acquire all the spectra required. The fifth overtone region was acquired using pyridine 2, and the sixth overtone was acquired using DCM. The pressures used were between ~300-500 torr of sample.

Curve fit analysis was done for the second through fourth overtones using Win-IR software [80]. All peaks were fitted as a mixture of Gaussian and Lorenztian line shapes. The initial guess for the number and position of peaks was based on the second derivative spectrum; these were adjusted as necessary during the fitting procedure. Intensities from the curve fit analysis are compared with the predictions of the HCAO/LM model. Apart from unavoidable ambiguity in the number and nature of the peaks, the amount of error in the curve fitting procedure depends on the amount of noise and the amount of overlap

between adjacent bands. A correlation coefficient of $R^2 \geq 0.99$.was achieved for all curve fits reported here.

## 2.2.3 Theory

### 2.2.3.1 Geometry and internal rotation

The minimum energy conformers of TMA and DMS are known to be those shown in Figure 2-1. The structures of TMA and DMS were optimized with the HF/6-311++G(2d,2p) basis set with Gaussian 94 [81]. The optimized parameters (bond lengths and bond angles) are summarized in Table 2-1.

**Table 2-1.** Calculated bond lengths and angles for TMA and DMS. All values were calculated using RHF/6-311++G(2d,2p).

| Trimethyl Amine | | Dimethyl Sulfide | |
|---|---|---|---|
| | Bond Length (Å) | | Bond Length (Å) |
| NC | 1.444 | SC | 1.808 |
| $CH^{gauche}$ | 1.082 | $CH^{gauche}$ | 1.080 |
| $CH^{trans}$ | 1.093 | $CH^{trans}$ | 1.080 |
| | Bond Angles(°) | | Bond Angles(°) |
| C-N-C | 111.75 | C-S-C | 100.40 |
| $N\text{-}C\text{-}H^{gauche}$ | 109.91 | $S\text{-}C\text{-}H^{gauche}$ | 107.08 |
| $N\text{-}C\text{-}H^{trans}$ | 112.74 | $S\text{-}C\text{-}H^{trans}$ | 110.89 |
| $H^{gauche}\text{-}C\text{-}H^{gauche}$ | 107.98 | $H^{gauche}\text{-}C\text{-}H^{gauche}$ | 109.98 |
| $H^{gauche}\text{-}C\text{-}H^{trans}$ | 108.08 | $H^{gauche}\text{-}C\text{-}H^{trans}$ | 108.96 |

Though the barrier to internal rotation in trimethyl amine is high enough to decouple the CH stretching from internal methyl rotation, calculations of the energy at various dihedral angles (varying only one of the methyl groups) of the CH bond with respect to the lone pair were carried out in order to determine whether there were any local minima that could be reflected in the spectra. The results of these calculations are shown in Figure 2-10.

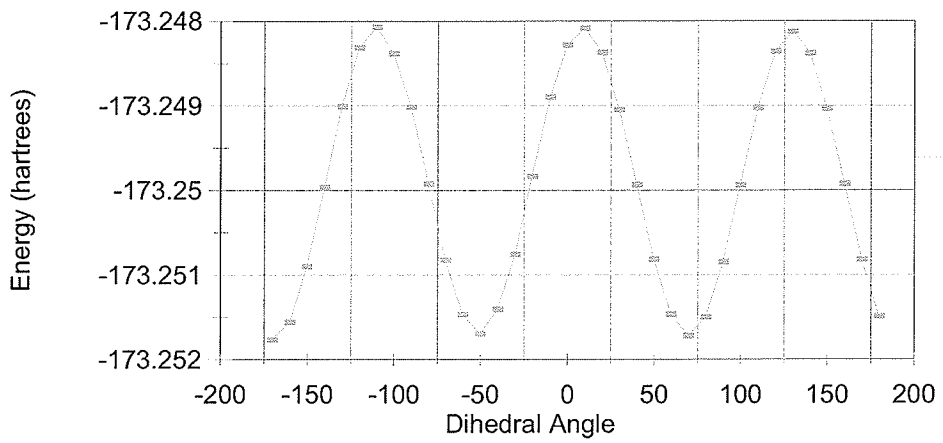


**Figure 2-10.** Energy versus dihedral angle between CH and the lone pair of electrons, calculated at HF/6-31G** level with Gaussian 94.

Since all of the minima observed in the results are at equivalent geometries, it can be assumed that there are no other geometries that will significantly affect the spectra. This calculation was not carried out for dimethyl sulfide, since it has far less steric crowding than trimethyl amine, and therefore is assumed to be less likely to have any local minima.

### 2.2.3.2 The HCAO/LM model and Intensities

The HCAO/LM model is used to describe the CH stretching vibrational modes. This procedure has been described previously [65],[66]; an overview is presented here. Coupling between CH bonds on different centers has been neglected, since such coupling is significant only when the CH bonds are attached to the same center. This was shown to be the case for propane by Kjaergaard *et al.* [65]. In that paper calculations were done with and without the inter-methyl coupling and the results were essentially the same in both

cases. It should be noted that propane does not exhibit the lone pair *trans* effect and whether that makes a difference has yet to be tested.

The oscillator strength of a vibrational transition between the ground state **g** and an excited state **e** is given by

**Equation 2-2.**

$$f_{eg} = [4.702 \text{cmD}^{-1}]\tilde{\nu}_{eg}\left|\vec{\mu}_{eg}\right|^2$$

where $\tilde{\nu}_{eg}$ is the vibrational frequency of the transition and $\vec{\mu}_{eg}$ is the dipole matrix element $\langle e|\vec{\mu}|g\rangle$ in debyes (D). For a methyl group the Hamiltonian is simply that of three coupled Morse oscillators. The zeroth-order Hamiltonian can be written:

**Equation 2-3.**

$$\frac{[H^o - E^o_{|00\rangle|0\rangle}]}{hc} = (v_1 + v_2)\tilde{\omega}_1 - (v_1^2 + v_2^2 + v_1 + v_2)\tilde{\omega}_1\chi_1 + v_3\tilde{\omega}_3 - (v_3^2 - v_3)\tilde{\omega}_3\chi_3$$

where $\omega_i$ is the LM frequency, $\omega_i\chi_i$ is the anharmonicity, $E^o_{|00\rangle|0\rangle}$ is the energy at the ground vibrational state and $v_i$ refers to the vibrational quantum number. The subscripts 1 and 2 refer to the *gauche* CH bonds for TMA and the *trans* for DMS, and 3 refers to the remaining CH bond in each case. For each CH bond type, values for the LM frequency and anharmonicity are determined from a least squares fit of the pure LM peak overtone positions to a Birge-Spöner plot. The values for the local mode parameters will be presented in Section 2.3.3.

The HCAO/LM model implies the inclusion of perturbation-only terms that are quadratic in momentum and position operator. The creation and annihilation operators [82] ($a^+$, a) may be introduced, and the perturbation can be written as,

**Equation 2-4.**

$$H^{1}_{intra} / hc = -\gamma'_{12}(a_1 a_2^{+} + a_1^{+} a_2) - \gamma'_{13}(a_1 a_3^{+} + a_1^{+} a_3 + a_2 a_3^{+} + a_2^{+} a_3)$$

where the coupling parameters are

**Equation 2-5.**

$$\gamma'_{12} = (\gamma_{12} - \phi_{12})\tilde{\omega}_1$$

**Equation 2-6.**

$$\gamma'_{13} = (\gamma_{13} - \phi_{13})\sqrt{\tilde{\omega}_1 \tilde{\omega}_3}$$

with

**Equation 2-7.**

$$\gamma_{ij} = -\frac{1}{2}\frac{G^{o}_{ij}}{\sqrt{G^{o}_{ii} G^{o}_{jj}}}$$

**Equation 2-8.**

$$\phi_{ij} = \frac{1}{2}\frac{F_{ij}}{\sqrt{F_{ii} F_{jj}}}$$

where the $G^{o}_{ij}$ are the elements of the Wilson G matrix evaluated at the optimized geometry, and $F_{ij}$ are the force constants. The operators $a^{+}$ and a are assumed to have step-up and step-down properties known from harmonic oscillators even though in this case they are operating on Morse oscillators [34]. With this approximation, $H^{1}_{intra}$ will only couple states within the same manifold that differ by one vibrational quantum in two CH oscillators.

The dipole moment function is expanded as a Taylor series about the equilibrium position

**Equation 2-9.**

$$\mu = \sum_{ijk} \mu_{ijk} q_1^{\,i} q_2^{\,j} q_3^{\,k}$$

where $\mu_{ijk}$ is the derivative of the dipole moment multiplied by (1/i!j!k!). The q coordinates are displacements in the bond length (R) from equilibrium with $q_1$ pointing in the positive y direction. The expansion is limited to terms of third order and lower when they involve at most two coordinates. The only third order term neglected involves $\mu_{111}$, which would affect primarily the intensity of the peak corresponding to one quantum in each CH bond; this peak is expected to be relatively small. The coefficients $\mu_{ijk}$, are obtained from two-dimensional grids of dipole moment as a function of both ($q_1$,$q_2$) and ($q_1$,$q_3$). The grids are calculated by varying the two coordinates in steps of 0.05 Å from -0.15 to 0.15 Å, with the rest of the molecule remaining at the equilibrium geometry. The grid points are calculated using a MO calculation at the SCF level with a 6-311G++(2d,2p) basis set with the Gaussian 94 program package [81]. The coefficients $\mu_{ijk}$ are obtained via these grids using a numerical technique to fit a n-1 order polynomial to n points.

It should be noted that all HCAO/LM calculations were done for non deuterated molecules and for $N(CD_3)_2(CD_2H)$. They are compared with the deuterated molecules.

## 2.3 Results and Discussion

### 2.3.1 Spectral Assignments for Trimethyl Amines

Before the local mode parameters can be evaluated and the predicted intensities compared to those measured experimentally, it is necessary to assign the bands as completely as possible. Previous papers on the overtone spectra of trimethyl amine have primarily assigned the pure local modes [68][70]. In this thesis, the assignments have been extended to L-L combinations and L-N combination bands. However, many of the assignments are tentative due to the difficulties inherent with assigning combinations bands in these high energy regions. In many cases, peaks are assigned as a group of unresolved vibrations. Since LM vibrations are expected to be the only significant source of intensity in the regions studied, the relative intensities of bands have been calculated as a percentage of the intensity observed over the entire region in question. The position and intensity of peaks treated in this manner are such that they match with the HCAO/LM model predictions well enough to support the assignment. L-N mode combinations are assumed to be Fermi resonances with pure local modes, as these combinations are not expected have any significant intrinsic intensity. The density of the possible states and the shift caused by the Fermi resonance complicates assignments of these bands. The assignments presented here are based on the expected position of the combination shifted by an amount that offsets the deviation of the pure local mode with which it is Fermi resonant. In most cases the assignments are further supported by analysis of the spectra of the deuterated molecules.

The $N(CHD_2)(CD_3)_2$ spectra are the simplest as there is only a single CH oscillator; thus only two vibrations are expected to have any intensity in any particular overtone region. Because of the simplicity expected for the $N(CHD_2)(CD_3)_2$ spectra, they are often

highly instructive in the assignment of other the molecules; therefore, they will be discussed first.

Spectra of $N(CD_3)_3$ revealed that the only significant peaks due to CD vibrations observed in the CH overtone regions are in the first and fourth overtone regions. The intensities of the first overtone regions have not been discussed. The CD vibrations observed in the fourth overtone CH stretching region are the fifth overtone of CD stretching and have intensity that is too low to be significant compared to the intensity of the CH stretching. Thus, we are able to discount any contribution from CD vibrations to the intensities.

Descriptions of the normal modes involved in combinations are taken from the harmonic force field of trimethyl amine described by McKean *et al.* [54].

For comparisons between the HCAO/LM model and the observed values it is generally considered acceptable for the predicted local-local combination frequencies to differ by tens of wavenumbers from the observed [75].

#### 2.3.1.1 Note on curve fitting

The curve fitting procedures must be used with great caution and they must be understood for what they are: an approximation. In most attempts to perform a curve fit, there is a great deal of ambiguity about the result. There may be situations where a spectrum may be fitted equally well by two peaks or by three peaks. It is not sufficient in these situations to rely on Ockham's razor (the simplest answer is the best), as in many cases the simplest possible answer is *not* always the best. This is particularly true in spectroscopy, where limits to the resolution of the spectrum, and linewidths that are broad and overlapping, may obscure details that would show that more peaks are present. To the same extent, one can

not simply use as many peaks as is needed to get a perfect fit. As in any situation, an infinite number of peaks will lead to a perfect solution even if there is no underlying physical reason for all the peaks. Therefore, curve fitting a spectrum is a compromise. In considering the curve fit data, one must realize that the curve fit procedure is (hopefully) the best that can be done with the available data. This includes the resolution, knowledge of the expected number of peaks, second derivative spectra and intuition. In any curve fit, the results must be considered to be an approximation: it is always possible that a poorly resolved peak was omitted or that one of the peaks included has no physical basis. The shapes of the peaks are also open to ambiguity, as they are taken as a mixture of Gaussian and Lorenztian functions. Considering these points, one must conclude that each peak fitted in this manner has some of uncertainty associated with it depending on the magnitude of the peak and how well it is resolved. From personal experience, it is the suggestion of the author that one should consider the error in any curve fit to be between 5-20% (for reasonably well resolved peaks). The assignments that are presented in the following sections rely heavily on curve fitting data, and should be considered to be plausible, not definitive. To reduce the chance of bias in the curve fitting, all curve fits were done without the aid of predicted values. The starting positions and number of peaks were based on the second derivative of the spectrum. Peaks were added to the curve fit spectrum if, after iteration, it was apparent from the residual that another peak was likely to be present.

#### 2.3.1.2 First Overtone

The first overtone still displays a large amount of normal mode character. This makes comparison to the HCAO/LM calculations difficult. In addition there is a lot of rotational structure that makes it impossible to perform a reliable curve fitting analysis on this

part of the spectrum. Therefore, the analysis of the first overtone is limited to the assignment of the bands and to intensity defined only as strong, medium, weak and very weak (see Table 2-2).

**Table 2-2.** Experimental vs. Calculated peak positions and intensities for the first overtone of $N(CH_3)_3$, $N(CH_3)_2(CD_3)$, $N(CD_3)_2(CH_3)$, and $N(CD_3)_2(CD_2H)$.

| Observed | | Calculated | | | |
|---|---|---|---|---|---|
| Frequency ($cm^{-1}$) | Intensity | Frequency ($cm^{-1}$) | Intensity ($10^{-7}$) | Relative Intensity (%) | Assignment |
| $N(CH_3)_3$ | | | | | |
| | | 5415 | 0.253 | 4.5 | $\|0,0\rangle\|2\rangle$ |
| 5544 | w | | | | Combination |
| 5596 | w | | | | Combination |
| 5706 | s | 5701 | 1.48 | 26.5 | $\|1,0\rangle_+\|1\rangle$ |
| | | 5733 | 0.319 | 5.7 | $\|1,0\rangle_-\|1\rangle$ |
| 5789 | s | 5763 | 1.18 | 21.1 | $\|2,0\rangle_+\|0\rangle$ |
| 5799 | s | 5772 | 1.18 | 21.1 | $\|2,0\rangle_-\|0\rangle$ |
| 5937 | s | 5899 | 1.18 | 21.1 | $\|1,1\rangle\|0\rangle$ |
| 6046 | w | | | | Combination |
| $N(CH_3)_2(CD_3)$ | | | | | |
| | | 5415 | 0.253 | 4.5 | $\|0,0\rangle\|2\rangle$ |
| 5543 | w | | | | Combination |
| 5707 | w | 5701 | 1.48 | 26.5 | $\|1,0\rangle_+\|1\rangle$ |
| | | 5733 | 0.319 | 5.7 | $\|1,0\rangle_-\|1\rangle$ |
| 5785 | s | 5763 | 1.18 | 21.1 | $\|2,0\rangle_+\|0\rangle$ |
| 5789 | s | 5772 | 1.18 | 21.1 | $\|2,0\rangle_-\|0\rangle$ |
| 5938 | s | 5899 | 1.18 | 21.1 | $\|1,1\rangle\|0\rangle$ |
| 6054 | | | | | Combination |
| $N(CD_3)_2(CH_3)$ | | | | | |
| | | 5415 | 0.253 | 4.5 | $\|0,0\rangle\|2\rangle$ |
| 5542 | s | | | | Combination |
| 5704 | s | 5701 | 1.48 | 26.5 | $\|1,0\rangle_+\|1\rangle$ |
| 5722 | w | 5733 | 0.319 | 5.7 | $\|1,0\rangle_-\|1\rangle$ |
| 5791 | s | 5763 | 1.18 | 21.1 | $\|2,0\rangle_+\|0\rangle$ |
| 5800 | w | 5772 | 1.18 | 21.1 | $\|2,0\rangle_-\|0\rangle$ |

| Observed | | Calculated | | | |
|---|---|---|---|---|---|
| Frequency ($cm^{-1}$) | Intensity | Frequency ($cm^{-1}$) | Intensity ($10^{-7}$) | Relative Intensity (%) | Assignment |
| 5935 | s | 5899 | 1.18 | 21.1 | \|1,1>\|0> |
| 6053 | w | | | | Combination |
| $N(CD_3)_2(CD_2H)$ | | | | | |
| | | 5416 | .0865 | 11.0 | \|0,0>\|2> |
| 5488 | w | | | | CD |
| 5587 | w | | | | |
| 5785 | s | 5766 | .702 | 89.0 | \|2,0>\|0> |
| 5945 | w | | | | Combination |

**$N(CD_2H)(CD_3)_2$**

The first overtone of $N(CHD_2)(CD_3)_2$ has a greatly simplified spectrum as the local mode combinations are no longer a factor (see Figure 2-11). Four major peaks are observed in this spectrum. It would be tempting to assign the band at 5488 $cm^{-1}$ as |0,0>|2> however it is significantly higher in energy than the predicted value and is more likely a be a combination band. The actual |0,0>|2> peak is likely obscured by other vibrations and noise. A peak at 5587 $cm^{-1}$ can be assigned as a combination of 2953 $cm^{-1}$ (37 $S_{25}$ asym gauche CH str, 30 $S_{13}$ sym gauche CH str, 18 $S_8$ asym

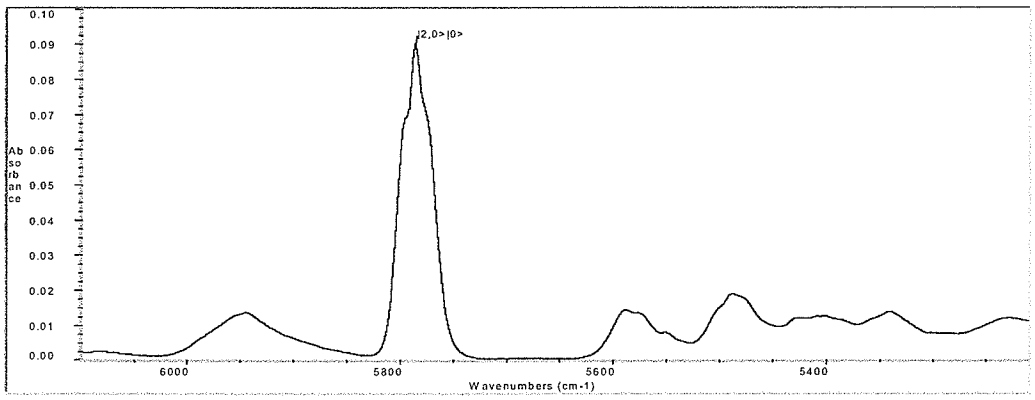


**Figure 2-11.** Spectrum of the first overtone of $N(CD_2H)(CD_3)_2$ and spectrum of the first overtone of $N(CD_3)_3$ collected at 250 torr, 1.6 meter gas path length, 2048 co-added scans.

gauche CH str and 15 $S_2$ sym gauche CH str), 1296 $cm^{-1}$ (50 $S_{17}$, 28 $S_5$ Me sym def‘ and 13 $S_{29}$ Me asym def‘‘) and 1336 $cm^{-1}$ (30 $S_{16}$Me sym def, 22 $S_{31}$ Me rock‘‘, 20 $S_4$ Me sym def, 10 $S_{29}$ Me asym def‘ and 10 $S_{26}$ asym NC str). A similar combination is found at ~5544 $cm^{-1}$ in the first overtone of every isotopomer. A combination of a CH stretch mode with two CH deformation modes is observed in many CH overtone spectra. A peak at 5785 $cm^{-1}$ is assigned as |2,0>|0>. Finally a peak at 5945 $cm^{-1}$ could possibly be a combination of |2,0>|0> and 185 $cm^{-1}$ (torsion). It should be noted however that the 185 $cm^{-1}$ was not observed in the fundamental and was only calculated in the force field analysis by McKean *et al.*[54].

**$N(CH_3)_3$**

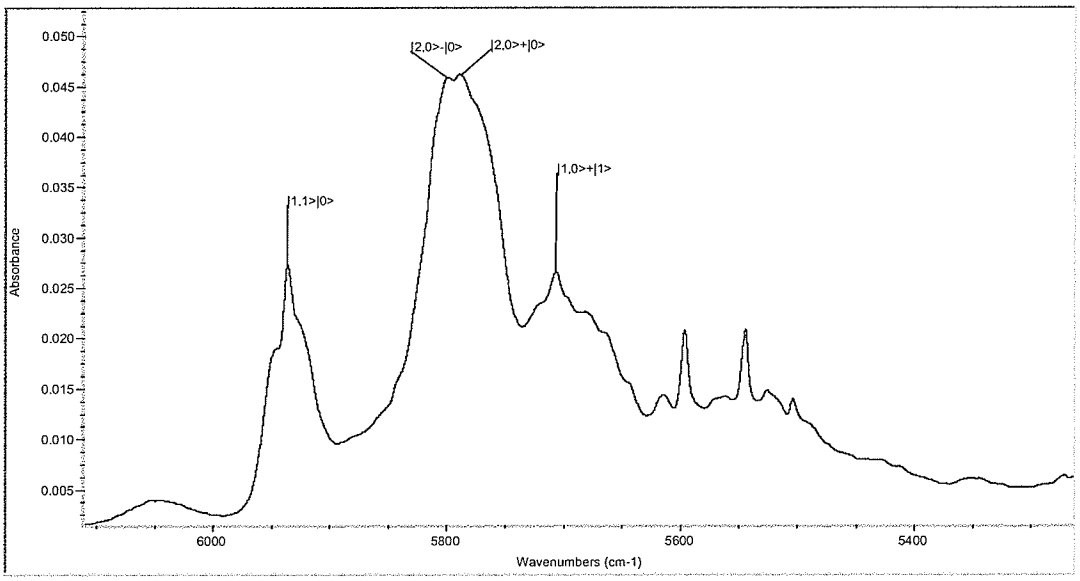


**Figure 2-12.** Spectrum of the first overtone of $N(CH_3)_3$ collected at 343 torr, 1.6 meter pass length, 2048 co-added scans.

For the trimethyl amine $d_0$ first overtone region, many bands are observed, the most prominent seven of which are discussed here. (See Figure 2-12). The positions of these

peaks have been found using the peak pick function in the Win-IR program [80] and compared to the values predicted by the HCAO/LM calculations (see Table 2-2). Two peaks are observed at 5544 $cm^{-1}$ and at 5596 $cm^{-1}$. These peaks are relatively weak and both have A/B character (where A,B,C refer to the profile of the band made of the P, Q and R branches [1]). The positions of these bands do not correlate with any of the predicted local mode vibrations, therefore it is assumed that they must be due to a combination of normal modes. This could be explained as a combination of 2 x 2774.8 $cm^{-1}$ Fermi resonant with 2 x 2775.9 $cm^{-1}$. However, there are several problems with this assignment. First of all, these two combinations are basically local modes, as they are multiple quanta of CH stretching vibrations. They should be affected by anharmonicity and therefore appear lower by ~160 $cm^{-1}$ (which is about where the HCAO/LM would predict them to be). Also, if there is a Fermi resonance here, it must be considered that the intensity of these peaks is nearly equal. This being the case, it would be expected that the two vibrations were very close in energy. If the energy of the two vibrations were very close, the splitting due to the Fermi resonance would be symmetric and the original position of the peaks would be expected to be at the mid-point between the observed peaks. However, this is not the case. Both of these combinations would be at ~ 5550 $cm^{-1}$ (if the anharmonic effects are not included), as opposed to 5570 $cm^{-1}$, which is the mid-point between the two observed peaks. Thus, other schemes for peak assignments must be considered.

A survey of the fundamental region shows that there are no combination of two fundamentals that can explain these peaks. However, a number of combinations of the following three fundamental bands are possible: 2953 $cm^{-1}$($S_2$ sym gauche CH str), 1444 $cm^{-1}$(92 $S_4$ 12 $S_5$ Me sym and asym def respectively) and 1186 $cm^{-1}$(80 $S_6$ Me rock) which leads to

a total of 5583 $cm^{-1}$; and 2953 $cm^{-1}$, 1409 $cm^{-1}$(106 $S_{16}$ Me def) and 1186 $cm^{-1}$ leading to a total of 5548 $cm^{-1}$. These assignments are the most likely ones, based on the fact that these combinations would fall near where they are observed.

A strong peak at 5706 $cm^{-1}$ with C character is assigned as $|1,0>_+|1>$. The absence of a band corresponding to the $|1,0>_-|1>$ vibration is consistent with its predicted low intensity and the likelihood that it would be obscured by the stronger $|1,0>_+|1>$. Two very strong overlapping peaks at 5789 and 5799 $cm^{-1}$ are assigned as $|2,0>_+|0>$ and $|2,0>_-|0>$, respectively. A peak at 5937 $cm^{-1}$ with C character is assigned as $|1,1>|0>$. Finally a peak at 6046 $cm^{-1}$ is assigned as a combination of 5789 $cm^{-1}$ ($|2,0>_+|0>$) and 256 $cm^{-1}$ (Me torsion).

It is interesting to note that the HCAO/LM calculations seem to underestimate the energies of the vibrations for this region. This is to be expected since vibrational behavior does deviate considerably from the local mode model in this region. It is also interesting to note that the *trans* CH vibration is not observed in this spectrum. This is not surprising since the HCAO/LM model does predict that it will be relatively weak.

**$N(CH_3)_2(CD_3)$**

The first overtone of $N(CH_3)_2(CD_3)$ is very similar to that of $N(CH_3)_3$. (See Figure 2-13) This suggests that there is little coupling between the methyl groups. However, there are some differences to be noted. Most noticeable is the lack of a peak at 5596 $cm^{-1}$. A peak is still observed at 5543 $cm^{-1}$; this can be assigned as a combination band of 2955 $cm^{-1}$ (63 $S_2$, 31 $S_{13}$ gauche CH str), 1436 $cm^{-1}$ (71 $S_4$, 28 $S_{16}$ Me sym def) and 1168 $cm^{-1}$ (68 $S_6$, 14 $S_{19}$ Me rock'). From this assignment, we can see why the 5596 $cm^{-1}$ band does not appear. In the non deuterated molecule, the 5544 $cm^{-1}$ and 5596 $cm^{-1}$ peaks were

due to basically the same combinations except for one involved the $S_4$ methyl deformation and the other the $S_{16}$; in the partially deuterated molecules both of these appear mixed in one vibration, hence only one combination peak is observed. The rest of the assignments are basically the same as for the non deuterated molecule (see Table 2-2).

It should be noted that the spectrum for $N(CH_3)_2(CD_3)$ seems less congested than for the non deuterated molecule. This may be due to a small amount of coupling between the methyl groups, causing a large number of weak combination vibrations. The number of these would be reduced in the deuterated molecule.

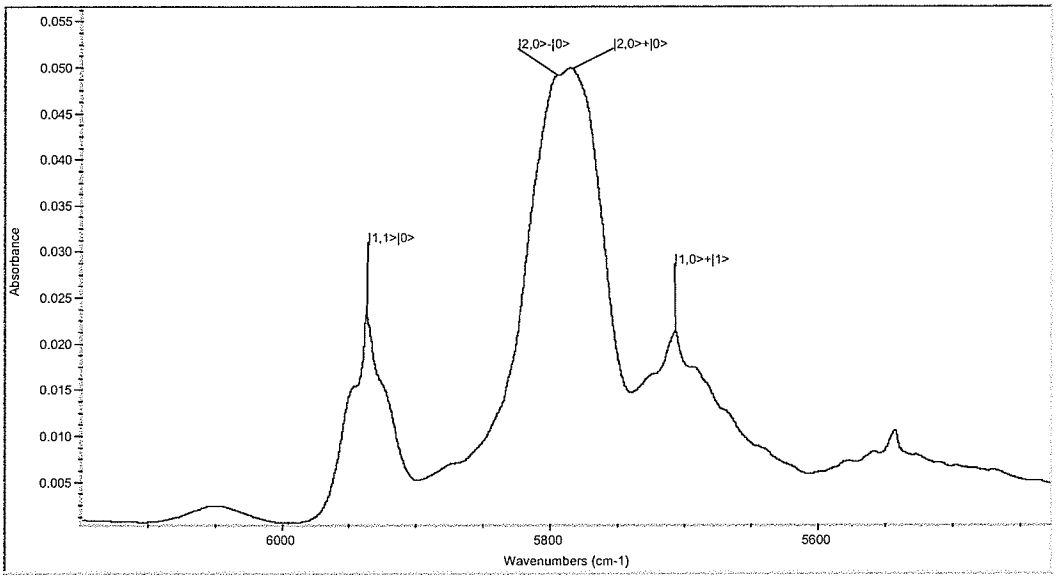


**Figure 2-13.** Spectrum of the first overtone of $N(CH_3)_2(CD_3)$ collected at 250 torr, 1.6 meter gas path length, 2048 co-added scans.

### $N(CD_3)_2(CH_3)$

The first overtone of $N(CH_3)(CD_3)_2$ is similar to its previously described counter-parts (see Figure 2-14). Further evidence that only weak coupling exists between the methyl groups is seen in this spectrum. The positions of the peaks are basically the same as

for $N(CH_3)_2(CD_3)$, however the spectrum again seems less congested. A band at 5542 $cm^{-1}$ is observed and can be assigned as the combination of 2950.5 $cm^{-1}$ (62 $S_{13}$, 31 $S_2$ sym gauche CH str), 1453 $cm^{-1}$ (60 $S_{17}$, 32 $S_5$ sym Me def'), and 1144 $cm^{-1}$ (48 $S_6$ 35 $S_{19}$ Me rock'). Notice that this is basically the same combination that was observed for trimethyl amine $d_6$ except that Me sym def, replaces the Me sym def. The |0,0>|2> might be assigned at 5487 $cm^{-1}$, though this is somewhat higher than predicted. In fact, this may be too far from the predicted value; it could be a combination band. The rest of the assignments for this spectrum are similar to those for trimethyl amine d3 (see Table 2-2).

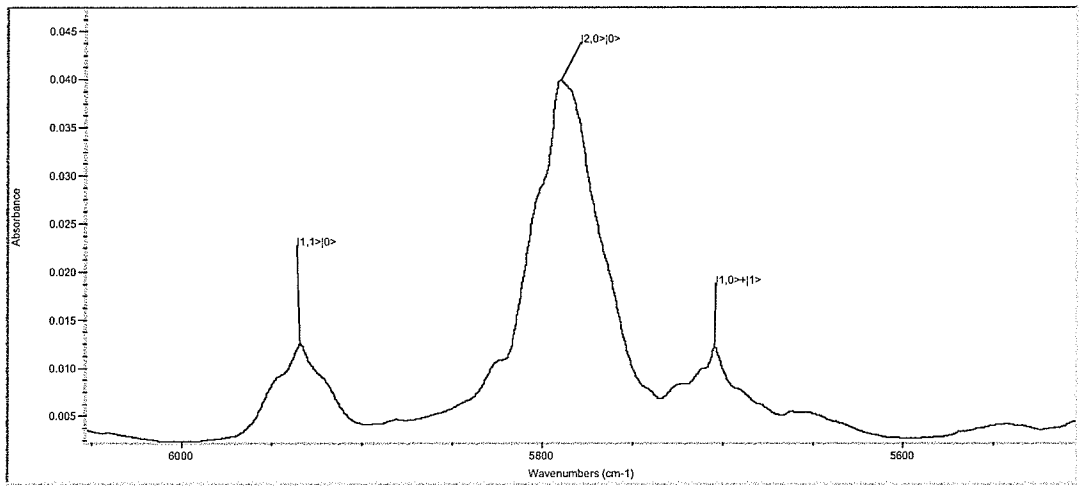


**Figure 2-14.** Spectrum of the first overtone of $N(CH_3)(CD_3)_2$ collected at 250 torr, 1.6 meter gas path length, 2048 co-added scans.

### 2.3.1.3 Second Overtone

The second overtone is primarily local mode in character, however there is still some evidence of local-normal mode combinations. There is little rotational structure observed in this region, thus a reasonable curve fit analysis may be done more easily. The curve fit analysis is very helpful in the comparison of the experimental value to the HCAO

/LM model predictions. However, curve fitting must be considered an approximation. (See Section 2.3.1.1)

The following protocol is used for comparisons of the HCAO/LM model calculations to the observed data. Peak positions taken from the curve fit results are directly compared to predicted values. For intensities, both the predicted and observed values were converted into relative intensities by taking the intensity of a given peak as a percentage of the sum of all of the peaks in the region. These relative intensity values could then be compared. The intensities are discussed in this chapter only as they relate to assignments. A more detailed discussion of intensities is presented in Section 2.3.4. The experimental and calculated positions and intensities are shown in Table 2-3.

**Table 2-3.** Experimental vs. Calculated peak positions and intensities for the second overtone of $N(CH_3)_3$, $N(CH_3)_2(CD_3)$, $N(CD_3)_2(CH_3)$, and $N(CD_3)_2(CD_2H)$.[a]

| Observed | | | Calculated | | | | |
|---|---|---|---|---|---|---|---|
| Frequency ($cm^{-1}$) | Relative Intensity (%) | Summed Intensity (%) | Frequency ($cm^{-1}$) | Intensity ($10^{-8}$) | Relative Intensity (%) | Summed Intensity (%) | Assignment |
| $N(CH_3)_3$ | | | | | | | |
| 7858 | 8.1 | | | | | | FR |
| 7941 | 7.7 | 19.3 | 7916 | 2.3 | 27.3 | 27.3 | $\|0,0\rangle\|3\rangle$ |
| 8003 | 3.5 | | | | | | FR |
| 8262 | 4.2 | 7.3 | 8342 | .45 | 5.4 | 5.5 | $\|1,0\rangle_+\|2\rangle$ |
| | | | 8375 | .007 | .1 | | $\|1,0\rangle_-\|2\rangle$ |
| 8369 | 10.8 | | | | | | FR |
| | | | 8455 | 2.2 | 26.1 | | $\|3,0\rangle_+\|0\rangle$ |
| 8444 | 17.2 | | 8457 | 2.0 | 24.1 | 50.2 | $\|3,0\rangle_-\|0\rangle$ |
| 8482 | 27.1 | 55.1 | | | | | FR |
| | | | 8541 | 0.55 | 6.6 | | $\|2,0\rangle_+\|1\rangle$ |
| | | | 8549 | 0.47 | 5.6 | | $\|2,0\rangle_-\|1\rangle$ |

| Observed | | | Calculated | | | | |
|---|---|---|---|---|---|---|---|
| Frequency ($cm^{-1}$) | Relative Intensity (%) | Summed Intensity (%) | Frequency ($cm^{-1}$) | Intensity ($10^{-8}$) | Relative Intensity (%) | Summed Intensity (%) | Assignment |
| 8589 | 15.4 | 15.4 | 8662 | 0.03 | 0.4 | 14.3 | $\|1,1\rangle\|1\rangle$ |
| | | | 8697 | 0.15 | 1.7 | | $\|2,1\rangle_+\|0\rangle$ |
| 8764 | 2.9 | 2.9 | 8747 | 0.23 | 2.7 | 2.7 | $\|2,1\rangle_-\|0\rangle$ |
| $N(CH_3)_2(CD_3)$ | | | | | | | |
| 7867 | 13.9 | 23.5 | 7916 | 2.3 | 27.3 | 27.3 | $\|0,0\rangle\|3\rangle$ |
| 7942 | 5.3 | | | | | | FR |
| 7997 | 4.3 | | | | | | FR |
| 8308 | 5.1 | 5.1 | 8342 | .45 | 5.4 | 5.5 | $\|1,0\rangle_+\|2\rangle$ |
| | | | 8375 | .007 | .1 | | $\|1,0\rangle_-\|2\rangle$ |
| 8364 | 1.5 | | | | | | FR |
| | | | 8455 | 2.2 | 26.1 | | $\|3,0\rangle_+\|0\rangle$ |
| 8444 | 27.2 | 58.1 | 8457 | 2.0 | 24.1 | 50.2 | $\|3,0\rangle_-\|0\rangle$ |
| 8486 | 29.3 | | | | | | FR |
| | | | 8541 | 0.55 | 6.6 | | $\|2,0\rangle_+\|1\rangle$ |
| | | | 8549 | 0.47 | 5.6 | | $\|2,0\rangle_-\|1\rangle$ |
| 8585 | 8.3 | 11.8 | 8662 | 0.03 | 0.4 | 14.3 | $\|1,1\rangle\|1\rangle$ |
| 8630 | 3.5 | | 8697 | 0.15 | 1.7 | | $\|2,1\rangle_+\|0\rangle$ |
| 8767 | 1.5 | 1.5 | 8747 | 0.23 | 2.7 | 2.7 | $\|2,1\rangle_-01\rangle$ |
| $N(CD_3)_2(CH_3)$ | | | | | | | |
| 7852 | 3.9 | | | | | | FR |
| 7898 | 4.1 | | | | | | FR |
| 7975 | 9.0 | 17.0 | 7916 | 2.3 | 27.3 | 27.3 | $\|0,0\rangle\|3\rangle$ |
| 8213 | 2.9 | 5.6 | 8342 | .45 | 5.4 | 5.5 | $\|1,0\rangle_+\|2\rangle$ |
| 8296 | 2.7 | | 8375 | .007 | .1 | | $\|1,0\rangle_-\|2\rangle$ |
| 8356 | 14.6 | | | | | | FR |
| | | | 8455 | 2.2 | 26.1 | | $\|3,0\rangle_+\|0\rangle$ |
| 8448 | 33.5 | 60.4 | 8457 | 2.0 | 24.1 | 50.2 | $\|3,0\rangle_-\|0\rangle$ |
| 8504 | 12.3 | | | | | | FR |
| 8576 | 7.2 | 7.2 | 8541 | 0.55 | 6.6 | | $\|2,0\rangle_+\|1\rangle$ |
| | | | 8549 | 0.47 | 5.6 | | $\|2,0\rangle_-\|1\rangle$ |
| 8621 | 6.8 | 6.8 | 8662 | 0.03 | 0.4 | 7.7 | $\|1,1\rangle\|1\rangle$ |
| | | | 8697 | 0.15 | 1.7 | | $\|2,1\rangle_+\|0\rangle$ |

| Observed | | | Calculated | | | | |
|---|---|---|---|---|---|---|---|
| Frequency ($cm^{-1}$) | Relative Intensity (%) | Summed Intensity (%) | Frequency ($cm^{-1}$) | Intensity ($10^{-8}$) | Relative Intensity (%) | Summed Intensity (%) | Assignment |
| 8768 | 3.0 | 3.0 | 8747 | 0.23 | 2.7 | 2.7 | \|2,1>_\|0> |
| $N(CD_3)_2(CD_2H)$ | | | | | | | |
| 7800 | 6.1 | | | | | | |
| 7864 | 6.0 | | | | | | |
| 7959 | 12.2 | 24.4 | 7917 | 0.76 | 31.4 | 31.4 | \|0,0>\|3> |
| 8283 | 16.1 | | | | | | |
| 8389 | 19.3 | | | | | | |
| 8506 | 40.3 | 75.7 | 8463 | 1.66 | 68.7 | 68.7 | \|3,0>_\|0> |

[a]Thin lines separate groups of bands that will be associated for comparison between theoretical and experimental intensities.

**$N(CD_2H)(CD_3)_2$**

Since there is only one CH oscillator, and it must occupy either the *gauche* or *trans* position, we would expect to find only two peaks in this region, however, six peaks are observed (see Figure 2-15). These are considered to be due to Fermi resonant interactions with L-N combinations. The peak at 7959 $cm^{-1}$ is assigned to the |0,0>|3> vibration. The fact that it is observed 42 $cm^{-1}$ higher in energy than predicted lends further support to the assignment of the peaks at 7800 $cm^{-1}$ and 7864 $cm^{-1}$ as L-N combinations in Fermi resonant interaction with it. The 7800 $cm^{-1}$ peak is assigned as the combination of 5415 $cm^{-1}$(|0,0>|2>), 1325 $cm^{-1}$ (Me sym def, Me rock) and 1123 $cm^{-1}$ (Me sym def, sym NC str, Me sym def). The 7864 $cm^{-1}$ peak is assigned as the combination of 5415 $cm^{-1}$(|0,0>|2>) and 2 quanta of 1224 $cm^{-1}$ (Asym NC str, Me rock" Asym $NC_3$ def). A more complete description of these Fermi resonant assignments can be found in Section 6.1.2.

The intensities of the L-N combinations are attributed to the pure LM with which they are Fermi resonant (|0,0>|3>) the relative intensity of these three peaks is 24% compared to a predicted 31%.

The other three peaks are also assigned as a pure local mode and two combination bands Fermi resonant with it. The 8506 $cm^{-1}$ band is the |3,0>|0> pure LM; 8390 $cm^{-1}$ is assigned as the combination of 5785 $cm^{-1}$ (|2,0>|0>) with two quanta of 1336 $cm^{-1}$ (Me sym def, Me rock", Me asym def, asym NC str); and the band at 8283 $cm^{-1}$ is assigned as 5785 $cm^{-1}$ (|2,0>|0>), 1297 $cm^{-1}$ (Me asym def; Me asym def") and 1207 $cm^{-1}$ (asym NC str, Me sym def) (details may be found in Section 6.1.3). The summed intensity of the three bands associated with the |3,0>|0> is 76%, which is quite reasonable compared with the predicted value of 69%.

In order to simplify the remaining text in this section, references will be made to Appendix 1 where detailed tables of the combination bands may be found.

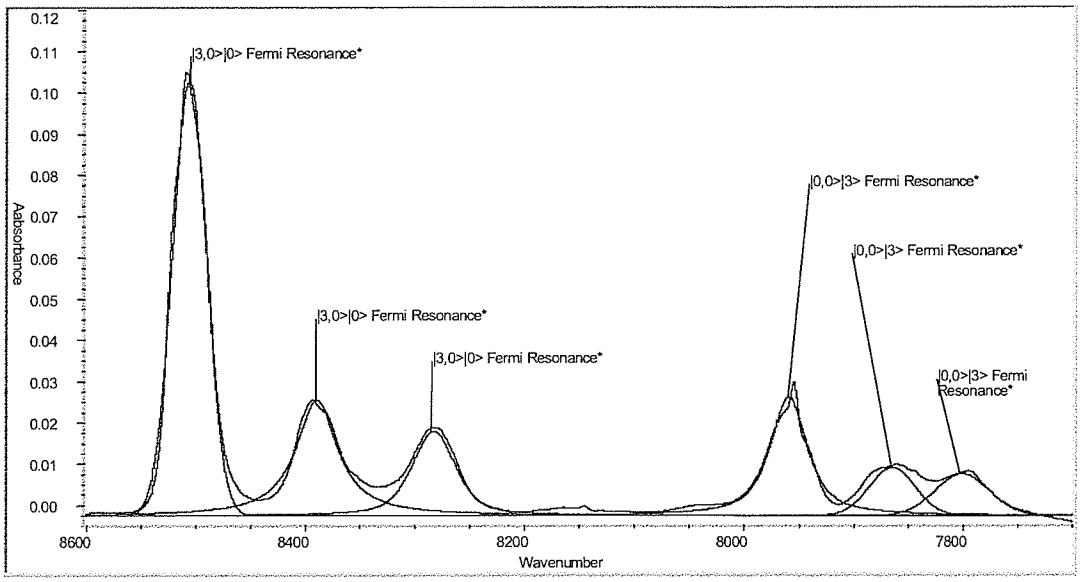


**Figure 2-15.** Spectrum of the second overtone of $N(CD_2H)(CD_3)_2$ collected at 250 torr, 1.6 meter gas path length, 2048 co-added scans. *Fermi resonance between pure local mode and local-normal combination, see text for further description.combinations

### $N(CH_3)_3$

Nine peaks were used to fit the second overtone region of $N(CH_3)_3$ (see Figure 2-16 and Table 2-3). Peaks at 7858 $cm^{-1}$, 7941 $cm^{-1}$ and 8002 $cm^{-1}$ are of particular interest. The region encompassed by these peaks corresponds to the |0,0>|3> local mode vibration, predicted by the HCAO/LM model to be at 7914 $cm^{-1}$. However, the predictions only account for one peak, therefore, it is assumed that there must be some L-N combinations to account for these peaks. However, there are no combinations of one normal mode with one local mode vibration that would fall within this region.

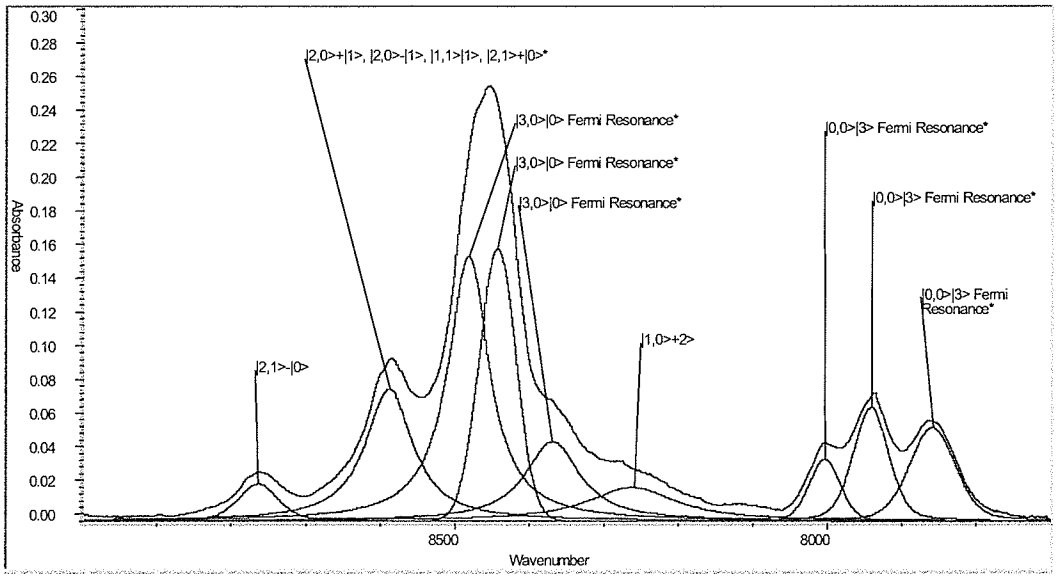


**Figure 2-16.** Spectrum of the second overtone of $N(CH_3)_3$ collected at 343 torr, 1.6 meter gas path length, 2048 co-added scans. *Fermi resonance between pure local mode and local-normal combination, see text for further description.

There are a number of combinations of a local mode with two normal modes that could fall within this region. These would be expected to be intrinsically very weak vibrations and therefore the relatively large intensity of these peaks are assumed to be due to Fermi resonance with the |0,0>|3> vibration. The fact that there are two vibrations Fermi resonant with one LM adds considerable complication to the analysis of these peaks. Competing forces causing shifts in wave number and intensity must be considered. The details of the assignments of Fermi resonance are given in Appendix 1; an explanation of these tables can be found on page 233. The results for this analysis for $N(CH_3)_3$ are shown in Section 6.1.4. The combinations are shown fit to within experimental error and are considered to be in line with what was found for the deuterated molecules. Because of the intensity sharing through Fermi resonance, the sum of the observed intensities of these three peaks was compared with the predicted intensity. The observed value was 19.2%, com-

pared to the 27.3% predicted. Given the error inherent in curve fitting, this is considered to be a fairly good agreement.

A similar, group of peaks is observed at 8369 $cm^{-1}$, 8443 $cm^{-1}$ and 8482 $cm^{-1}$. The same treatment was performed on these peaks, the results of which are shown in Section 6.1.5. This solution yields a very low error. Taking the sum of the intensities of these peaks to compare to the predicted value, we find 55.1% compared to 50.2%. It should be noted here that the observed value here is 5% higher than the predicted, whereas, for the *trans* region it was found to be 8% lower. It is possible that the calculation favors the *gauche* vibration more than is appropriate.

The peak observed at 8589 $cm^{-1}$ is relatively broad and contributes a relative intensity of 15.4%. There is no single predicted peak that matches well with it. However, it is possible that this peak is due to several of the local modes that are simply not resolved in this spectrum. The HCAO/LM model calculation predicts peaks at 8541 $cm^{-1}$, 8549 $cm^{-1}$, 8662 $cm^{-1}$ and 8697 $cm^{-1}$; the summed predicted intensity of these bands is 14.2%. This gives a good agreement with the intensity observed for 8589 $cm^{-1}$ and these predicted peaks fall into the region covered by the 8589 $cm^{-1}$ observed peak. Note that, if the peak predicted at 8541 $cm^{-1}$ was used in the assignment of the 8482 $cm^{-1}$ peak, this agreement would be lost.

Finally a peak with 2.9% intensity is observed at 8764 $cm^{-1}$; this matches well with the |2,1>-0> vibration predicted to appear at 8747 $cm^{-1}$ with a relative intensity of 2.7%.

**$N(CH_3)_2(CD_3)$**

The second overtone spectrum of $N(CH_3)_2(CD_3)$ is very similar to that of $N(CH_3)_3$ (see Figure 2-17), therefore the assignments are made in the same way. Three peaks are observed at 7866 $cm^{-1}$, 7942 $cm^{-1}$ and 8002 $cm^{-1}$. The analysis of the possible Fermi resonances explaining these peaks is shown in Section 6.1.6. The observed relative intensity of these three peaks is 25%, in good agreement with the predicted intensity (27%) for the |0,0>|3> mode (see Table 2-3). The peak observed at 8307 $cm^{-1}$ is attributed to the |1,0>|2>, predicted to fall at 8342 $cm^{-1}$. The observed intensity of this peak is 6.7%, in good agreement with the predicted intensity of 5.3%.

The peaks observed at 8374 $cm^{-1}$, 8444 $cm^{-1}$ and 8489 $cm^{-1}$ are assigned as Fermi resonance of the |3,0>|0> local mode vibration and combinations between a local mode and two normal modes (see Section 6.1.7). The same considerations made for $N(CH_3)_3$ hold here as well. The relative intensity of the three observed peaks is 58.1%, which agrees well with the predicted intensity of 50.2%. A peak at 8586 $cm^{-1}$ is assigned to the following predicted, but unresolved vibrations: 8541 $cm^{-1}$, 8549 $cm^{-1}$, 8661 $cm^{-1}$ and 8696 $cm^{-1}$. The predicted intensity in total for these vibrations is 14.3% which is in good agreement with the observed 11.8%.

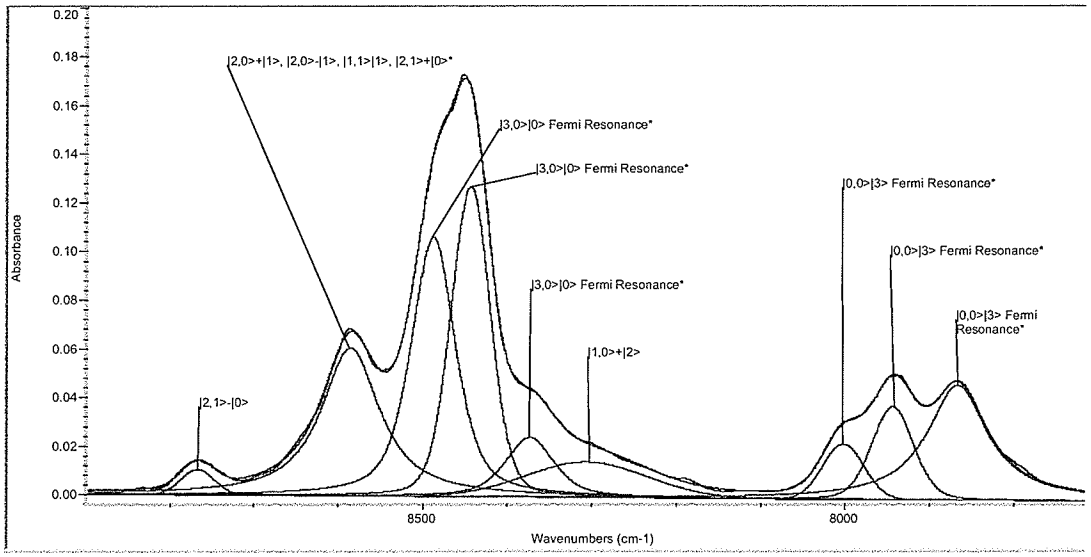


**Figure 2-17.** Spectrum of the second overtone of $N(CH_3)_2(CD_3)$ collected at 250 torr, 1.6 meter gas path length, 2048 co-added scans. *Fermi resonance between pure local mode and local-normal combination, see text for further description.

A peak at 8768 $cm^{-1}$ is assigned to |2,1>_|0>, predicted to fall at 8747 $cm^{-1}$ with 2.7% intensity, which is in reasonable agreement with the 1.3% observed in the spectrum.

### $N(CH_3)(CD_3)_2$

The spectrum recorded for $N(CH_3)(CD_3)_2$ is similar to that for the previous molecules (See Figure 2-18), however, more features are observable in this spectrum. Contributions from CD vibrations is considered unlikely since no CD vibrations are observed to fall within this region. More likely possibility is that, in the other molecules, weak coupling between the methyl groups produced a large number of local mode combinations that obscured the features now observed in this spectrum.

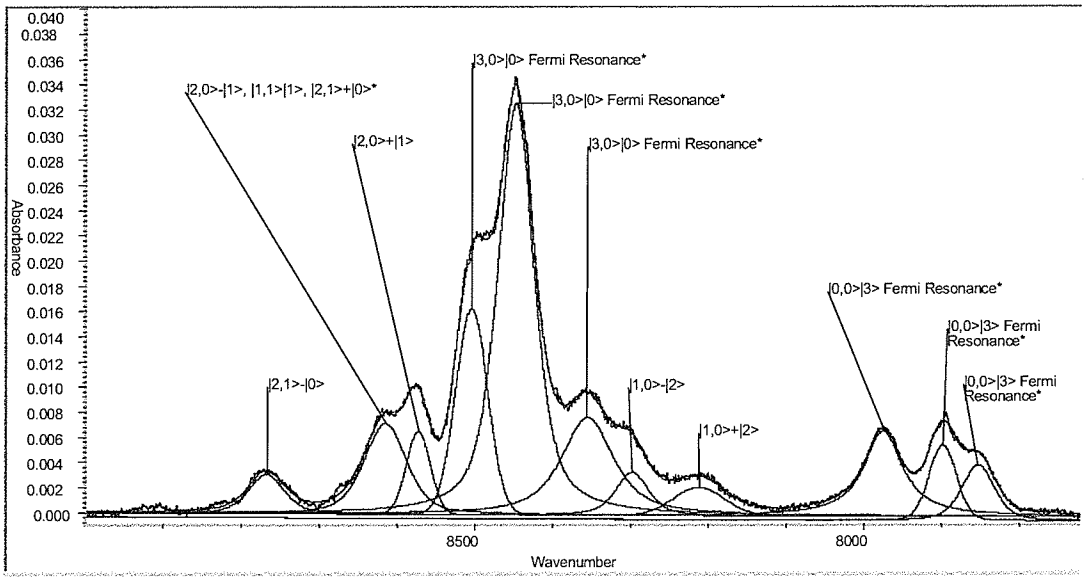


**Figure 2-18.** Spectrum of the second overtone of $N(CH_3)(CD_3)_2$ collected at 300 torr, 1.6 meter gas path length, 2048 co-added scans. *Fermi resonance between pure local mode and local-normal combination, see text for further description.

Three peaks observed at 7853 $cm^{-1}$, 7898 $cm^{-1}$ and 7975 $cm^{-1}$ are assigned in the same manner as in the previous compounds, see Section 6.1.8 for details. The summed intensity of these observed peaks is 17.0% compared to a predicted value of 27.3%. The peak observed at 8213 $cm^{-1}$ is assigned to $|1,0>_+|2>$, which is predicted to be found at 8342 $cm^{-1}$. The peak observed at 8296 $cm^{-1}$ is assigned as $|1,0>_-|2>$, which was predicted to fall at 8375 $cm^{-1}$. The intensities of the 8213 $cm^{-1}$ and 8296 $cm^{-1}$ bands are 2.9 and 2.7%, respectively.

Three peaks are observed at 8356 $cm^{-1}$, 8448 $cm^{-1}$ and 8504 $cm^{-1}$. These are assigned as Fermi resonances with the |3,0>|0> local mode vibrations. For details, see Section 6.1.9. The summed intensity of the observed peaks is 60.4% compared to the predicted value of 50.2%.

The peak observed at 8576 $cm^{-1}$ is assigned as $|2,0>_+|1>$, predicted to appear at 8541 $cm^{-1}$. The intensities, observed and calculated, respectively, are 7.2% and 6.5%.

The peak at 8622 $cm^{-1}$ is assigned to three unresolved vibrations: $|2,0>_-|1>$, $|1,1>|1>$ and $|2,1>_+|0>$ (see Table 2-3 for the predicted positions). The observed intensity is 6.8%, in good agreement with the predicted value of 14.3%. Finally, the peak that is observed at 8768 $cm^{-1}$ is assigned as $|2,1>_-|0>$, predicted to be at 8747 $cm^{-1}$. The observed intensity is 3.0% compared to 2.7% predicted.

### 2.3.1.4 Third Overtone

The third overtone offers some new challenges as the local-normal mode combinations fall closer to the *trans* CH stretch peak than in the lower overtones, due to the anharmonic nature of the *trans* CH bond. However, the energy separation between the local mode and local-normal "regions" is still large (~200 $cm^{-1}$), significant resonance effects would not be expected. The predicted and calculated energies and intensities for $N(CH_3)_3$, $N(CH_3)_2(CD_3)$, $N(CD_3)_2(CH_3)$, and $N(CD_3)_2(CD_2H)$ are compared in Table 2-4.

**Table 2-4.** Experimental vs. Calculated peak positions and intensities for the third overtone of $N(CH_3)_3$, $N(CH_3)_2(CD_3)$, $N(CD_3)_2(CH_3)$, and $N(CD_3)_2(CD_2H)$.[a]

| Observed | | | Calculated | | | | |
|---|---|---|---|---|---|---|---|
| Frequency ($cm^{-1}$) | Relative Intensity (%) | Summed Intensity (%) | Frequency ($cm^{-1}$) | Intensity ($10^{-9}$) | Relative Intensity (%) | Summed Intensity (%) | Assignment |
| $N(CH_3)_3$ | | | | | | | |
| 10270 | 20.0 | 20.4 | 10279 | 3.38 | 33.2 | 33.2 | $\|0,0>\|4>$ |
| 10306 | 0.5 | | | | | | |
| | | | 10844 | 0.295 | 2.9 | | $\|1,0>_+\|3>$ |
| | | | 10877 | 0.004 | 0.0 | | $\|1,0>_-\|3>$ |
| 10893 | 10.2 | | | | | | FR |
| 11042 | 58.6 | 74.6 | 11031 | 2.75 | 27.0 | 61.1 | $\|4,0>_+\|0>$ |

| Observed | | | Calculated | | | | |
|---|---|---|---|---|---|---|---|
| Frequency ($cm^{-1}$) | Relative Intensity (%) | Summed Intensity (%) | Frequency ($cm^{-1}$) | Intensity ($10^{-9}$) | Relative Intensity (%) | Summed Intensity (%) | Assignment |
| | | | 11031 | 3.09 | 30.3 | | $\|4,0\rangle_-\|0\rangle$ |
| 11215 | 5.8 | | 11166 | 0.05 | 0.5 | | $\|2,0\rangle_+\|2\rangle$ |
| | | | 11174 | 0.04 | 0.4 | | $\|2,0\rangle_-\|2\rangle$ |
| 11319 | 2.7 | 2.7 | 11247 | 0.184 | 1.8 | 3.6 | $\|3,0\rangle_+\|1\rangle$ |
| | | | 11248 | 0.149 | 1.46 | | $\|3,0\rangle_-\|1\rangle$ |
| | | | 11311 | 0.0009 | 0.01 | | $\|1,1\rangle\|2\rangle$ |
| | | | 11383 | 0.03 | 0.3 | | $\|3,1\rangle_+\|0\rangle$ |
| | | | 11409 | 0.197 | 1.93 | | $\|3,1\rangle_+\|0\rangle$ |
| 11440 | 2.2 | 2.2 | 11468 | 0.0094 | 0.09 | 2.1 | $\|2,1\rangle_+\|1\rangle$ |
| | | | 11527 | 0.0078 | 0.08 | | $\|2,1\rangle_-\|1\rangle$ |
| | | | 11556 | 0.0037 | 0.04 | | $\|2,2\rangle_-\|0\rangle$ |
| $N(CH_3)_2(CD_3)$ | | | | | | | |
| 10263 | 19.9 | 20.7 | 10279 | 3.38 | 33.2 | 33.2 | $\|0,0\rangle\|4\rangle$ |
| 10307 | 0.8 | | | | | | |
| | | | 10844 | 0.295 | 2.9 | | $\|1,0\rangle_+\|3\rangle$ |
| | | | 10877 | 0.004 | 0.0 | | $\|1,0\rangle_-\|3\rangle$ |
| 10947 | 21.4 | | | | | | FR |
| 11045 | 50.4 | 74.1 | 11031 | 2.75 | 27.0 | 61.1 | $\|4,0\rangle_+\|0\rangle$ |
| | | | 11031 | 3.09 | 30.3 | | $\|4,0\rangle_-\|0\rangle$ |
| 11213 | 2.3 | | 11166 | 0.05 | 0.5 | | $\|2,0\rangle_+\|2\rangle$ |
| | | | 11174 | 0.04 | 0.4 | | $\|2,0\rangle_-\|2\rangle$ |
| 11289 | 3.2 | 3.2 | 11247 | 0.184 | 1.8 | 3.6 | $\|3,0\rangle_+\|1\rangle$ |
| | | | 11248 | 0.149 | 1.46 | | $\|3,0\rangle_-\|1\rangle$ |
| | | | 11311 | 0.0009 | 0.01 | | $\|1,1\rangle\|2\rangle$ |
| | | | 11383 | 0.03 | 0.3 | | $\|3,1\rangle_+\|0\rangle$ |
| | | | 11409 | 0.197 | 1.93 | | $\|3,1\rangle_+\|0\rangle$ |
| 11432 | 2.1 | 2.1 | 11468 | 0.0094 | 0.09 | 2.1 | $\|2,1\rangle_+\|1\rangle$ |
| | | | 11527 | 0.0078 | 0.08 | | $\|2,1\rangle_-\|1\rangle$ |
| | | | 11556 | 0.0037 | 0.04 | | $\|2,2\rangle_-\|0\rangle$ |
| $N(CD_3)_2(CH_3)$ | | | | | | | |
| 10246 | 15.0 | 20.8 | 10279 | 3.38 | 33.2 | 33.2 | $\|0,0\rangle\|4\rangle$ |
| 10314 | 1.5 | | | | | | FR |

| Observed | | | Calculated | | | | |
|---|---|---|---|---|---|---|---|
| Frequency ($cm^{-1}$) | Relative Intensity (%) | Summed Intensity (%) | Frequency ($cm^{-1}$) | Intensity ($10^{-9}$) | Relative Intensity (%) | Summed Intensity (%) | Assignment |
| 10355 | 4.3 | | | | | | FR |
| | | | 10844 | 0.295 | 2.9 | | $\|1,0\rangle_+\|3\rangle$ |
| | | | 10877 | 0.004 | 0.0 | | $\|1,0\rangle_-\|3\rangle$ |
| 10902 | 11.8 | | | | | | FR |
| 10988 | 11.8 | | | | | | FR |
| 11058 | 42.3 | 70.3 | 11031 | 2.75 | 27.0 | 61.1 | $\|4,0\rangle_+\|0\rangle$ |
| | | | 11031 | 3.09 | 30.3 | | $\|4,0\rangle_-\|0\rangle$ |
| | | | 11166 | 0.05 | 0.5 | | $\|2,0\rangle_+\|2\rangle$ |
| 11199 | 4.4 | | 11174 | 0.04 | 0.4 | | $\|2,0\rangle_-\|2\rangle$ |
| 11297 | 4.4 | 4.4 | 11247 | 0.184 | 1.8 | 3.6 | $\|3,0\rangle_+\|1\rangle$ |
| | | | 11248 | 0.149 | 1.46 | | $\|3,0\rangle_-\|1\rangle$ |
| | | | 11311 | 0.0009 | 0.01 | | $\|1,1\rangle\|2\rangle$ |
| | | | 11383 | 0.03 | 0.3 | | $\|3,1\rangle_+\|0\rangle$ |
| 11432 | 2.3 | 2.3 | 11409 | 0.197 | 1.93 | 2.0 | $\|3,1\rangle_+\|0\rangle$ |
| | | | 11468 | 0.0094 | 0.09 | | $\|2,1\rangle_+\|1\rangle$ |
| 11586 | 2.2 | 2.2 | 11527 | 0.0078 | 0.08 | | $\|2,1\rangle_-\|1\rangle$ |
| | | | 11556 | 0.0037 | 0.04 | | $\|2,2\rangle_-\|0\rangle$ |
| $N(CD_3)_2(CD_2H)$ | | | | | | | |
| 10178 | 5.2 | | | | | | |
| 10247 | 16.1 | 36.1 | 10280 | 1.1 | 35.4 | 35.4 | $\|0,0\rangle\|4\rangle$ |
| 10335 | 13.8 | | | | | | |
| 10417 | 1.1 | | | | | | |
| 10533 | 1.3 | | | | | | |
| 10728 | 1.4 | | | | | | |
| 10850 | 2.5 | | | | | | |
| 10967 | 16.9 | | | | | | |
| 11059 | 28.9 | 63.9 | 11036 | 1.01 | 32.3 | 64.7 | $\|4,0\rangle_+\|0\rangle$ |
| | | | 11036 | 1.01 | 32.3 | | $\|4,0\rangle_-\|0\rangle$ |
| 11078 | 2.5 | | | | | | |
| 11159 | 7.1 | | | | | | |
| 11251 | 1.2 | | | | | | |

| Observed | | | Calculated | | | | |
|---|---|---|---|---|---|---|---|
| Frequency ($cm^{-1}$) | Relative Intensity (%) | Summed Intensity (%) | Frequency ($cm^{-1}$) | Intensity ($10^{-9}$) | Relative Intensity (%) | Summed Intensity (%) | Assignment |
| 11358 | 0.9 | | | | | | |
| 11442 | 1.2 | | | | | | |

[a]Thin lines separate groups of bands that will be associated for comparison between theoretical and experimental intensities.

**$N(CD_3)_2(CD_2H)$**

In the $N(CD_2H)(CD_3)$ molecule, we expect that there will only be two vibrations that have significant intensity, the |0,0>|4> and |4,0>|0> pure LMs. However, more than 14 peaks are observed (see Figure 2-19). All the intensity for these additional peaks is assumed to be derived through Fermi resonance with the two pure local mode vibrations and are assigned to the pure LM to which they are closest in energy. Since, upon summing the intensities of all the peaks associated with each pure LM (see Table 2-4), we find that the predicted intensities match the observed intensities to within 1%, this seems to have been a reasonable choice.

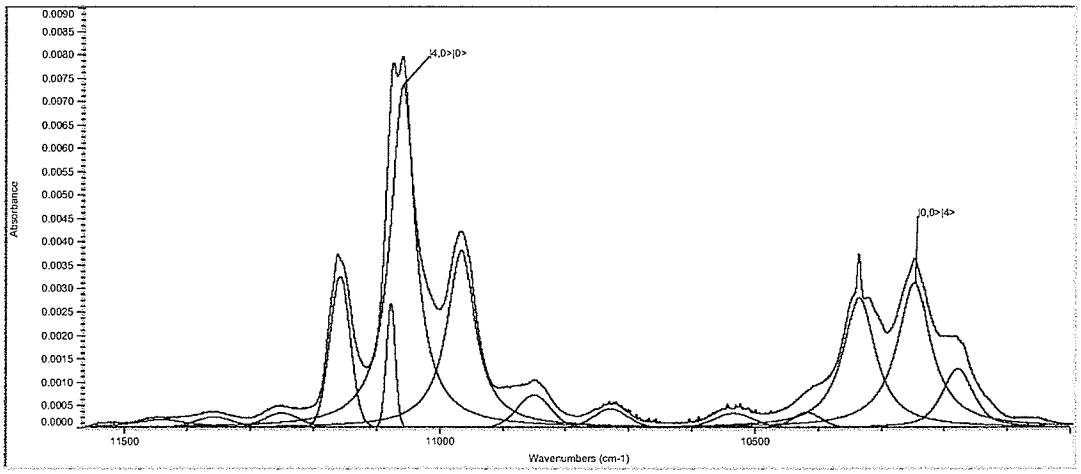


**Figure 2-19.** Spectrum of the third overtone of $N(CD_2H)(CD_3)_2$. Collected with a 10 meter path length, 16384 co-added scans. *Fermi resonance between pure local mode and local-normal combination, see text for further description

## $N(CH_3)_3$

The spectrum of $N(CH_3)_3$ in the third overtone region (See Figure 2-20) bears some resemblance to the second overtone, as expected. The peak at 10270 $cm^{-1}$ is quite asymmetric and it is likely that this peak is actually several overlapping modes. However, there is no way to resolve these bands with any satisfactory degree of certainty; curve fitting analysis of this band is ambiguous. Given that any bands that would fall in this region, other than |0,0>|4>, would be expected to be very weak, this entire peak is attributed to the |0,0>|4> vibration. In the curve fitted analysis, a small band was placed at 10307 $cm^{-1}$. This was done simply to improve the curve fit result. No physical meaning is attributed to this curve, as a similar quality of fit could have been achieved in any number of different ways, with no way to determine which is valid. For the purposes of intensity analysis, the intensity of the 10306 $cm^{-1}$ peak is combined with the 10270 $cm^{-1}$ peak (See Table 2-4).

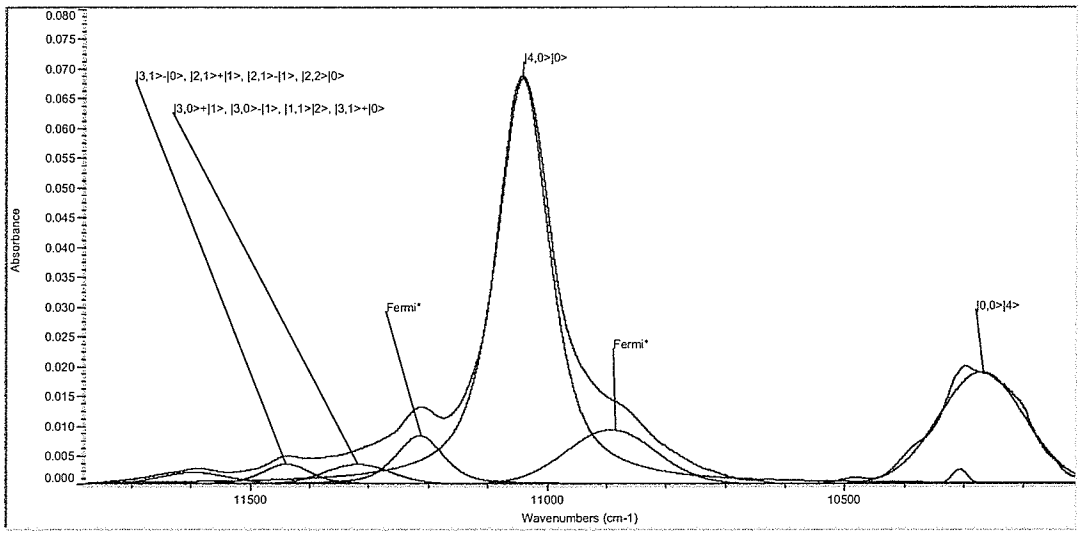


**Figure 2-20.** Spectrum of the third overtone of $N(CH_3)_3$. Collected with a 10 meter path length, 16384 co-added scans. *Fermi resonance between pure local mode and local-normal combination, see text for further description.

The peak that appears at 10893 $cm^{-1}$ is a shoulder on the stronger 11042 $cm^{-1}$peak, and presents some difficulty in assignment. As it is a shoulder, the intensity of this peak is somewhat difficult to determine. Depending on parameters used for the curve fit, the intensity may be 10% or more. At 10% relative intensity, this band is stronger than any of the predicted local mode combinations. Fermi resonance with the |4,0>|0> vibration, predicted to fall at 11031 $cm^{-1}$ but observed at 11042 $cm^{-1}$, is a likely explanation.

A peak at 11215 $cm^{-1}$ is assigned to both $|2,0\rangle_{+}|2\rangle$, predicted to be at 11166 $cm^{-1}$, and $|2,0\rangle-|2\rangle$, predicted to appear at 11174 $cm^{-1}$.

The peak observed at 11319 $cm^{-1}$ is assigned to the following unresolved set of predicted peaks: 11247 $cm^{-1}$ ($|3,0\rangle+1\rangle$), 11248 $cm^{-1}$ ($|3,0\rangle-|1\rangle$), 11311 $cm^{-1}$ ($|1,1\rangle|2\rangle$) and 11383 $cm^{-1}$ ($|3,1\rangle+|1\rangle$). The predicted combined intensity of this set of peaks is 3.6%, which agrees well with the observed 2.7%.

The peak observed at 11440 $cm^{-1}$ is assigned as the unresolved peaks predicted as: 11409 $cm^{-1}$ ($|3,1\rangle_{-}|0\rangle$), 11468 $cm^{-1}$ ($|2,1\rangle_{+}|1\rangle$), 11527 $cm^{-1}$ ($|2,1\rangle_{-}|1\rangle$) and 11556 $cm^{-1}$ ($|2,2\rangle_{-}|0\rangle$). The combined predicted intensity of these peaks is 2.1%, which is in good agreement with the observed value of 2.2%.

**$N(CH_3)_2(CD_3)$**

The spectrum of the third overtone of $N(CH_3)_2(CD_3)$ (See Figure 2-21) is very similar to that of $N(CH_3)_3$. At 10263 $cm^{-1}$, an asymmetric peak is observed. It is unlikely to be due to a single vibration; however, it would seem that one vibration is the primary source of intensity. Unfortunately again, it is not possible to curve fit this peak with any degree of certainty. A second peak at 10307 $cm^{-1}$ has been included in the curve fit as before, just to

fill the region. For the purpose of analysis, the intensity of this peak is added to that at 10263 $cm^{-1}$. Together, these peaks are assigned to the |0,0>|4> vibration, predicted to fall at 10279 $cm^{-1}$. Note that the observed relative intensity of the $|4,0>_{+}|0>$, 19.9%, is under-estimated by the HCAO/LM model. (See Table 2-4)

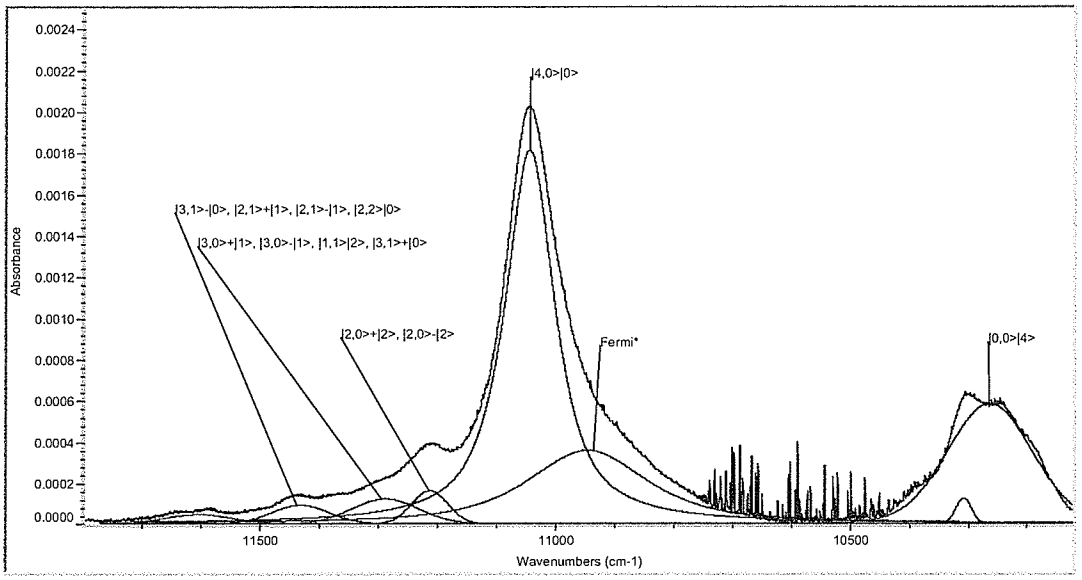


**Figure 2-21.** Spectrum of the third overtone of $N(CH_3)_2(CD_3)$. Collected with a 10 meter path length, 16384 co-added scans. *Fermi resonance between pure local mode and local-normal combination, see text for further description.

A peak at 11045 $cm^{-1}$ is assigned as the |4,0>|0> pure LM. A shoulder is observed at 10947 $cm^{-1}$. It would seem that this peak must be getting at least some of its intensity from the |4,0>|0> pure LM. The assignment of this shoulder is not obvious; there are local-local combination peaks that are predicted to fall at 10844 $cm^{-1}$ and at 10877 $cm^{-1}$, but they are predicted to have much lower intensity than observed. This shoulder could be due to a local-normal mode combination, Fermi resonant to the |4,0>|0>. The intensity of the shoul-

der is added to that of the observed for $|4,0\rangle|0\rangle$ for analytical purposes, as it is assumed that the pure local mode is the source of the majority of the intensity.

The peak at 11213 $cm^{-1}$ is assigned as the unresolved $|2.0\rangle_+|2\rangle$ and $|2,0\rangle_-|2\rangle$ vibrations, which are predicted to appear at 11166 $cm^{-1}$ and 11174 $cm^{-1}$, respectively. The observed intensity of this band is higher than that of the predicted vibrations by about 1.4%.

The band at 11289 $cm^{-1}$ is assigned as a series of unresolved local-local vibrations: $|3,0\rangle_+|1\rangle$, $|3,0\rangle_-|1\rangle$, $|1,1\rangle|2\rangle$ and $|3,1\rangle_+|0\rangle$ (for predicted position and intensities see Table 2-4). The sum of the predicted intensities of these bands is 3.6%, which compares well with the observed 3.2%.

The band observed at 11432 $cm^{-1}$ is assigned as the unresolved $|3,1\rangle_-|0\rangle$, $|2,1\rangle_-|1\rangle$, $|2,1\rangle_+|1\rangle$ and $|2,2\rangle_-|0\rangle$ vibrations (for predicted positions and intensities see Table 2-4). The sum of the predicted intensities of these vibrations is 2.1%, which compares well with the observed 2.1%.

**$N(CD_3)_2(CH_3)$**

The spectrum of the third overtone of $N(CH_3)(CD_3)_2$ is similar to that of the previous isotopomers, however, more structure can be observed. This is difficult to resolve via curve fitting procedures (See Figure 2-22). It is apparent that there are stronger Fermi resonances in this spectrum in comparison to the previous examples.

There is an asymmetric peak at 10246 $cm^{-1}$, clearly due to more than one vibration. However, it is not possible to resolve these peaks unambiguously using curve fitting procedures. Therefore, as before, this peak was fitted with three peaks and the intensities summed for comparison to predicted value, under the assumption that the majority of the

intensity is due to the |0,0>|4> vibration. (See Table 2-4) While some of the intensity may be due to the 4th overtone of a *gauche* CD vibration, that contribution will be negligible, as it is at least an order of magnitude less than the third overtone CH vibrations. The intensity of these peaks is 21%. This is 12% lower than the predicted value of 33%, but not out of line with previous observations.

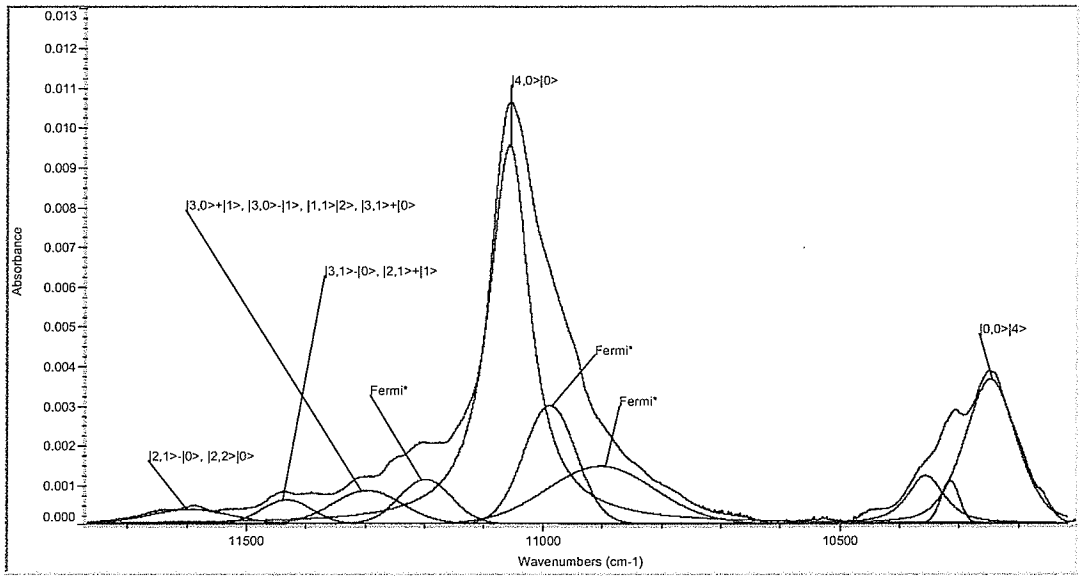


**Figure 2-22.** Spectrum of the third overtone of $N(CH_3)(CD_3)_2$. Collected with a 10 meter path length, 16384 co-added scans. *Fermi resonance between pure local mode and local-normal combination, see text for further description.

There are two shoulders observed on the peak at 11058 $cm^{-1}$ assigned to the |4,0>|0> vibration. The curve fit analysis places these shoulders at 10902 $cm^{-1}$ and at 10998 $cm^{-1}$. There are several possibilities for their assignment, including the $|1,0>_+|3>$ and $|1,0>_-$ |3> modes, and several local-normal combinations. The intensity observed in these shoulders is far greater than predicted, (see Table 2-4) thus, it could be assumed that there is Fermi resonance with the |4,0>|0> vibration, for which the observed intensity is lower than predicted. However, for this to be true, the predicted positions would have to be too low by about 100 to 150 $cm^{-1}$. Only one shoulder was observed in this region for the spectra of

$N(CH_3)_3$ and $N(CH_3)_2(CD_3)$. It is possible that there were actually two vibrations that made up the shoulder in the spectra of $N(CH_3)_3$ and $N(CH_3)_2(CD_3)$, however it is still difficult to explain the increased intensity using the local mode vibrations as an explanation for these shoulders. If these peaks are due to local-normal mode combinations, then differences between the spectra of deuterated compounds are easily explained, as the local-normal combinations would lead to different peak positions.

A peak observed at 11199 $cm^{-1}$ is assigned to the $|2,0\rangle_-|2\rangle$ and $|2,0\rangle_+|2\rangle$ vibrations, however, the observed intensity is 4.4% compared to the 1% predicted. This suggests there may be some Fermi resonance involved here also.

The peak observed at 11297 $cm^{-1}$ is assigned as the unresolved vibrations: $|3,0\rangle_+|1\rangle$, $|3,0\rangle_-|1\rangle$ $|1,1\rangle|2\rangle$ and $|3,1\rangle_+|0\rangle$. For predicted positions and intensities see Table 2-4. Although these peaks are semi-resolved, curve fitting cannot reliably give unique specific values.

The peak observed at 11432 $cm^{-1}$ is assigned as the unresolved $|3,1\rangle_-|0\rangle$ and $|2,1\rangle_+|1\rangle$ vibrations; for predicted intensities and positions see Table 2-4. The observed intensity is 2.3%, which compares well with the predicted 2.0%.

### 2.3.1.5 Fourth Overtone

With the exception of $N(CD_2H)(CD_3)$, all of the spectra for the fourth overtone region showed the expected two "peaks" carrying most of the intensity. Their asymmetry suggested that, as previously observed in the lower overtones, some Fermi effects are present. Unfortunately, in most cases, the component bands were not resolved enough to allow sufficiently unambiguous curve fitting to permit the assignments of individual com-

ponents. In the case of $N(CD_2H)(CD_3)$, there are a multitude of different bands observed. Since there are only two vibrations that were expected to have any significant intensity in this region, it is concluded that these peaks must be due to Fermi resonances. However, the concentration of dark states in this region makes it impossible to make assignments of these resonances with any degree of certainty.

**Table 2-5.** Experimental vs. Calculated pear positions and intensities for the fourth overtone of $N(CH_3)_3$, $N(CH_3)_2(CD_3)$, $N(CD_3)_2(CH_3)$, and $N(CD_3)_2(CD_2H)$.[a]

| Observed | | | Calculated | | | | |
|---|---|---|---|---|---|---|---|
| Frequency ($cm^{-1}$) | Relative Intensity (%) | Summed Intensity (%) | Frequency ($cm^{-1}$) | Intensity ($10^{-10}$) | Relative Intensity (%) | Summed Intensity (%) | Assignments |
| $N(CH_3)_3$ | | | | | | | |
| 12082 | 1.2 | | | | | | |
| 12142 | 0.2 | | | | | | |
| 12333 | 7.5 | | | | | | |
| 12459 | 5.0 | | | | | | |
| 12513 | 19.6 | 37.0 | 12504 | 4.87 | 36.3 | 36.3 | $\|0,0\rangle\|5\rangle$ |
| 12740 | 3.3 | | | | | | |
| 13292 | 3.5 | 3.5 | 13207 | .273 | 2.0 | 2.1 | $\|1,0\rangle_+\|4\rangle$ |
| | | | 13240 | .0152 | 0.1 | | $\|1,0\rangle_-\|4\rangle$ |
| 13425 | 11.9 | | | | | | |
| 13508 | 39.5 | 55.1 | 13481 | 3.24 | 24.1 | 57.8 | $\|5,0\rangle_+\|0\rangle$ |
| | | | 13841 | 4.52 | 33.7 | | $\|5,0\rangle_-\|0\rangle$ |
| 13734 | 3.6 | | | | | | |
| | | | 13671 | .0006 | <0.1 | | $\|2,0\rangle_+\|3\rangle$ |
| | | | 13679 | .00006 | <0.1 | | $\|2,0\rangle_-\|3\rangle$ |
| 13838 | 1.5 | 1.5 | 13801 | 0.167 | 1.2 | 2.2 | $\|4,0\rangle_+\|1\rangle$ |
| | | | 13801 | 0.111 | 0.8 | | $\|4,0\rangle_-\|1\rangle$ |
| | | | 13813 | 0.005 | <0.1 | | $\|1,1\rangle\|3\rangle$ |
| | | | 13891 | 0.010 | 0.1 | | $\|3,0\rangle_-\|2\rangle$ |
| | | | 13971 | 0.015 | 0.1 | | $\|4,1\rangle_+\|0\rangle$ |
| 13963 | 2.9 | 2.9 | 13975 | 0.19 | 1.4 | 1.6 | $\|4,1\rangle_-\|0\rangle$ |
| | | | 14088 | 0.0006 | <0.1 | | $\|2,1\rangle_+\|2\rangle$ |

| Observed | | | Calculated | | | | |
|---|---|---|---|---|---|---|---|
| Frequency ($cm^{-1}$) | Relative Intensity (%) | Summed Intensity (%) | Frequency ($cm^{-1}$) | Intensity ($10^{-10}$) | Relative Intensity (%) | Summed Intensity (%) | Assignments |
| | | | 14150 | 0.0012 | <0.1 | | $\|2,1\rangle_-\|2\rangle$ |
| | | | 14168 | 0.0038 | <0.1 | | $\|3,1\rangle_+\|1\rangle$ |
| | | | 14202 | 0.0028 | <0.1 | | $\|3,1\rangle_-\|1\rangle$ |
| | | | 14335 | 0.0002 | <0.1 | | $\|2,2\rangle\|1\rangle$ |
| $N(CH_3)_2(CD_3)$ | | | | | | | |
| 12047 | 1.4 | | | | | | |
| 12147 | 0.6 | | | | | | |
| 12356 | 3.9 | | | | | | |
| 12471 | 21.1 | 27.6 | 12504 | 4.87 | 36.3 | 36.3 | $\|0,0\rangle\|5\rangle$ |
| 12552 | 0.6 | | | | | | |
| 13247 | 6.9 | 6.9 | 13207 | .273 | 2.0 | 2.1 | $\|1,0\rangle_+\|4\rangle$ |
| | | | 13240 | .0152 | 0.1 | | $\|1,0\rangle_-\|4\rangle$ |
| 13480 | 49.3 | 64.7 | 13481 | 3.24 | 24.1 | 60.0 | $\|5,0\rangle_+\|0\rangle$ |
| | | | 13841 | 4.52 | 33.7 | | $\|5,0\rangle_-\|0\rangle$ |
| | | | 13671 | .0006 | <0.1 | | $\|2,0\rangle_+\|3\rangle$ |
| | | | 13679 | .00006 | <0.1 | | $\|2,0\rangle_-\|3\rangle$ |
| 13767 | 15.5 | | 13801 | 0.167 | 1.2 | 2.2 | $\|4,0\rangle_+\|1\rangle$ |
| | | | 13801 | 0.111 | 0.8 | | $\|4,0\rangle_-\|1\rangle$ |
| | | | 13813 | 0.005 | <0.1 | | $\|1,1\rangle\|3\rangle$ |
| | | | 13891 | 0.010 | 0.1 | | $\|3,0\rangle_-\|2\rangle$ |
| | | | 13971 | 0.015 | 0.1 | | $\|4,1\rangle_+\|0\rangle$ |
| | | | 13975 | 0.19 | 1.4 | 1.6 | $\|4,1\rangle_-\|0\rangle$ |
| 14010 | 0.8 | 0.8 | 14088 | 0.0006 | <0.1 | | $\|2,1\rangle_+\|2\rangle$ |
| | | | 14150 | 0.0012 | <0.1 | | $\|2,1\rangle_-\|2\rangle$ |
| | | | 14168 | 0.0038 | <0.1 | | $\|3,1\rangle_+\|1\rangle$ |
| | | | 14202 | 0.0028 | <0.1 | | $\|3,1\rangle_-\|1\rangle$ |
| | | | 14335 | 0.0002 | <0.1 | | $\|2,2\rangle\|1\rangle$ |
| $N(CD_3)_2(CH_3)$ | | | | | | | |
| 12050 | 0.9 | | | | | | |
| 12145 | 0.3 | | | | | | |
| 12484 | 5.3 | | | | | | |

| Observed | | | Calculated | | | | |
|---|---|---|---|---|---|---|---|
| Frequency ($cm^{-1}$) | Relative Intensity (%) | Summed Intensity (%) | Frequency ($cm^{-1}$) | Intensity ($10^{-10}$) | Relative Intensity (%) | Summed Intensity (%) | Assignments |
| 12469 | 20.9 | 28.1 | 12504 | 4.87 | 36.3 | 36.3 | $\|0,0\rangle\|5\rangle$ |
| 12551 | 0.6 | | | | | | |
| | | | 13207 | .273 | 2.0 | 2.1 | $\|1,0\rangle_+\|4\rangle$ |
| 13261 | 8.9 | | | | | | |
| 13479 | 45.2 | 71.9 | 13240 | .0152 | 0.1 | | $\|1,0\rangle_-\|4\rangle$ |
| | | | 13481 | 3.24 | 24.1 | 60.0 | $\|5,0\rangle_+\|0\rangle$ |
| | | | 13841 | 4.52 | 33.7 | | $\|5,0\rangle_-\|0\rangle$ |
| 13756 | 17.8 | | | | | | |
| | | | 13671 | .0006 | <0.1 | | $\|2,0\rangle_+\|3\rangle$ |
| | | | 13679 | .00006 | <0.1 | | $\|2,0\rangle_-\|3\rangle$ |
| | | | 13801 | 0.167 | 1.2 | 2.2 | $\|4,0\rangle_+\|1\rangle$ |
| | | | 13801 | 0.111 | 0.8 | | $\|4,0\rangle_-\|1\rangle$ |
| | | | 13813 | 0.005 | <0.1 | | $\|1,1\rangle\|3\rangle$ |
| | | | 13891 | 0.010 | 0.1 | | $\|3,0\rangle_-\|2\rangle$ |
| | | | 13971 | 0.015 | 0.1 | | $\|4,1\rangle_+\|0\rangle$ |
| 14015 | 0.3 | 0.3 | 13975 | 0.19 | 1.4 | 1.6 | $\|4,1\rangle_-\|0\rangle$ |
| | | | 14088 | 0.0006 | <0.1 | | $\|2,1\rangle_+\|2\rangle$ |
| | | | 14150 | 0.0012 | <0.1 | | $\|2,1\rangle_-\|2\rangle$ |
| | | | 14168 | 0.0038 | <0.1 | | $\|3,1\rangle_+\|1\rangle$ |
| | | | 14202 | 0.0028 | <0.1 | | $\|3,1\rangle_-\|1\rangle$ |
| | | | 14335 | 0.0002 | <0.1 | | $\|2,2\rangle\|1\rangle$ |
| $N(CD_3)_2(CD_2H)$ | | | | | | | |
| 12080 | 2.2 | | | | | | |
| 12062 | 4.3 | | | | | | |
| 12245 | 2.6 | | | | | | |
| 12306 | 1.9 | | | | | | |
| 12380 | 4.6 | | | | | | |
| 12477 | 5.5 | | | | | | |
| 12548 | 5.4 | 33.4 | 12505 | 1.59 | 37.8 | 37.8 | $\|0,0\rangle\|5\rangle$ |
| 12764 | 1.2 | | | | | | |
| 12648 | 4.2 | | | | | | |
| 12874 | 1.5 | | | | | | |

| Observed | | | Calculated | | | | |
|---|---|---|---|---|---|---|---|
| Frequency ($cm^{-1}$) | Relative Intensity (%) | Summed Intensity (%) | Frequency ($cm^{-1}$) | Intensity ($10^{-10}$) | Relative Intensity (%) | Summed Intensity (%) | Assignments |
| 13137 | 9.8 | | | | | | |
| 13263 | 1.8 | | | | | | |
| 13385 | 9.8 | | | | | | |
| 13478 | 19.5 | 66.6 | 13485 | 1.30 | 31.1 | 62.2 | $\|5,0\rangle_+\|0\rangle$ |
| | | | 13485 | 1.30 | 31.1 | | $\|5,0\rangle_-\|0\rangle$ |
| 13564 | 7.8 | | | | | | |
| 13651 | 6.5 | | | | | | |
| 13778 | 6.4 | | | | | | |
| 13898 | 2.1 | | | | | | |
| 14037 | 2.9 | | | | | | |

[a]Thin lines separate groups of bands that will be associated for comparison between theoretical and experimental intensities.

**$N(CD_2H)(CD_3)_2$**

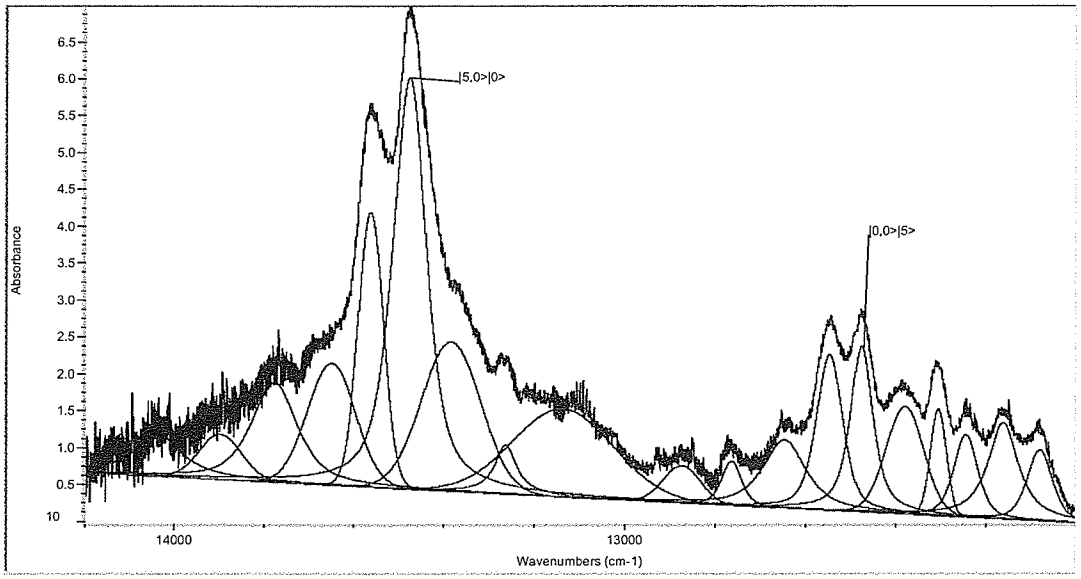


**Figure 2-23.** Spectrum of the fourth overtone of $N(CD_2H)(CD_3)_2$. Collected with a 10 meter path length, 16384 co-added scans. *Fermi resonance between pure local mode and local-normal combination, see text for further description.

The fourth overtone of $N(CD_3)(CD_2H)$ is rather complex, considering that there are only 2 predicted vibrations (see Figure 2-23). Since there are no possible vibrations that would have significant intensity in this region, it is concluded that all of the observed bands in this region are getting their intensity through Fermi resonant interactions with the 2 predicted local mode vibrations. In this region there is high density of possible combinations and the sixth overtone of the CD vibrations as well. Therefore it is not possible to assign the Fermi resonances with any degree of certainty. Considering that the intensity of the aforementioned CD vibrations would be significantly less than the CH overtones predicted for this region and that a spectrum of $N(CD_3)_3$ for this region did show any significant intensity, all of the observed peaks have been assigned to get their intensity from one or other of the local mode CH vibrations. The sum of the observed intensities compares well with the predicted (See Table 2-5).

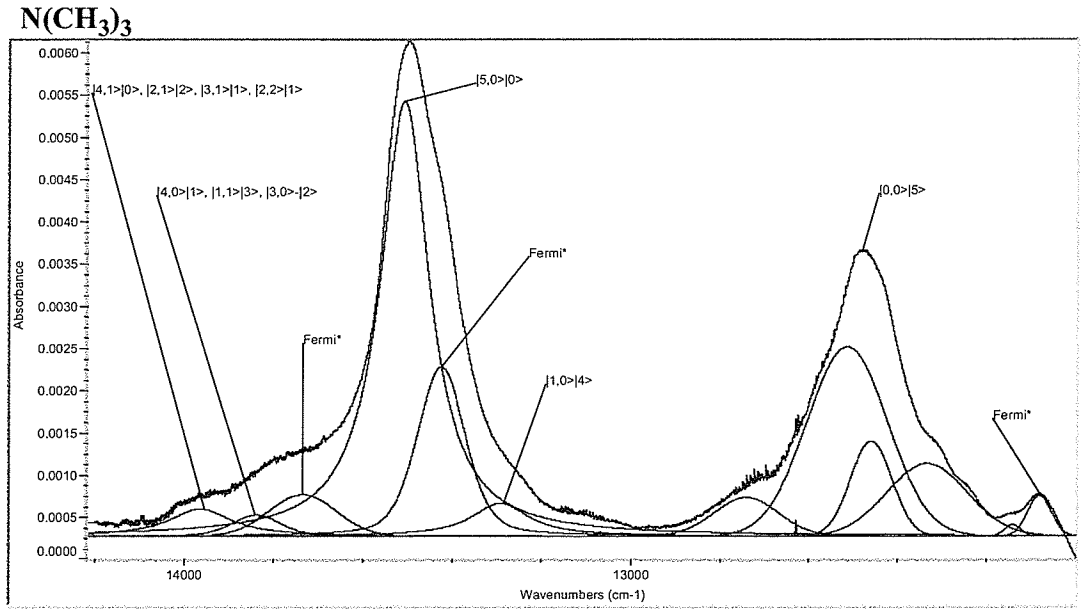


**Figure 2-24.** Spectrum of the fourth overtone of $N(CH_3)_3$. Collected with a 10 meter path length, 16384 co-added scans. *Fermi resonance between pure local mode and local-normal combination, see text for further description.

The fourth overtone of $N(CH_3)_3$ is divided into two regions of intensity (see Figure 2-24), which can be assigned as being due to the *trans* and the *gauche* vibrations, respectively. A peak appears at 12082 $cm^{-1}$ that is somewhat removed from the rest. However, the intensity of this band is higher than would be expected if it was not gaining intensity from some form of resonance interaction with the overtone vibrations. This could be assigned as the combination of the |4,0>|0> (11031 $cm^{-1}$) vibration with the fundamental vibration that appears at 1103 $cm^{-1}$ (Me rock") in a Fermi resonant interaction with the |0,0>|5> vibration. Above this there is an asymmetric peak at ~ 12500 $cm^{-1}$. Unfortunately unambiguous curve fitting was not possible for this peak as the component bands are not well enough resolved. Therefore the component bands could not be assigned. Curve fitting was done to allow intensity estimates to be made but these should not be considered as true band positions or shapes. (See Table 2-5). It is clear, though, that the |0,0>|5> vibration is

being affected by Fermi resonances in this area, as no other bands that would appear in this region would have any significant intensity. A host of expected dark states lie in this region.

A shoulder, observed at 13292 $cm^{-1}$, can be resolved with some degree of certainty. The observed intensity is 3.5%. This is assigned as the unresolved |1,0>+|4> and |1,0>-|4> vibrations, predicted to have 2.1% intensity. The predicted positions of these peaks is somewhat lower than observed, as is the summed intensity. However, they are within the error associated with the curve fitting analysis. (See Table 2-5).

Another shoulder observed at 13425 $cm^{-1}$, is likely due to Fermi resonance of a combination band with the |5,0>|0> mode. The |5,0>|0> band is observed at 13508 $cm^{-1}$, compared to the predicted value of 13481 $cm^{-1}$. This has likely been shifted up field by the Fermi resonance. The shoulder at 13734 $cm^{-1}$ is also likely due to a Fermi resonance with a dark state. Table 15 shows the Fermi resonance assignments and fit. Since the intensity of these 3 peaks would all be due to the |5,0>|0> vibration, the intensity was summed and found to be 55.1%, which compares well to the predicted 57.8%.

The next observed peak is at 13838 $cm^{-1}$. This is likely the unresolved $|4,0>_{+}|1>$, $|4,0>_{-}|1>$, |1,1>|1> and $|3,0>_{-}|2>$ vibrations (see Table 2-5 for predicted positions). The observed intensity was 1.5%, which matches well with the predicted 2.2%.

Finally, the peak at 13963 $cm^{-1}$ is likely the unresolved $|4,1>_{+}|0>$, $|4,1>_{-}|0>$, $|2,1>_{+}|2>$, $|2,1>_{-}|2>$, $|3,1>_{+}|1>$, $|3,1>_{-}|1>$ and |2,2>|1> vibrations (see Table 2-5 for predicted positions). The observed intensity was 2.9% which compares well to the predicted intensity of 1.6%.

**$N(CH_3)_2(CD_3)$**

The fourth overtone of $N(CH_3)_2(CD_3)$ has a very similar spectrum to $N(CH_3)_3$, except that, in of the former, the S/N ratio was somewhat poorer. Only a small amount of the $N(CH_3)_2(CD_3)$ was available and the spectrum had to be acquired at lower pressure (see Figure 2-25). Therefore, in some cases, it was not possible specify peak positions as well as for $N(CH_3)_3$. A peak observed at 12047 $cm^{-1}$ is assigned as Fermi resonance of the combination band of |4,0>|0> and the fundamental band at 1100 $cm^{-1}$ (Me rock").

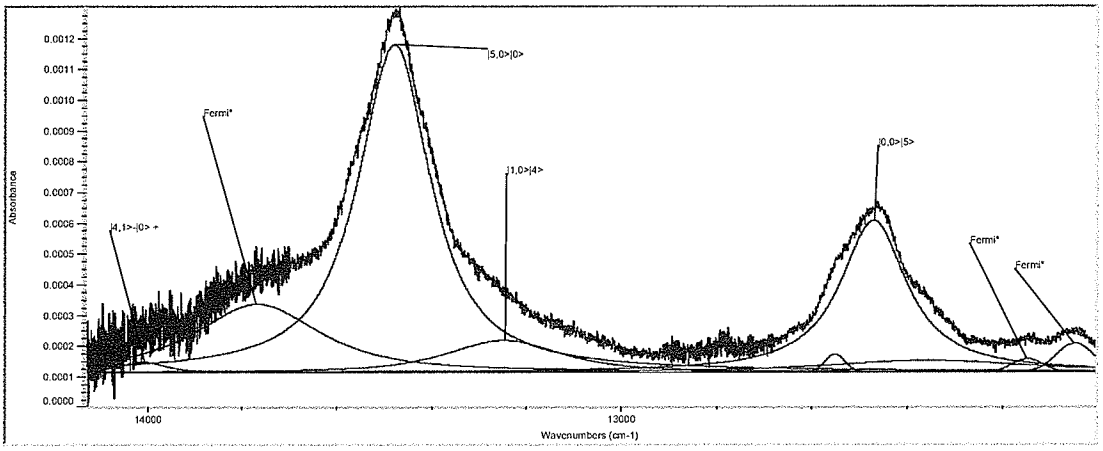


**Figure 2-25.** Spectrum of the fourth overtone of $N(CH_3)_2(CD_3)$. Collected with a 10 meter path length, 16384 co-added scans. *Fermi resonance between pure local mode and local-normal combination, see text for further description.

The peak centered at 12471 $cm^{-1}$ is assigned as the |0,0>|5> vibration, however this is an asymmetric band that cannot be resolved unambiguously. A shoulder is observed at ~13247 $cm^{-1}$, however its exact position and intensity are unclear. Its intensity has been estimated at 6.9% and it likely incorporates the predicted $|1,0>_+|4>$ and $|1,0>_-|4>$ vibrations. However, these are only predicted to have 2.1% intensity, therefore it is likely that some of the intensity is being taken from the |5,0>|0> vibration either through Fermi interactions or difficulties in resolving the bands. The shoulder at 13767 $cm^{-1}$ has an intensity of 15.5%. It is likely due to Fermi resonances, but due to the poor resolution no assignments

can be made, though some predicted local mode vibrations fall in this region. See Table 2-5 for details.

The last band, appearing at 14010 $cm^{-1}$, has 0.8% intensity and is likely the remaining unresolved predicted local mode vibrations that, when summed together, are predicted to have an intensity of 1.6%. See Table 2-5 for details.

**$N(CD_3)_2(CH_3)$**

The fourth overtone $N(CD_3)_2CH_3$ is very similar to $N(CH_3)_2(CD_3)$ (see Figure 2-26) The assignments are basically the same save for some small differences in position and intensity. (See Table 2-5 for the positions and intensities) A peak observed at 12050 $cm^{-1}$ is assigned as Fermi resonance of the combination band of |4,0>|0> and the fundamental band at 1143 $cm^{-1}$ (Me rock').

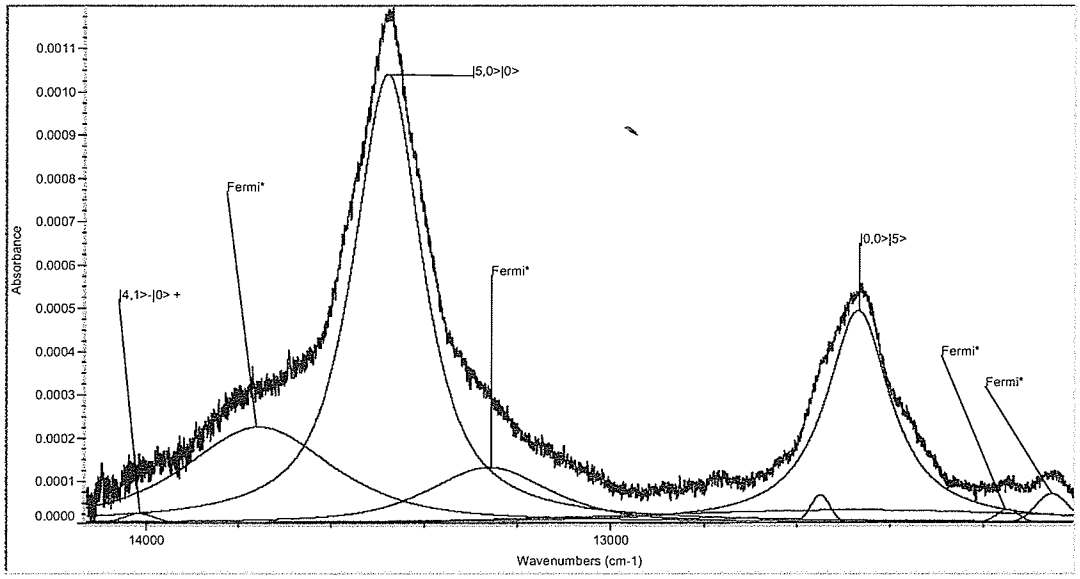


**Figure 2-26.** Spectrum of the fourth overtone of $N(CH_3)(CD_3)_2$. Collected with a 10 meter path length, 16384 co-added scans. *Fermi resonance between pure local mode and local-normal combination, see text for further description.

### 2.3.1.6 Rotational alternative for Fermi resonance assignments

It cannot be ignored that the three peaks in $N(CH_3)_3$, $N(CH_3)_2(CD_3)$ and $N(CH_3)(CD_3)_2$, that have been repeatedly assigned to Fermi resonances with the |0,0>|X> vibration, and the three similarly assigned to Fermi resonances with the |X,0>|0> vibration, may be rotational structure, particularly where X=3. For |0,0>|X>, the oscillation of the electric dipole is nearly parallel with the symmetry axis and the band shape observed does resemble that of a typical parallel vibration. Though the |X,0>|0> is not as parallel with the symmetry axis, the observed bands would still be consistent with what would be expected for rotational structure; see for example, the analysis of Edgell and Moynihan [83]. In their paper, they show that the Coriolis effect has a pronounced influence on the band shape and, for positive values of the Coriolis constant, the P and R branches contract towards the band center. However, this explanation fails to explain the appearance of the trio of well-resolved peaks in both the |3,0>|0> and the |0,0>|3> regions of the $N(CHD_2)(CD_3)_2$ spectrum; the contour formed by these sets of peaks cannot be explained in terms of rotational structure.

Futhermore, Manzanares *et al.* found that the FWHM of the *gauche* CH transitions were always three times larger than the width estimated for their rotational envelopes ($4^{th}$ –$6^{th}$ overtones) [70]. Thus, rotational arguments can only partially explain the band contour observed; whereas, the Fermi resonance assignments given above explain the observed contours in a consistent manner. It is therefore likely that Fermi resonance plays an important role in the appearance of these contours.

#### 2.3.1.7 Fourth and Fifth overtones by ICL-PAS

Much of the early data on this project was obtained with ICL-PAS system. It is perhaps somewhat ironic that very little of that early work appears in the final analysis. In fact, the data acquired through ICL-PAS will only be discussed in this section, and the discussion itself will for the most part focus on why these data were put aside in favor of other data.

The major reason that much of the data collected using the ICL-PAS system was put aside was the access to a modern FT-IR with which it was possible to collect data up to the fourth overtone. Prior to access to the Nicolet 870 FT-IR, the fifth overtone of all the compounds was collected using the ICL-PAS system. The first differences that should be noted about the two techniques are the level of difficulty and the time requirement. The ICL-PAS system had to be aligned and calibrated often, to ensure that the results obtained would be accurate. Any change in room temperature, humidity etc. would require this process, which takes 1-4 days to complete. The FT-IR has automatic self alignment which takes only 1-10 minutes. Depending on the resolution and wavelength range required, collecting a single spectrum using the ICL-PAS system could take as much as 6 hours. A single scan using the FT-IR takes less than a minute, but since many scans must be co-added to get an acceptable S/N ratio, data collection could take up to 8 hours. The ICL-PAS system required that constant power readings be taken so that corrections could be made to the spectrum. The FT-IR does not have this requirement, hence it is far more efficient. In fact, the work of 6 months using the ICL-PAS was repeated using the FT-IR in less than a month. Beyond the time constraints, the dependence on readings of the power taken by

hand, in order to correct the intensity for power fluctuations over the energy range scanned, added error.

Despite these drawbacks the ICL-PAS system was capable of producing very good results, see for example the fourth overtone of Dimethyl sulfide shown in Figure 2-27

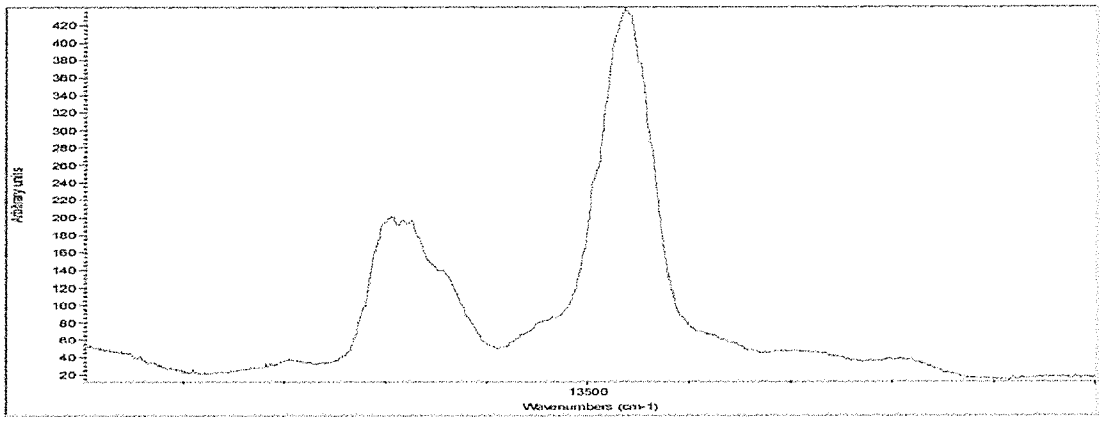


**Figure 2-27.** Fourth Overtone of dimethyl sulfide collected using the ICL-PAS system, at 113 torr, with a chop rate of 281 Hz.

This spectrum is almost the same as that collected by the FT-IR system (see Figure 2-33). In fact it does not have the anomaly previously described (Section 2.2.2 on page 41). However, looking at the fourth overtone of trimethyl amine (see Figure 2-28), a different problem is evident.

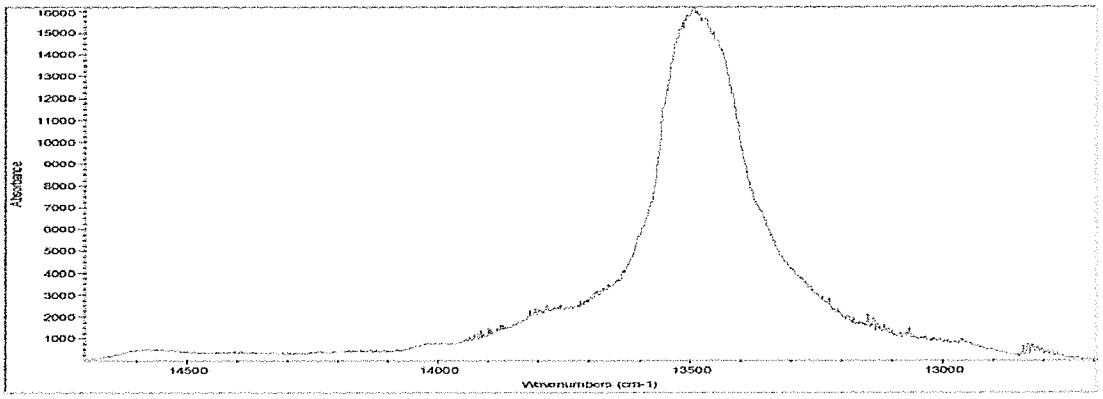


**Figure 2-28.** Fourth Overtone of trimethyl amine collected using the ICL-PAS system, at 434 torr with a 296 Hz chop rate.

Though the region observed in this spectrum is the same region observed in the FT-IR spectra of the fifth overtone, the low energy region where the *trans* band is found could not be collected as it fell outside of the dye range. Obviously, this data cannot be used for a study of relative intensities. Even if another dye was available to collect the *trans* band, the differences in the laser power produced by changing dyes would make it extremely difficult to get reliable intensity data, whereas the relative intensity for the FT-IR spectra are very reliable.

With the more sensitive ICL-PAS system, higher overtones can be observed than with the FT-IR system. For example, the fifth overtone of trimethyl amine is shown in Figure 2-29.

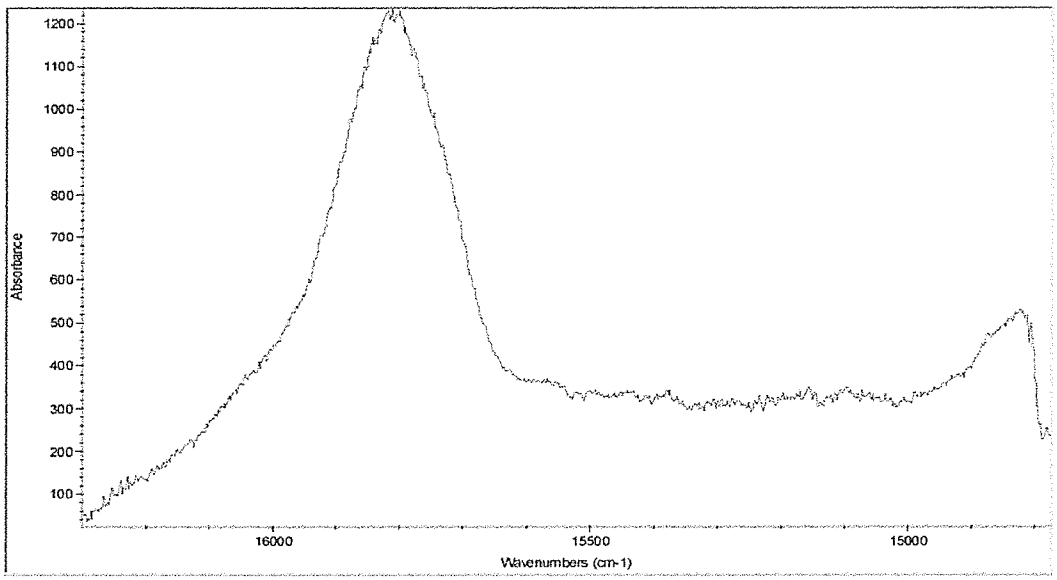


**Figure 2-29.** Fifth Overtone of trimethyl amine collected using the ICL-PAS system, at 300 torr with a 350 Hz chop rate.

In this case only the *gauche* band is observable in the dye range. Therefore, again this spectrum of little use for the study of relative intensities (however, it was used in the calculation of the local mode parameters). It is important to note that most molecules do not have bands

as widely as separated as the molecules studied here, therefore ICL-PAS techniques are often very useful. ICL-PAS type experiments offer additional opportunities, as described in Chapter 4.

## 2.3.2 Spectral Assignments for Dimethyl Sulfide

A new complication appears for dimethyl sulfide, due to the smaller difference in anharmonic behavior between *gauche* and *trans* CH bonds. The overtones are much closer together, resulting in significant overlap and making it difficult to get reliable curve fits and thus intensities.

**Table 2-6.** Experimental vs. Calculated peak positions and intensities for Dimethyl sulfide.

| Observed | | | Calculated | | | | |
|---|---|---|---|---|---|---|---|
| Frequency ($cm^{-1}$) | Relative Intensity (%) | Summed Intensity (%) | Frequency ($cm^{-1}$) | Intensity ($10^{-9}$) | Relative Intensity (%) | Summed Intensity (%) | Assignments |
| First Overtone | | | | | | | |
| | | | 5739 | 94.2 | 12.8 | | $\|2,0\rangle_+\|0\rangle$ |
| 5757 | s | n/a | 5749 | 210 | 28.5 | | $\|2,0\rangle_-\|0\rangle$ |
| 5784 | s | n/a | 5799 | 108 | 14.7 | | $\|0,0\rangle\|2\rangle$ |
| 5799 | s | n/a | | | | | 2935+2860 |
| 5805 | s | n/a | | | | | 2969+2841 |
| 5903 | s | n/a | 5874 | 199 | 27.0 | | $\|1,1\rangle\|0\rangle$ |
| 5905 | s | n/a | 5909 | 74.9 | 10.2 | | $\|1,0\rangle_+\|1\rangle$ |
| 5918 | s | n/a | 5916 | 50 | 6.8 | | $\|1,0\rangle_-\|1\rangle$ |
| 5955 | s | n/a | | | | | |
| 5959 | s | n/a | | | | | |
| 5972 | w | n/a | | | | | |
| Second Overtone | | | | | | | |
| 8358 | 6.7 | | | | | | |
| 8405 | 3.9 | | | | | | |
| 8457 | 48.2 | 58.9 | 8436 | 21.1 | 32.0 | 62.1 | $\|3,0\rangle_+\|0\rangle$ |
| | | | 8437 | 19.8 | 30.0 | | $\|3,0\rangle_-\|0\rangle$ |
| 8545 | 16.1 | 23.7 | 8541 | 15.4 | 23.4 | 23.4 | $\|0,0\rangle\|3\rangle$ |
| 8572 | 0.5 | | | | | | |
| 8591 | 7.1 | | | | | | |
| 8657 | 3.1 | 6.5 | 8649 | 3.05 | 4.6 | 6.2 | $\|2,1\rangle_+\|0\rangle$ |
| 8679 | 3.4 | | 8693 | 1.06 | 1.6 | | $\|2,0\rangle_+\|1\rangle$ |

| Observed | | | Calculated | | | | |
|---|---|---|---|---|---|---|---|
| Frequency ($cm^{-1}$) | Relative Intensity (%) | Summed Intensity (%) | Frequency ($cm^{-1}$) | Intensity ($10^{-9}$) | Relative Intensity (%) | Summed Intensity (%) | Assignments |
| 8714 | 3.8 | 3.8 | 8694 | 2.26 | 3.4 | 3.4 | $\|2,0\rangle_-\|1\rangle$ |
| 8746 | 5.8 | 5.8 | 8727 | 0.771 | 1.2 | 4.6 | $\|2,1\rangle_-\|0\rangle$ |
| | | | 8762 | 2.29 | 3.5 | | $\|1,0\rangle_+\|2\rangle$ |
| 8802 | 1.2 | 1.2 | 8780 | 0.172 | 0.3 | 0.3 | $\|1,0\rangle_-\|2\rangle$ |
| Third Overtone | | | | | | | |
| 10726 | 1.9 | | | | | | |
| 10877 | 0.6 | | | | | | |
| 10999 | 50.6 | 53.2 | 11003 | 1.84 | 36.9 | 68.2 | $\|4,0\rangle_+\|0\rangle$ |
| | | | 11003 | 1.56 | 31.3 | | $\|4,0\rangle_-\|0\rangle$ |
| 11135 | 36.6 | 40.1 | 11173 | 1.16 | 23.3 | 23.3 | $\|0,0\rangle\|4\rangle$ |
| 11160 | 1.2 | | | | | | |
| 11199 | 2.3 | | | | | | |
| | | | 11351 | 0.0746 | 1.5 | | $\|3,1\rangle_+\|0\rangle$ |
| | | | 11369 | 0.187 | 3.8 | | $\|3,1\rangle_-\|0\rangle$ |
| 11394 | 5.2 | 5.2 | 11397 | 0.0218 | 0.4 | 5.7 | $\|3,0\rangle_+\|1\rangle$ |
| | | | 11403 | 0.0004 | <.1 | | $\|3,0\rangle_-\|1\rangle$ |
| | | | 11458 | 0.133 | 2.7 | | $\|1,0\rangle_+\|3\rangle$ |
| 11507 | 1.5 | 1.5 | 11486 | 0.0003 | <.1 | 2.8 | $\|1,0\rangle_-\|3\rangle$ |
| | | | 11518 | 0.0042 | 0.1 | | $\|2,2\rangle\|0\rangle$ |
| | | | 11586 | 0.0003 | <.1 | | $\|2,0\rangle_-\|2\rangle$ |
| | | | 11623 | 0.0003 | <.1 | | $\|2,1\rangle_+\|1\rangle$ |
| | | | 11688 | 0.0018 | <.1 | | $\|2,1\rangle_-\|1\rangle$ |
| Fourth Overtone | | | | | | | |
| 13184 | 5.2 | | | | | | |
| 13292 | 3.2 | | | | | | |
| 13449 | 52.5 | 62.0 | 13445 | 0.139 | 32.7 | 72.3 | $\|5,0\rangle_-\|0\rangle$ |
| | | | 13445 | 0.168 | 39.6 | | $\|5,0\rangle_+\|0\rangle$ |
| 13538 | 1.2 | | | | | | |
| 13647 | 23.9 | 33.0 | 13694 | 0.0872 | 20.5 | 20.5 | $\|0,0\rangle\|5\rangle$ |
| 13684 | 6.2 | | | | | | |
| 13786 | 2.9 | | | | | | |
| | | | 13928 | 0.0044 | 1.0 | | $\|4,1\rangle_+\|0\rangle$ |

| Observed | | | Calculated | | | | |
|---|---|---|---|---|---|---|---|
| Frequency ($cm^{-1}$) | Relative Intensity (%) | Summed Intensity (%) | Frequency ($cm^{-1}$) | Intensity ($10^{-9}$) | Relative Intensity (%) | Summed Intensity (%) | Assignments |
| 13941 | 5.0 | 5.0 | 13931 | 0.0145 | 3.4 | 7.2 | $\|4,1\rangle_-\|0\rangle$ |
| | | | 13969 | 0.00002 | <.1 | | $\|4,0\rangle_+\|1\rangle$ |
| | | | 13696 | 0.0033 | 0.8 | | $\|4,0\rangle_-\|1\rangle$ |
| | | | 14090 | 0.0068 | 1.6 | | $\|4,0\rangle_+\|1\rangle$ |
| | | | 14120 | 0.0007 | 0.2 | | $\|4,0\rangle_-\|1\rangle$ |
| | | | 14150 | 0.0002 | <.1 | | $\|3,2\rangle_+\|0\rangle$ |
| | | | 14222 | 0.0002 | .1 | | $\|3,0\rangle_+\|2\rangle$ |
| | | | 14226 | 0.00007 | <.1 | | $\|3,0\rangle_-\|2\rangle$ |
| | | | 14242 | 0.00002 | <.1 | | $\|3,2\rangle_-\|0\rangle$ |
| | | | 14319 | 0.00005 | <.1 | | $\|3,1\rangle_+\|1\rangle$ |
| | | | 14333 | 0.0001 | <.1 | | $\|2,0\rangle_+\|3\rangle$ |
| | | | 14335 | 0.00005 | <.1 | | $\|2,0\rangle_-\|3\rangle$ |
| | | | 14350 | 0.00005 | <.1 | | $\|3,1\rangle_-\|1\rangle$ |
| | | | 14411 | 0.00006 | <.1 | | $\|1,1\rangle\|3\rangle$ |
| | | | 14475 | 0.000006 | <.1 | | $\|2,2\rangle\|1\rangle$ |
| | | | 14534 | 0.00001 | <.1 | | $\|2,1\rangle_+\|2\rangle$ |
| | | | 14542 | 0.000004 | <.1 | | $\|2,1\rangle_-\|2\rangle$ |

### 2.3.2.1 First Overtone

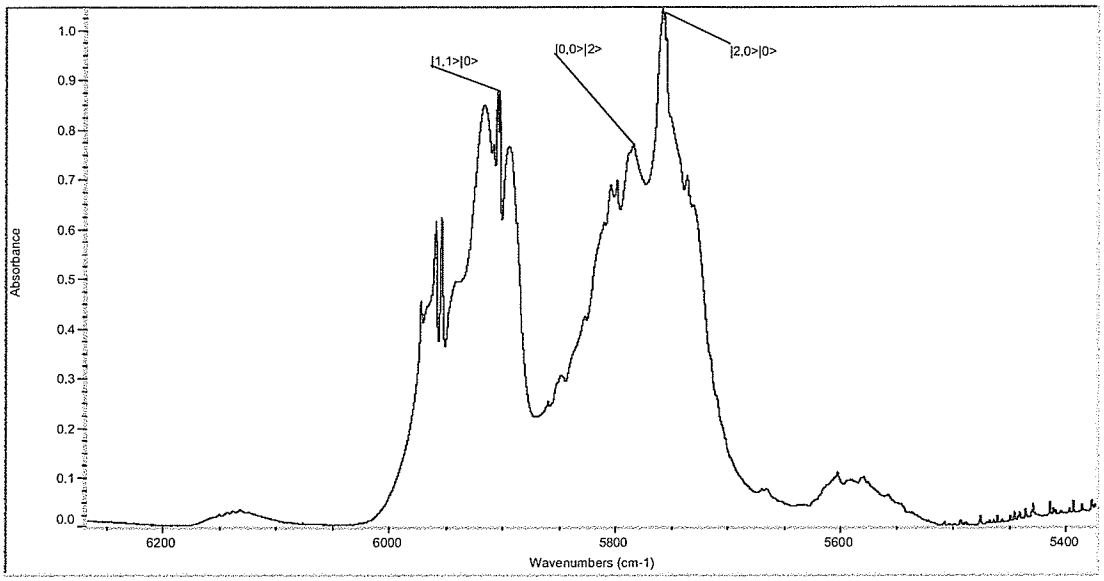


**Figure 2-30.** Spectrum of the first overtone of dimethyl sulfide, collected with a 10 meter path length, 4048 co-added scans.

The first overtone of dimethyl sulfide contains a number of characteristics that make it difficult to get much quantitative information (see Figure 2-30). The predicted difference between the |2,0>|0> and |0,0>|2> vibrations is only 50 $cm^{-1}$; these are not well resolved within the spectrum. Nominally they are observed at 5757 $cm^{-1}$ and 5784 $cm^{-1}$, respectively. However, the overlap is so significant that these positions are questionable and curve-fitting is not feasible due to the broad rotational envelopes. A peak with B character observed at 5903 $cm^{-1}$ is likely due to the |1,1>|0> vibration (predicted to be at 5874 $cm^{-1}$) and likely encompasses the |1,0>-|1> and $|1,0>_{+}|1>$ bands. The very sharp peak with C character, observed at 5959 $cm^{-1}$, is possibly due to a combination of the |2,0>|0> vibration with the out-of-phase torsion of the methyl group observed at 227 $cm^{-1}$ in the fundamental (see Table 2-6 for details).

### 2.3.2.2 Second Overtone

The second overtone still shows a large amount of overlap in the spectrum (see Figure 2-31). The largest peak that is observed is at 8457 $cm^{-1}$; this peak is asymmetric. This peak is assigned to the |3,0>|0> vibration. Two shoulders are observed at 8358 $cm^{-1}$ and 8405 $cm^{-1}$; these are assigned as combinations of first overtone CH stretch vibrations and two fundamental vibrations. A number of possible combinations could cause these shoulders, for example, both shoulders could be explained as the combinations of 2x 1303 $cm^{-1}$ (Me sym def, HCS asym bend, $CH_2$ rock)[84] with the |2,0>|0> or |0,0>|2> LM, respectively.

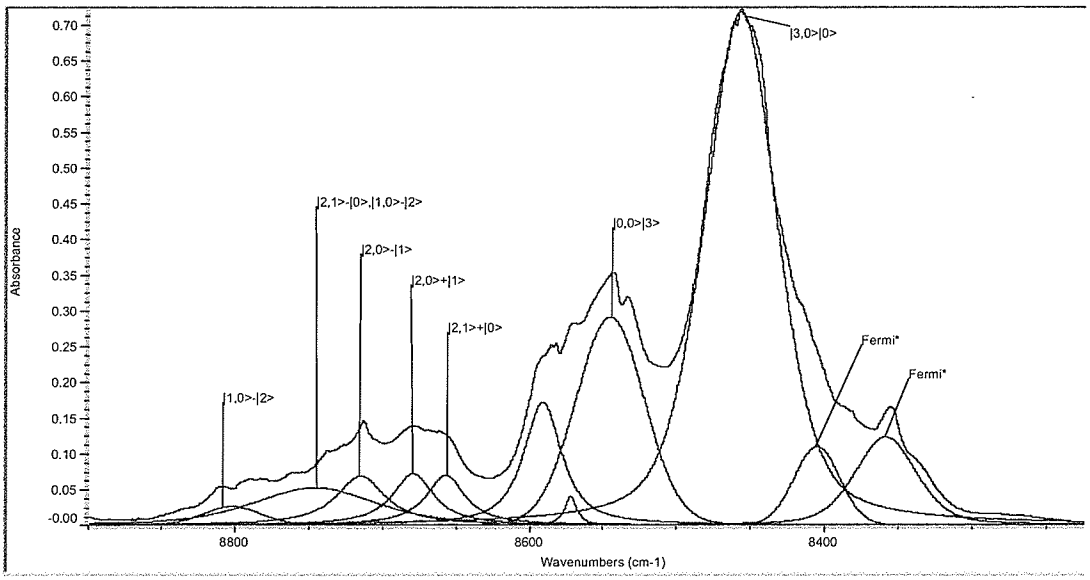


**Figure 2-31.** Spectrum of the second overtone of dimethyl sulfide, collected with a 10 meter path length, 4048 co-added scans.* See text for detailed intensities.

The assignments of some other combinations are also possible. Their intensity is likely due to weak Fermi resonance with the local mode vibration and therefore is added to that of the local mode vibration for purposes of comparison to predicted values. The observed intensity is 59%, which compares well with the predicted 62%.

The peak observed at 8545 $cm^{-1}$ is assigned to the |0,0>|3> vibration; it is asymmetric and, in order to account for all of the intensity, it has been fitted to 3 curves. However, there is a large amount of ambiguity in this fit, therefore the intensity and position of the individual bands are not useful. The intensity in this area would come from the |0,0>|3> vibration, and any other vibration that appears in this region would have to gain intensity from it. Therefore all of the intensity of these peaks is summed for comparison with the predicted value. The observed intensity is 23.7%, which compares well with the 23.4% predicted.

There are several combination bands that may fall in this region that may indeed be Fermi resonant, however the region is too poorly resolved for any assignments to be made. Two observed peaks at 8657 $cm^{-1}$ and 8679 $cm^{-1}$ are assigned to the $|2,1>_{+}|0>$ and $|2,0>_{+}|1>$ modes, respectively. It is likely that the total intensity of the two bands (6.6%) is approximately correct, especially when compared with their total predicted intensity (6.2%). The next observed peak, at 8714 $cm^{-1}$, is assigned as the |2,0>|1> vibration. The observed and predicted intensities are in good agreement (see Table 2-6 for details). The peak at 8746 $cm^{-1}$ is assigned as the unresolved $|2,1>_{-}|0>$ and $|1,0>_{+}|2>$ vibrations, with reasonable agreement between predicted and observed intensities. The peak observed at 8802 $cm^{-1}$ is assigned as the $|1,0>_{-}|2>$ vibration, though position and intensity for this peak are high in comparison to the predicted values.

#### 2.3.2.3 Third Overtone

The most intense band in the third overtone region, at 10999 $cm^{-1}$ (see Figure 2-32), is assigned to the |4,0>|0> LM. The observed intensity is 50.6%, somewhat lower than the predicted 68.2%. Two weak shoulders are seen at 10726 $cm^{-1}$ and 10877 $cm^{-1}$ respectively.

These are assigned to combination bands of local mode vibrations of the second overtone plus two fundamentals: (8436 $cm^{-1}$ +1303 $cm^{-1}$ +953 $cm^{-1}$) and (8541 $cm^{-1}$ +1328 $cm^{-1}$ +1032 $cm^{-1}$), respectively [84]. The intensity of these shoulders is low. It is therefore unclear if their intensity is due to weak Fermi interactions or intrinsic to the combinations. The band observed at 11135 $cm^{-1}$ is asymmetric, but it cannot be resolved into any consistent group of bands. This band is assigned to the |0,0>|4> vibration for the purpose of determining intensity; it has been fitted to 3 bands and the intensity is summed for comparison with predicted values. The observed intensity is 40.1%, which is much higher than the predicted value of 23.3%. Bands observed at 11394 $cm^{-1}$ and 11507 $cm^{-1}$ are assigned as unresolved local mode vibrations and the intensities match well. (See Table 2-6 for details).

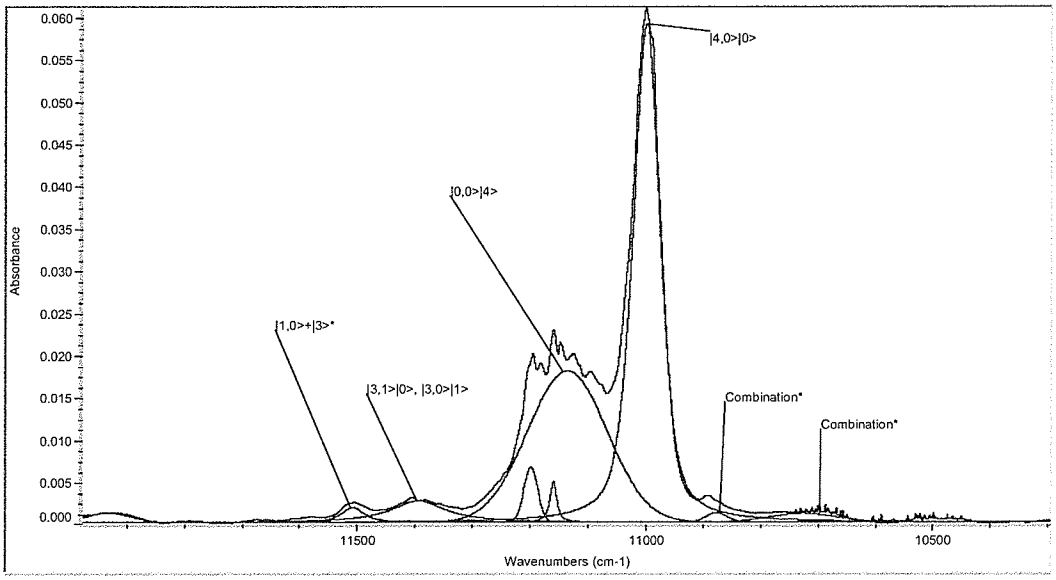


**Figure 2-32.** Spectrum of the third overtone of dimethyl sulfide, collected with a 10 meter path length, 4048 co-added scans. See text for details.

### 2.3.2.4 Fourth Overtone

The peak at 13449 $cm^{-1}$ is assigned as the |5,0>|0> vibration. A peak observed at 13538 $cm^{-1}$ has also been included to deal with the asymmetry of this peak (this peak is not resolved enough to speculate on any cause of the asymmetry). The sum of the intensities of these peaks is 62% (~10% lower than predicted). The peaks at 13647 $cm^{-1}$, 13684 $cm^{-1}$ and 13786 $cm^{-1}$ are assigned to the |0,0>|5> vibration (the 3 peaks being used to estimate intensity since the peak is asymmetric, but not well enough resolved to assign component bands). There are two small shoulders at 13184 $cm^{-1}$ and 13292 $cm^{-1}$ (see Figure 2-33) which have intensities that are unlikely to exist at this energy without some gain from Fermi resonance. There are several combinations that could fall in this region however considering that they have likely shifted somewhat due to the Fermi resonance it is difficult to assign these with any degree of certainty. The intensity is 12% above the predicted. The peak at 13941 $cm^{-1}$ is assigned to a group of unresolved local mode vibrations that have enough intensity to appear in this region. See Table 2-6 for details.

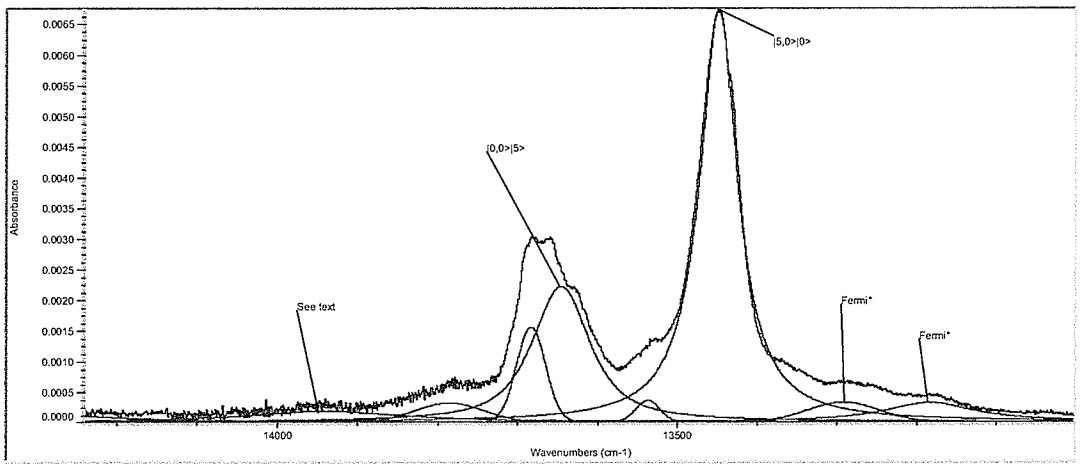


**Figure 2-33.** Spectrum of the fourth overtone of dimethyl sulfide, collected with a 10 meter path length, 4048 co-added scans. See text for details

### 2.3.3 Local mode parameters and dipole moment functions

The values of the local mode parameters are found in Table 2-7. The peaks used for Birge-Spöner plots were taken from our data for the $2^{nd}$–$4^{th}$ overtones with the assumption that the most intense peaks were the pure local modes. Values for the $5^{th}$ and $6^{th}$ overtones of trimethyl amine were taken from the paper by Fang and Swofford [68]; those for the $5^{th}$ overtone of dimethyl sulfide were taken from the paper by Manzanares *et al.* [70].

**Table 2-7.** LM Frequency and anharmonicity determined from Birge-Spöner plots.

| | LM Frequency ($cm^{-1}$) | | | Anharmonicity ($cm^{-1}$) | | |
|---|---|---|---|---|---|---|
| | This work | Fang et al. | Manzanares *et al.* | This work | Fang et al. | Manzanares *et al.* |
| TMA | | | | | | |
| *Gauche* | 3069+/-5 | 3085+/-26 | 3074+/-4 | 62+/-1 | 64+/-6 | 63+/-1 |
| *Trans* | 2915+/-8 | 2877+/-15 | 2892+/-8 | 69+/-2 | 65+/-3 | 66+/-2 |
| DMS | | | | | | |
| *Gauche* | 3062+/-7 | 3060+/-32 | | 55+/-1 | 54+/-5 | |
| *Trans* | 3070+/-4 | 3038+/-34 | | 62+/-2 | 58+/-6 | |

The LM frequency and anharmonicity parameters calculated from this work agree within experimental error (See Table 2-7) with those reported previously by Fang *et al.* [68] and Manzanares *et al.* [70]. The error associated with the values found here is lower than in earlier works, and, given the greater number of points in the fit, is expected to be more reliable.

The experimental results from this thesis show a smaller difference between the local mode frequencies and a greater difference between the anharmonicities for the *trans* and *gauche* CH in TMA than previously reported. Both these parameters and the optimized geometries show the differences anticipated to arise from the lone pair *trans* effect: the longer, weaker bond has lower LM frequency and greater anharmonicity.

In contrast, the effect of the lone pair on the bond length of dimethyl sulfide is seen to be nearly negligible as the geometry optimization produced CH bonds that were nearly equal in length, within possible experimental error. For dimethyl sulfide, the Birge-Spöner plot gives a greater difference between the anharmonicities of *trans* and *gauche* CH bonds than previously reported, while the LM frequencies are nearly identical to those previously reported. This difference in anharmonicity is responsible for the eventual resolution of the CH stretching bands, in the higher overtones of dimethyl sulfide. This relatively large difference in anharmonicity between *trans* and *gauche* is somewhat surprising considering the lack of significant difference in bond lengths.

In general, there was very good agreement between the frequencies of the vibrations observed and the HCAO/LM model predictions. Deviations are reasonably explained by shifts due to Fermi resonance, which is not accounted for in the HCAO/LM model. In many cases, significantly fewer bands were observed in regions where L-L combinations were predicted by the HCAO/LM model. These regions contained broad bands that generally covered the range where several of the L-L combinations were expected to appear, thus it is assumed that they are not resolved.

The *ab initio* calculated coupling parameters, seen in Equation 2-4 on page 52, repeated below here for convenience

$$H^{1}_{\text{intra}} / hc = -\gamma'_{12}(a_1 a_2^{+} + a_1^{+} a_2) - \gamma'_{13}(a_1 a_3^{+} + a_1^{+} a_3 + a_2 a_3^{+} + a_3^{+} a_2)$$

can be similar even when bonds are different, since they arise from HCH angles and potential coupling between the CH stretches. In this case, the coupling constants are: 17 $cm^{-1}$ ($\gamma'_{12}$) and 10 $cm^{-1}$ ($\gamma'_{13}$) for TMA, and 15 $cm^{-1}$ ($\gamma'_{12}$) and 16 $cm^{-1}$ ($\gamma'_{13}$) for DMS with the

first number being the coupling between the two identical CHs, *i.e.*, *gauche* for TMA and *trans* for DMS. These couplings between the identical CHs are considered to be very similar. They have an effect only on the intensities of the L-L bands [65].

**Table 2-8.** Dipole moment expansion coefficients for CH bonds in Trimethyl amine and Dimethyl sulfide.

| | Trimethyl Amine | | Dimethyl Sulfide | |
|---|---|---|---|---|
| $\mu_i$[a] | $CH_{gauche}$ | $CH_{trans}$ | $CH_{gauche}$ | $CH_{trans}$ |
| $\mu_1$ | 0.986 | 2.028 | 0.319 | 0.612 |
| $\mu_2$ | 2.019 | 2.939 | 1.408 | 2.206 |
| $\mu_3$ | 0.021 | 0.082 | 0.040 | 0.168 |
| $\mu_4$ | 0.053 | 0.091 | 0.053 | 0.033 |

[a] Calculated as the sum of the squared cartesian components for the diagonal terms.

The dipole moment function used by Kjaergaard and Low has been expanded as a fourth degree polynomial in the internal bond displacement coordinates. Values for the expansion coefficients are shown in Table 2-8. The $\mu_i$ are the *i*th derivatives of the dipole, calculated as the sum of the three squared Cartesian components for the different bonds. These terms may be examined for an initial, rough estimate of the intensities of the different overtones [65]. The fundamental is dependent on $\mu_1$ and to a lesser extent, $\mu_2$. The first overtone is the most complicated, being dependent on both $\mu_1$ and $\mu_2$, however, depending on the sign, either summation or partial cancellation of contributions could occur. The next overtones ($2^{nd}$ to $4^{th}$) depend greatly on $\mu_2$, with variable contributions from the higher order terms. The absolute magnitudes of the $\mu_1$ and $\mu_2$ in trimethyl amine are greater than their counterparts in dimethyl sulfide. Within each molecule, the ratio of the *gauche:trans* components is about the same at each level (*e.g.*; for $\mu_2$, the *gauche* coefficient is about two thirds that of the *trans*, in trimethyl amine and in dimethyl sulfide). According to guidelines

above, the absolute intensities of the trimethyl amine modes will likely be greater than those of the dimethyl sulfide but the influence of the dipole moment functions on the relative intensities of *gauche* and *trans* should be similar throughout the overtones.

### 2.3.4 Intensities

The calculated and observed relative intensities of the L-L combinations and the pure LM, *gauche* and *trans*, are shown in Table 2-9 for all compounds, through the three overtones. Comparable data for dimethyl ether (DME) [66] are also presented. Italicized entries indicate lower reliability of experimental results. In the fourth overtone of $N(CHD_2)(CD_3)_2$, one or more of the L-N bands may be resonant with both of the pure LMs, but are assigned to the *gauche* CH only. In the fourth overtone of $N(CH_3)_2(CD_3)$ and $N(CH_3)(CD_3)_2$, the *trans* CH intensity may have been underestimated due to baseline problems in that region. Finally, the curvefit in the third overtone of DMS has an elevated uncertainty, attributable to the proximity of the *gauche* and *trans* pure LMs.

**Table 2-9.** Relative contributions (L-L:*gauche:trans*) to intensity, for CH stretching overtones[a]

| | Second Overtone (%) | | Third Overtone (%) | | Fourth Overtone (%) | |
|---|---|---|---|---|---|---|
| | Observed | Calculated | Observed | Calculated | Observed | Calculated |
| $N(CHD_2)(CD_3)_2$ | 0:76:24 | 0:69:31 | 0:64:35 | 0:67:35 | *0:67:33* | 0:62:38 |
| $N(CH_3)_3$ | 26:55:19 | 23:50:27 | 11:69:21 | 10:57:33 | 8:55:37 | 6:59:37 |
| $N(CH_3)_2(CD_3)$[b] | 18:58:24 | | 8:72:21 | | *8:65:28* | |
| $N(CH_3)(CD_3)_2$[b] | 23:60:17 | | 13:66:21 | | *9:63:28* | |
| $S(CH_3)_2$ | 17:24:59 | 15:23:62 | *7:40:53* | 9:23:68 | 5:33:62 | 7:21:72 |
| $O(CH_3)_2$[c] | | | 16:22:62 | 8:31:61 | 5:36:60 | 5:30:65 |

[a] Numbers in italics are less reliable due to experimental factors. See text for details.

[b] Separate calculations for $N(CH_3)_2(CD_3)$ and $N(CH_3)(CD_3)_2$ were not performed. Observed values may be compared to the calculated values for $N(CH_3)_3$.

[c] Experimental and theoretical data for dimethyl ether obtained from Kjaergaard *et al.* [66].

Sets of intensities will be considered in groups that can be readily compared to each other. For the sake of simplicity these considerations will be divided into sections comparing (1) single molecules over all observed overtones and (2) single overtones for different molecules.

The HCAO/LM intensity model takes into consideration the potential energy surface (including anharmonicity parameters from experiment) and the calculated dipole moment functions. In this model, the more anharmonic oscillator gains intensity in relation to the less anharmonic oscillator. On a per CH bond basis, the calculated intensity for the more anharmonic *trans* CH bonds is usually greater than that for the *gauche* in both TMA and DMS.

#### 2.3.4.1 $N(CHD_2)(CD_3)_2$ Comparison of the relative Intensities through the overtones

Since $N(CHD_2)(CD_3)_2$ has only one CH oscillator and no L-L coupling, it is appropriate to consider it separately from the other molecules. The CH oscillator may be in the *trans* position or in one of two *gauche* positions. In order to make the intensities directly comparable, the *gauche* intensities are scaled to a per position basis.

The agreement observed here between calculated and observed values is very good, particularly at the third overtone. The difference between experimental and calculated results is the highest for the second overtone. This could be due to remaining normal mode character in the second overtone. The slightly higher difference between experimental and calculated results at the fourth overtone is likely due to a complicated Fermi resonance

involving combinations and both of the pure local modes, instead of just the *gauche* as assumed.The results are shown in Figure 2-34.

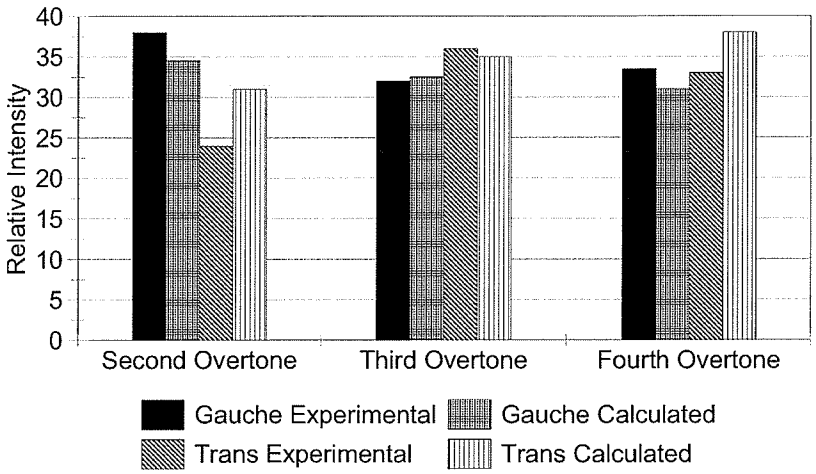


**Figure 2-34.** Comparison of $N(CHD_2)(CD_3)_2$ intensities on a per bond basis.

### 2.3.4.2 Comparison of the second overtones of $N(CH_3)_3$, $N(CH_3)_2(CD_3)$, and $N(CH_3)(CD_3)_2$

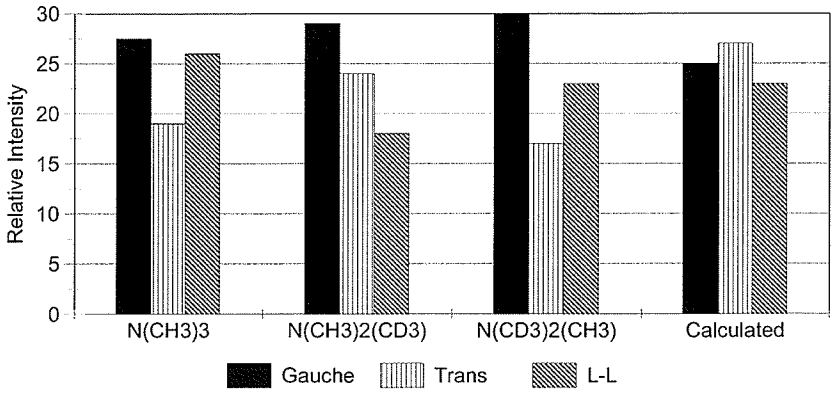


**Figure 2-35.** Comparison of calculated and observed intensities for the second overtones of $N(CH_3)_3$, $N(CH_3)_2(CD_3)$, and $N(CH_3)(CD_3)_2$ on a per bond basis.

HCAO/LM calculations were only done for $N(CH_3)_3$. Since it was assumed that there was no inter-methyl coupling, no differences between $N(CH_3)_3$, $N(CH_3)_2(CD_3)$, and $N(CH_3)(CD_3)_2$ are expected. Note, however, that there is experimental evidence (Section 2.3.1) that low-level coupling may exist. In this section, the intensities of the second overtones on a per bond basis are compared (see Figure 2-35).

There is much to consider when analyzing the change in intensity that occurs as the methyl groups become deuterated. The experimentally observed relative intensities for the second overtones of $N(CH_3)_3$, $N(CH_3)_2(CD_3)$ and $N(CH_3)(CD_3)_2$ consistently have *trans* bands ~17-43% less intense than the *gauche*. Whereas, the HCAO/LM model predicts that the trans bands should be ~8% more intense than the *gauche*. This is likely due to some inaccuracies in the HCAO/LM calculation, perhaps caused by a small error in the LM parameters. This is in line with the results from the second overtone of $N(CHD_2)(CD_3)_2$ in which the experimental relative intensity for the *trans* band was observed to be ~37% lower than the *gauche* and the HCAO/LM model predicted that it would only be ~10% less intense. This is also be consistent with a small error in the LM parameters. It is interesting to note that on a qualitative level the fact that the *gauche* per bond intensity is observed to be greater than the *trans* observed for $N(CH_3)_3$, $N(CH_3)_2(CD_3)$ and $N(CH_3)(CD_3)_2$, is the same situation that occurs with both the observed results and the calculated results for $N(CHD_2)(CD_3)_2$. Perhaps this suggests that the HCAO/LM attributes an unduly large intensity to L-L combinations at the expense of the *gauche* vibration. One also might consider the possibillity of Fermi resonance between the L-L modes and the pure LM vibrations. However, all possible Fermi resonances would involve the *gauche* vibration and thus

the gauche vibration would be expected to be overestimated by the HCAO/LM model, which is the opposite of what is observed.

It is interesting that the L-L combinations for $N(CH_3)(CD_3)_2$ agree exactly with HCAO/LM predictions. Hence this could be considered further evidence that there is some inter-methyl coupling. Of course then it would be expected that $N(CH_3)_2(CD_3)$ would be in better agreement than $N(CH_3)_3$, which is the opposite of what is observed. This is likely due to errors in the curve fit. It is easy to imagine that, in one case, too much intensity was attributed to the pure LM and in the other, too much to a L-L combination. Additionally, the pure LM and L-L bands are not clearly resolved, thus some intensity may have been misassigned between them. The *trans* band should be less affected as there are no L-L combinations close to it. At any rate, the differences between the observed values of all three are too low to make any definitive statements. What is clear is that the predicted *trans* intensity is too high. Probable explanations include errors in LM parameters and mis-assignment of L-L contributions to *gauche* rather than *trans* modes. Much of the conjecture made in the analysis of the second overtone can be tested in the analysis of the third overtone. Less L-L combination intensity will be expected and effects of anharmonicity should be increased.

#### 2.3.4.3 Comparison of the third overtones of $N(CH_3)_3$, $N(CH_3)_2(CD_3)$, and $N(CH_3)(CD_3)_2$

The comparison for the third overtone is shown in Figure 2-36. It is very interesting to note that the relative intensity of the *trans* band is invariant to deuteration. This eliminates inter-methyl coupling as an explanation for its low intensity, however, such coupling would expected to be very weak by the third overtone. The intensity of the *trans* band is

also very low compared with the predicted value and with the intensity observed for the third overtone of $N(CHD_2)(CD_3)_2$ (Figure 2-34).

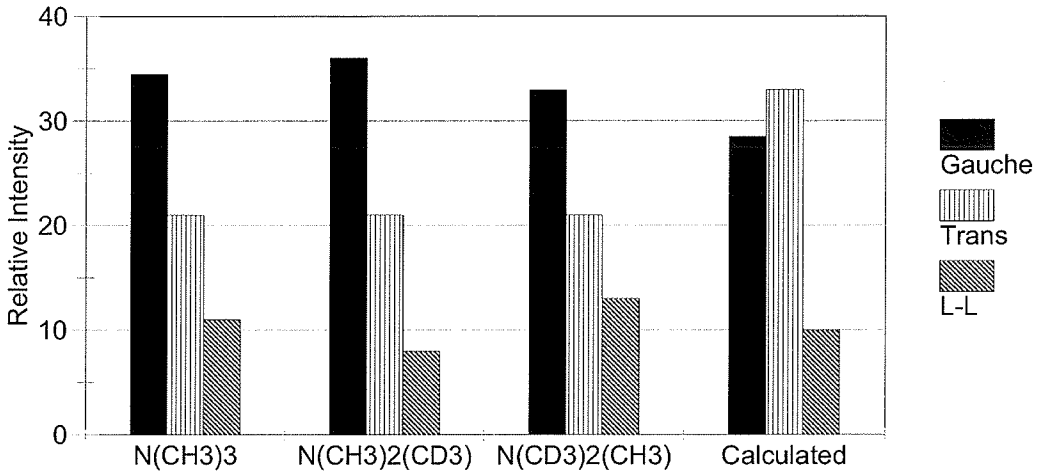


**Figure 2-36.** Comparison of calculated and observed intensities for the third overtones of $N(CH_3)_3$, $N(CH_3)_2(CD_3)$, and $N(CH_3)(CD_3)_2$ on a per bond basis.

The low *trans* intensity is inconsistent with the hypothesis that the disagreement between observed and calculated values are simply due to errors in the LM parameters (though it does not preclude them as a factor). If LM parameter errors were the only factor, then the error would be expected to appear in $N(CHD_2)(CD_3)_2$ as well. The L-L combination intensity is in approximate agreement with the calculated value, in all the observed data. The relative intensity of the *gauche* band is consistently too high. Perhaps the L-L mode combinations take more of their intensity from the *trans* than predicted by the HCAO/LM and consequently less from the *gauche*, which would be in keeping with all of the preceding observations.

### 2.3.4.4 Comparison of the fourth overtones of $N(CH_3)_3$, $N(CH_3)_2(CD_3)$, and $N(CH_3)(CD_3)_2$

In the fourth overtone, there should be very little L-L intensity, so many of the theories put forth so far may be tested further. The problem of assigning L-L intensities inappropriately to the pure LM's is thereby greatly reduced. The comparison of the relative intensities of the fourth overtones of $N(CH_3)_3$, $N(CH_3)_2(CD_3)$, and $N(CH_3)(CD_3)_2$ is shown in Figure 2-37.

Since the intensities of $N(CH_3)_2(CD_3)$, and $N(CH_3)(CD_3)_2$ are somewhat suspect due to baseline issues they are not discussed in detail.

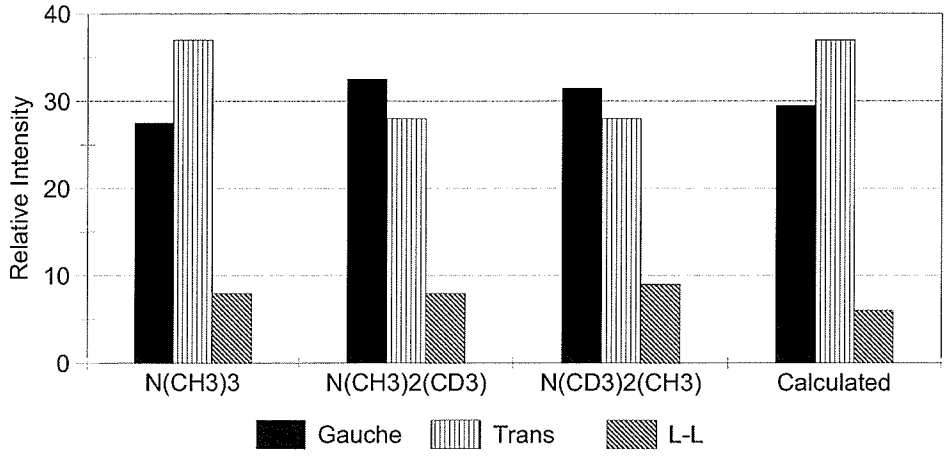


**Figure 2-37.** Comparison of calculated and observed intensities for the fourth overtones of $N(CH_3)_3$, $N(CH_3)_2(CD_3)$, and $N(CH_3)(CD_3)_2$ on a per bond basis.

As expected, the observed relative intensity of the fourth overtones of $N(CH_3)_3$ agrees well with the predicted values, which supports the theory that the HCAO/LM model does not accurately distribute the contributions of the pure LM's to the L-L combinations.

### 2.3.4.5 $N(CH_3)_3$ comparison relative intensities through the overtones

In the previous sections the relative intensities of $N(CH_3)_3$, $N(CH_3)_2(CD_3)$, and $N(CH_3)(CD_3)_2$ have been compared with each other for each overtone. Since the HCAO/LM model predictions were calculated for $N(CH_3)_3$, it is helpful to focus on this molecule alone through all of the overtones (Figure 2-38). The worst agreement between the experimental values and the HCAO/LM model predictions occurs at the third overtone. This is unexpected, since generally any error would either get consistently worse with increasing quantum number, or consistently better. The most likely explanation therefore is that there is in fact more than one factor contributing to the disagreement between the predicted and observed relative intensities. These factors may well offset each other at the second overtone. Also it is interesting that the intensity of the *trans* band does not increase at a constant rate with increased quanta. The increase between the second and third overtone is very minor, but quite large between third and fourth. This disagrees with the HCAO/LM predictions, and may be indicative of an error in the local mode parameters.

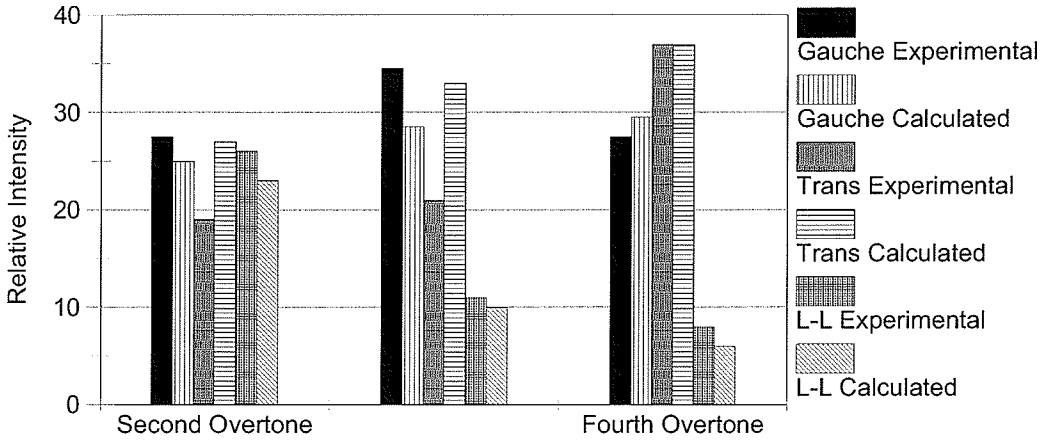


**Figure 2-38.** Comparison of $N(CH_3)_3$ intensities on a per bond basis.

### 2.3.4.6 Comparison relative intensities of $S(CH_3)_2$ through the overtones

The intensities of dimethyl sulfide are shown here in Figure 2-39. The agreement between the experimentally observed intensities and the predicted intensities at the second overtone is very good. The experimental values for the third overtone are questionable due to overlap between the *trans* and *gauche* bands so the third overtone is not discussed in detail. However, at the fourth overtone the agreement is not as good. This is most likely due to errors in the local mode parameters.

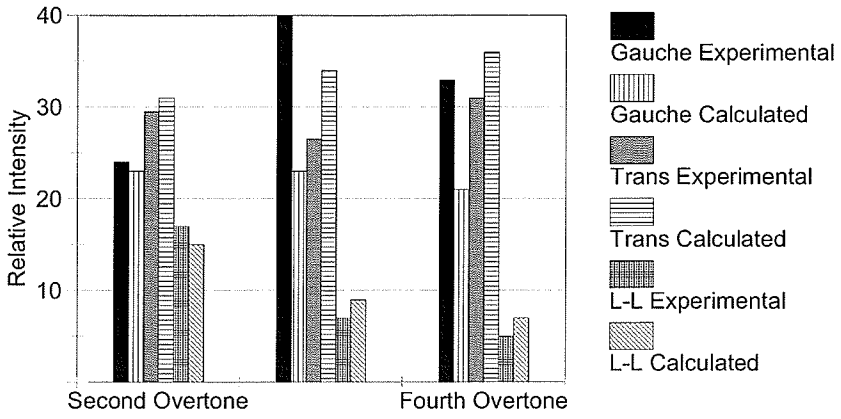


**Figure 2-39.** Comparison of $S(CH_3)_2$ intensities on a per bond basis.

There is a significant difference between the *trans* and *gauche* anharmonicities in DMS, particularly as compared to the earlier results from Kjaergaard et al. [66] for DME in which a value of 62.5+/-1.0 for the *gauche* CH and 67.3 for the *trans* was obtained. This seems unusual since the lone pair *trans* effect, as manifested by the bond lengths, appears to be small in DMS as opposed to DME where the bond lengths suggest a larger manifestation of the lone pair *trans* effect (1.0890 Å for *trans* and 1.0814 Å *gauche* [66]). Of course, the bond lengths reflect the equilibrium, and not the potential energy surface. Good

agreement was found between the observed and calculated relative intensities in DME [66]. The DMS spectra do not exhibit Fermi resonance in the higher overtones but the *gauche* band is not well resolved, so that the anharmonicity is perhaps less accurate. Thus, the discrepancy between calculated and observed relative intensity for DMS could arise in part from errors in the derived anharmonicity parameters.

#### 2.3.4.7 Final thoughts on intensities: TMA and DMS

Given that the lone pair *trans* effect is much weaker in dimethyl sulfide than in trimethyl amine, and that the error between the observed intensities and the predicted relative intensities is similar, any effects of the lone pair *trans* effect on the intensities must be considered minor in comparison to other factors. The foregoing discussion shows that there is no simple explanation for the discrepancies between the HCAO/LM predictions and the observed values. In trimethyl amine, errors in the LM parameters, the possibility of intermethyl coupling at lower overtones, and L-L combination intensities being derived from pure LM's differently than expected seem to be the most likely factors. For dimethyl sulfide, errors in the LM parameters are the most likely factor. Finally one must consider that the L-N combinations that are involved in the Fermi resonance could in fact have some intensity of their own, in which case the intensity ratios would be affected. However, this is unlikely to be the main factor, particularly at the higher overtones.

## 2.4 Conclusions

The $1^{st}$ – $4^{th}$ overtones of TMA and DMS have been reported. All of the major peaks were assigned to pure local mode, L-L combination or L-N combinations involved in Fermi resonant interactions with LM bands. Calculations of relative intensities made

using the HCAO/LM model are shown to agree well with the experimental observations. However, a tendency for the HCAO/LM model to overestimate the intensity of the *trans* CH vibration and underestimate the *gauche* is noted. The rotational envelope cannot adequately explain the contours of the bands, thus, there is likely some significant influence from Fermi resonance. Modest but noticeable intensity in the LN combination bands, assumed to be negligible, may have contributed to the residual discrepancies. The assumption that the methyl groups are isolated may be incorrect. Coupling between the methyl groups in TMA and DMS could be facilitated by the lone pair(s), and would give rise to additional L-L combinations.

# 3 Vibrational overtone spectra of organometallics: Effect of the coordinating metal on the CH bond lengths

## 3.1 Introduction

### 3.1.1 General

This chapter focuses on the application of overtone spectroscopy to the study of the effect of the coordinating metal on the organic ligand in organometallic compounds. In particular the effect on the CH bonds is examined. Two projects are discussed within this chapter. The first, on the vibrational spectroscopy of cyclohexadiene iron tricarbonyl (CHDIT), is a collaborative project involving me, D. L. Snavely, H. G. Kjaergaard, K. M. Gough and A. V. Fedorov. Since I was not the primary researcher on this project the discussion of this work is somewhat truncated. (For a more complete discussion the reader is referred to the published paper Federov *et al.* [85]). However, this project led to the second project that comprises the majority of this chapter and therefore warrants some discussion. The CHDIT project was focussed on the change in the CH bond vibrations of the ligand caused by coordination with a metal atom. The study of the change in the ligand is accomplished by comparing the free ligand spectrum to the organometallic compound. That is, spectra of 1,3-cyclohexadiene are compared to those of CHDIT revealing the changes in the cyclohexa-

diene geometry caused by coordination. The second project expands this methodology to the comparison of spectra of a ligand coupled with different metal atoms, in order to characterize the influence of the different metal atoms on the compound. For this study metallocenes are studied for two reasons. First, they are common compounds in synthetic chemistry [86] and any knowledge gained about them may be of value to synthetic chemists, as the length of the CH bond length is directly related to the bond strength. Features common to both projects are discussed first, followed by those specific to each project.

### 3.1.2 The relationship between CH stretching frequency and CH bond length.

In Section 2.1, the relationship between CH stretching vibrational frequencies and the CH bond length was touched on. In this chapter, it is appropriate to consider this topic in more detail. The correlation between the CH stretching frequencies and bond length was made clear by McKean *et al.*[62] and by Duncan [87], who were building on the work of Bernstein [88] and Badger [89][90]. In these papers, large numbers of molecules were considered; the CH stretching frequencies found for these molecules were compared with bond lengths determined from various experimental techniques such as x-ray or microwave spectroscopy. They found a linear relationship between the CH stretching frequency and the bond length. The few cases that were outside of this linear relationship could, in general, be explained by Fermi resonance. The practical use of this relationship for studying the geometry of molecules is evident, and has been applied to the effects of conformation and substitution by McKean [91], in addition to the results found by McKean that relate to the lone pair *trans* effect discussed in Section 2.1, McKean looked at a number of other systems as well. The linear relationship between the CH stretching frequencies and bond

length was applied to the study of α and β methyl and halogen groups in saturated compounds. In olefinic compounds, spectral observations show that the position of the substitution, α, *cis* or *trans* results in different effects on the CH bond stretching frequency. The greatest effect was on the *trans* CH. In the more complex molecule $O(CH_3)_2$, McKean *et al.* [92] studied the effect of substitution of one hydrogen with various halogens using deuteration to aide in the analysis. Upton *et al.* [93] demonstrated that the relationship between the bond length and the stretching frequency also applied to NH bonds although it is not quite linear. These types of relationships were later shown to extend to a number of X-H bonds [94].

### 3.1.3 The Correlation between CH overtones and CH bond length

Given the correlation between the fundamental CH stretching frequencies and bond length, it is reasonable to conclude that a similar relationship should exist between bond length and overtone vibrations. In fact, due to the LM nature of the overtones, such a relationship exists, and has been shown to be more generally applicable, since LM vibrations are those of uncoupled oscillators rather than of harmonically coupled oscillators. In the fundamental region, selective deuteration is used to decouple the oscillators so that single oscillators may be observed. With overtone vibrations, this is not necessary. The correlation of CH bond length to vibrational frequency has been extended to the overtone region as mentioned in Section 2.1. Since this chapter focuses on such a correlation, some further discussion of the previous work is appropriate. In 1980, Mizugai and Katayama [95] compared the CH stretching fifth overtone of several heterocyclic compounds to experimentally determined bond lengths. They found that there is a good linear relationship which is characterized by the following equation:

**Equation 3-1.**

$$r_{CH} = 1.084 - 8 \times 10^{-5} \frac{\Delta\omega}{(v+1)}$$

where $\Delta\omega$ is the shift of the $v^{th}$ overtone from the benzene absorption maximum. This work was followed by work by Wong and Moore in which the correlation between bond length and the fifth overtone frequency was extended to alkanes and alkenes [96]. They found a good correlation between bond length determined from *ab initio* calculations with the 4-31G basis set. The relationship followed the equation:

**Equation 3-2.**

$$r_{CH}^{0}(calc) = (1.32 \pm 0.02) - (1.4 \pm 0.1) \times 10^{-5} v$$

with a correlation coefficient of -0.966.

Since experimental CH bond lengths can be difficult to obtain, it is frequently necessary to use *ab initio* calculations to determine the bond length needed for the correlation. However, the level of theory has a large effect on the results. Using both the STO-G3 and 4-21G basis sets to calculate the bond lengths, Gough and Henry [64] have shown good correlations between the shift in the overtone frequency and *ab initio* calculated bond lengths as expressed by the following equation:

$$r_{CH}^{LM} = 1.084 - \left(\frac{\Delta\omega}{11v}\right)0.001$$

Not surprisingly, the correlation was much better (coefficient 0.988) for the bond lengths calculated with the larger 4-21G basis set, compared 0.792 for the more limited STO-3G basis set. Thus demonstrating the ned for good basis set functions.

### 3.1.4 Overtone studies of Organometallics

There are relatively few reports of vibrational overtone spectra of organometallics in the literature. In 1982, Lewis reported the spectra of a number of organometallic compounds including ferrocene [97]. In general, this work showed that overtone spectra had features which were indicative of the organic groups coordinated to the metal. Specifically, different iron organometallic complexes containing cyclopentadienyl rings had a common peak due to the CH stretching in the ring. This demonstrated the usefulness of overtone spectroscopy in the study of organometallics.

Much of the rest of the work on the overtone spectroscopy of organometallic compounds has been done by Snavely *et al.* In 1991, Blackburn, Snavely and Oref examined the third overtone spectra of solid ferrocene [98]. They observed only two peaks, both of which they assigned to the |4> pure LM of the CH stretch, and theorized that the split was due to the rotation of the cyclopentadienyl ring. To test this theory, VanMarter, Olsen and Snavely [99] acquired better quality spectra of ferrocene, ruthenocene, acetylferrocene and cyclopentadienyl titanium trichloride. It was anticipated that, if the "splitting" of the overtone peaks were due to the rotation of the cyclopentadienyl ring, changes in the spectrum should be observed in molecules that have different barriers to internal rotation. Ruthenocene has a significantly higher barrier to internal rotation than ferrocene. However, they found no differences in the spectra that could be attributed to internal rotation. Therefore they developed another theory based on comparisons of the ferrocene spectra to that of free cyclopentadiene. Since a number of peaks observed in the metallocenes were not observed in the cyclopentadiene, they theorized that these peaks are dark in the cyclopentadiene but are brightened by the coordination of the metal. This point is of significant inter-

est to the metallocene project to be presented in this chapter. In 1999, Fedorov and Snavely recorded the first through third overtones of ferrocene, ruthenocene and several other cyclopentadienyl containing organometallics [100]. In all of these spectra, the combination bands associated with the cyclopentadienyl ring are observed. A thorough and highly consistent set of assignments for these bands was presented. These assignments are invaluable to the work on metallocenes presented here.

To some degree, most of the papers discussed above focus on metallocenes and are directly related to the metallocene work presented here. In 1997, Fedorov and Snavely compared 1,3-butadiene to butadiene iron tricarbonyl [101] and used the correlation between the CH stretching overtones and CH bond length to great advantage for the assignment of the overtone spectra of the complexes. They observed that the changes between the spectra of 1,3-butadiene and the complexes could all be directly related to the changes in the CH bond length predicted from *ab initio* studies. In a study of cycloheptatriene chromium tricarbonyl, Fedorov and Snavely did not observe changes in the differences in the overtone frequencies for the CH stretching frequencies between the complex and the free ligand that should have been present if there is $\mu_4/\mu_2$ (i.e., the chromium is coordinated to a set of four conjugated carbon atoms and a set of two conjugated carbon atoms), as proposed by x-ray studies [102]. Instead, they suggested that $\mu_6$ bonding (*i.e.,* the chromium is coordinated to one set of six conjugated carbon atoms) is more likely.

### 3.1.5 Vibrational Overtone Spectroscopy and Overtone Intensities of Cyclohexadiene Iron Tricarbonyl and 1,3-Cyclohexadiene

The project discussed here was a collaborative project, in which I was fortunate to have a role as it afforded a perfect transition between the work presented in Chapter 2 and the work on metallocenes for which I was the primary investigator. Though my role in this work was somewhat limited, it warrants some discussion as it leads directly to the metal-locene project.

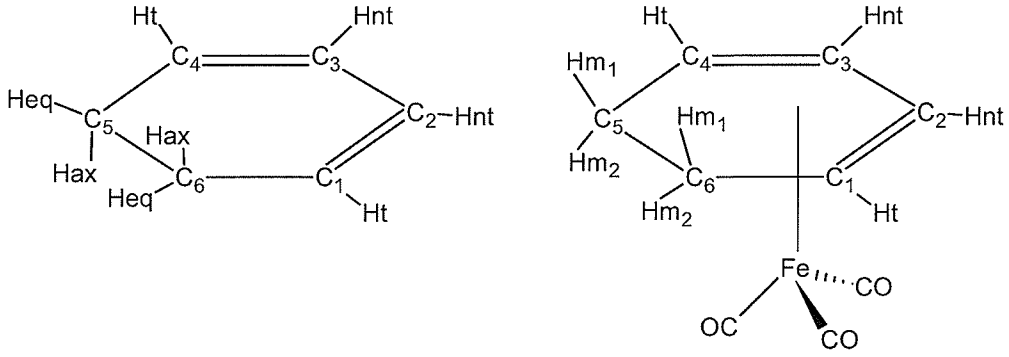


**Figure 3-1.** Structure of Cyclohexadiene (left) and Cyclohexadiene iron tricarbonyl (right).

Many transition metal complexes have catalytic activity that is derived from the ability of unoccupied d-orbitals of the metal atom to share electrons with the lone pair, $\pi$ or aromatic clouds of the ligand. This interaction significantly alters the electronic structure of the ligand. Cyclohexadiene iron tricarbonyl (CHDIT) is a good example of a $\pi$–bonded organometallic complex [85]. In this study, the first through third overtones of CHDIT are compared with the spectra of 1,3-cyclohexadiene, previously studied by Gough *et al.* [103]. Both microwave spectroscopy [104] and x-ray diffraction [105] show that CHDIT has a "piano stool" type structure (see Figure 3-1). Comparison of the microwave determined CC

bond lengths for the CHDIT [104] and those for the free ligand [106] show that complexation results in the shortening of the bond adjacent to both of the double bonds and the lengthening of the double bonds. In this work, the goal was to determine the effect of the complexation on the CH bonds.

### 3.1.6 Vibrational overtone spectra of metallocenes: Effect of the coordinating metal on the CH bond lengths

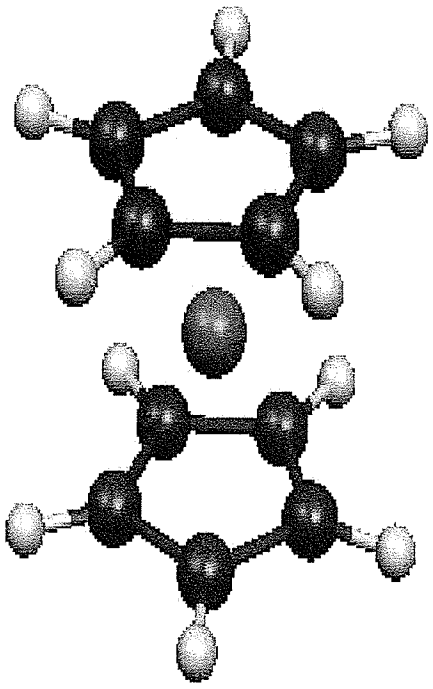

Overtone spectra can provide bond specific information and thus are very useful for the study of the C-H bonds of metallocenes. These organometallic compounds are characterized by two cyclopentadienyl rings bound to a central metal atom. In this study, the spectra of both ruthenocene and ferrocene have been reeaxamined in addition to previously unexamined nickelocene, cobaltocene, bis(cyclopentadienyl) magnesium and sodium cyclopentadienyl, with particular attention to the CH bond vibrational energies and their correlation to bond length.

**Figure 3-2.** Geometry of metallocenes.

In the metallocenes, two separate geometries are possible: eclipsed and staggered. However, calculations have shown that there is no difference in the geometry of the cyclopentadienyl groups in the two conformations [107] simplifying many of the considerations by eliminating concerns about changes during internal rotation. However this precludes any determination of the preferred geometry from overtone spectra.

Cyclopentadienyl is aromatic and, with the possible exception of cobaltocene, only one pure LM vibration is anticipated at each overtone. The expectation that there will only be one pure LM does not preclude the possibility of local-normal combination bands. However these local-normal combination bands bands would be expected to have low intensity, particularly at higher overtones. However, Fermi resonance may cause these peaks to exhibit higher than expected intensities (see Section 1.2.3).

In previous work [99], the spectra of ferrocene and ruthenocene were compared to that of cyclopentadiene. The appearance of peaks in the spectra of metallocenes that were absent in the cyclopentadiene spectra led the authors to suggest that these vibrations are brightened by the influence of the metal atom on the cyclopentadienyl ring. However, since cyclopentadiene is not aromatic, it is also possible that the disparity is due to the structural differences between the aromatic cyclopentadienyl and the non aromatic cyclopentadiene, rather than to the effect of the metal atom. To investigate this possibility, sodium cyclopentadienyl was selected for comparison to the metallocene spectra. Sodium cyclopentadienyl is characterized as ionic and provides the best possible approximation to the spectrum of independent cyclopentadienide.

There is some question as to whether bis(cyclopentadienyl) magnesium is ionic or is covalently bonded [86]. The nature of the metal-ligand bond will affect the ligand structure, and therefore the spectrum of this compound. This study will help clarify the nature of bis(cyclopentadienyl) magnesium.

Cobaltocene is of spin multiplicity 2, therefore it is expected to manifest the Jahn-Teller effect [107][108], with distortion of the cyclopentadienyl ring. If the effect is significant, the reduction in symmetry to $C_2$ would result in three separate sets of CH bonds, with

different lengths [107]. In this case, we would expect three separate bands instead of one in each of the overtone spectra of cobaltocene.

The effect of the metal atom on the CH bond length is studied by determining the correlation between the pure LM CH stretching vibration frequency and CH bond length calculated at several levels of theory. These correlations can then be used to estimate the relative CH bond lengths of the metallocenes. To this end, no scaling was done on any of the calculated bond lengths. The results of this analysis are compared to bond lengths calculated with the BLYP level of theory using the 6-311G(d,p) basis set for the carbon and hydrogen atoms and a 3-21G basis set for the metal atoms (hereafter referred to as BLYP/ hybrid), and to bond lengths determined experimentally. Note that the basis set used for the metal is very low, and therefore the metal is only being treated in a approximate fashion, though this reduces the accuracy of the results. Also the parameters of the of elements with different basis sets may be optimized with different criteria this may cause inaccuuracies in the results. However,the use of the hybrid basis set was necessary as higher basis set will not work for all of the metals involved.

## 3.2 Experimental

### 3.2.1 Vibrational Overtone Spectroscopy and Overtone Intensities of Cyclohexadiene Iron Tricarbonyl and 1,3-Cyclohexadiene

In this collaborative project, the carbon tetrachloride solution and liquid spectra were collected by Fedorov and Snavely; ( Bowling Green State University, Bowling Green, Ohio, U.S.A) the gas phase and some liquid spectra were collected by me, Gough and Fedorov (University of Manitoba, Winnipeg, Manitoba, Canada); the HCAO LM calculations were done by Kjaergaard (University of Otago, Dunedin, New Zealand).

#### 3.2.1.1 Collection of spectra

1,3-cyclohexadiene (97% purity) and CHDIT (97% purity) were purchased from Aldrich and Strem Chemicals, respectively. All transfers of CHDIT were carried out under an inert atmosphere, and the solvents were degassed by passing nitrogen through them for 2 hours.

All of the solution and the second and third overtone liquid spectra were recorded at 2 $cm^{-1}$ resolution on a Mattson Galaxy FTIR spectrometer, with a 1 cm path length. In all cases, 1000 co-added scans were used. The first and second overtones were collected using a Pb/Se detector and the third using a Si detector.

The first overtone of both liquid and gas phase CHDIT were collected using a Wilmad Glass variable path length cell with a nominal 3 m path length and a Bio-Rad FTS-40 spectrometer. In order to introduce gaseous CHDIT to the cell, a sidearm containing liquid CHDIT was attached to the cell. The sidearm and cell were heated; once the required temperature was reached (100 $^{o}C$ for the cell and 120 $^{o}C$ for the sidearm), background scans

were collected and the CHDIT gas was allowed to enter the cell. Upon cooling, CHDIT collected on the windows of the cell, forming a thin layer (~5 mm) of CHDIT on the windows; this allowed liquid phase spectra to be collected. All spectra were composed of 128 co-added scans. Curve fits were obtained for all spectra with either Mattson peak solve or Bomem-Grams software.

Experimental oscillator strengths ( $f_{e \leftarrow g}$ ) were determined from the following equations [109][110]:

**Equation 3-3.** Gas phase

$$f_{e \leftarrow g} = (8.026 \times 10^{-7}(\text{Torr} \cdot \text{m} \cdot \text{cm}))\frac{1}{pl}\int A(\tilde{\nu})d\tilde{\nu}$$

**Equation 3-4.** Liquid phase

$$f_{e \leftarrow g} = \left(4.335 \times 10^{-11}\left(\frac{\text{mol}}{\text{l}} \cdot \text{m} \cdot \text{cm}\right)\right)\frac{9n}{(n^2+2)} \cdot \frac{1}{Ml}\int A(\tilde{\nu})d\tilde{\nu}$$

where p is the pressure of the gas, n is the refractive index of the liquid, M is the concentration, l is the path length and A is the absorbance.

### 3.2.1.2 Calculations of Geometries and HCAO LM intensities

The geometries of 1,3-cyclohexadiene and CHDIT were calculated using the HF/3-21G* and HF/6-311+G(d,p) levels of theory. The effect of electron correlation was investigated with density functional theory using the perturbative Becke-Perdew method with full polarization basis set (pBP/DN(p,d)).

The intensity calculations were carried out according to the HCAO LM model, as described in Section 2.2.3. Aside from carrying out the calculations for the geometries of 1,3-cyclohexadiene and CHDIT (*i.e.*, a single CH oscillator for the olefinic CH and asymmetric $CH_2$ for the aliphatic CH bonds), there was only one major difference between the procedure used here and that described in Section 2.2.3. Experimentally determined LM parameters (as in Section 2.2.3) were replaced with the LM parameters calculated from force constants and their derivatives of along the internal CH stretching coordinate, given by the following equations [111]:

**Equation 3-5.**

$$\omega = \frac{(F_{ii}G_{ii})^{\frac{1}{2}}}{2\pi c}$$

**Equation 3-6.**

$$\omega x = \frac{hG_{ii}}{72\pi^2 c}\left(\frac{F_{ii}}{F_{iii}}\right)$$

where $F_{ii}$ and $F_{iii}$ are the second and third order force constants, respectively.

The force constants were determined from the same molecular energies used in the grids for calculation of the dipole moment functions. Scaling factors for olefinic and aliphatic CH bonds were determined from the average ratio of calculated to experimental values of previously studied compounds. (For a more complete discussion, see reference) [85].

## 3.2.2 Vibrational overtone spectra of metallocenes: Effect of the coordinating metal on the CH bond lengths

Sodium cyclopentadienyl (2 molar in THF), ferrocene (98% purity), ruthenocene (99% purity), bis(cyclopentadienyl) magnesium (99.9% purity), cobaltocene (98% purity)

and nickelocene (99% purity) were obtained from Strem Chemicals. The sodium cyclopentadienyl solution was used directly. Saturated solutions of the pure compounds in carbon tetrachloride (99% purity, Aldrich) and THF (Fisher Scientific, purified using methods described by D.D Perrin and W.L.F Armarego [112]), were prepared under an argon atmosphere. The concentration varied depending on the solubility. The solvent was degassed by repeated freeze-pump-thaw cycles.

All spectra were acquired with a Nicolet 870 FT-IR spectrometer and a white light source. The first and second overtones required a quartz beam splitter and MCT-A detector. For metallocenes, a 1 cm cell was used and 2048 scans were co-added. For the third overtone, a silicon detector and a 10 cm cell path length were used and 4096 scans were co-added. In all cases, the spectra were ratioed against a carbon tetrachloride background. Sodium cyclopentadienyl spectra were acquired using the parameters described above, except that a 3 mm cell was used and the spectrum were ratioed against the empty cell. The THF spectrum was subsequently subtracted.

#### 3.2.2.1 CH bond length and wave number correlation

In order to evaluate relationships between CH bond length and frequency for the metallocenes, it was necessary to establish a bond length-frequency correlation based on compounds with well defined geometric and spectral parameters, for which the spectra had been recorded in the liquid phase. The spectra of *o*-xylene (Eastman), cycloheptatriene (J.T. Baker Chemical Co.), cyclooctadiene (J. T. Baker Chemical Co.), indene (Aldrich) and 1,4-cyclohexadiene (Aldrich) were chosen for the correlation, because they offered an appropriate range of CH bond lengths which correspond to well-defined LM vibrations. All spectra were collected in the liquid phase using a 3 mm path length; 2048 scans were collected

and co-added for the first and second overtones and 4096 for the third overtone. The CH bond lengths used for the correlations were calculated at the HF/6-311G(d,p) and BLYP/6-311G(d,p) levels of theory. Calculations of the metallocene geometries were done with Gaussian 98 software [81] using only the BLYP/hybrid as the HF/6-311G(d,p) level of theory cannot be used for molecules containing heavy atoms.

## 3.3 Results

Results for the vibrational overtone spectroscopy and overtone intensities of cyclopentadiene iron tricarbonyl and 1,3-cyclohexadiene can be found in reference [85]. Since most of the data was collected and interpreted by my collaborators it is inappropriate to present it here as part of this thesis. A brief summary and general discussion appear within the next section, where pertinent to the extended study actually conducted for this thesis.

### 3.3.1 Vibrational overtone spectra of metallocenes: Effect of the coordinating metal on the CH bond lengths

#### 3.3.1.1 Correlation between *ab initio* CH bond length and overtone frequencies

The data from the molecules used in the determination of the CH bond length correlation are given in Table 3-1. This includes the band positions for the first, second and third overtones and the lengths of the CH bonds to which they are assigned, calculated at both the HF/6-311G(d,p) and BLYP/6-311G(d,p) level of theory. In many cases, the pure LM for the first overtone could not be assigned reliably due to significant normal mode character in that region.

The spectra of the molecules used to produce the correlation between CH bond length and the first overtone are shown in Figure 3-3. Generally, only very strong bands are assigned, and only bands that are considered to be pure local modes of CH stretch are assigned. No attempts were made to account for Fermi resonances in determining the position of the peaks that were used in the correlation. This may be considered a source of error, and will lead to a poorer fit in the correlation. However, the increased error introduced by

neglecting the Fermi resonance is accepted, in order to avoid inappropriately fitting the peak positions to a correlation.

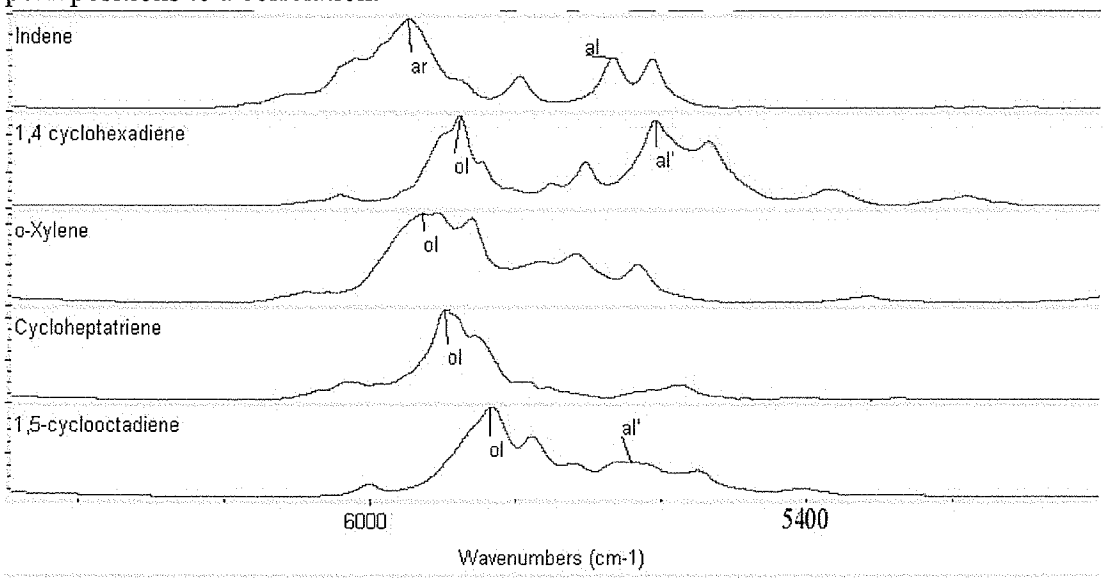


**Figure 3-3.** First overtone spectra used for bond length frequency correlation, collected using a 3mm path length and 2048 co-added scans. Absorbance plotted on the vertical axes and annotation according to Table 3-1

The spectra of indene show a peak of equal intensity to the $CH_{al}$ band just below it in energy. This may be due to a Fermi resonant interaction with a local normal combination. In o-xylene, only the $CH_{ol}$ was sufficiently well defined to use in the correlation, though other peaks could be assigned; the same is true for cycloheptatriene. For 1,5-cyclooctadiene, two bands are considered well enough defined to be assigned; there are others but spectral crowding makes their assignment too tentative to use in the correlation. The spectra used for the second overtone CH bond length frequency correlation are shown in Figure 3-4. The assignments are relatively straight forward (Table 3-1).

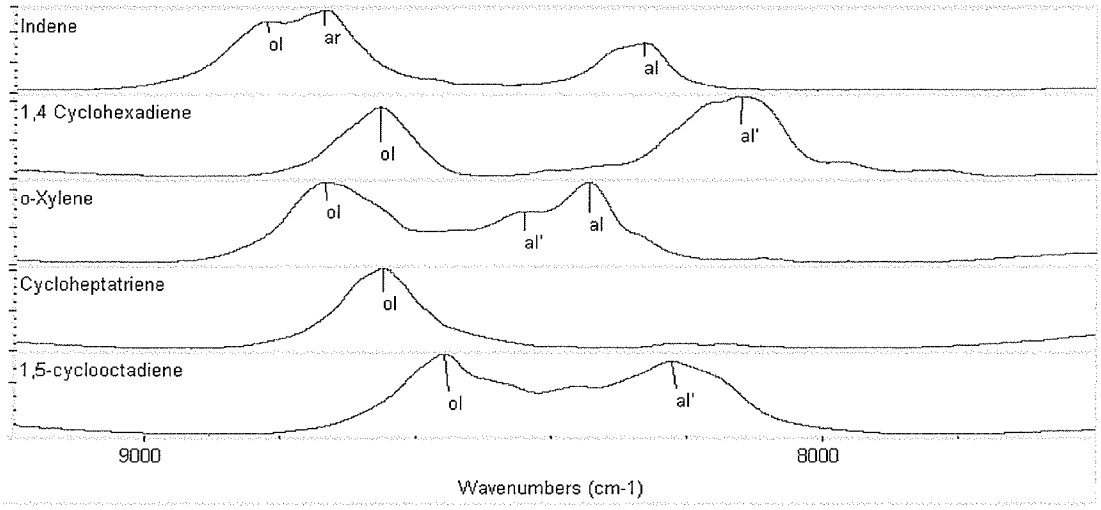


**Figure 3-4.** Second overtone spectra used for bond length frequency correlation, collected using a 3mm path length and 2048 co-added scans. Absorbance plotted on the vertical axes and annotation according to Table 3-1

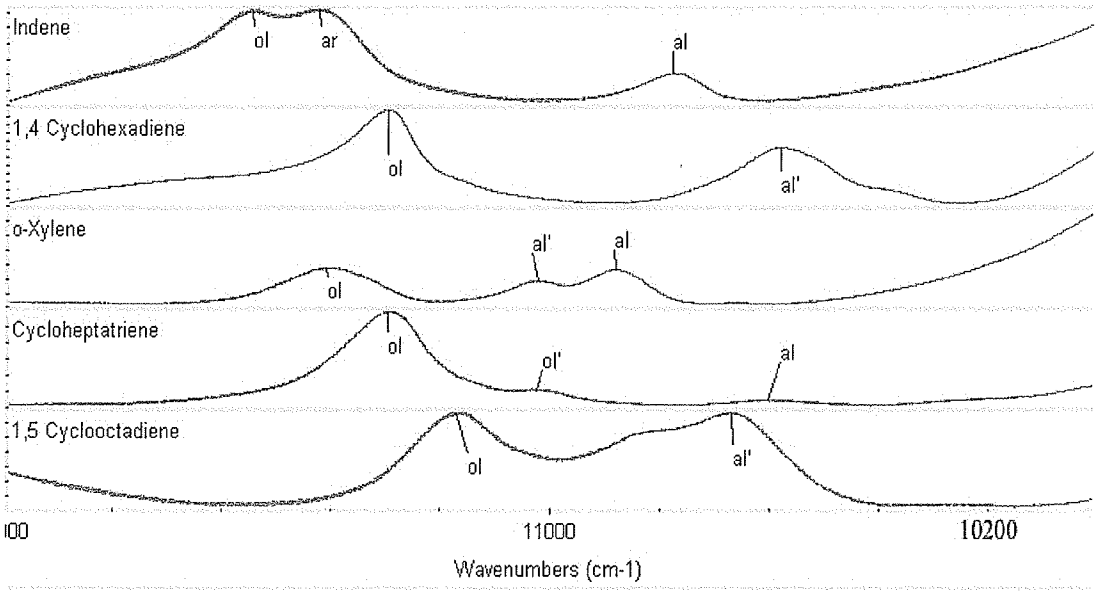


**Figure 3-5.** Third overtone spectra used for bond length frequency correlation, collected using a 3mm path length and 2048 co-added scans. Absorbance plotted on the vertical axes and annotation according to Table 3-1

**Table 3-1.** Bond lengths (Å) and energies ($cm^{-1}$) used for correlations.

| Compound[a] | | HF/6-311G(d,p) | BLYP | First Overtone | Second Overtone | Third Overtone |
|---|---|---|---|---|---|---|
| Indene | ar | 1.076 | 1.091/1.092d | 5954 | 8740 | 11426 |
| | ol | 1.074 | 1.088/1.089d | | 8824 | 11548 |
| | al | 1.088 | 1.104 | 5669 | 8268 | 10784 |
| 1,4-cyclohexadiene | ol | 1.078 | 1.092 | 5883 | 8658 | 11301 |
| | al | 1.090 | 1.109/1.110[d] | 5615 | 8126 | 10585 |
| *o*-Xylene[b] | ol | 1.076 | 1.092 | 5934 | 8740 | 11411 |
| | ol' | | 1.091 | | | |
| | al | 1.087 | 1.102 | | 8351 | 10889 |
| | al' | 1.083 | 1.098 | | 8447 | 11030 |
| Cycloheptatriene[c] | ol | 1.078 | 1.094 | 5902 | 8653 | 11298 |
| | ol' | 1.077 | 1.093 | | | |
| | al | 1.083 | 1.098 | | | 11040 |
| | al' | 1.089 | 1.105 | | | 10615 |
| Cyclooctadiene | ol | 1.079 | 1.095 | | | |
| | ol' | 1.080 | 1.096 | 5837 | 8563 | 11176 |
| | al | 1.081 | 1.097 | | | |
| | al' | 1.089 | 1.105 | 5644 | 8229 | 10680 |
| | al" | 1.090 | 1.107 | | | |
| | al"' | 1.086 | 1.101 | | | |

a) All energies from liquid phase spectra. (ar=aromatic, ol=olefinic, al=aliphatic)

b) Spectra of the second and third overtones of liquid benzene and *o*-xylene previously published by Henry *et al.*[24]

c) Spectrum of the third overtone of liquid cycloheptatriene have been published by Snavely *et al.* [113]

d) In these cases BLYP/6-311G(d,p) showed 2 different bond length where HF/6-311G** had one; for the purpose of correlation, the shorter bond length was used.

At the third overtone, the spectra are essentially LM in character and the assignments therefore are straightforward (see Table 3-1). The increases in intensity that appear at the edges of the spectra are artifacts that come from the baseline correction of truncated spectra. This is a relatively common occurrence. Since the intensities are not of interest, these artifacts do not cause a problem.

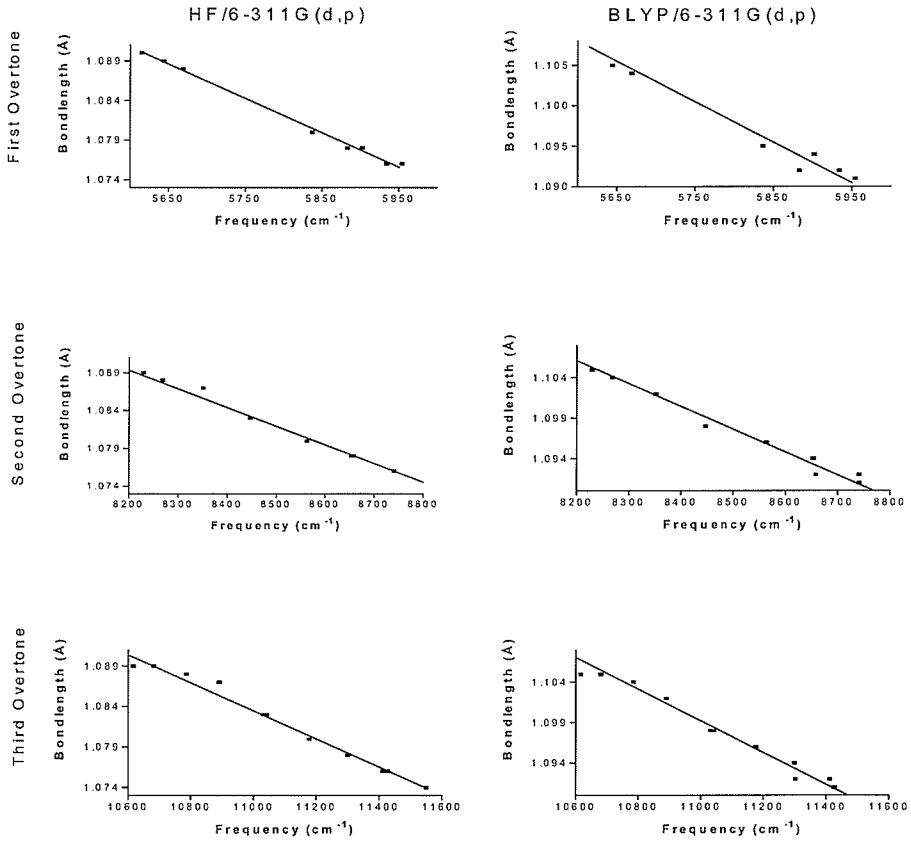


**Figure 3-6.** . Correlation between calculated bond lengths and CH stretching overtone vibration frequency, at each overtone, with different basis sets.

The data shown in Table 3-1 are used to calculate correlations between bond length and frequency. Figure 3-6 shows the correlation between CH bond length, calculated at HF/6-311G(d,p) and BLYP/6-311G(d,p) level of theory, and the pure LM CH stretching vibra-

tional energy for the first, second and third overtones. The general relationship correlating the bond length calculated at the HF/6-311G(d,p) or BLYP/6-311G(d,p) level to wavenumber of the overtone may be expressed as:

**Equation 3-7.**

$$R_{CH}^{Basis} = I^{Basis} - S^{Basis} \times \overline{\nu}$$

where $\nu$ is the wave number of the pure LM vibration, while I (intercept) and S (slope) have the values listed in Table 3-2 for the overtone considered; $r^2$ values of 0.995, 0.989 and 0.986 were obtained for the first, second and third overtones, respectively, for the HF calculations.

**Table 3-2.** Constants for correlations

| | I(Å) | Error in I | S(Å/cm$^{-1}$) | Error in S | $r^2$ of fit |
|---|---|---|---|---|---|
| HF/6-311G(d,p) | | | | | |
| First Overtone | 1.33 | 0.01 | $4.3 \times 10^{-5}$ | $0.2 \times 10^{-5}$ | 0.995 |
| Second Overtone | 1.29 | 0.01 | $2.5 \times 10^{-5}$ | $0.1 \times 10^{-5}$ | 0.989 |
| Third Overtone | 1.27 | 0.01 | $1.7 \times 10^{-5}$ | $0.1 \times 10^{-5}$ | 0.986 |
| BLYP | | | | | |
| First Overtone | 1.38 | 0.02 | $4.5 \times 10^{-5}$ | $0.4 \times 10^{-5}$ | 0.968 |
| Second Overtone | 1.34 | 0.01 | $2.8 \times 10^{-5}$ | $0.1 \times 10^{-5}$ | 0.988 |
| Third Overtone | 1.32 | 0.01 | $2.0 \times 10^{-5}$ | $0.1 \times 10^{-5}$ | 0.980 |

The correlation of frequency to bond length calculated at the BLYP/hybrid level of theory yielded $r^2$ values of 0.968, 0.988 and 0.980 for the first through third overtones, respectively.

The parameters from the HF/6-311G(d,p) and BLYP/6-311(d,p) regressions and the experimental values for the frequency of the pure LM CH vibrations were used to estimate the CH bond lengths in the metallocenes and cyclopentadienide. Results of these calculations are given in Table 3-5 on page 149, along with the CH bond lengths calculated for the

metallocenes at the BLYP/hybrid level of theory and the experimentally determined bond lengths from other sources where available.

### 3.3.1.2 Metallocene Spectra

Figures 3-7 through 3-9 show the overtone spectra of the metallocenes studied for the first through third overtones, respectively. Assignments for the peaks observed in these spectra are based on those made by Fedorov *et al.* [100] on ferrocene and are shown in Table 3-3. The pure LM vibrations used for the estimation of the CH bond length are in boldtype.

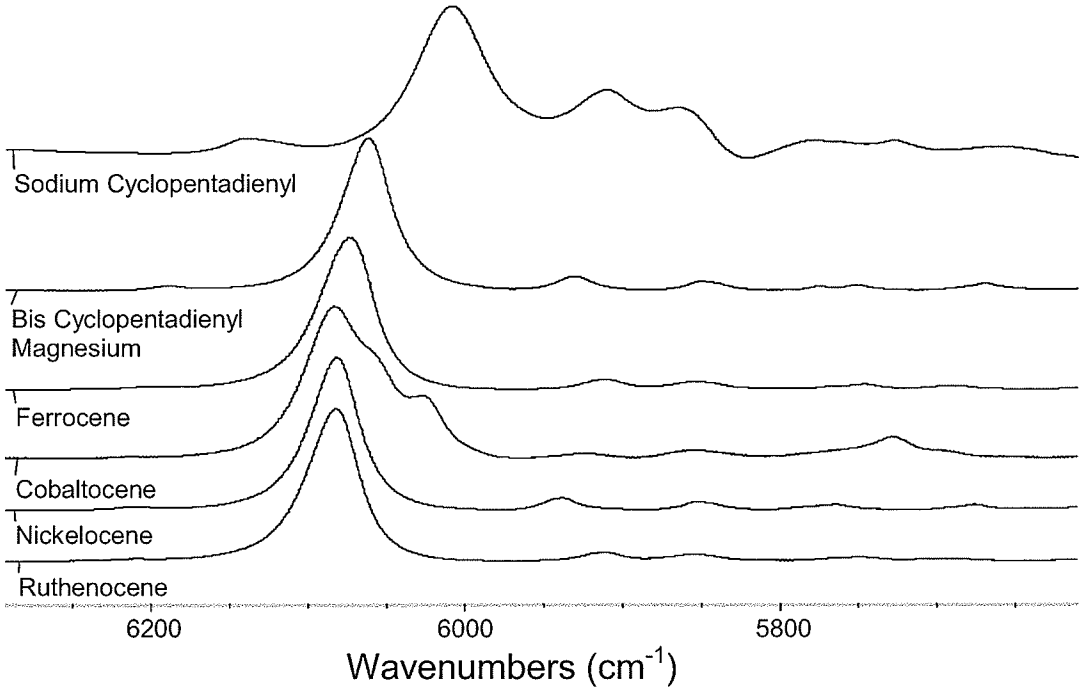


**Figure 3-7.** First overtone spectra of metallocenes in carbon tetrachloride, and sodium cyclopentadienyl in THF. Spectra acquired at room temperature with a 1 cm path length.

**Table 3-3.** Observed frequencies ($cm^{-1}$) and assignments for metallocenes

| Overtone | $Mg(C_5H_5)_2$ | $Fe(C_5H_5)_2$ | $Co(C_5H_5)_2$ | $Ni(C_5H_5)_2$ | $Ru(C_5H_5)_2$ | $Na(C_5H_5)$ | Assignment |
|---|---|---|---|---|---|---|---|
| 1[a] | | 5503 | | | | 5498 | |
| | | 5555 | | | | Shoulder | |
| | 5669 | 5686 | Shoulder | 5676 | 5698 | 5662 | $\nu_{CH}+\nu_{CCstr(as)}+\nu_{CHbend}$ |
| | 5751 | 5746 | 5729 | 5766 | 5748 | 5727 | $\nu_{CH}+\nu_{CCstr(as)}+\nu_{CHbend}$ |
| | 5775 | Shoulder | | Shoulder | Shoulder | 5780 | |
| | 5849 | 5855 | 5856 | 5853 | 5854 | 5865 | $\nu_{CH}+\nu_{CCstr(}+\nu_{CHbend}$ |
| | 5930 | 5911 | 5923 | 5938 | 5912 | 5910 | $\nu_{CH}+2\nu_{CCstr(as)}$ |
| | | | 6028 | | | | |
| | | | Shoulder | | | | |
| | **6062** | **6074** | **6084** | **6082** | **6082** | **6009** | $2\nu_{CH}$ |
| | 6190 | 6201 | 6211 | 6210 | shoulder | 6139 | $\nu_{CH}+2\nu_{CCstr}$ |
| 2[a] | | | | 8665 | | | |
| | 8734 | 8732 | | 8758 | 8738 | 8693 | $2\nu_{CH}+\nu_{CCstr(as)}+\nu_{CHbend}$ |
| | 8828 | 8833 | 8873 | 8837 | 8842 | 8776 | $2\nu_{CH}+\nu_{CCstr(as)}+\nu_{CHbend}$ |
| | 8898 | 8891 | 8921 | 8922 | 8898 | 8903 | $2\nu_{CH}+2\nu_{CCstr(as)}$ |
| | **8949** | **8956** | **8977** | **8974** | **8967** | **8833** | $3\nu_{CH}$ |
| 3[b] | 11363 | | | | | | |
| | 11459 | | | | | | |
| | 11542 | | 11563 | | | | |
| | 11610 | 11609 | 11636 | | 11620 | Shoulder | $3\nu_{CH}+\nu_{CCstr(as)}+\nu_{CHbend}$ |
| | **11675** | **11669** | **11698** | | **11684** | **11489** | $4\nu_{CH}$ |
| | 11756 | 11748 | 11763 | | 11752 | | $3\nu_{CH}+\nu_{CCstr}+\nu_{CHbend}$ |
| | 11845 | 11821 | 11863 | | 11822 | | $3\nu_{CH}+2\nu_{CCstr(as)}$ |
| $\omega\chi$[c] | 56±5 | 60±5 | 59±5 | | 60±5 | 66±5 | |
| $\omega$[c] | 3090±7 | 3100±7 | 3104±7 | | 3104±7 | 3139±7 | |

a) Peak energies based on center of gravity.

b) Peak energies estimated based on curve fitting.

c) $\omega\chi$ and $\omega$ determined from Birge-Spöner plots.

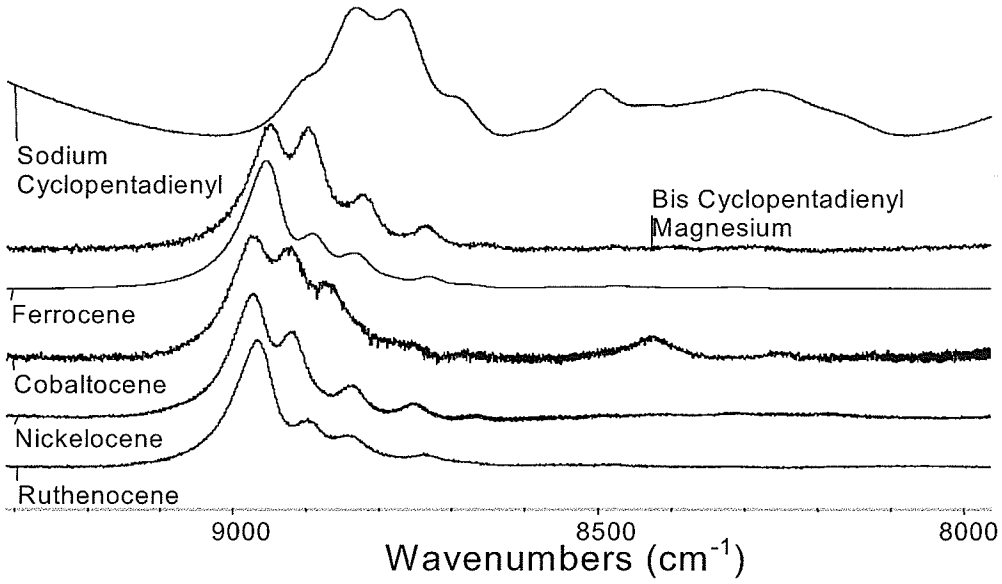


**Figure 3-8.** Second overtone spectra of metallocenes in carbon tetrachloride, and sodium cyclopentadienyl in THF. Spectra acquired at room temperature with a 1 cm path length.

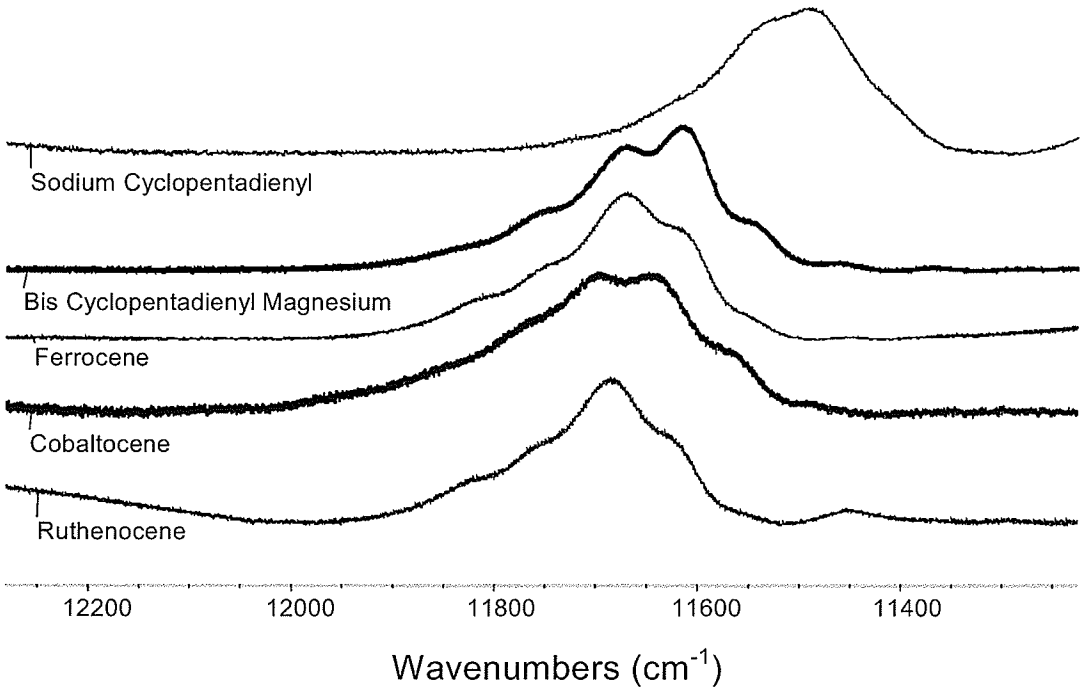


**Figure 3-9.** . Third overtone spectra of metallocenes in carbon tetrachloride, and sodium cyclopentadienyl in THF. Spectra acquired at room temperature with a 10 cm path length

# 3.4 Discussion

## 3.4.1 Vibrational Overtone Spectroscopy and Overtone Intensities of Cyclohexadiene Iron Tricarbonyl and 1,3-Cyclohexadiene

The calculated LM parameters for 1,3-cyclohexadiene agreed well with the experimentally observed values [85]. Generally, the agreement was better for the vapor than for the liquid phase. For CHDIT, the agreement was not quite as good, with the mechanical frequencies being underestimated by ~50-100 $cm^{-1}$ and the anharmonicities overestimated by ~2-10 $cm^{-1}$. A summary of the experimental and calculated local mode parameters is provided in Table 3-4. For both molecules, the experimental and calculated LM parameters showed the expected trends, with the olefinic CH bonds having higher mechanical frequencies and lower anharmonicities than the aliphatic CH bonds.

**Table 3-4.** Selected experimental and calculated (and scaled) Local Mode parameters ($cm^{-1}$), taken from reference [85]

| | Mechanical Frequency experimental | | Anharmonicity Experimental | | Mechanical Frequency calculated | | Anharmonicity Calculated | |
|---|---|---|---|---|---|---|---|---|
| Bond | Liquid | Vapor | Liquid | Vapor | Liquid | Vapor | Liquid | Vapor |
| 1,3-Cyclohexadiene | | | | | | | | |
| $CH_{ax}$ | 3014∓6 | 2997∓2 | 76.5∓1.4 | 70.2∓0.4 | 2971 | 2994 | 62.2 | 63.3 |
| $CH_{eq}$ | 3050∓6 | 3074∓17 | 63.5∓1.4 | 64.9∓3.2 | 3031 | 3055 | 61.0 | 62.1 |
| $CH_{nt}$ | 3128∓7 | 3155∓1 | 56.0∓1.7 | 58.9∓0.1 | 3132 | 3145 | 58.2 | 59.2 |
| $CH_t$ | 3128∓7 | 3155∓1 | 56.0∓1.7 | 58.9∓0.1 | 3139 | 3153 | 58.0 | 58.9 |
| Cyclohexadiene Iron Tricarbonyl | | | | | | | | |
| $CH_{m1}$ | 3006∓11 | | 66.5∓2.3 | | 2954 | | 64.3 | |
| $CH_{m2}$ | 3065∓7 | | 68.0∓1.7 | | 2983 | | 63.4 | |
| $CH_t$ | 3170∓31 | | 72.0∓7.5 | | 3033 | | 61.5 | |
| $CH_{nt}$ | 3206∓5 | | 68.0∓1.2 | | 3106 | | 59.3 | |

Agreement between the calculated and observed intensities and energies was generally good, and similar to what was presented in chapter 2. However, there were fewer Fermi resonances to cause errors.

The comparison of the 1,3-cyclohexadiene spectra and the CHDIT spectra revealed dramatic differences upon complexation. The band associated with the olefinic CH bonds in the 1,3-cyclohexadiene spectra split into two peaks in the first overtone of the CHDIT, and three in the second and third overtones. The peaks associated with the aliphatic CH bonds, that appeared as two well separated peaks for 1,3-cyclohexadiene, and were assigned as equatorial and axial CH bond vibrations, now appeared in the CHDIT spectra as two heavily overlapping peaks. These observations give some general insights as to the changes in the geometry of the cyclohexadiene geometry upon complexation. The olefinic bonds, which are equivalent in 1,3-cyclohexadiene, become different in the complex while the difference between the axial and equatorial aliphatic CH bonds is reduced. This is consistent with the results of the geometry optimizations, which predict that the difference between axial and equatorial aliphatic CH bonds is reduced from 0.005 Å to 0.002 Å and the olefinic CH bonds go from being roughly equal in length to differing by approximately 0.005 Å.

The relationship between the change in CH bond length and the overtone frequency shift of the CH stretch can be expressed as:

**Equation 3-8.**

$$\Delta r = \frac{\Delta \tilde{\nu}}{13.2\nu}(0.001)$$

From this relationship, changes to the various CH bond lengths upon complexation may be estimated. In turn, these changes can give insight into the changes to the CC bonds, caused by complexation.

Referring to Figure 3-1 on page 126, the $CH_{nt}$ bonds are shortened by 0.001 Å, and the $CH_t$ are lengthened by 0.002 Å, upon complexation. This leads to some insight about the CC bonds in CHDIT. Since the $CH_t$ bonds lengths moved closer to what would be expected for aliphatic CH bonds and the $CH_{nt}$ seemed to gain more olefinic character, it can be concluded that upon complexation, the $C_2$-$C_3$ bond gained more double bond character while the $C_1$-$C_2$ and $C_3$-$C_4$ bonds gain more single bond character. This in turn suggests that the iron tricarbonyl is coordinating to the $C_1$ and $C_4$ carbons and the $C_2$-$C_3$ bond.

The $CH_{eq}$ and $CH_{ax}$ bonds become closer in length upon complexation (labeled $CH_{m1}$ and $CH_{m2}$ for CHDIT). This suggests that the complexation removes the 15 degree dihedral angle that is present between the $C_1$-$C_2$ and $C_3$-$C_4$ bonds in cyclohexadiene. In other words, the complexation forces the $C_1$-$C_2$ and $C_3$-$C_4$ bonds to be co-planar. This supports the complexation scheme described in the previous paragraph.

### 3.4.2 Vibrational overtone spectra of metallocenes: Effect of the coordinating metal on the CH bond lengths

### 3.4.3 Assignments

In all of the overtones recorded, significant similarities are observed between bis(cyclopentadienyl) magnesium, ferrocene, nickelocene and ruthenocene (hereinafter referred to as group 1). In the first overtone of all group 1 compounds, the dominant band at ~6070 $cm^{-1}$ is assigned to the pure LM CH stretching vibration. Several weak bands,

observed in all of the group 1 compounds, have been assigned as combinations of CH stretching, CH bending and CC stretching. In the second overtone spectra, all of the observed bands appear in a fairly narrow region. Since, at the second overtone, combination bands are not expected to have any significant intensity, it is reasonable to assume that the dominant vibration is the pure LM CH stretch, while the other bands are combinations that gain intensity through Fermi resonance interactions with it. The bands are assigned to the same combinations as in the first overtone, plus one quantum of CH stretch. The relative intensity of these bands is greater than that observed for the first overtone, due to the stronger Fermi resonance. This interaction increases at the second overtone due to the greater anharmonicity of the pure LM, which decreases the separation between the pure LM and the combination bands. Similar arguments apply to the third overtone, where different combinations appear as they become closer to the pure LM CH stretching energy and previously observed combinations fade as they shift away from it.

### 3.4.4 Bond lengths

As a general guideline, the first overtone should be avoided for the estimation of bond lengths, since the spectra are still largely of normal mode character and are complicated by the presence of many combination bands. However, in the case of these metallocenes, the first overtone spectra typically do display a single, narrow, intense pure LM peak that is generally free of interference from other vibrations. In the higher overtones, the greater anharmonicity of the CH stretching modes causes the pure LM CH vibration to shift in energy relative to the combination bands. As a result, many of the combination bands are closer to the pure LM band and their relative intensity is increased. The coupling between the pure LM band and the combination bands in question may shift the pure LM band and

lead to errors in the estimation of the bond length. For this reason, the first through third overtones are considered together so that any effects of coupling may be monitored.

As anticipated, cobaltocene shows several differences when compared to group 1 molecules. Two shoulders observed at approximately 6028 $cm^{-1}$ and 6050 $cm^{-1}$ may be due to Jahn-Teller distortion of the cyclopentadienyl ring. From the correlation between experimental frequencies and bond lengths calculated with the HF/6-311 G(d,p) basis set, the position of these peaks translates into bond lengths of 1.070, 1.071 and 1.072 Å, respectively. The BLYP/6-311G(d,p) correlation gives bond lengths of 1.084, 1.086 and 1.087 Å. Geometry optimization of cobaltocene at the BLYP/hybrid level shows that the cyclopentadienyl ring is distorted from $D_{5h}$ to $C_2$ symmetry and the CH bonds are predicted to have different lengths. The predictions show six CH bonds with a length of 1.085 Å and four at 1.086 Å; this agrees within experimental error with the predictions of the BLYP/6-311G(d,p) correlation. However, it should be noted that the lower basis set used for the cobalt may cause the effect of the metal to be underestimated. It should also be noted that the relative intensities of the observed peaks do not appear to be in the expected 1:2:2 ratio; however, the true relative intensities are difficult to estimate due to the amount of overlap. It is also possible that there is some Fermi resonance involved, but there is insufficient data for further conjecture. Using the equation correlating the CH bond length calculated at the HF/6-311G(d,p) and BLYP/6-311G(d,p) levels of theory and the pure LM band for CH stretch at the first overtone level, we find that the CH bond lengths for all the metallocenes are approximately the same (Table 3-5).

**Table 3-5.** Metallocene CH bond lengths (Å)

| | From Standard correlation | | | | | | Calculated | Experimental |
|---|---|---|---|---|---|---|---|---|
| | First Overtone | | Second Overtone | | Third Overtone | | | |
| | HF/[a] | BLYP[a] | HF/[a] | BLYP[a] | HF/[a] | BLYP[a] | BLYP[b] | |
| $Mg(C_2H_5)_2$ | 1.071 | 1.085 | 1.071 | 1.085 | 1.072 | 1.086 | 1.087 | |
| $Fe(C_2H_5)_2$ | 1.070 | 1.084 | 1.071 | 1.085 | 1.072 | 1.086 | 1.086 | 1.104±0.006[114] |
| $Co(C_2H_5)_2$ | 1.070 | 1.084 | 1.070 | 1.084 | 1.071 | 1.085 | 1.085 | 1.095±0.006[115] |
| | 1.071 | 1.086 | | | | | 1.085 | |
| | 1.072 | 1.087 | | | | | 1.086 | |
| $Ni(C_2H_5)_2$ | 1.070 | 1.084 | 1.070 | 1.084 | | | 1.085 | 1.083±0.0095[116] |
| $Ru(C_2H_5)_2$ | 1.070 | 1.084 | 1.070 | 1.084 | 1.072 | 1.086 | 1.086 | 1.130±0.006[117] |
| $Na(C_2H_5)$ | 1.073 | 1.088 | 1.074 | 1.088 | 1.075 | 1.090 | 1.089 | |
| Uncertainty | ±0.002 | ±0.002 | ±0.002 | ±0.003 | ±0.002 | ±0.003 | | |

[a]6-311G(d,p) basis set
[b]Hybrid basis set

The results of the correlation for the second overtone are similar to those for the first overtone (Table 3-5), thus it may be concluded that any Fermi resonance coupling did not cause a significant frequency shift. For cobaltocene, it is impossible to distinguish between possible combination bands and those attributed to LM from CH bonds of different lengths. However, had the bands observed in the first overtone actually been combination bands, then at the second overtone they should have appeared at energies of ~100 $cm^{-1}$ above that of the pure LM. Such bands are not observed; therefore it is more likely that the bands observed in the first overtone are pure LM vibrations, due to the Jahn Teller distortion.

Similar observations are made for the third overtone; however, the bond lengths obtained from the correlation equation are approximately 0.001 Å longer (Table 3-5). The combination bands in the third overtone appear at higher frequency than the pure LM bands and have considerably more intensity than would be expected in the absence of coupling.

The strong coupling with the combination bands will have shifted the pure LM bands to lower frequencies. In any event, this difference of 0.001 Å is within the error associated with the correlation, and is not significant.

### 3.4.5 Cyclopentadiene, cyclopentadienide and cyclopentadienyl

In evaluating the metallocene spectra, the possible differences between the parent molecule cyclopentadiene, the ionic cyclopentadienide, and the coordinated cyclopentadienyl ligand must be considered. Previously, the spectrum of ferrocene had been compared to that of cyclopentadiene [99]. This comparison led to the hypothesis that the appearance of many of the combination bands was due to the influence of the metal on the ring. However, this theory neglects the change in geometry of the cyclopentadiene ring when it becomes cyclopentadienide.

Sodium cyclopentadienyl is characterized as essentially ionic and therefore the spectra should be interpreted as that of the cyclopentadienide. These spectra are quite different from those of group 1, however, the combination bands observed are quite similar. To determine whether the difference in solvents contributed to the observed dissimilarity between the sodium cyclopentadienyl and group 1 spectra, the spectrum of ferrocene in THF was acquired. No significant variation could be detected between the latter and its spectrum in carbon tetrachloride. Poor solubility, in conjunction with the strong absorptions of the THF in the same region, prevented spectra being obtained of the other metallocenes in THF. On the basis of the ferrocene results, it may be concluded that the differences observed for the sodium cyclopentadienyl are not solvent dependent, but are due to its essentially ionic character.

Very little similarity is observed between the overtone spectra of cyclopentadienide and those of cyclopentadiene obtained by VanMarter *et al.* [99]. There is only the one aromatic CH bond type in cyclopentadienyl, thus the aliphatic band at 8322 $cm^{-1}$ is absent. The CC stretching and CH bending normal modes of vibration are the most likely combination bands to appear in the overtone regions, but their probable location is shifted far from the pure LM CH stretching band because of significant differences between the frequencies of these modes for cyclopentadiene and cyclopentadienide. Therefore, Fermi resonance interaction is unlikely in cyclopentadiene. In the absence of Fermi resonance, these combination bands would be expected to have very low intensity, and it is not surprising that they are not observed in the cyclopentadiene spectra.

The principal difference between sodium cyclopentadienyl (considered to be a prototypical ionic form) and the metallocenes of group 1 is the red shift of the pure LM CH stretching band of sodium cyclopentadienyl. It is concluded that the coordination of the metal ions to the ligand causes a shortening of about 0.002 Å-0.003 Å in the CH bonds. Geometry optimizations at the BLYP/hybrid level of theory agree with the change change in geometry upon coordination described above.

The energies of the combination bands observed in sodium cyclopentadienyl are similar to those observed in the group 1 compounds and are ascribed to similar fundamental modes (Table 3-3). This is most evident for the first overtone. Since the pure LM CH stretching band is red shifted in sodium cyclopentadienyl, it lies closer to these combination bands and stronger Fermi resonance interactions can occur. Thus, while the positions of the combination bands in the sodium cyclopentadienyl are similar to those in the group 1 spectra, they are more intense. Similar interpretations apply to the $2^{nd}$ and $3^{rd}$ overtones, where

different bands are involved in Fermi resonance interaction for the group 1 compounds and the sodium cyclopentadienyl.

It has been assumed that sodium cyclopentadienyl is ionic and that its spectra may be considered to be essentially that of cyclopentadienide. The combinations in sodium cyclopentadienyl spectra resemble those of the group 1 molecules, and both are quite different from those in the cyclopentadiene spectra. Based on this evidence, it may be concluded that the appearance of combination bands in the metallocenes, and their absence in the cyclopentadiene spectra, can be attributed to differences in structure between cyclopentadiene and cyclopentadienide rather than to the influence of the metal atoms, as has been suggested in earlier works [99][100].

It is also interesting to note that there has been some question as to whether bis(cyclopentadienyl) magnesium is ionic in solution [86]. If bis(cyclopentadienyl) magnesium were ionic, its spectra would be expected to be more similar to the ionic sodium cyclopentadienyl spectra. Instead, the spectrum of this compound in carbon tetrachloride are very similar to that of ferrocene, which is not ionic.

### 3.4.6 Comparison with X-ray crystal structure data

The CH bond lengths found from the method described here show little agreement with those determined by x-ray crystallography (Table 3-5). The most significant explanation for this disagreement is likely the technique itself: it is very difficult to determine the position of hydrogen atoms using X-ray crystallography since hydrogen diffracts poorly. A second possible factor is the influence of crystal structure on the CH bond lengths, not present in solution. Differences in crystal packing could arise from the different relative

sizes of these molecules. Third, the overtone spectroscopic method relies on the accuracy of *ab initio* calculations in the formulation of the correlation plots. The correlation is only as accurate as the level of theory used to determine the bond lengths and it is generally accepted that the relative bond lengths are more reliable than the absolute values. As has been shown, this varies between levels of theory. Undoubtedly, these factors explain the large differences reported between the CH bond lengths within different metallocenes, from crystallographic measurements [114]-[118], that are not observed by the spectroscopic method used here. Overtone spectroscopy provides direct information on the bonds in question and the results are corroborated by high level *ab initio* calculations. Therefore the results from the overtone spectroscopy presented here are deemed to be preferable.

## 3.5 Conclusions

### 3.5.1 Vibrational Overtone Spectroscopy and Overtone Intensities of Cyclohexadiene Iron Tricarbonyl and 1,3-Cyclohexadiene

In this project, the first through third overtones of CHDIT were compared to the first through third overtone spectra of the free ligand 1,3 cyclohexadiene. It was found the complexation caused the lengthening of the terminal olefinic CH bonds and the shortening of the non terminal olefinic CH bonds. It was noted that the difference between the axial and equatorial aliphatic CH's was lessened upon complexation. These observations support a structure for the CHDIT complex in which the bond adjacent to both double bonds gains double bond character while the terminal diene CC bonds become closer to single bonds.

### 3.5.2 Vibrational overtone spectra of metallocenes: Effect of the coordinating metal on the CH bond lengths

From the correlation between the frequency of CH LM vibrations and *ab initio* calculated bond lengths, evidence has been found that the CH bonds of cyclopentadienyl are shortened by coordination to a metal atom in comparison to the cyclopentadienide, studied via the sodium cyclopentadiene structure. However, the nature (*i.e.,* the electronic structure, bonding, size etc.) of the metal atom does not have a significant effect on the magnitude of this shortening. The observed CH bond length of bis(cyclopentadienyl) magnesium is approximately the same as that of the other metallocenes, indicating that bis(cyclopentadienyl) magnesium is not ionic.

The combination bands in the spectra of the metallocenes, previously postulated to arise from interactions with the metal atoms, are now ascribed to the aromatic nature of the cyclopentadienyl. There are significant differences between the spectrum of cyclopentadi-

ene and that of sodium cyclopentadienyl, presumably due to the aromatic nature of the latter compound. Differences in the structure, bond length and bond strength cause the combination bands to occur closer to the pure LM CH stretching band of the cyclopentadienide ion, allowing for increased Fermi resonance.

While semi-empirical correlations such as those used here are heavily reliant on the accuracy of the *ab initio* calculations, they can be of great value in determining relative CH bond lengths, if proper care is taken in the selection of the basis set and level of theory. They are particularly helpful in cases such as this where there is a limited number of basis sets available that can handle heavy metals.

# 4 An Instrument for measuring the Vibrational-Translational relaxation time of Overtone Vibrations.

## 4.1 Introduction

The basis behind this project was derived from work done in collaboration with Dr. Terry Gough (University of Victoria, British Columbia, Canada), in which an attempt was made to modify a cell equipped with a heated wire in order to find absolute intensities of absorption bands collected via photoacoustic spectroscopy. During the preliminary work on this system a phase shift was observed between the signal generated by the wire and that generated by the absorption, that may have been due to the Vibrational-Translational (V-T) relaxation of the excited species. Though the initial project was eventually discontinued because the arrival of new instrumentation in our lab allowed the acquisition of reliable intensity information by other means, a new project was undertaken to explore the possibility of using this system to measure accurate V-T relaxation times for overtone vibrations. It should be noted that although the original project was discontinued, the instrument designed for the project described here may be used to investigate absolute intensities with little modification if the need arises.

The long term goal of this project is to test the feasibility of measuring V-T relaxation by using photoacoustic spectroscopy with a heated wire signal as a reference. As such, the data described herein are preliminary and often have led to more questions than actual relaxation times. Presently the instrument has not been fully characterized. There remains the very real possibility of instrumental errors. These possibilities will be discussed and strategies for addressing them will be proposed. It is the hope of the author that this work can act as a starting point for further advances in this area of research.

**Hypothesis**

The V-T relaxation times of overtone vibrations can be measured using photoacoustic spectroscopy emploting a heated wire as a reference. This projects seeks to prove that the use of a heated wire reference for the acquistion of V-T relaxation times has the potential of leading to a viable instrument.

### 4.1.1 Vibrational-Translational (V-T) relaxation

#### 4.1.1.1 Basic concept of V-T relaxation

Consider a molecule with one of its vibrational modes excited. The method by which it was raised to the excited state is not of importance. The energy in this mode of vibration will be relatively quickly redistributed throughout the vibrational modes of the molecule. This internal vibrational relaxation (IVR) process is very fast, much faster than the V-T relaxation. After IVR, the molecule still contains the energy that was initially present in the vibration, though it is not localized in a single mode of vibration. This molecule is now said to be in a "bath state". This is a general term used to describe the molecule as being excited, but not to define the modes where the energy is located. If the molecule was completely isolated, the molecule would in theory remain in this "bath state" until it is de-excited by spontaneous emission. However, in a gas, the molecule will eventually collide with another molecule and several events may happen. The molecules may both remain in the states they were in prior to the collision. The energy may be completely or partially transferred from the vibrational states of one molecule to the vibrational states of the other, leaving the net vibrational energy of the system the same it was as prior to the collision. Finally, the energy may be completely or partially transferred to the translational energy of the molecules, thereby reducing the vibrational energy and increasing the temperature of the system. It is this last possibility that is the subject of this project. The V-T relaxation time is dependent on a number of factors, however they may be summed up by three: the probability of collision, the probability of the energy being transferred from vibrational energy to translational energy during the collision, and the amount of vibrational energy involved. The probability of collision can be determined by statistical methods, but the

probability of each collision leading to V-T relaxation is not as easily found. Hence, the need for experiment.

#### 4.1.1.2 V-T relaxation theory

V-T relaxation theory is primarily energy transfer physics. The following discussion uses Rosencwaig's [119] treatment of energy transfer physics and the reader is referred to his full treatment and the references therein for a more complete discussion.

There are two ways to consider the energy transfer physics; in both cases the considerations are basically the same, as both consider the equilibrium between internal and external degrees of freedom. One case is that the energy in the external degrees of freedom may be increased (this is done in ultrasonics, shock tubes and similar techniques) and the transfer to the internal degrees of freedom (vibrational and rotational, generally the equilibrium between translational and rotational is very fast so the vibrational degrees of freedom dominate in this area) cause excitation. Alternatively, energy is placed in the internal degrees of freedom (rotational-vibrational-electronic) and the transfer of energy goes from the internal degrees of freedom to the external. It is this latter case which is of interest in this project. However, in both cases, the mechanism for transfer is collision.

Assuming that the most important event is the single collision between two particles, it follows that the deactivation rate is dependant on two factors: the probability of collision and the probability of the collision resulting in energy transfer. Therefore, we can define:

**Equation 4-1.**

$$c_{ij} = Z_{AB} p_{ij}$$

where, $c_{ij}$ is the collisional deactivation rate, $Z_{AB}$ is the collisional density (the number of collisions between two species per unit volume per unit time) and $p_{ij}$ is the probability that a collision will lead to energy transfer between the molecules. There are a number of treatments of $Z_{AB}$ depending on what assumptions are made. The most general will be sufficient for the discussion presented here[120]:

**Equation 4-2.**

$$Z_{AB} = \sigma\left(\frac{8kT}{\pi\mu}\right)N_A^2[A][B]$$

where $\sigma$, the collisional cross-section which may be defined by:

**Equation 4-3.**

$$\sigma = \pi d^2$$

and

**Equation 4-4.**

$$d = \frac{1}{2}(d_A + d_B)$$

The $d_A$ and $d_B$ are the diameters of the molecules involved. Returning to equation 4-2, k is the Boltzmann constant, T is temperature, $\mu$ is the reduced mass of the particles involved in the collision, $N_A$ is Avogadro's constant and the squared brackets are the molar concentrations of the particles. Note the concentrations may be considered analogous to pressure. The probability of each collision resulting in the deactivation of the vibration is ($p_{ij}$) a somewhat more difficult problem. However, Landau and Teller [121] have shown that:

**Equation 4-5.**

$$p_{ij} \sim e^{-\omega l/u}$$

$\omega$ is the vibrational angular frequency defined by $\omega=2\pi/t_v$ where $t_v$ is the period of the vibration. If the collision time is defined as $\tau_c$ then $l=u\tau_c$ and u is the relative velocity between the molecules, defined as:

**Equation 4-6.**

$$u = \left(\frac{\pi l k T}{\mu}\right)^{\frac{1}{3}}$$

From equations 4-5 and 4-6 and assuming that the processes involve strong short-range potentials, it is found that probability of energy transfer per gas kinetic collision varies as:

**Equation 4-7.**

$$p_{ij} \sim e^{-\left(\frac{\mu(l\Delta E)^2}{\left(\frac{h}{2\pi}\right)^2 kT}\right)^{\frac{1}{3}}}$$

where $\Delta E$ is the energy transferred. Note that there is a strong relationship between the amount of energy transferred and the probability of transfer. Therefore we can expect there to be significantly larger relaxation times for overtone vibrations, which are much higher in energy than the fundamentals. It is also important to note that equation 4-7 only shows that the probability of transitions is proportional to the given parameters; if one wants to know more specific information it is necessary to acquire more data, which is why experimental procedures like those presented here are important.

### 4.1.1.3 Why study V-T relaxation?

Now that V-T relaxation has been described, it is appropriate to ask the question "why study it?". In general the answer is fairly straight forward. The V-T relaxation time is a measure of how long energy will remain in a molecule under a given set of circum-

stances. The importance of this can be related to a host of gas phase applications. A number of examples are given in the following paragraphs.

Gas phase laser systems are dependant on achieving a population inversion in the gas molecules. The importance of V-T relaxation to gas phase lasers is therefore evident. Because of this, a considerable number of papers have been published on the V-T relaxation in systems relevant to gas phase lasers. Taylor and Bitterman published a survey of research on relaxation processes that are important to $CO_2$-$N_2$ laser systems [122]. There have also been a number of studies into the V-T relaxation of excited hydrogen fluoride with various collision partners[123][124], due to the interest in pulsed HF chemical lasers [125].

V-T relaxation processes are important to the chemical kinetics of gases phase radiative processes, which are of interest in many fields including atmospheric modeling, (see for example the study by V. Zenianari, B.A Tikhomirov, Yu. N. Ponomarev and D. Courtois on the relaxation of selectively excited ozone and binary mixtures [126]).

A potential for new applications also exists. These fall into the area of instrumentation. Photoacoustic depth profiling is a well known technique [127] based on phase shifts in the photoacoustic signal from solid substrates. In essence, this is the same feature of the photoacoustic signal that is used to determine the V-T relaxation time of gases using photoacoustic spectroscopy. The source of the phase shift used in depth profiling is the distance that the sound wave must travel through the material before it reaches the detector. This is clearly different from what is seen in gas phase photoacoustic spectroscopy, however both rely on a phase shift in an acoustic wave. The same technology that applies to depth profiling can be applied to gas phase photoacoustic spectroscopy, with V-T relaxation time

instead of depth associated with the phase data. This could be of significant benefit in the spectroscopy of mixtures of gases.

It has been shown that the V-T relaxation time of a gas is a characteristic of that gas. For example Cottrell *et al.* found that at a pressure of 1 atmosphere $CO_2$ had a V-T relaxation time 5 times longer than that of methane [128]. If an instrument could be built to take advantage of the difference in relaxation rates of various gases, then the components of a spectrum related to different gases could be separated, allowing for much easier analysis, and thus make previously impossible quantitative studies possible.

There are many issues that must be considered before such an instrument can be designed. One very important issue is that the presence of other gases will affect the relaxation rate of the initial gas. For example, work by Yardley *et al.* showed that the deactivation of the CH stretching modes of methane is affected by the presence of another gas. It was found that pure methane had a relaxation time of 1.9 μsec atm, while if a small amount of ethane was added this decreased to 0.77 μsec atm. In that paper, a number of different measurements were made for the relaxation of methane mixed with different gases and at different mole fractions. That the contaminating gas has a large effect on the relaxation time was evident [129], however, this would not preclude the possibility of an instrument like the one proposed here since as long as there is some difference in the relaxation times, they can be used to resolve the peaks.

More research would be needed determine whether the difference in the relaxation rates of several gases in a mixture would be sufficient to differentiate between the absorptions of the gases. A literature search failed to reveal any research into this possibility. The previously described idea for a technique assumes that the relaxation rate for an molecule

would be the same for all of the vibrations. Considering that IVR is much faster than V-T relaxation, this is not unreasonable; however the dependence of the relaxation time on the amount of energy involved would suggest otherwise. Barocchi and Vallauri found that in liquid carbon tetrachloride there are several different relaxation times associated with different modes of vibration [130]. Even though this may make using relaxation times to differentiate between gases in a mixture more difficult, it does offer a new possibility. If there is a significant difference between the relaxation of various modes, then the relaxation may be used to further resolve the spectra, aiding significantly in the analysis.

In the previous paragraphs, the reasons for interest into V-T relaxation have been discussed. Most of these issues will not be directly studied in this project, because it is a feasibility study of a method for studying V-T relaxations. It is the hope of the author that this method could one day be used to address the issues described above.

### 4.1.2 Photoacoustic spectroscopy

Since the basis of the instrument described in this project is photoacoustic spectroscopy, it is important that photoacoustic spectroscopy be well described. The general formalism used by Rosencwaig will be used for this description [119].

The absorption of a photon is the cause of excitation in photoacoustic spectroscopy. Once the photon is absorbed, there are several methods by which the molecule can relax: it may re-radiate a photon, some photochemistry may take place, it may collide with another particle and transfer the energy to that molecule's vibrational modes or it may collide with another particle and the vibrational energy may be changed into translational energy. It is the last possibility that leads to the photoacoustic signal. For the sake of simplicity, and since IVR is faster than V-T relaxation, a two-level model will be considered in which the molecule is either in its ground state ($E_i$) or in an excited state ($E_j$). To include the time dependence of the number of atoms in the excited state, all possible methods of transition must be considered. The radiative transition rate ($r_{ij}$) may be stated as:

**Equation 4-8.**

$$r_{ij} = \rho_v B_{ij} + A_{ij}$$

where $\rho_\upsilon$ is the radiation density and $B_{ij}$ and $A_{ij}$ are the Einstein coefficients for stimulated and spontaneous emission respectively. In this case $B_{01}=B_{10}$ and $A_{01}=0$ since $E_1>E_0$.

The time dependence of the number of molecules in the excited state ($N_1$) is simply the rate at which molecules are excited minus the rate at which they are deactivated:

**Equation 4-9.**

$$\frac{dN_1}{dt} = (r_{01} + c_{01})N_0 - (r_{10} + c_{10})N_1$$

where $c_{ij}$ is the collisionally induced non-radiative transition rate. Substituting in equation 4-8, and taking advantage of the previously mentioned relations as well as assuming that $c_{01}$ is essentially zero:

**Equation 4-10.**

$$\frac{dN_1}{dt} = \rho_\nu B_{10}(N_0 - N_1) - (A_{10} + c_{10})N_1$$

The inverse of the rates $A_{10}$ and $c_{10}$ are the relaxation times from the excited states for radiative ($\tau_r$)and collisional ($\tau_c$) processes respectively. Therefore equation 4-10 may be written:

**Equation 4-11.**

$$\frac{dN_1}{dt} = \rho_\nu B_{10}(N_0 - N_1) - \left(\frac{1}{\tau_r} + \frac{1}{\tau_c}\right)N_1$$

It is a simple matter to get the same type of equation for $N_0$. The total relaxation time $\tau$ is simply $\tau_r+\tau_c$. Defining I as the intensity of the light, the following definitions can be used to simplify things:

**Equation 4-12.**

$$\rho_\nu = \frac{Ih\nu}{c}$$

**Equation 4-13.**

$$B = B_{10}\left(\frac{h\nu}{c}\right)$$

Using these equations and assuming a steady state, it can be shown that:

**Equation 4-14.**

$$N_1 = \frac{BIN}{2BI + \tau^{-1}}$$

This equation defines the state that will occur when there is a constant radiation incident on the sample. This system would not lead to an acoustic signal. The result of this would be

that the molecules remained in the same ratio of excited and ground state while energy was constantly being transferred into the translational modes of the molecules, thereby continually heating the system.

Now that the rate equation of the system has been defined, it must be modified to the experimental parameters of the photoacoustic system. The main issue here is that a steady state will not lead to a sound wave and therefore there will be no acoustic signal. There are many variations on photoacoustic spectrometers, but they all have two things in common: the incident radiation is modulated and the signal is measured by either a microphone or a pressure transducer. It is this modulation of the incident radiation that causes the sound wave to be produced. The intensity of the modulated radiation may be defined using the following equation:

**Equation 4-15.**

$$I = I_0(1 + \delta e^{i\omega t})$$

where $I_0$ is the full intensity, $\omega$ is the frequency of the modulation, $0 \leq \delta \leq 1$ and t is time. If this is substituted into equation 4-14, the kinetics for the excited energy state population change becomes:

**Equation 4-16.**

$$N_1 = N\frac{BI_0(1 + \delta e^{i\omega t})}{2BI_0(1 + \delta e^{i\omega t}) + \tau^{-1}}$$

Now that the kinetics for the excited state of the molecules population change have been defined, this must be translated into the signal that is measured. The acoustic signal is defined as the negative of the pressure inside the cell. From the ideal gas law the pressure for a gas inside a cell of constant volume is:

**Equation 4-17.**

$$p = NkT$$

In order to know the temperature we must know the amount of kinetic energy (K). For the two level approximation being used the total energy of the system is

**Equation 4-18.**

$$U = N_1 E_1 + K$$

Thus the change in energy is simply the difference between the absorbed energy and the energy that is reradiated:

**Equation 4-19.**

$$\frac{dU}{dt} = (r_{01} N_0 - r_{10} N_1) E_1$$

The change in kinetic energy may be stated as

**Equation 4-20.**

$$\frac{dK}{dt} = c_{10} N_1 E_1$$

From equations 4-17 through 4-20 the following equation for the time dependence of pressure may be found.

**Equation 4-21.**

$$\frac{dp}{dt} = \frac{k}{C_v} N(c_{10} N_1 E_1)$$

The modulation of the incident beam can be accounted for by substituting equation 4-16 for $N_1$.

**Equation 4-22.**

$$\frac{dp}{dt} = \frac{k}{C_v}\frac{N^2 E_1}{\tau_c}\frac{BI_0(1+\delta e^{i\omega t})}{2BI_0(1+\delta e^{i\omega t})+\tau^{-1}}$$

Rosencwaig shows that by expanding in powers of $\delta e^{i\omega t}$, retaining only the $e^{i\omega t}$ term and integrating this becomes [119]:

**Equation 4-23.**

$$p = \frac{kE_1N^2}{C_v\omega}\left\{\frac{2\tau_c^{-2}BI_0\delta}{(2BI_0+\tau^{-1})\left[(2BI_0+\tau^{-1})^2+\omega^2\right]^{\frac{1}{2}}}\right\}e^{i(\omega t-\omega\tau-\pi/2)}$$

Since, in most cases, $I_0$ is small and the optical pumping term $2BI_0 << \tau^{-1}$, the photoacoustic signal can be written:

**Equation 4-24.**

$$q \cong \frac{kE_1N^2}{C_v\omega}\left(\frac{\tau}{\tau_c}\right)^2\frac{2BI_0\delta}{(1+\omega^2\tau^2)^{1/2}}e^{i(\omega t-\omega\tau-\pi/2)}$$

If there is no significant radiative relaxation, then $\tau=\tau_c$. It is the value of $\tau_c$ that the experiment described here is designed to find. It should be evident in the photoacoustic signal as a phase shift.

It is clear from the equation that there are a number of variables that may affect the signal other than $\tau_c$, and this does not include any of the instrumental parameters such as the response time of the microphone, the delay due to electronics and the possible presence

of resonances. All of these things add serious complications to the determination of relaxation time via photoacoustic spectroscopy.

Previously electronic factors have been dealt with by using systems that are known to relax very quickly, in order to zero the instrument. One example of this is in the work of Vasconcllos *et al.* [131], who used the relaxation of a fundamental mode of $NH_3$ to zero their instrument because it has a relaxation time of less than 0.01 μsec, which is too fast to be determined by typical photoacoustic instruments. This is of course an effective way of zeroing an instrument, however it limits the design of the instrument. This also requires that either a single cell must be filled with $NH_3$ and then filled with the sample of interest, or two cells must be used. Both of these options add error into the experiment. In this case, the instrument in question has been designed to study overtone vibrations, and therefore it is unable to excite the fundamental modes of $NH_3$.

#### 4.1.2.1 The use of photoacoustic spectroscopy to study V-T relaxation

The dependence of the photoacoustic signal on $\tau_c$ makes photoacoustic spectroscopy a viable option for the study of V-T relaxation. The first proposal to use the phase shift in the photoacoustic signal to determine V-T relaxation was made by Gorelik in 1946. The first successful experiment was done by Slobodskaya in 1948 [119]. The possibility of determining the V-T relaxation time by monitoring the DC pressure rise was also suggested by Cottrell, however this will not be discussed here as Cottrell found that this method was not possible [132].

Since then, phase shift of a photoacoustic signal has been used to determine the relaxation time of a vibration. In 1957, Jacox and Bauer used this technique to study the

relaxation of carbon dioxide. They were unable to make any quantitative measurements of the relaxation times but did observe the pressure dependence of the phase shift [133]. Cottrell *et al.* [128] used a very simple apparatus to measure relaxation times; essentially the apparatus was a typical photoacoustic spectrometer with a reference diode to determine the zero point of the phase of the incident beam. The data were analyzed by fitting phase shifts recorded at various pressures to the following equation:

**Equation 4-25.**

$$\tan\phi = \omega\frac{\tau}{p}$$

where $\phi$ is the phase shift. In some of the preliminary experiments, Cottrell *et al.* found that there was a resonance for the cell that caused significant phase shifts which had no relation to the relaxation process. Once these were eliminated, more reliable phase shifts were collected. In all cases, a phase lead due to the heat of conduction had to be considered. This phase lead was most prominent for the light molecules studied. To account for these, ammonia was used as a reference, since its phase shift was expected to be very low and any phase shift observed could be assumed to be due to the heat of conduction.

A more recent study using photoacoustic phase shifts takes the heat of relaxation into account mathematically [126]. The observed phase shift is divided into two components, one due to the V-T relaxation of the gases and the other due to the heat relaxation time defined by:

**Equation 4-26.**

$$\tau_{TR} = \left(\frac{\rho C_v D^2}{10Q}\right)/P$$

where D is the gas density and Q is the thermal conductivity of the gas. To this, a relaxation time due to the microphone ($\tau_{TC}$) is added. The heat relaxation time is then defined as:

**Equation 4-27.**

$$\frac{1}{\tau_T} = \frac{1}{\tau_{TR}} + \frac{1}{\tau_{TC}}$$

From this a correction to the phase shift ($\phi_2$) was calculated using:

**Equation 4-28.**

$$\phi_2 = \arctan(\omega\tau_T P)$$

The corrected phase shift is then fitted to a three level kinetic model, which will not be described here.

### 4.1.3 The use of a Heated Wire reference

The first use of an electrically heated wire in photoacoustic spectroscopy was reported by T.E. Gough *et al.* [134]. In this experiment, the heated wire was used to calibrate the line intensities measured by the photoacoustic instrument. There was no intention to measure the relaxation time. However, even though the purpose of the instrument described here differs from that of the T. E. Gough experiment, the methodology is basically the same. The essential point of both is that a signal generated by a heated wire can mimic a photoacoustic signal. Since the success of the experiment done by T.E Gough *et al.* demonstrates the ability of the heated wire to mimic the photoacoustic signal, it is appropriate to discuss the results here in some detail. It must be noted that the experimental set up in that work was markedly different from what will be presented here. The cell used by T. E. Gough was not designed to take advantage of resonant enhancement of the signal. Basically the cell was a tube with windows on the end for the laser light to pass through. An 18 μm diameter tungsten wire was mounted within the cell, slightly off-axis. The microphone was mounted on the cell wall in the middle of the cell. This difference in position of the wire relative to the position of the laser led to a 15.1% increase in efficiency in producing signal from the wire compared to the laser. It was shown that, for DC heating, the fractional rise in pressure at the cell wall (and hence, at the microphone) is essentially identical for the heated wire and the laser. For a step rise in heating, it was found that the variation in pressure at the walls of the cell could be fitted to an exponential relaxation curve:

**Equation 4-29.**

$$\Delta P(t) = \frac{\alpha P_0}{\kappa}\left(1 - e^{-t/\left(\frac{\beta P_0}{\kappa}\right)}\right)$$

where $\alpha$ and $\beta$ are scaling constants and $\kappa$ is the thermal conductivity of the gas. The time constant for the pressure rise, which determines the frequency response of the system, was found to be identical for the heated wire and the laser. However, the heated wire was 5% more efficient in its conversion of input energy to increase in pressure. The chopping frequency dependence of the pressure changes was found using the Fourier transform of equation 4-27:

**Equation 4-30.**

$$\Delta P(\omega) = \frac{1}{\sqrt{2\pi}} \frac{\left(\frac{\alpha P_0}{\kappa}\right)\left(\frac{\beta P_0}{\kappa}\right)}{1 + \omega^2\left(\frac{\beta P_0}{\kappa}\right)^2}$$

After making corrections for the microphone response, this was found to agree well with experimental results using the heated wire. They applied the use of the hot-wire to an overtone band of acetylene and found that 16.4 mW of electrical power to the wire were needed to mimic the laser induced signal. Taking into account the higher efficiency of the wire in producing signal, they found that this meant that 20.3 mW of laser radiation was absorbed by the sample. Since 13.9 watts of laser power were being used, the absorbance was found to be $1.47 \times 10^{-3}$. From this, the transition dipole moment of $2.58 \times 10^{-4}$ D was calculated which compared well to the value of $2.47 \times 10^{-4}$ D found in previous studies.

The work by T. E. Gough *et al.* has a highly relevant to the project presented here. In fact it is the basis for the project: a signal produced by a heated wire may mimic a pho-

toacoustic signal. This project, however, focuses on the difference between the photoacoustic signal and the heated wire signal. In this project, the interest is in a single step of the process of the acoustic signal production, that is the transfer of energy from the excited media, either the heated wire or the excited molecules. Previous investigations using photoacoustic spectroscopy in the study of V-T relaxation have had to consider factors that could affect the phase of the acoustic wave after the relaxation (Section 4.1.2.1). Since it has been shown that the heated wire signal is essentially the same as the laser induced signal after the relaxation, it can provide a very useful reference. In order to use the wire as a reference, certain assumptions about the transfer of heat must be made. Since the intensity of the signal is not of concern, and anything that affects the signal after the energy transfer is not a concern, then the only thing left is the relaxation time of the wire. This is the equivalent of $\tau$ in the laser induced experiment. Since in either case this will be dependant on the collisional deactivation rate, it is appropriate to refer to Equation 4-1 on page 159. Note there are only two factors: one is the average number of collisions; since a very thin wire is used it is assumed that the number of collisions will be the same or greater than it will be for the excited gas molecules; the other factor, probability of energy transfer, requires more consideration. First, it is assumed that the time between the electric pulse and the heating of the wire is negligible. Therefore, the system that must be considered is a heated wire surrounded by gas. In this case, each collision only has to transfer the heat from the wire (translational energy) to the gas molecule. Here it is assumed that the probability of this occurring is very high in comparison to the situation described in Section 4.1.1.2. If these assumptions are correct, then the relaxation of the wire will be much faster than that of an excited molecule. Therefore, a signal created by a typical photoacoustic experiment will be equiv-

alent to that of a wire with an electric current modulated at the same frequency, except that the photoacoustic experiment will be out of phase with the signal from the wire by an amount proportional to the V-T relaxation time.

### 4.1.4 Helmholtz resonators

The amplification of the signal in the instrument described here depends on the fact that the cell is a Helmholtz resonator. Although a Helmholtz resonator is a very efficient amplifier, it may also cause a great deal of complication in the determination of the phase shifts. This has been made clear by both Rosencwaig [119] and Cottrell [128]. One goal of this project is to determine whether the use of the heated wire can eliminate this problem, since the any shift due to resonance should be the same for both the laser induced signal and the wire induced reference signal. However, a fairly in-depth discussion of Helmholtz resonators is warranted.

There have been a number of papers that have dealt with the theory of Helmholtz resonators. However, none of these have really given a complete characterization of how the amplification of the resonator is affected by the parameters of the experiment. To try to get as complete as possible a view of Helmholtz resonators, several of these papers will be discussed in detail. In general, a Helmholtz resonator is characterized by a cavity with a small open end. The simplest example is a bottle: think of blowing over the top of a bottle to make a sound. Of course, the present experiment is more complicated, as it is a closed system.

The simplest treatment of a Helmholtz cell was presented by Schattka *et al.* [135]. The cell used was fairly typical, consisting of a tube with windows on the ends mounted at the Brewster angle. Near one of the ends was placed a short connecting tube leading to a large cavity. The cavity was assumed to effectively create an open end, leading to the following equation for the resonance frequency [135]:

**Equation 4-31.**

$$\omega = \frac{V_s n}{4l}$$

where $V_s$ is the velocity of sound through the gas, n is any odd number (typically 1) and l is the length of the cell. This equation for the resonance condition of the cell is accurate only for the specific case of the cell that was used. A number of parameters that were not considered are of great importance to the resonant frequency of these types of cells in general cell. However, the paper by Schattka *et al.* [135] does demonstrate the importance of the position of the microphone when longitudinal resonances are used. It was shown that the optimum placement of the microphone is at the opposite end of the cell from the connection between the cavity and the cell. This is due to the fact that, at resonance, a standing wave is established within the cell. It was also shown that the signal strength from a Helmholtz cell increases linearly with pressure, up to the highest pressure tested (700 torr).

There are more general expressions for the resonant frequency of a Helmholtz resonator.The most widely used expression today is probably that proposed by Quimby *et al.* [136].

**Equation 4-32.**

$$\omega = \left( \left( c\left(\frac{A}{l_c V_r}\right)^{\frac{1}{2}} \right)^2 + \left(\frac{4\pi\eta}{\rho A}\right)^2 \right)^{\frac{1}{2}}$$

The first term in this equation is the undamped resonant frequency. This part depends on the speed of sound through the sample (c), the cross-sectional area of the tube connecting

the two compartments of the cell (A), the length of the connecting tube ($l_c$) and the reduced volume ($V_r$) of the cell.

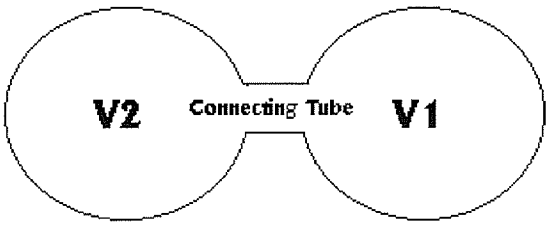


**Figure 4-1.** Simplified diagram of a Helmholtz cell; V1 and V2 represent volumes which can either be the channel through which the laser is passed or the cavity added to produce the Helmholtz resonance.

The reduced volume may be defined referring to Figure 4-1 as:

**Equation 4-33.**

$$V_r = \frac{V1 \times V2}{V1 + V2}$$

Perhaps the most complete treatment of Helmholtz resonance was presented by McClenny *et al.* [137], and is worth in-depth discussion here.

The treatment of McClenny *et al.* [137] uses the equation for a harmonically driven harmonic oscillator:

**Equation 4-34.**

$$\left(\frac{\rho l'}{S}\right)\left(\frac{\partial^2 x}{\partial t^2}\right) + R_a\left(\frac{dx}{dt}\right) + X_a x = P\cos\omega t$$

where x is the product of the cross-sectional area of the connecting tube and the displacement of the gas in the connecting tube, P is the amplitude forcing term (which is the function that defines how the pressure is put into the system) and $R_a$ is the acoustic resistance. The remaining parameters are defined in the following equations:

**Equation 4-35.**

$$X_a = \left[\left(\frac{\rho c^2}{V1}\right) + \left(\frac{\rho c^2}{V2}\right) + X_v\right]$$

**Equation 4-36.**

$$X_v = \left(\left(\frac{2\mu\rho}{\omega}\right)^{\frac{1}{2}} l'\right) / (\pi a^3)$$

**Equation 4-37.**

$$l' = l_c + 1.7a$$

where a is the radius of the connecting tube and $\mu$ is the coefficient of shear viscosity.

The forcing function was defined as

**Equation 4-38.**

$$P(\omega) = A\tau_t / \left(1 + \tau_c \tau_r^{-1}\right)\left[1 + (\omega\tau_t)^2\right]^{\frac{1}{2}} \times \left[1 + \left[\omega\left(\tau_c^{-1} + \tau_r^{-1}\right)^{-1}\right]^2\right]^{\frac{1}{2}}$$

where $\tau_c$, $\tau_r$ and $\tau_t$ are the collisional, radiative and thermal relaxation times respectively. A is a constant determined by the system parameters. Assuming typical values for the relaxation times and modulation frequencies this becomes:

**Equation 4-39.**

$$P(\omega) = \frac{A}{\omega}$$

It is important to note here that, for typical parameters, the forcing function is essentially independent of any of the relaxation times. This is important because it shows that, for longitudinal resonances, the resonant frequency is not dependent on the relaxation times. This fact simplifies the considerations in the project being done here. If there were a dependence between the relaxation and the resonance frequency, then the signal included by the heated

wire would have a different resonant frequency than the laser induced signal, which would cause major complications in analysis. Solving for equations 4-34 and 4-38, McClenny *et al.* [137] found:

**Equation 4-40.**

$$x = P\sin(\omega t - \phi')/(\omega Z_a)$$

**Equation 4-41.**

$$Z_a = (R_a^2 + \chi_a^2)^2$$

**Equation 4-42.**

$$\phi' = \arctan\left(\frac{\chi_a}{R_a}\right)$$

**Equation 4-43.**

$$\chi_a = \frac{1.568\mu^{\frac{1}{2}}\rho^{\frac{1}{2}}l'\omega^{\frac{1}{2}}}{a^3} + \frac{2\rho l'\omega}{a^2} - \frac{0.159\rho c^2}{\omega V'}$$

**Equation 4-44.**

$$R_a = \frac{1.568\mu^{\frac{1}{2}}\rho^{\frac{1}{2}}l'\omega^{\frac{1}{2}}}{a^3}$$

Assuming adiabatic compression, the periodic pressure variation ($P_h$) in the cavity was found to be:

$$P_h = \left(\frac{\gamma P P_0}{\omega Z_a V_2}\right)\sin(\omega t - \phi' - \pi)$$

**Equation 4-45.**

Resonance occurs when $\chi_a$=0.

Thus, although the resonance frequency is dependent on a complex number of factors related to the design of the cell and nature of the gas, it is eventually independent of the relaxation time.

### 4.1.5 Philosophy and assumptions of this project

The purpose of this project wasto build an instrument to measure V-T relaxation time of overtone vibrations. Since photoacoustic spectroscopy is a very useful method of accessing overtone vibrations and can be used for measuring V-T relaxation (Section 4.1.2.1), it lends itself well to such a study. In this project, a new method of referencing the phase shift indicative of the V-T relaxation is investigated. This method is expected to be independent of many factors that affect the phase shift but unrelated to the V-T relaxation, due to the fact that these factors have the same effect on the reference as they do on the laser induced signal. This method involves using an electrically heated wire to mimic the photoacoustic signal free of V-T relaxation (Section 4.1.3). The basic assumption here is that the amount of time it takes for the electrical pulse to cause a pressure wave in the cell is much smaller than the V-T relaxation time of the sample. This is a basic assumption of the design of this instrument and must be tested. Secondly this instrument uses a Helmholtz resonance cell in an attempt to take advantage of the amplification offered by such a cell. In previous experiments, Helmholtz resonance has caused serious problems in measuring phase shifts, as the resonance may cause large phase shifts, that are unrelated to the V-T relaxation of the sample. However, the presence of the heated wire reference should allow the effect of any of these types of phase shifts to be nullified. For this to work, the Helmholtz resonance created by the hot wire must be the same as that created by the laser-driven signal.

# 4.2 Experimental

## 4.2.1 Instrument design

The instrument designed for this project is based on a typical photoacoustic spectrometer. In order to get good signal intensity from overtone vibrations, the sample cell is placed inside a dye laser cavity. A heated wire was incorporated into the cell to be used as a reference. The measurement of interest is the phase shift between a signal induced by the heated wire and that induced by the laser. Hence, the technique describe herein is termed Intra Cavity Laser- Photoacoustic Referenced Phase Shift or ICL-PARPS.

### 4.2.1.1 Instrumental Overview.

A schematic of the ICL-PARPS system is shown in Figure 4-2. A CW

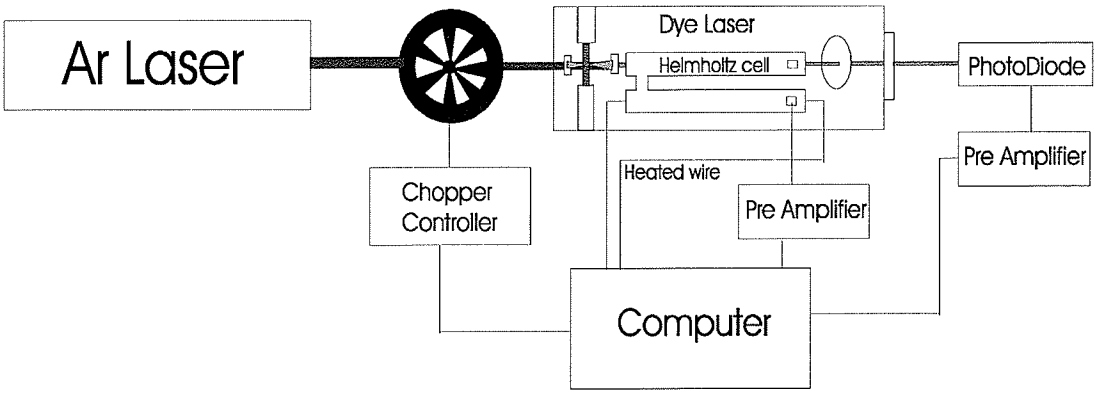


**Figure 4-2.** Schematic of the ICL-PARPS system.

argon ion laser is used to pump the dye laser. Modulation of the laser is achieved via an optical chopper placed between the Argon ion laser and the dye laser. The frequency of the chopper is controlled by a computer running a custom design LabView program (described later). The modulation frequency is chosen to coincide with the resonant frequency of the cell under the conditions of the experiment being done. While in theory one could deter-

mine the resonance frequency from the equations in Section 4.1.4, it is more straight forward to obtain it experimentally by varying the frequency until the largest signal strength is found. The frequency of the radiation is determined by the choice of dye and the birefringent filter. Each dye has a range in which it may lase. The birefringent filter, is used to tune the dye laser to the desired frequency within the dye range. For this experiment, only one frequency of radiation is used at a time. The frequency is chosen before the rest of the experiment is done. The cell is placed within the dye cavity so that the beam travels through the sample. A photo diode is placed in the path of the external beam. This is used as a trigger for the collection of the signal. The photo diode signal is passed through a simple preamplifier before going to the computer, which controls the data collection. The cell has two microphones, one is used to collect the reference signal and the other is used to collect the laser induced signal. Both are passed through a low phase shift pre amplifier.

#### 4.2.1.2 Cell design

The most novel aspects of the ICL-PARPS system are apparent in the design of the cell. This cell design is based on an earlier design made in collaboration with Dr. T. E. Gough.

The symmetry of this cell is of primary importance. It consists of two tubes connected via a thin tube. The cell is filled via a small opening at the center of the connecting tube which leads to a valve. The position of this opening was chosen so as not to affect the symmetry of the cell. The two main tubes are almost exactly the same; they have the same diameter and length. Both tubes have both ends cut at the Brewster angle and both have microphones mounted at the opposite ends from the connecting tube. However, where one side has fused silica windows capping the end, the other has plastic caps with small holes

in the centers. Through these holes a 0.000008 inch diameter wire is strung and the holes are then filled with epoxy. For this cell, depending on which source of energy is being used, one side of the cell will be where the signal is created and the other will act as the cavity. For example if the hot-wire is being used to create the signal, the side with the windows will act as the cavity, and vice versa. Since the cell is symmetric and the gas composition, temperature and pressure will be the same on both sides, in theory the resonance of both sides should be the same.

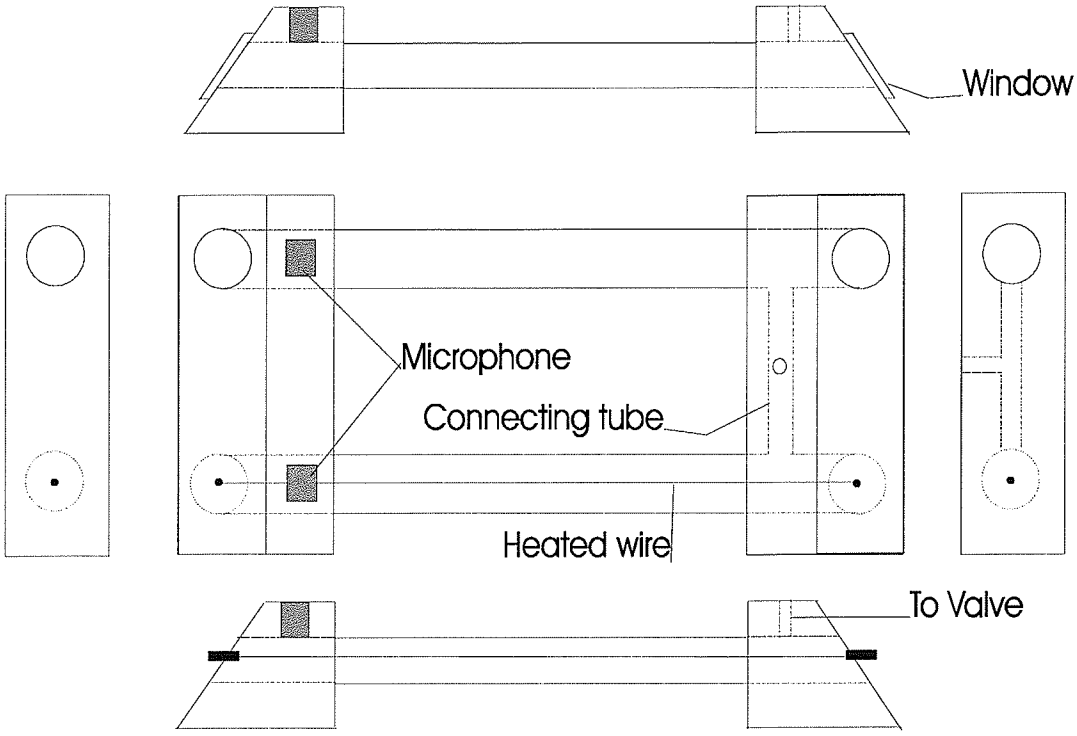


**Figure 4-3.** ICL-PARPS cell design

Since any effects of the resonance on the phase of the signal should manifest themselves in the heated wire signal equally to that of the laser induced signal, the use of the heated wire signal as a reference should account for any resonance effects. Therefore, with this type of

a cell it is possible to take advantage of the amplification of signal offered by resonance while still obtaining an accurate phase shift reading.

### 4.2.2 Computer control and software

The success of this experiment depends upon the control and timing of the data acquisition. This is achieved using a computer equipped with a National Instruments PCI-6052 analog to digital converter controlled by a custom made LabView (version 6.1) pro-ram. Details of the wiring of the instrument and the software may be found in Appendices 2 and 3, respectively.

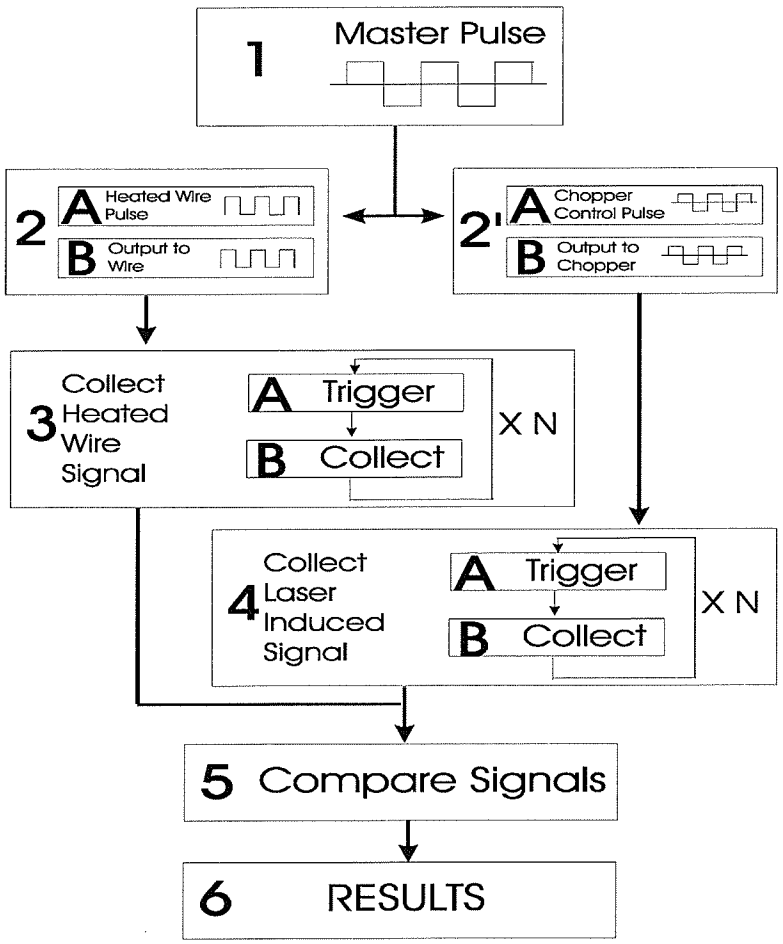


**Figure 4-4.** Flow chart of ICL-PARPS system.

The description of the computer control of the ICL-PARPS system follows the flow chart shown in Figure 4-4; within the description reference is made to the bold numbers given to each step in the flow chart. In so far as possible, these steps are described in the order they appear in the flow chart.

The first function of the software is to create a master pulse that will be used throughout the experiment. (1 in Figure 4-4). The master pulse is a square wave of the desired modulation frequency, which will be used to define the output of the computer. At this stage it is only one second in duration, and has a 50% duty cycle. Since this signal will eventually be converted into a continuous output, an algorithm had to be designed to ensure that the signal would be uniform. In order to accomplish this, the number of points per second used to define the square wave must be a number exactly divisible by the frequency. To accomplish this the number of points per second is defined as 8 times the frequency. At this point (for convenience) the amplitude of the wave is set to be from 1 to -1 volts.

Two copies of the master pulse are then made. The first is used to make the heated wire pulse. (2A in Figure 4-4). This pulse is the same as the Master pulse, except the amplitude is changed from 0 to the desired amplitude (any voltage between 0 and 10 volts). The second copy is used to create the chopper control pulse (2′A in Figure 4-4). This pulse is the same as the master pulse except its amplitude is from -5 to 5 volts. Both pulses are then output continuously through the analog output channels of the PCI-6052 DAQ board. One pulse is output through the tungsten wire (2B in Figure 4-4); the other is output to the chopper control box (2′B in Figure 4-4) which controls the speed of rotation such that the signal from its internal diode matches the chopper control pulse. Thus, the chopping frequency

and the electrical pulses that go through the tungsten wire have the same frequency and phase. However, there are a couple of complicating factors involving the chopper.

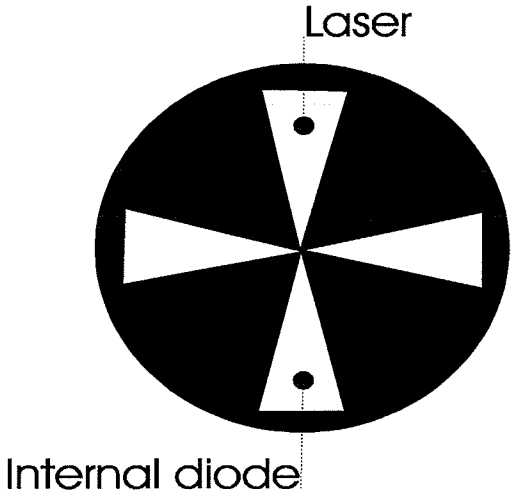


**Figure 4-5.** Schematic drawing of how the internal diode and laser would have to be positioned for perfect phase alignment to be possible. Both must be exactly at the center of a opening in the chopper disk at the same time.

The first is that the signal of the internal diode of the optical chopper is not necessarily in phase with the resulting laser pulses that pass through the cell. This is because it is difficult to ensure that the beam passes through the chopping disk at a point exactly across from the point where the disk passes across the diode (see Figure 4-5). The phase alignment in this manner is very difficult, though technically possible. (A simpler solution to this problem is discussed later.) The second problem is that the speed of the chopper is being continually changed to try to match the phase of the chopper control pulse; this leads to the result that at any given time the phase may actually be slightly off the phase of the control pulse, in one direction or the other. However, on *average,* the signal will be exactly in phase.

Once the optical chopper and the heated wire have the appropriate signals, data collection may begin. Since it takes some time for the chopper to come up to speed and match that of the chopper control pulse, the heated wire reference signal is collected first. During

this portion of the experiment the pump laser is blocked so that only signal due to the heated wire is measured. In order to ensure reliable phase data the collection of data must start on the rising edge of the pulse. To accomplish this, the heated wire voltage is fed through a trigger channel of the PCI-6052 DAQ board, which monitors the heated wire pulse and triggers collection on the rising edge (3A in Figure 4-4). The collection parameters are very important, the sampling rate and buffer size must be chosen carefully. Though the incoming frequency is analog, it is converted to digital data by the DAQ board which samples the analog signal at distinct intervals defined by the sampling frequency. The sampling frequency must be greater than the Nyquist frequency, or twice the modulation frequency. For this experiment, a sampling frequency much higher than the modulation frequency is desired, as otherwise the phase information will be lost. Generally, a sampling frequency of 100 kHz is adequate, since in most of the experiments done for this project use modulation frequencies below 1000 Hz, therefore each cycle has more then 100 points to define it. This is enough to reliably get phase data. Higher frequencies are possible, but they use up large amounts of the system resources and may significantly slow down the experiment. The buffer size is also of importance. Since the signal will eventually be fitted to a sinusoidal function to determine the phase, a larger buffer is preferable, as this gives a larger section of wave to fit. However, a large buffer may also take up a lot of memory resources and once the memory resources are depleted, the collection will necessarily be halted. Generally, a 3000 point buffer gives an adequate length of signal for a reliable fit and does not deplete the memory resources, as long as the modulation frequency is significantly higher than 3 Hz (which it always is in this experimental arrangement). The length of collection is defined by the sampling frequency and the buffer size: for a sampling frequency of 100000

Hz and a buffer size of 3000 points, the collection time would be 0.03 seconds (3B in Figure 4-4). In order to get a good signal to noise ratio, it is beneficial to co-add a number of scans. For this reason step 3 is repeated and the results from each repeat unit are added together (3 in Figure 4-4). Generally, a sum of 1000 scans has been found to be the best compromise between signal to noise ratio and the time required to run the experiment. For strong signals, this can be reduced to save time, while for weak signals, more scans can be added to achieve better signal to noise ratio.

Once the signal from the heated reference wire is collected, the wire is disconnected from the cell and the pump laser is unblocked. The data collection procedure for the laser induced signal (4 in Figure 4-4) is virtually the same as that for the heated reference wire, except for the trigger (4A in Figure 4-4). The trigger used for the collection of the laser induced signal comes from a photo diode placed at the output of the dye laser (see Figure 4-2 on page 184). This diode has a response time of 6 ns, much faster than the V-T relaxation. This diode allows the collection to be triggered at the beginning of each laser pulse through the cell. In this way, both the heated wire reference and the laser induced signal begin collection at the rising edge of a pulse. Because of each collection is trigger on the rising edge, it is not important that the modulation of the laser and the wire be exactly in phase.

Once the signal from the reference wire and the laser induced signal are collected, both are fitted to sinusoidal functions. This gives the phase, frequency and amplitude of each signal. The results of the fitting are then compared, and the difference between the phase of the reference wire and the laser induced signal is found (5 in Figure 4-4 on page 187). Finally, using Equation 4-25 on page 171, the relaxation time is calculated.

### 4.2.3 Samples and Laser Frequencies

Several different experiments were performed in order to test the ICL-PARPS system. Data were collected for trimethyl amine (Matheson of Canada Limited) and methane (Matheson of Canada Limited). For gas mixture experiments, Argon (Praxair) was used. Laser frequencies were chosen to fall on overtone absorption bands. For trimethyl amine, three frequencies were used, one at 14612 $cm^{-1}$, which falls the |0,0>|6> band; one at 15782 $cm^{-1}$, which falls within the |6,0>|0> band; and one at 16540 $cm^{-1}$, which falls within the |0,0>|7> band. The first two frequencies fall within the range of DCM dye, and the thrid falls in the range of the rhodamine 6G laser dye. Readings of several mixtures of trimethyl amine and Argon were taken at 14612 $cm^{-1}$. Several readings were also taken at a number of different pressures. For methane, the laser frequency was set to 16169 $cm^{-1}$, which is in the range of the rhodamine 6G laser dye. Again multiple readings were taken at a number of pressures.

## 4.3 Results

### 4.3.1 Tests of assumptions

Two major assumptions had to be tested: the assumption that the heat transfer of the heated wire is much faster than the V-T relaxation time and the assumption that both sides of the cell (one containing a wire, the other for the laser beam) have the same resonance including the same phase shift due to resonance.

#### 4.3.1.1 Hot-wire heat transfer

With the equipment available, it wasnot possible to get a quantitative measurement of the rate of heat transfer from the wire to the gas. However, it waspossible to determine a lower limit to the transfer rate. If the wire does not reach thermal equilibrium with the gas within half a cycle, then the wire will gain more heat before the original heat has been dissipated. In this scenario, the wire will constantly be transferring energy to the gas, the gas temperature will never decrease and no sound wave will be formed. Instead the most likely thing to happen is that the gas and the wire will simply continue to get hotter and hotter untill the wire is vaporized. To describe this using an analogy, consider an hour glass with an open top, such that more sand can be added at various intervals. The sand represents the heat energy; the top compartment of the hourglass, the wire; and the bottom compartment, the gas. The center constriction represents the rate at which the energy can be transferred. Now assume that sand is dropped into the top compartment in discrete amounts and regular intervals. If the constriction is wide enough so that all the sand in each discrete amount can pass from the top to the bottom before the next portion of sand is dropped, the sand will fall in pulses into the bottom level. This is analogous to the sound wave measured in the PAS

experiment. If the constriction is so narrow that not all of the sand makes it to the bottom compartment between the intervals, then the sand will build up in the top and the flow of sand to the bottom will be a constant stream. If we consider an analogous situation in the wire, the gases will get hotter and hotter with no oscillating pattern and therefore no signal will be measured. Following this theory, in principle, it should be possible to increase the the modulation frequency of the signal applied to the wire until no signal is observed from the microphone. At the point where no signal is observed, the time required to transfer one pulse of energy will be approximately half the wavelength of the modulation. The highest modulation frequency that the ICL-PARPS system can achieve for the heated wire is 50 kHz. The signal recorded for a 50 kHz modulation frequency is shown in Figure 4-6. At high frequencies, skin effects could cause the heat to be localized at the outer surfaces of the wire, however even at 50 kHz, for the thin wire that used here, skin effects are not an issue.

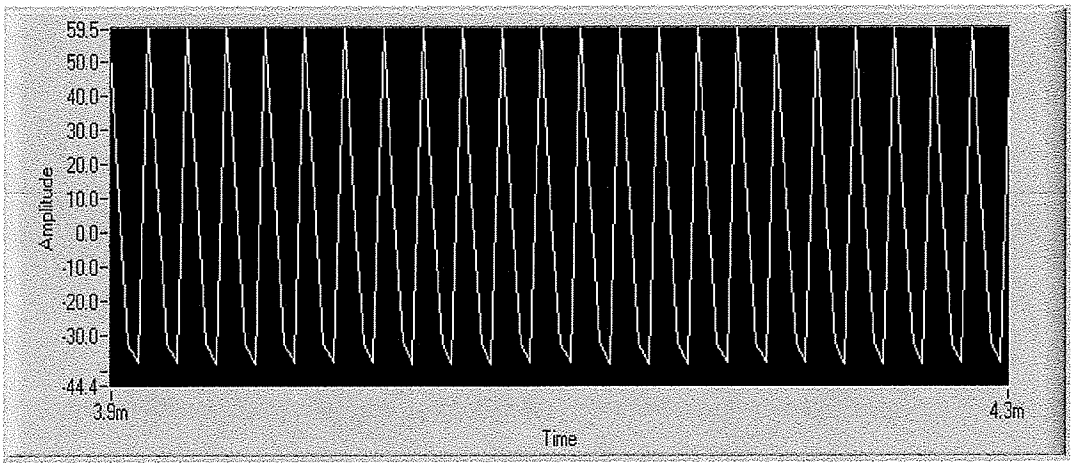


**Figure 4-6.** Signal recorded using heated wire at a modulation frequency of 50 khz. the cell filled with 700 torr of trimethyl amine. The observed parameters are frequency 50 khz, amplitude 52.129 and the phase was 62.601 degrees.

The scan rate used was 200 kHz, thus the waveform is very sharp. Though a scan rate of 330 kHz is possible, the combination of scanning and outputting a pulse at such high rates caused problems in the system. However, since a signal is produced and the length of a cycle is $2 \times 10^{-5}$ seconds, the time required for the dissipation of heat from the wire to the gas must be less than $1 \times 10^{-5}$ seconds.

#### 4.3.1.2 Equivalence of Resonance

Due to the symmetry of the cell, the resonance frequency of both sides should be the same. However, any difference between sides of the cell may cause measurable differences in the resonances. Fortunately this can easily be checked by replacing the windows on the laser channel side with a second wire. The results of these tests are shown in Table 4-1.

**Table 4-1.** Test of equivalence of resonances of the two sides of the cell

| Side #1 | | | Side #2 | | | Phase |
|---|---|---|---|---|---|---|
| Frequency | Amplitude | Phase | Frequency | Amplitude | Phase | difference |
| 560.036 | 11.536 | 266.061 | 560.036 | 11.792 | 266.829 | 0.768 |
| 560.035 | 11.516 | 265.943 | 560.036 | 11.935 | 266.650 | 0.707 |
| 560.037 | 11.543 | 265.978 | 560.036 | 11.671 | 266.907 | 0.929 |
| 560.036 | 11.482 | 265.689 | 560.036 | 11.743 | 266.819 | 1.13 |

From these results, it is evident that there is little difference between the two sides of the cell. The phase difference between readings on each side is consistently around 1 degree. Some difference is to be expected, since the reading depends on fitting the signal to a function and noise will introduce some variability. However, it does seem that the phase of the second side (the laser channel) is consistently higher. Also, this side seems to consistently have greater amplitude. This could indicate some minor instrumental non equivalence, such as a slight difference in microphone sensitivities. As shown later, this difference is not significant compared to the results in the V-T experiments.

#### 4.3.1.3 The effect of voltage through the wire

The next experiment is designed to test whether the voltage passed through the wire will have an effect on the phase shift observed. If the voltage of the wire has an effect on the shift, then, for each experiment, the signal amplitude between the wire and the laser

would have to be matched. If the phase difference is constant then the highest voltage and hence the highest signal can always be used. In this test the voltage sent through the wire was varied while all the other parameters were kept constant. The results are shown in Table 4-2. This test was done on a sample of 700.05 torr of trimethyl amine. Note that, for clarity, the negatives of the observed phases are used; this is because the Labview software reports a phase lead as a positive and a phase shift as a negative, which is the opposite of how I wish to consider them.

**Table 4-2.** Effect of wire voltage

| Heated Reference Wire | | | | Laser induced | | | Phase Difference |
|---|---|---|---|---|---|---|---|
| Voltage | Frequency | Amplitude | Phase | Frequency | Amplitude | Phase | |
| 10.00 | 345.02 | 59.31 | 24.63 | 345.05 | 14.74 | -26.46 | -51.08 |
| 1.00 | 345.02 | 40.99 | 22.94 | 345.02 | 18.24 | -29.45 | -52.40 |
| 0.7 | 345.02 | 21.36 | 19.79 | 345.02 | 19.34 | -32.30 | -52.10 |
| 0.5 | 345.02 | 11.10 | 20.79 | 345.02 | 18.86 | -30.49 | -51.29 |

From this data, it is evident that the amplitude of the wire signal is not linear with voltage. This is not surprising as the amount of energy in the wire is dependent on the amperage and the resistance of the wire (not directly on voltage), and the resistance of the wire is dependent on temperature. In the rest of the experiments, the maximum voltage will always be used to ensure the maximum signal.

Some variation is observed in the phase of the wire signal, however, this seems to be unrelated to the voltage. The phase of the reading at 0.7 volts is lower than at either 0.5 or 1.0 volts. It is important to note that the laser induced signal has a phase that varies in a manner that mimics that of the heated wire signal; as a result, the phase difference remains relatively constant. Since the laser parameters are kept constant and the two signals are essentially independent of each other, the variation of the laser induced signal is somewhat

surprising. The only explanation is that some conditions which are common to both must be changing. There are two possibilities evident. The first is that the cell has a slow leak which causes the pressure to rise throughout the experiment. Since the 0.5 volt experiment was done before the 0.7 volt experiment, this is entirely consistent with the observations. However, the fact that no leaks were found in the cell does not preclude this possibility as a very slow leak would be very difficult to detect. Another possibility is that the average temperature within the cell changes, which would also affect the pressure in the cell. Either explanation is possible. Unfortunately there are not enough data to determine which explanation is true. It is noted however that the changes are essentially equal for both the signal induced by the heated wire and by the laser, which shows that the reference wire is acting as intended, and accounting for changes in the cell conditions. Some concern does remain because the laser induced signal readings are always taken after that of the reference wire which may lead to an instrument-induced over estimation of the phase shift. Since this would be dependent on the time between the readings, it is impossible to account for with the current design. Returning to the reason these readings were taken, it is clear that the phase of the heated wire signal is independent of voltage, therefore, constantly using the highest possible voltage is an acceptable course of action.

## 4.3.2 Experiments

Several experiments have been performed using this system. As explained the desired result is the phase difference between the sound waves induced by the laser and by the heated wire. The raw data are in the form of two waves; since the actual waves are generally not instructive on their own, only one example is shown (see Figure 4-7). All of the raw data take this form.

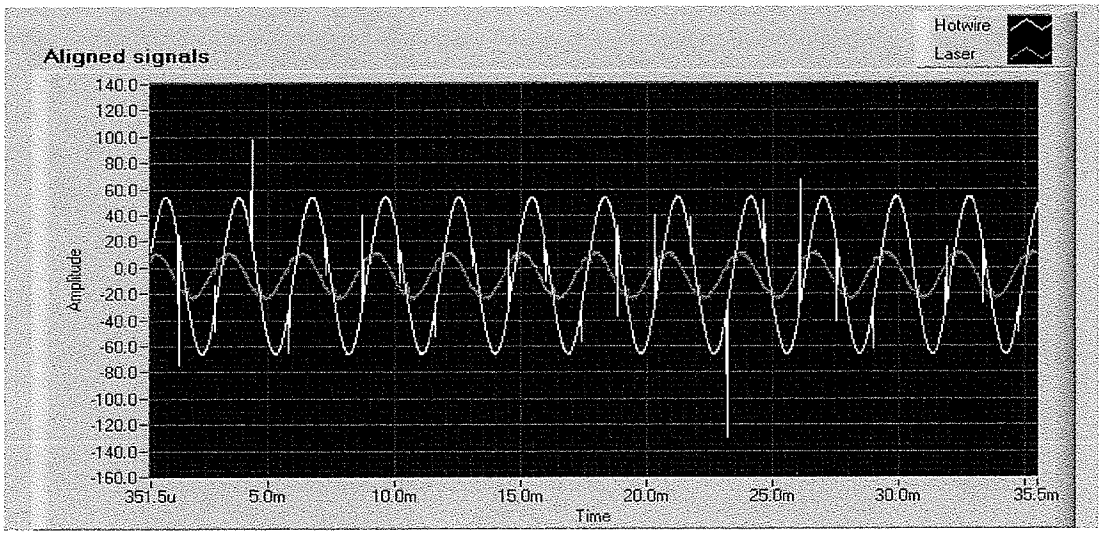


**Figure 4-7.** Signal for 700.5 torr of trimethyl amine, modulation frequency 345.00 hz. The white trace is the signal produced by the heated wire, and the red trace is the signal produced by the laser

These waves are fitted to a sine wave from which the frequency, amplitude and phase are determined.

### 4.3.2.1 Trimethyl amine

The majority of the tests done were on trimethyl amine. Trimethyl amine was of interest because of its two well separated CH stretching overtone vibrations. The first transition studied was the |0,0>|6> band at 14612 $cm^{-1}$. Multiple readings were taken at a

number of pressures. The results are shown in Table 4-3. For analysis the average of phase

**Table 4-3.** Data for the |0,0>|6> band of trimethyl amine

| Pressure (torr) | Heated Wire | | | Laser induced | | | Phase difference (deg) | Relaxation time ($10^{-4}$ sec) |
|---|---|---|---|---|---|---|---|---|
| | Frequency ($cm^{-1}$) | Amplitude | Phase Lag (deg) | Frequency ($cm^{-1}$) | Amplitude | Phase Lag (deg) | | |
| 207.50 | 346.98 | 18.57 | 40.85 | 346.98 | 4.23 | -27.89 | -68.74 | -3.22 |
| 207.50 | 346.98 | 17.57 | 31.34 | 346.97 | 2.06 | -40.70 | -72.03 | -3.86 |
| 247.00 | 355.02 | 25.51 | 49.65 | 354.41 | 4.23 | 5.22 | -44.44 | -1.43 |
| 247.00 | 355.02 | 25.21 | 40.85 | 355.22 | 5.33 | -12.96 | -53.81 | -1.99 |
| 247.00 | 355.02 | 19.42 | 11.00 | 355.01 | 5.44 | -54.48 | -65.49 | -3.20 |
| 333.30 | 346.98 | 26.35 | 43.13 | 346.99 | 5.47 | -22.92 | -66.05 | -4.53 |
| 333.30 | 346.98 | 26.95 | 33.85 | 346.99 | 4.12 | -28.55 | -62.40 | -3.85 |
| 355.00 | 354.01 | 30.73 | 24.50 | 354.14 | 5.37 | -4.63 | -29.14 | -1.17 |
| 355.00 | 354.01 | 29.60 | 17.41 | 354.12 | 5.88 | -25.56 | -42.96 | -1.96 |
| 355.00 | 353.01 | 26.50 | 7.11 | 353.24 | 3.05 | -29.39 | -36.50 | -1.56 |
| 453.00 | 346.98 | 35.84 | 8.48 | 346.98 | 4.65 | -47.08 | -55.56 | -3.99 |
| 453.00 | 346.98 | 35.13 | 5.39 | 346.99 | 3.64 | -52.30 | -57.69 | -4.32 |
| 577.00 | 346.98 | 51.50 | 20.69 | 347.02 | 9.60 | -34.94 | -55.63 | -5.09 |
| 700.50 | 345.02 | 59.31 | 24.63 | 345.05 | 14.74 | -26.46 | -51.08 | -5.27 |

readings at the same pressure will be used.

The last column of Table 4-3 represents an estimate of the relaxation time at 1 atmosphere calculated using Equation 4-25 on page 171; this is only an estimate more reliable values are derived later. As shown later, these values do not reflect the actual relaxation times; they were used only to follow the operation of the instrument so that major instrumental failures could be detected. However, this set of data points is less precise than desirable with an average value of $-3.25 \pm 1.17 \times 10^{-4}$ sec. At this point the cause of the variation in the results is unclear.

Data were also collected for the |6,0>|0> band of trimethyl amine found at 15782 $cm^{-1}$. (See Table 4-4)

**Table 4-4.** Data for the |6,0>|0> band of trimethyl amine.

| Pressure (torr) | Heated Wire | | | Laser induced | | | Phase difference (deg) | Relaxation time ($10^{-4}$ sec) |
|---|---|---|---|---|---|---|---|---|
| | Frequency ($cm^{-1}$) | Amplitude | Phase Lag (deg) | Frequency ($cm^{-1}$) | Amplitude | Phase Lag (deg) | | |
| 308.9 | 384.97 | 16.97 | 15.81 | 384.97 | 52.19 | -49.95 | -65.76 | -3.73 |
| 308.9 | 384.97 | 16.26 | 10.64 | 384.97 | 48.87 | -52.88 | -63.53 | -3.37 |
| 308.9 | 384.97 | 15.47 | 8.07 | 384.97 | 50.91 | -56.51 | -64.57 | -3.53 |
| 402.00 | 364.01 | 23.22 | 20.51 | 364.01 | 80.72 | -42.66 | -63.17 | -4.57 |
| 402.00 | 364.01 | 20.84 | 8.79 | 364.01 | 73.97 | -52.83 | -61.61 | -4.28 |
| 402.00 | 364.01 | 19.16 | 2.37 | 364.01 | 69.91 | -58.41 | -60.78 | -4.13 |
| 501.50 | 347.97 | 27.40 | 14.09 | 348.00 | 116.38 | -38.81 | -52.90 | -3.99 |
| 501.50 | 348.00 | 29.69 | 11.42 | 348.00 | 98.97 | -42.07 | -53.49 | -4.08 |
| 501.50 | 348.00 | 29.15 | 9.36 | 348.00 | 99.60 | -45.45 | -54.81 | -4.28 |
| 602.00 | 340.00 | 34.03 | 28.98 | 339.99 | 96.30 | -23.06 | -52.04 | -4.75 |
| 602.00 | 340.00 | 33.75 | 25.47 | 340.00 | 97.44 | -25.49 | -50.96 | -4.57 |
| 602.00 | 340.00 | 33.43 | 22.94 | 340.0 | 57.47 | -28.47 | -51.44 | -4.65 |

The results observed for the |6,0>|0> band of trimethyl amine are more consistent than those of the |0,0>|6> band ($-4.16\pm0.36 \times 10^{-4}$ sec) and is likely due to the increased signal intensity achieved by the stronger absorption of that band.

Results were also collected for the |0,0>|7> band of trimethyl amine. Since this is at the sixth overtone, this band is very weak. There is some concern therefore that the signal collected may be due to noise rather than the actual band absorption. However, the signal was strong enough that it seemed reasonable to assume that an absorption was present. The results are shown in Table 4-5.

**Table 4-5.** Data for the |0,0>|7> band of trimethyl amine.

| Pressure (torr) | Heated Wire | | | Laser induced | | | Phase difference (deg) | Relaxation time ($10^{-4}$ sec) |
|---|---|---|---|---|---|---|---|---|
| | Frequency ($cm^{-1}$) | Amplitude | Phase lag (deg) | Frequency ($cm^{-1}$) | Amplitude | Phase lag (deg) | | |
| 104.30 | 360.06 | 8.49 | 37.20 | 359.60 | 1.28 | -40.52 | -77.72 | -2.79 |
| 114.00 | 360.07 | 7.90 | 29.76 | 369.70 | 0.94 | -45.60 | -75.36 | -2.54 |
| 114.00 | 360.09 | 7.34 | 24.02 | 359.66 | 0.83 | -52.71 | -76.72 | -2.81 |
| 212.70 | 352.08 | 14.65 | 60.07 | 352.01 | 2.37 | 5.05 | -55.02 | -1.81 |
| 212.70 | 352.10 | 14.53 | 47.56 | 351.77 | 2.27 | -11.86 | -59.42 | -2.14 |
| 212.70 | 352.11 | 14.25 | 41.88 | 351.71 | 2.30 | -19.02 | -60.90 | -2.28 |
| 314.00 | 349.92 | 19.75 | 41.24 | 350.15 | 2.66 | -15.76 | -57.00 | -2.89 |
| 314.00 | 349.91 | 19.54 | 32.62 | 350.00 | 3.25 | -24.18 | -56.80 | -2.87 |
| 314.00 | 349.91 | 19.03 | 27.80 | 350.06 | 3.34 | -31.29 | -59.08 | -3.14 |
| 314.00 | 343.99 | 25.01 | 33.23 | 344.16 | 8.69 | -20.23 | -53.46 | -2.58 |
| 314.00 | 344.00 | 24.94 | 28.02 | 344.00 | 9.22 | -24.89 | -52.91 | -2.53 |
| 314.00 | 343.98 | 24.36 | 24.02 | 344.06 | 8.58 | -28.36 | -52.37 | -2.48 |
| 314.00 | 343.97 | 24.14 | 21.35 | 344.09 | 8.06 | -30.76 | -52.13 | -2.46 |
| 414.40 | 344.98 | 25.09 | 44.22 | 345.04 | 7.29 | -8.56 | -52.80 | -3.31 |
| 404.40 | 343.77 | 26.02 | 41.21 | 344.04 | 9.62 | -21.55 | -62.76 | -4.78 |
| 404.40 | 343.99 | 26.18 | 31.98 | 344.09 | 8.66 | -25.43 | -57.41 | -3.85 |
| 404.40 | 343.97 | 25.81 | 26.78 | 344.00 | 8.49 | -31.16 | -57.94 | -3.93 |
| 404.40 | 343.97 | 25.26 | 22.82 | 344.00 | 8.47 | -35.68 | -58.50 | -4.02 |
| 404.40 | 343.96 | 23.06 | 13.15 | 343.97 | 8.57 | -46.11 | -59.25 | -4.14 |
| 508.60 | 343.96 | 29.94 | 38.83 | 344.02 | 11.14 | -16.34 | -55.17 | -4.45 |
| 508.60 | 343.96 | 30.89 | 33.92 | 343.96 | 10.48 | -19.95 | -53.87 | -4.24 |
| 508.60 | 343.96 | 31.05 | 31.85 | 343.96 | 8.65 | -22.10 | -53.95 | -4.25 |
| 605.40 | 342.98 | 37.90 | 36.34 | 342.99 | 9.20 | -14.96 | -51.30 | -4.61 |
| 605.40 | 342.98 | 38.14 | 33.11 | 343.02 | 9.04 | -17.29 | -50.40 | -4.47 |
| 605.40 | 342.98 | 37.93 | 31.82 | 342.98 | 7.92 | -20.34 | -52.16 | -4.76 |

#### 4.3.2.2 Trimethyl amine- Argon mixtures

The presence of a buffer gas can have a very large effect on the V-T relaxation time; however this effect would not be expected to be the same for wire as it would for the relaxation of excited molecules. In this section, readings taken for different mixtures of Argon

gas and trimethyl amine are reported. At 433 torr the estimated relaxation time values are

**Table 4-6.** Data for the |6,0>|0> band of trimethyl amine mixed with Argon in various ratios.

| Pressure (torr) | | Heated Wire | | | Laser induced | | | Phase diff. (deg) | Relaxation time ($10^{-4}$ sec) |
|---|---|---|---|---|---|---|---|---|---|
| TMA | Ar | Frequency ($cm^{-1}$) | Amplitude | Phase (deg) | Frequency ($cm^{-1}$) | Amplitude | Phase (deg) | | |
| 596.00 | 111.00 | 403.03 | 27.03 | 71.17 | 403.04 | 12.87 | 5.22 | -65.95 | -8.23 |
| 596.00 | 111.00 | 403.03 | 29.90 | 43.34 | 403.03 | 6.87 | -26.25 | -69.59 | -9.87 |
| 596.00 | 111.00 | 403.03 | 30.40 | 42.11 | 403.03 | -24.75 | -66.86 | -66.86 | -8.59 |
| 514.60 | 202.00 | 445.00 | 24.39 | 67.06 | 445.00 | 8.15 | -4.85 | -71.91 | -10.2 |
| 514.60 | 202.00 | 445.00 | 25.28 | 66.70 | 444.99 | 6.33 | -4.06 | -70.76 | -9.53 |
| 514.60 | 202.00 | 445.00 | 25.29 | 66.75 | 445.00 | 6.29 | -1.52 | -68.27 | -8.35 |
| 402.00 | 305.00 | 350.98 | 51.18 | 36.23 | 350.98 | 21.77 | -16.14 | -52.38 | -5.47 |
| 402.00 | 305.00 | 350.98 | 53.08 | 34.77 | 350.98 | 26.22 | -17.39 | -52.16 | -5.43 |
| 402.00 | 305.00 | 350.98 | 53.79 | 34.40 | 350.97 | 22.07 | -18.99 | -53.39 | -5.68 |
| 506.00 | 259.00 | 342.00 | 67.74 | 25.60 | 342.00 | 17.83 | -27.92 | -53.52 | -6.33 |
| 506.00 | 259.00 | 342.00 | 68.21 | 24.78 | 342.00 | 18.82 | -27.80 | -52.58 | -6.12 |
| 506.00 | 259.00 | 342.00 | 68.52 | 24.88 | 342.00 | 18.09 | -27.26 | -52.14 | -6.03 |
| 433.00 | 318.80 | 342.98 | 66.27 | 26.01 | 342.99 | 13.93 | -71.50 | -97.50 | 34.9 |
| 433.00 | 318.80 | 342.98 | 68.25 | 24.72 | 342.98 | 6.39 | -69.64 | -94.36 | 60.3 |
| 433.00 | 318.80 | 342.98 | 71.81 | 27.44 | 342.98 | 16.36 | -72.00 | -99.44 | 27.6 |
| 306.40 | 424.20 | 349.99 | 58.17 | 25.28 | 349.99 | 10.13 | -35.51 | -60.79 | -7.82 |
| 306.40 | 424.20 | 349.99 | 59.26 | 24.39 | 350.00 | 12.43 | -31.98 | -56.38 | -6.57 |
| 306.40 | 424.20 | 349.99 | 58.26 | 23.56 | 349.99 | 9.42 | -33.84 | -57.40 | -6.84 |
| 202.10 | 519.20 | 367.00 | 43.91 | 36.19 | 367.01 | 7.91 | -31.27 | -67.45 | -9.91 |
| 202.10 | 519.20 | 367.00 | 44.09 | 35.11 | 367.00 | 11.29 | -26.27 | -61.39 | -7.54 |
| 202.10 | 519.20 | 367.00 | 44.10 | 34.32 | 367.01 | 8.96 | -29.92 | -64.24 | -8.53 |

large and positive, compared to the rest which are negative. These numbers are not inconsistent with the rest, they appear that way because this way of treating the data is incorrect, as will be shown later.

#### 4.3.2.3 Methane

Since methane is a very simple molecule that has been extensively studied, a set of readings were taken for various pressures at the 16169 $cm^{-1}$ band of methane. The 16169 $cm^{-1}$ band was the only prominent methane band that fell in a region accessible with the available laser dyes and optics.

**Table 4-7.** Data for the 16169 $cm^{-1}$ band of methane

| Pressure (torr) | Heated Wire | | | Laser induced | | | Phase difference (deg) | Relaxation time ($10^{-4}$ sec) |
|---|---|---|---|---|---|---|---|---|
| | Frequency ($cm^{-1}$) | Amplitude | Phase (deg) | Frequency ($cm^{-1}$) | Amplitude | Phase (deg) | | |
| 698.50 | 674.94 | 9.92 | 84.83 | 675.08 | 2.81 | 3.39 | -81.45 | -14.4 |
| 698.50 | 674.93 | 10.00 | 85.13 | 675.09 | 4.34 | 6.67 | -78.47 | -10.6 |
| 698.50 | 674.93 | 9.98 | 85.20 | 674.66 | 2.76 | 1.57 | -83.63 | -19.4 |
| 698.50 | 674.93 | 9.94 | 85.55 | 675.04 | 1.85 | 0.93 | -84.62 | -23.0 |
| 698.50 | 674.94 | 9.96 | 86.00 | 674.76 | 2.16 | 1.47 | -84.52 | -22.6 |
| 698.50 | 674.94 | 9.93 | 86.37 | 673.60 | 1.65 | -8.19 | -94.56 | -27.2 |
| 598.50 | 690.03 | 9.35 | 69.21 | 689.93 | 4.02 | -12.97 | -82.18 | -15.5 |
| 598.50 | 690.03 | 9.20 | 80.76 | 689.61 | 5.66 | 1.49 | -79.27 | -11.2 |
| 598.50 | 690.01 | 9.22 | 80.69 | 689.73 | 6.70 | 2.74 | -77.95 | -9.94 |
| 502.50 | 672.94 | 9.75 | 72.75 | 672.93 | 3.63 | -5.19 | -77.95 | -7.32 |
| 502.50 | 672.95 | 9.81 | 73.24 | 672.89 | 5.76 | -3.34 | -76.58 | -6.55 |
| 502.50 | 672.94 | 9.74 | 73.49 | 672.90 | 3.89 | -4.13 | -77.62 | -7.12 |
| 392.60 | 615.01 | 11.00 | 72.02 | 614.94 | 3.96 | -6.40 | -78.43 | -6.53 |
| 392.80 | 615.02 | 10.06 | 55.94 | 614.86 | 3.60 | -29.37 | -85.31 | -16.3 |
| 392.80 | 615.01 | 10.26 | 56.14 | 615.03 | 3.45 | -28.78 | -84.92 | -15.1 |
| 392.80 | 615.01 | 10.26 | 56.31 | 614.98 | 3.59 | -28.19 | -84.50 | -13.9 |
| 298.00 | 603.00 | 9.65 | 92.92 | 602.82 | 3.27 | 9.85 | -83.07 | -8.52 |
| 298.00 | 602.99 | 9.85 | 92.34 | 602.96 | 2.65 | 9.19 | -83.14 | -8.61 |
| 298.00 | 603.00 | 10.12 | 91.59 | 602.95 | 2.21 | 8.63 | -82.96 | -8.38 |

## 4.4 Discussion

In the results section, the estimated relaxation times at one atmosphere are almost all negative. Even though these are just estimates, the negative values are physically impossible. From these results, it must be concluded that the equation used to get these estimates from the phase difference:

**Equation 4-46.**

$$\tau = \frac{\tan(\phi)}{2\pi\omega}$$

was incorrect. There are three other theories that can be applied to the data, to try to provide a better explanation of the results. These are presented in the following subsections; in each, averages of the phases for repeated trials of the same pressure will be analyzed using a different theory. The results are analyzed to determine which theory is the most consistent with the expected trends. In each of the following subsections, values for relaxation time at each pressure based on the theory being tested are plotted against inverse pressure. These values are referred to as the nominal relaxation time ($\tau_n$). Linear regression analysis is used to determine the relaxtion time at one atmosphere for each case, however, since it is not known which theory is correct, these are called apparent relaxation times ($\tau_a$).

### 4.4.1 Case 1: Heat transfer of the wire slower than V-T relaxation

The first method of analysis considers the heat transfer from the wire being slower than the V-T relaxation time. For this method to be reasonable, the statements of Section 4.3.1.1 must be discounted. This is not unreasonable, if the assumption is made that with each pulse the temperature of the wire rises and along with it the rate of energy transfer to the gas. In this scenario, the pressure in the cell would oscillate as would the temperature

of the wire. However, the average temperature of the wire would steadily increase eventually resulting in the wire vaporizing. However, if the temperature increments involved are low enough then the time before the wire actually burns may be much longer than the time needed for the experiment.

Since the modulation frequency changes with changing pressure, a plot of the phase lag against the inverse of pressure is not useful for linear regression. Instead the nominal relaxation time ($\tau_n$) defined by:

**Equation 4-47.**

$$\tau_n = \frac{\tan(\phi)}{2\pi\omega}$$

plotted against the inverse of the pressure in atmospheres and using these plots in the linear regression analysis, the slope gives time difference between the heated wire and the laser induced signal at one atmosphere. If the theories behind this method of analysis are correct then this value would be $\tau_c$. However, without further analysis it is not clear which of the theories used to analyze the data is correct, hence, it would be inappropriate to refer to any of them as relaxation times.

The plot of the nominal relaxation time against the inverse pressure in atmospheres for the $|0,0>|6>$ (14612 $cm^{-1}$) mode of trimethyl amine is shown in Figure 4-8.

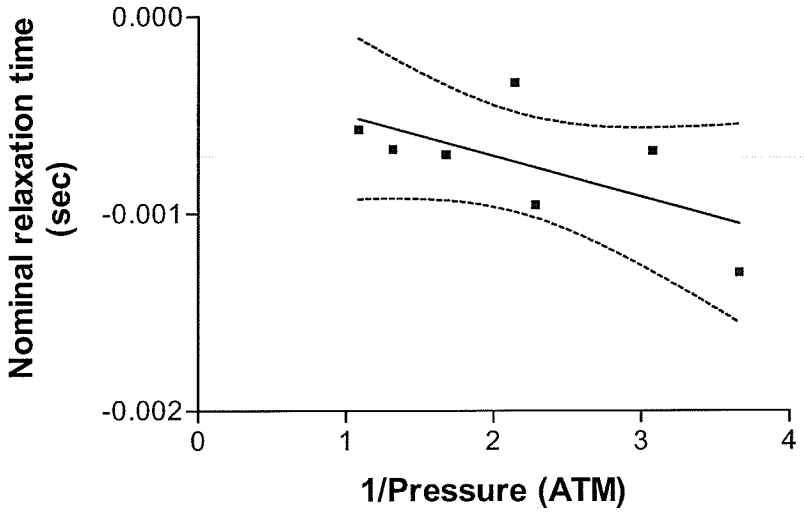


**Figure 4-8.** Plot of the nominal relaxation time against the inverse of pressure (atm) for the |0,0>|6> (14612 $cm^{-1}$) mode of trimethyl amine, assuming that the unmodified phase lags are correct. The dotted lines represent the 95% confidence interval.

The nominal relaxation time decreases with decreasing pressure, becoming more negative. This result would be expected if the heated wire energy transfer was slower than the V-T relaxation. In this situation, both the V-T relaxation timeand the relaxation time associated with the wire would be a function of pressure, but the wire would be more sensitive to pressure decreases. The same trend is also found for the |6,0>|0> (15782 $cm^{-1}$) and |0,0>|7> (16540 $cm^{-1}$) modes of trimethyl amine as well as the 16169 $cm^{-1}$ band of methane, shown in figures 4-9 through 4-11.

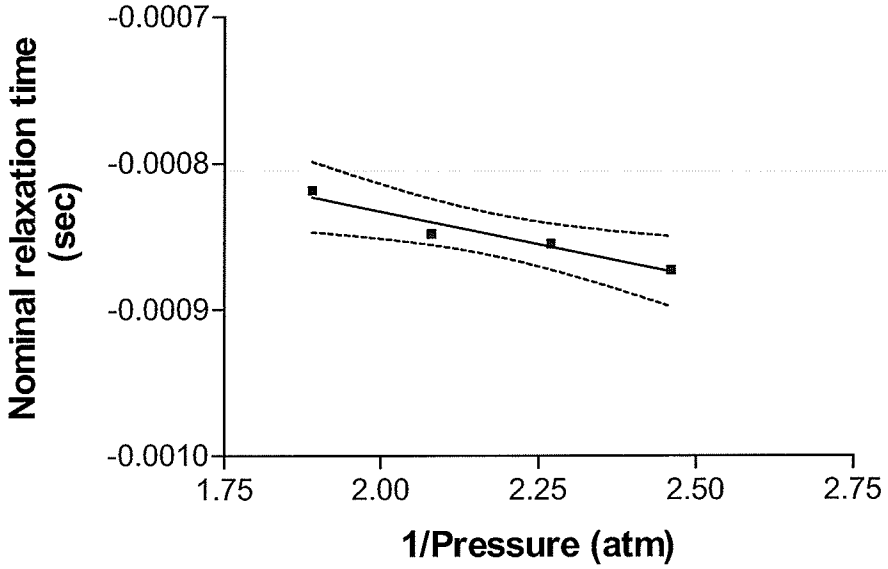


**Figure 4-9.** Plot of the nominal relaxation time against the inverse of pressure (atm) for the |6,0>|0> (15782 $cm^{-1}$) mode of trimethyl amine, assuming that the unmodified phase lags are correct. The dotted lines represent the 95% confidence interval.

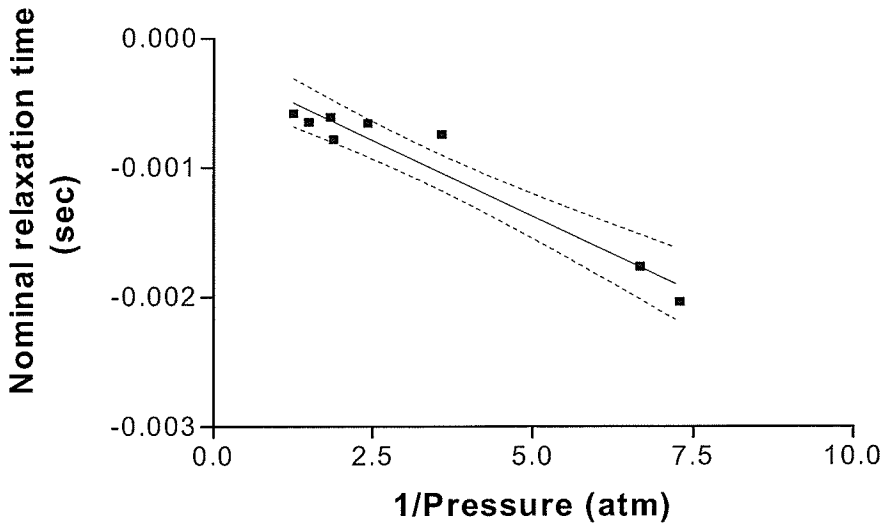


**Figure 4-10.** Plot of the nominal relaxation time against the inverse of pressure (atm) for the |0,0>|7> (16540 $cm^{-1}$) mode of trimethyl amine, assuming that the unmodified phase lags are correct. The dotted lines represent the 95% confidence interval.

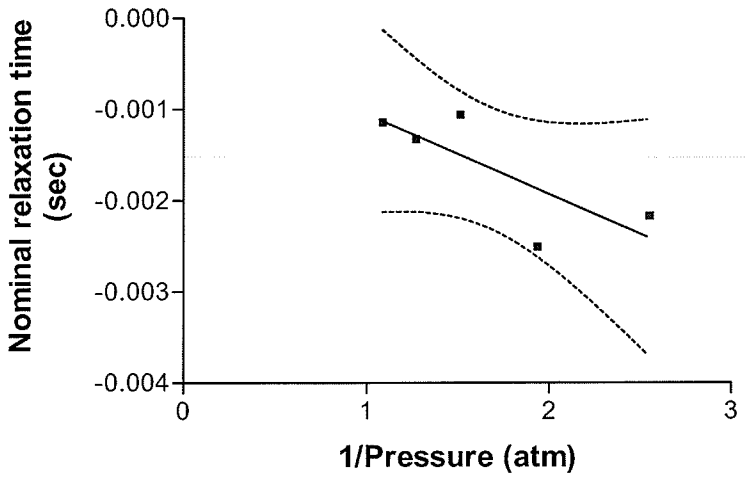


**Figure 4-11.** Plot of the nominal relaxation time against the inverse of pressure (atm) for the 16169 $cm^{-1}$ mode of methane, assuming that the unmodified phase lags are correct. The dotted lines represent the 95% confidence interval.

The results of the linear regression analysis for all of the molecules tested are shown in Table 4-8.

**Table 4-8.** Results of linear regression assuming that the heated wire relaxation time is longer than the V-T relaxation time.

| Molecule | Mode | Frequency of Band ($cm^{-1}$) | $\tau_a$ time at one atmosphere (sec) |
|---|---|---|---|
| Trimethyl Amine | \|0,0>\|6> | 14612 | -0.0002 ± 0.0001 |
| Trimethyl Amine | \|6,0>\|0> | 15782 | -0.00009 ± 0.00002 |
| Trimethyl Amine | \|0,0>\|7> | 16540 | -0.00023 ± 0.00003 |
| Methane | | 16169 | -0.0008 ± 0.0004 |

For the most part the results are consistent with the heat transfer time being longer the V-T relaxation time. Since the heat transfer time is independent of the wavelength of light used for the laser signal, any differences between the apparent relaxation times for different modes must be due to changes in the V-T relaxation time. In this case because, the apparent relaxation time for the |0,0>|6> (14612 $cm^{-1}$) of trimethyl amine is much shorter than for |6,0>|0> (15782 $cm^{-1}$), the actual relaxation time for the |6,0>|0> mode would

therefore be longer than the actual relaxation time than the |0,0>|6>, because in this case the relaxation of the heated wire is assumed to be longer. The |6,0>|0> mode having a longer relaxation time then the |0,0>|6> mode is consistent with what is expected since, from Section 4.1.1.2, the probability of relaxation and thus V-T relaxation time is expected to increase roughly exponentially with the increase of energy in the vibrational modes of the molecule. On the other hand, the apparent relaxation time of the |0,0>|7> (16540 $cm^{-1}$) mode of trimethyl amine is shorter than the |0,0>|6> (14612 $cm^{-1}$) mode. These results indicate a shorter V-T relaxation time, which is the opposite of what would be expected, based on the relationship between the amount of energy in the molecule and the probability of relaxation. However, since the experimental error is larger than the difference in relaxation times, the shorter relaxation time for the |0,0>|7> mode does not eliminate this as an adequate way to interpret the data.

Lastly, it is important to note that the heat transfer from the wire would have to take times in excess of the absolute value of the apparent relaxation times if this interpretation is true. That being the case, the relaxation times would exceed the length of a cycle at 50 kHz (for which signal has been observed, see Section 4.3.1.1) by more than ten times. In other words, ten cycles would pass before the first energy from the first cycle had completely relaxed.

Though there are a number of places in which this interpretation does not fit with the expected results, none of these is clear enough to eliminate this interpretation as a possibility. If this interpretation of the data is correct then this instrument cannot be considered a viable technique for the study of relaxation times.

### 4.4.2 Case 2: V-T relaxation causes more than a 180 degree phase lag

Another interpretation of the results is that the phase lag from V-T relaxation and other factors that can cause phase lag is in excess of 180 degrees. Since anything more than a 180 degree phase lag will be read as a phase lead, this could explain the observation of phase leads for the laser induced signal. Taken this way, the phase lag due to the V-T relaxation ($\phi$) would be calculated using the following equation:

**Equation 4-48.**

$$\phi = 360° - LP - HP$$

where LP is the observed phase lead of the laser induced signal and HP is the phase lag of the heated wire induced signal. The result of applying this interpretation to the data leads to phase lags of over 270 degrees. Equation 4-47 on page 206 would lead to negative times. Therefore, that equation cannot be used. Instead nominal relaxation times can be calculated assuming that the phase shift has a linear relationship to time, or that each degree of phase lag equals a discrete amount of time. In the paper by Cottrell *et al.* [128], the graphs of relaxation time versus pressure are curved at lower pressures and become close to linear at pressures over 30 cm Hg. Therefore at low pressures the assumption of a linear relationship between phase shift and time would lead to large errors, but at pressures over 30 cm Hg, it seems that an inverse relationship would be a reasonable approximation. The plots used for the linear regression, and based on the assumption that case 2 is correct, are shown in figures 4-12 through 4-15.

The apparent lag times at one atmosphere determined from linear regression analysis are shown in Table 4-9.

**Table 4-9.** Results of linear regression assuming that the V-T relaxation time causes a phase shift in excess of 180 degrees.

| Molecule | Mode | Frequency of Band ($cm^{-1}$) | $\tau_a$ at one atmosphere (sec) |
|---|---|---|---|
| Trimethyl Amine | \|0,0>\|6> | 14612 | -0.00005 ± 0.00003 |
| Trimethyl Amine | \|6,0>\|0> | 15782 | -0.00025 ± 0.000004 |
| Trimethyl Amine | \|0,0>\|7> | 16540 | -0.000055 ± 0.000004 |
| Methane | | 16169 | 0.00011± 0.00002 |

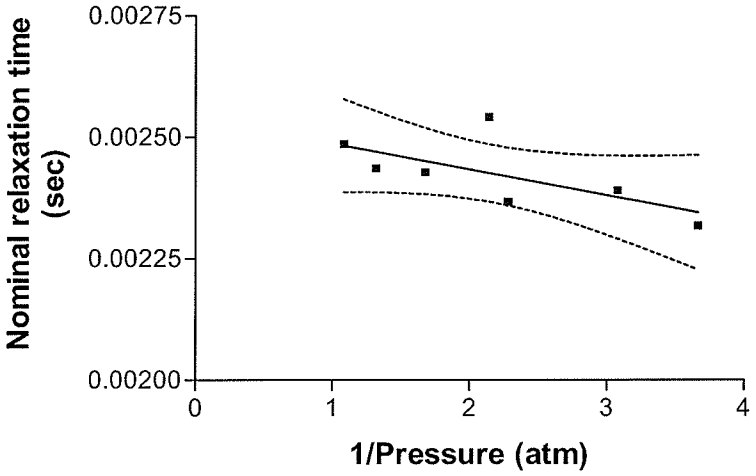


**Figure 4-12.** Plot of the nominal relaxation time against the inverse of pressure (atm) for the |0,0>|6> (14612 $cm^{-1}$) mode of trimethyl amine, assuming that the V-T relaxation time leads to a phase lag of over 180 degrees. The dotted lines represent the 95% confidence interval.

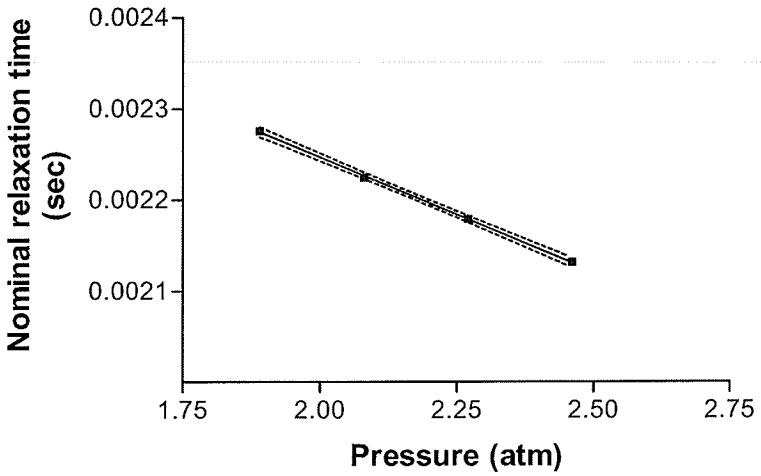


**Figure 4-13.** Plot of the nominal relaxation time against the inverse of pressure (atm) for the |6,0>|0> (15782 $cm^{-1}$) mode of trimethyl amine, assuming that the V-T relaxation time leads to a phase lag of over 180 degrees. The dotted lines represent the 95% confidence interval.

Even though the nominal relaxation times shown in the plots are all positive, the relaxation time increases with increasing pressure for all of the plots save methane. This is evident from the negative results for the apparent relaxation time at one atmosphere returned by the linear regression. Since this is impossible, V-T relaxation cannot be causing a 180 degree phase lag.

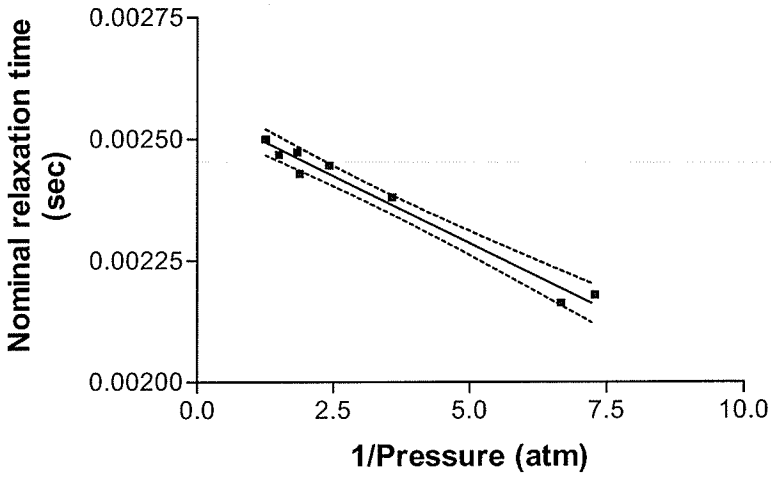


**Figure 4-14.** Plot of the nominal relaxation time against the inverse of pressure (atm) for the |0,0>|7> (16540 $cm^{-1}$) mode of trimethyl amine, assuming that the V-T relaxation time leads to a phase lag of over 180 degrees. The dotted lines represent the 95% confidence interval.

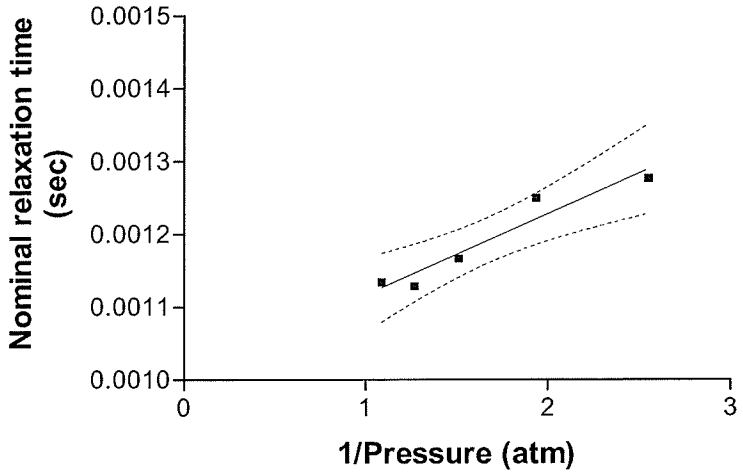


**Figure 4-15.** Plot of the nominal relaxation time against the inverse of pressure (atm) for the 16169 $cm^{-1}$ mode of methane, assuming that the V-T relaxation time leads to a phase lag of over 180 degrees. The dotted lines represent the 95% confidence interval.

### 4.4.3 Case 3: Resonance causes the inversion of phase shifts.

To the best of the author's knowledge, no work has previously been done on the effect that phase shifts due to V-T relaxation would have on the resonance, or vice versa. Phase shifts due to resonance were noticed by Cottrell *et al.* [128] however the resonance was removed and the effects were never studied. The papers by Schattka *et al.* [135] and by Quimby et al. [136] did not address phase shifts at all. In the paper by McClenny *et al.* [137], phase shifts are considered briefly, but it is assumed that any effect of the V-T relaxation is negligible. This paper does offer some hint as to what effect might be observed due to a long V-T relaxation time. First note that the V-T relaxation time does not delay the formation of the acoustic wave. As soon as there are molecules in the excited state there will be some signal. The phase shift observed is due to the fact that some molecules still have to relax after the laser is off. Essentially the wave length is being increased by an amount proportional to the V-T relaxation time. The increase in wavelength can be considered equivalent to a small change in the frequency compared to the modulation frequency. A more extreme version of the change in frequency is demonstrated in the paper by McClenny *et al.* [137] where they plot the phase lead observed as the modulation frequency is varied about the resonance frequency. As the modulation frequency moves below the resonance frequency (longer wavelength), less phase lead is observed, so it can be said that the longer modulation wavelength causes a phase lag. If the modulation frequency is higher than the resonance frequency the opposite is observed.

We can apply this observation to the phase shift observed in these experiments. To begin and for the sake of simplicity assume that the heated wire signal is exactly at the resonant frequency and that some time is needed to transfer the heat from the wire to the gas.

In this discussion, the side of the cell with the wire will be referred to as cavity 1 and the side without the wire will be referred to as cavity 2. When the pulse begins in the wire, a pressure wave builds in cavity 2. After the wire has stopped being heated, the pressure wave moves into cavity two. Since it only takes half the period of the resonant frequency for this pressure wave to pass from cavity 1 to cavity 2, when the next heat pulse starts in the wire the pressure wave is completely in cavity 2 and has been reflected so that it is now re-entering cavity 1, constructively interfering with the new pressure wave being formed. This gives the resonant enhancement. Now consider replacing the wire in cavity 1 with a laser modulated at the same frequency but with V-T relaxation time involved. In this scenario, we will have to consider that the microphone is at the end of cavity 1 opposite the channel which connects it to cavity 2. The pressure wave still moves through the cell at the same rate. This is a function of the cell design. But now when the first half of the period has passed, kinetic energy is still being added in cavity 1 even as the pressure wave is moving out of cavity 1. So when the wave is reflected its leading edge is already in cavity 1. Hence, this leading edge will reach the microphone before the next pulse begins. Since the beginning of the pulse is also the trigger for the data acquisition, a phase lead is observed as the pressure at the microphone starts to rise before be pulse begins. Therefore, on the basis of these arguments, the results of V-T relaxation time will be phase leads rather than phase lags. For sake of simplicity, in comparing these results with work done by non resonant techniques, it is convenient to say that phase lags and phase leads are interchanged by the resonance. Plots of the nominal relaxation time versus the inverse pressure, based on the assumption that the observed phase leads can be taken as phase lags and vice versa are shown in figures 4-16 through 4-20.

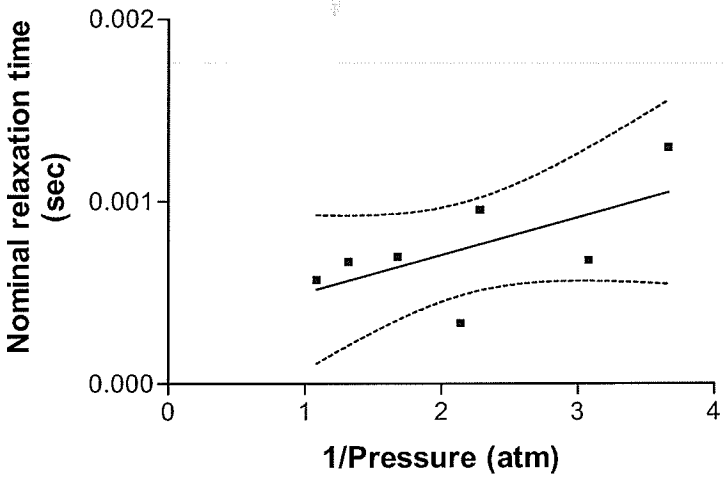


**Figure 4-16.** Plot of the nominal relaxation time against the inverse of pressure (atm) for the |0,0>|6> (14612 $cm^{-1}$) mode of trimethyl amine, assuming that the sign of the observed phase shift may be inverted. The dotted lines represent the 95% confidence interval.

The apparent relaxation times at 1 atmosphere (in this case $\tau_c$) found from the linear regression analysis are shown in Table 4-10.

**Table 4-10.** Results of linear regression assuming that the signs of the observed phase shifts may be reversed.

| Molecule | Mode | Frequency of Band ($cm^{-1}$) | $\tau_a$ at one atmosphere (sec) |
|---|---|---|---|
| Trimethyl Amine | \|0,0>\|6> | 14612 | 0.0002 ± 0.0001 |
| Trimethyl Amine | \|6,0>\|0> | 15782 | 0.00009 ± 0.00002 |
| Trimethyl Amine | \|0,0>\|7> | 16540 | 0.00023 ± 0.00003 |
| Methane | | 16169 | 0.0009 ± 0.0004 |

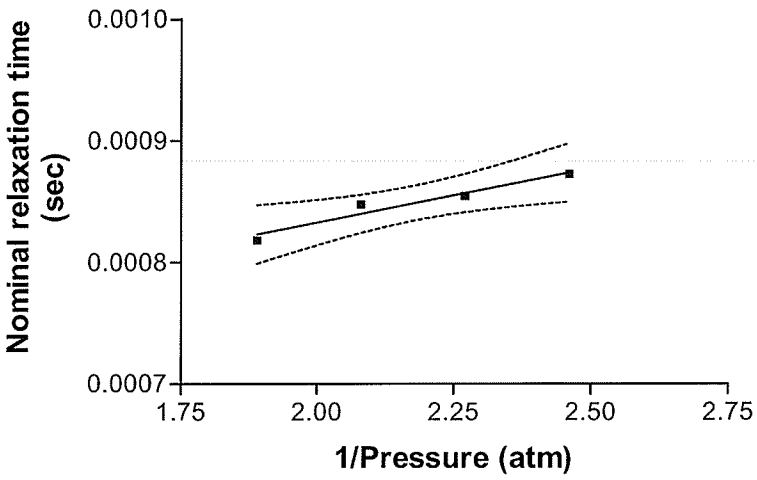


**Figure 4-17.** Plot of the nominal relaxation time against the inverse of pressure (atm) for the |6,0>|0> (15782 $cm^{-1}$) mode of trimethyl amine, assuming that the sign of the observed phase shift may be inverted. The dotted lines represent the 95% confidence interval.

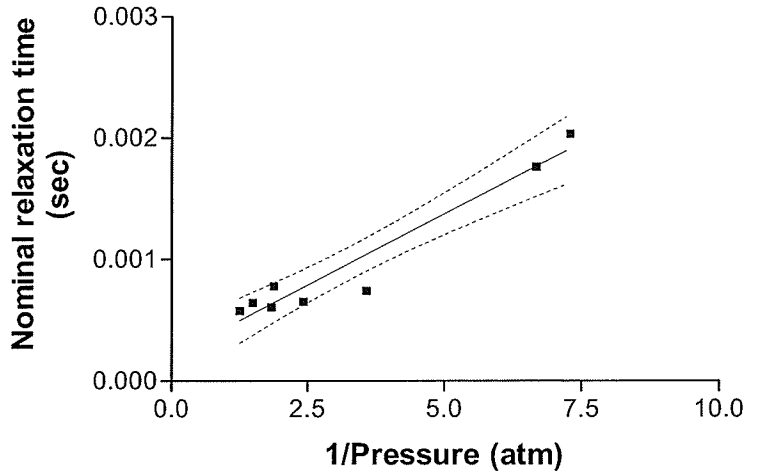


**Figure 4-18.** Plot of the nominal relaxation time against the inverse of pressure (atm) for the |0,0>|7> (16540 $cm^{-1}$) mode of trimethyl amine, assuming that the sign of the observed phase shift may be inverted. The dotted lines represent the 95% confidence interval.

The results based on this assumption are very good. All of the values for the V-T relaxation time at one atmosphere are positive, as expected. The results show a relaxation time at 1 atmosphere of 0.00009 ± 0.00002 sec for the |6,0>|0> mode of trimethyl amine.

It is interesting to note that the |6,0>|0> band appears to have a shorter relaxation time than the |0,0>|6> suggesting that there are different pathways for the relaxations of these two modes. Furthermore this difference in the relaxation time cannot be attributed to the difference in energy between the two bands, as the |6,0>|0> is at higher energy than the |0,0>|6> band, and therefore would be expected to have a longer relaxation time. From the data available, the exact cause of the decrease in the relaxation time between |0,0>|6> and |6,0>|0> cannot be determined. One could perhaps speculate that the IVR for these two modes leads to the energy ending up in different lower energy states which, in turn, would have different parameters affecting V-T relaxation. For example, it is possible that the |0,0>|6> mode relaxes by IVR into a group of levels with different characteristics.

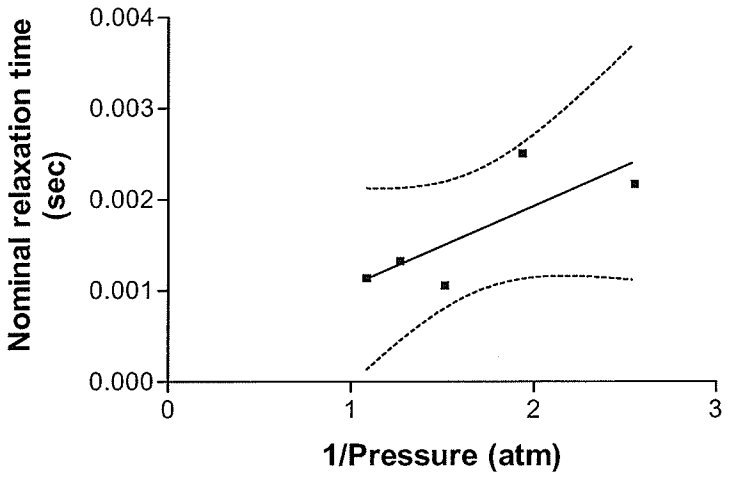


**Figure 4-19.** Plot of the nominal relaxation time against the inverse of pressure (atm) for the 16169 $cm^{-1}$ mode of methane, assuming that the V-T relaxation time leads to a phase lag of over 180 degrees. The dotted lines represent the 95% confidence interval.

There is no difference within experimental error between the apparent relaxation time ($\tau_a$) for the |0,0>|7> mode of trimethyl amine and the |0,0>|6> mode. However, the values that are observed without allowing for error are 0.002062 sec |0,0>|6> and 0.002346

sec for |0,0>|7>, which reflects the expected relationship because the relaxation time will increase as the amount of energy in the molecules vibrational modes increase. Also, since this is simply a higher overtone of the same vibration none of the possible differences described for the |6,0>|0> mode of trimethyl amine would be expected to apply. Also, note that as expected the |6,0>|0> mode does relax faster then the |0,0>|7> mode.

The 16169 $cm^{-1}$ mode of methane has a V-T relaxation time of 0.0009 sec at one atmosphere. This number can be compared to the V-T relaxations times of fundamental modes of methane. There have been a large number of studies on these, the values found range between 1.55-2.0 μsec atm. A list of these can be found in a paper by Avramides and Hunter [139]. The mode studied here has roughly 5 times the energy of the fundamental modes. The value for $\tau_c$ found for the 16169 $cm^{-1}$ mode of methane, was approximately 450 times that of the fundamentals, demonstrating clearly the exponential type of relationship between the energy in the vibrational modes and $\tau_c$.

### 4.4.4 Trimethyl amine - Argon Mixture

Since adding argon to methane has previously caused the relaxation time to increase [138], the effect of adding argon to trimethyl amine in different proportions was investigated. In this experiment, the overall pressure was kept relatively constant (between 700 and 760 torr), so the plots shown are of the V-T relaxation time at one atmosphere vs. the proportion of trimethyl amine. The results found for cases 1-3 were -0.0003 ± 0.005 sec, -0.0006 ± 0.0005 sec and 0.0003 ± 0.005 sec respectively.

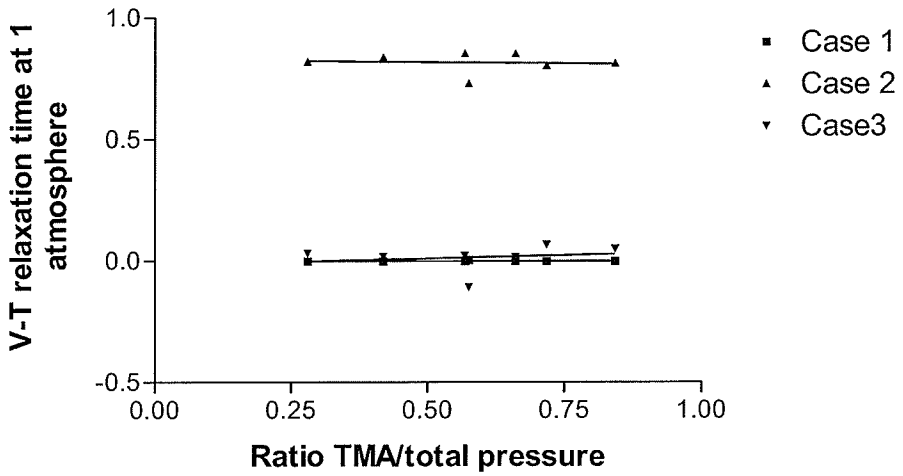


**Figure 4-20.** Plot of the effect of proportion of trimethyl amine in a argon-trimethyl amine mixture, for the |0.0>|6> mode of trimethyl amine.

It may be that within the observed range the proportion of trimethyl amine compared to argon makes little difference (there is no change within experimental error) and it is in fact just the presence of argon that causes the increase in the V-T relaxation. Though there is a fair amount of variability if the data are interpreted under the assumptions of case 3, the V-T relaxation times were generally about 0.001 sec, significantly slower than that observed for the same mode without the addition of argon. The relaxation time for fundamental vibrations of methane mixed with argon was found to be 1.5 times longer than that

for pure methane. For the fifth overtone the relaxation time was found to be 5 times longer. It is unclear whether this is a function of the nature of the molecules involved or to the amount of energy involved.

## 4.5 Conclusions and Future work

In this project, the goal was to develop an instrument for measuring V-T relaxation times, while taking advantage of resonance signal enhancements. The results found could be interpreted in several different ways. Though the possibility that the heat transfer from the heated wire was slower than the V-T relaxation time could not be eliminated, that interpretation does not fit with all of the data. The assumption that the resonance causes an inversion of phase shifts fits very well with the data. It would be beneficial to investigate the effect of resonance on the phase of the signal in more depth. There are a number of experiments that could be done that would allow this. The most important task would be to repeat the same experiments in the absence of resonance and compare the results. To accomplish this, the connecting tube between the two sides of the cell would have to be blocked; the addition of a couple of valves would accomplish this. However, without resonance to amplify it, the signal will be very weak, and a lock-in amplifier would be needed to get usable data. The shape and phase of the pulses through the heated wire could also be modified in a controlled fashion so that the effects of all these changes on the resonant signal could be studied.

The error in all of the results is often 50% or greater; modifications to the system will be needed to reduce this. The most likely sources of error are pressure and temperature changes that occur between the time of collecting the heated wire reference signal and the laser induced signal. Therefore, it would be beneficial if the system could be modified so that both of these signals were collected at the same time. The easiest way this can be accomplished would be to set the system up so that the signals cancel each other. This is an idea originally conceived by Dr. T. E. Gough for his experiments. It would require that the

heated wire signal be shifted to match the laser induced signal. To accomplish this, a different set of trigger and control electronics would be needed. First, a chopper that could lock to the reference signal would be needed. The current chopper does do this but its drift is too high for this type of experiment. Secondly, the ability to shift the phase of the reference wire would be required. Though this is not a difficult thing to add, if it is done then the reference wire pulse can no longer be used as a trigger; either the master timing signal or the signal from the photo diode would have to be used as the trigger. Third, the heated wire signal amplitude would have to be matched to the laser signal amplitude as in the paper by T. E. Gough *et al.* [134]. Alternatively temperature and pressure sensors could be added to the cell so that the average temperature and pressure could be monitored throughout the experiment.

Once these concerns are dealt with, a great many interesting lines of study could be undertaken with this instrument. A greater variety of buffer gases could be tested to determine what effect the nature of the buffer gas has. It would also be useful to study a wider range of overtones to get a better understanding of the effect of the amount of energy in the vibrational modes has on the V-T relaxation time. A large range of molecules could be studied, and relationships between the various possible differences in the molecules and the V-T relaxation time could be found.

In Section 4.1.1.3 the idea of developing an instrument that could further resolve bands based on their V-T relaxation time was introduced. Several experiments to further this goal can now be suggested. To test the possibility of differentiating between overlapping bands for different molecules in a mixture, the next step would be to try different mixtures of gases where each gas had a band within the same energy range. At first, it would

be easiest to start with bands that are well separated and then go to bands that overlap. The slight difference between the V-T relaxation times of the |6,0>|0> and |0,0>|6> modes of trimethyl amine supports the possible use of this type of system to further resolve overtone spectra. However, before the development of such a technique could be undertaken, significantly more data on the differences between the V-T relaxation times of different overtone modes of a molecule would have to be acquired.

As a final note, though the possibility that the heat transfer time of the wire is longer than expected cannot be eliminated entirely, it appears from the data shown that this is not the case. It also appears that, due to the resonance, the signs of the phase shifts observed must the inverted. Based on this, V-T relaxation times for the |0,0>|6>, |6,0>|0> and |0,0>|7> modes of trimethyl amine and the 16169 $cm^{-1}$ band of methane are reported. These values should be considered tentative as there are several issues that still have to be tested.

# 5 Summary

This thesis has investigated a number of aspects of Overtone spectroscopy; Intensity, frequency and Vibrational-Translational relaxation time. Each of these projects have given some insight into overtone spectroscopy. To conclude this thesis a summary of the conclusions of each project will be given.

## 5.1 CH-Stretch Overtone Study of Trimethyl Amine and Dimethyl Sulfide

The $1^{st}$ – $4^{th}$ overtones of TMA and DMS were reported. All of the major peaks were assigned to pure local mode, L-L combination or L-N combinations involved in Fermi resonant interactions with LM bands. Calculations of relative intensities made using the HCAO/LM model are shown to agree well with the experimental observations. However, a tendency for the HCAO/LM model to overestimate the intensity of the *trans* CH vibration and underestimate the *gauche* is noted. The assumption that the methyl groups are isolated may be incorrect. Coupling between the methyl groups in TMA and DMS could be facilitated by the lone pair(s), and would give rise to additional L-L combinations.

## 5.2 Vibrational overtone spectra of Organometallics: Effects of the coordinating metal on the CH bond lengths

This project contained two seperate studies which are summarized seperatly below.

### 5.2.1 Vibrational Overtone Spectroscopy and Overtone Intensities of Cyclohexadiene Iron Tricarbonyl and 1,3-Cyclohexadiene

In this project, the first through third overtones of CHDIT were compared to the first through third overtone spectra of the free ligand 1,3 cyclohexadiene. It was found the complexation caused the lengthening of the terminal olefinic CH bonds and the shortening of the non terminal olefinic CH bonds. It was noted that the difference between the axial and equatorial aliphatic CH's was lessened upon complexation. These observations support a structure for the CHDIT complex in which the bond adjacent to both double bonds gains double bond character while the terminal diene CC bonds become closer to single bonds.

### 5.2.2 Vibrational overtone spectra of metallocenes: Effect of the coordinating metal on the CH bond lengths

This project used the correlation between the frequency of CH LM vibrations and *ab initio* calculated bond lengths to investigate the effect of the coordinating metal on the ligand geometry. Evidence was found that the CH bonds of cyclopentadienyl are shortened by coordination to a metal atom in comparison to the cyclopentadienide, studied via the sodium cyclopentadiene structure. However, the nature (*i.e.,* the electronic structure, bonding, size etc.) of the metal atom does not have a significant effect on the magnitude of this shortening. The observed CH bond length of bis(cyclopentadienyl) magnesium is approximately the same as that of the other metallocenes, indicating that bis(cyclopentadienyl) magnesium is not ionic.

The combination bands in the spectra of the metallocenes, previously postulated to arise from interactions with the metal atoms, are now ascribed to the aromatic nature of the cyclopentadienyl. There are significant differences between the spectrum of cyclopentadi-

ene and that of sodium cyclopentadienyl, presumably due to the aromatic nature of the latter compound. Differences in the structure, bond length and bond strength cause the combination bands to occur closer to the pure LM CH stretching band of the cyclopentadienide ion, allowing for increased Fermi resonance.

While semi-empirical correlations such as those used here are heavily reliant on the accuracy of the *ab initio* calculations, they can be of great value in determining relative CH bond lengths, if proper care is taken in the selection of the basis set and level of theory. They are particularly helpful in cases such as this where there is a limited number of basis sets available that can handle heavy metals.

## 5.3 An Instrument for measuring the Vibrational-Translational relaxation time of Overtone Vibrations

In this project, the goal was to develop an instrument for measuring V-T relaxation times, while taking advantage of resonance signal enhancements. The results found could be interpreted in several different ways. The assumption that the resonance causes an inversion of phase shifts fits very well with the data. It would be beneficial to investigate the effect of resonance on the phase of the signal in more depth. There are a number of experiments that could be done that would allow this. The most important task would be to repeat the same experiments in the absence of resonance and compare the results. However, without resonance to amplify it, the signal will be very weak, and a lock-in amplifier would be needed to get usable data. The shape and phase of the pulses through the heated wire could also be modified in a controlled fashion so that the effects of all these changes on the resonant signal could be studied.

The error in all of the results is often 50% or greater; modifications to the system will be needed to reduce this. The most likely sources of error are pressure and temperature changes that occur between the time of collecting the heated wire reference signal and the laser induced signal. Therefore, it would be beneficial if the system could be modified so that both of these signals were collected at the same time. The easiest way this can be accomplished would be to set the system up so that the signals cancel each other. This is an idea originally conceived by Dr. T. E. Gough for his experiments. It would require that the heated wire signal be shifted to match the laser induced signal. To accomplish this, a different set of trigger and control electronics would be needed. First, a chopper that could lock to the reference signal would be needed. The current chopper does do this but its drift is too high for this type of experiment. Secondly, the ability to shift the phase of the reference wire would be required. Though this is not a difficult thing to add, if it is done then the reference wire pulse can no longer be used as a trigger; either the master timing signal or the signal from the photo diode would have to be used as the trigger. Third, the heated wire signal amplitude would have to be matched to the laser signal amplitude as in the paper by T. E. Gough *et al.* [132]. Alternatively temperature and pressure sensors could be added to the cell so that the average temperature and pressure could be monitored throughout the experiment.

Once these concerns are dealt with, a great many interesting lines of study could be undertaken with this instrument. A greater variety of buffer gases could be tested to determine what effect the nature of the buffer gas has. It would also be useful to study a wider range of overtones to get a better understanding of the effect of the amount of energy in the vibrational modes has on the V-T relaxation time. A large range of molecules could be stud-

ied, and relationships between the various possible differences in the molecules and the V-T relaxation time could be found.

In Section 4.1.1.3 the idea of developing an instrument that could further resolve bands based on their V-T relaxation time was introduced. Several experiments to further this goal can now be suggested. To test the possibility of differentiating between overlapping bands for different molecules in a mixture, the next step would be to try different mixtures of gases where each gas had a band within the same energy range. At first, it would be easiest to start with bands that are well separated and then go to bands that overlap. The slight difference between the V-T relaxation times of the |6,0>|0> and |0,0>|6> modes of trimethyl amine supports the possible use of this type of system to further resolve overtone spectra. However, before the development of such a technique could be undertaken, significantly more data on the differences between the V-T relaxation times of different overtone modes of a molecule would have to be acquired.

As a final note, though the possibility that the heat transfer time of the wire is longer than expected cannot be eliminated entirely, it appears from the data shown that this is not the case. It also appears that, due to the resonance, the signs of the phase shifts observed must the inverted. Based on this, V-T relaxation times for the |0,0>|6>, |6,0>|0> and |0,0>|7> modes of trimethyl amine and the 16169 $cm^{-1}$ band of methane are reported. These values should be considered tentative as there are several issues that still have to be tested.

## 5.4 Concluding Remark

It is hoped that this thesis has not only showed the usefulness of overtone spectroscopy as a tool for gaining a better understanding of molecules, but also that there is still

many areas in which a better understanding of overtone spectra and advances in instrumentation can lead to exciting new ways to gain information in the future.

# 6 Appendix 1

## 6.1 Introduction

This appendix contains the detailed descriptions of all of the Fermi resonant bands assigned in Chapter 2. They are presented in a Tablular format. The procedure used was based on Chapter 1, Section 1.2.3 on page 20. Since all the Fermi resonances involved 3 bands each table describes 3 bands. The highest and lowest energy bands both had the predicted positions of the bands compared to the actual position of the bands. The difference was taken to be the shift due to Fermi resonance. These shifts were then applied to the center band in the opposite direction. The result was compared to the observed position of the center peak. The combination bands that gave the best agreement were considered the most likely assignment.

### 6.1.1 Legend for Tables

| | Anharmonic factor | | | $A_1$ | $A_2$ | $A_3$ | | |
|---|---|---|---|---|---|---|---|---|
| #1 | $B_1$ | $B_2$ | $B_3$ | $C_1$ | $G_1$ | $I_1$ | | |
| | | | | E | | | | |
| #2 | $B_4$ | $B_5$ | $B_6$ | D | H | J | K | L |
| | | | | F | | | | |
| #3 | $B_7$ | $B_8$ | $B_9$ | $C_2$ | $G_2$ | $I_2$ | | |

| Details Number | Band | PED | Description | Notes |
|---|---|---|---|---|
| #1 | | | | |
| | | | | |
| | | | | |
| | | | | |
| | | | | |
| | | | | |
| | | | | |
| | | | | |
| | | | | |
| | | | | |
| #2 | | | | |
| | | | | |
| | | | | |
| | | | | |
| | | | | |
| | | | | |
| | | | | |
| | | | | |
| | | | | |
| | | | | |
| #3 | | | | |
| | | | | |
| | | | | |
| | | | | |
| | | | | |
| | | | | |
| | | | | |
| | | | | |
| | | | | |
| | | | | |

$A_i$ These three numbers are the corrections that are applied to account for anharmonicity, they applied to the combinations labeled #1, #2 and #3 respectively. These are variable parameters, which are generally kept low since most combinations have been found to

behave close to mutually excited but uncoupled oscillators. In the case of pure local modes no correction is applied as anharmonicity is already taken into account in the prediction.

$B_i$ These are the energies of the modes that make up the combinations or the mode.

$C_i$ and D These are the sums of the B's, in other words the predicted energies of the peaks in the absence of Fermi resonance.

E and F These are the separations between adjacent peaks. These are instructive as they must be reasonable values. For example if this number is small we would expect a large splitting and equivalent intensities, if this is not observed in the spectrum then the combination is not a reasonable candidate for consideration.

$G_i$ and H The differences between the observed and "predicted" peak positions and the observed peak positions. G's are considered the shifts due to Fermi resonance.

$I_i$ and J The observed peak positions.

K The predicted position of the center peak after Fermi resonance interactions (K=D+G(both)).

L The difference between the final predicted energy for the center band and the observed energy (L=J-K). The lower this value is the more trustworthy the assignments.

The section at the bottom contains the details of the vibrations involved in the interaction. **Number** is the band in which the vibrations are involved (equivalent to those above). Band is the band energies. **PED's** are the potential energy distributions for each band. These refer to the force field done by McKean *et al.* and are presented for reference purposes. **Description** is the description of each motion in the PED (*i.e.*, Me Str, Me rock etc.). **Notes** are points of interest that should be made about the modes involved.

## 6.1.2 Second Overtone $N(CD_3)_2(CD_2H)$ *Trans*

| | Anharmonic factor | 0 | 0 | 0 | | | |
|---|---|---|---|---|---|---|---|
| #1 | 0 | 0 | 7914 | 7914 | -45 | 7959 | | |
| | | | | 51 | | 93 | | |
| #2 | 5415 | 1325 | 1123 | 7863 | -3 | 7866 | 7881 | -15 |
| | | | | 0 | | 66 | | |
| #3 | 5415 | 1224 | 1224 | 7863 | 63 | 7800 | | |

| Details Number | Band | PED | Description | Notes |
|---|---|---|---|---|
| #1 | 7914 | \|0,0>3> | | Calculated Value |
| | | | | |
| | | | | |
| | | | | |
| | | | | |
| | | | | |
| | | | | |
| | | | | |
| | | | | |
| | | | | |
| #2 | 5415 | \|0,0>2> | | Calculated Value |
| | | | | |
| | 1325 | 38 S16 | Me sym def | |
| | | 28 S4 | Me sym def | |
| | | 14 S19 | Me rock' | |
| | | 11 S6 | Me rock' | |
| | 1123 | 63 S4 | Me sym def | Not observed in fundamental |
| | | 23 S3 | sym NC str | Calculated Value |
| | | 17 S16 | Me sym def | see (Mckean et al.) |
| | | | | |
| #3 | 5415 | \|0,0>2> | | Calculated Value |
| | | | | |
| | 1224 | 82 S15 | Asym NC str | Not observed in fundamental |
| | | 16 S20 | Me rock" | |
| | | 10 S21 | Asym NC3 def | |
| | | | | |
| | 1224 | 82 S15 | Asym NC str | Not observed in fundamental |
| | | 16 S20 | Me rock" | Calculated Value |
| | | 10 S21 | Asym NC3 def | see (Mckean et al.) |
| | | | | |

## 6.1.3 Second Overtone $N(CD_3)_2(CD_2H)$ *Gauche*

| | Anharmonic factor | | 0 | -18 | -3 | | | |
|---|---|---|---|---|---|---|---|---|
| #1 | 8455 | 0 | 0 | 8455 | -51 | 8506 | | |
| | | | | 16 | | 117 | | |
| #2 | 5785 | 1336 | 1336 | 8439 | 50 | 8389 | 8390 | -1 |
| | | | | -154 | | 106 | | |
| #3 | 5785 | 1296 | 1207 | 8285 | 2 | 8283 | | |

| Details Number | Band | PED | Description | Notes |
|---|---|---|---|---|
| #1 | 8455 | \|3,0>0> | | Calculated Value |
| | | | | |
| | | | | |
| | | | | |
| | | | | |
| | | | | |
| | | | | |
| | | | | |
| | | | | |
| | | | | |
| #2 | 5785 | \|2,0>0> | | |
| | | | | |
| | 1336 | 30 S16 | Me sym def | |
| | | 22 S31 | Me rock" | |
| | | 20 S4 | Me sym def | |
| | | 10 S29 | Me asym def" | |
| | | 10 S26 | asym NC str | |
| | 1336 | see above | | |
| | | | | |
| | | | | |
| #3 | 5785 | \|2,0>0> | | |
| | | | | |
| | 1296 | 50 S17 | Me asym def' | |
| | | 28 S5 | Me asym def' | |
| | | 13 S29 | Me asym def" | |
| | | | | |
| | 1207 | 52 S26 | asym NC str | Not observed in fundamental |
| | | 16 S15 | asym NC str | Calculated Value |
| | | 16 S4 | Me sym def | see (Mckean et al.) |
| | | 13 S27 | Me sym def | |

## 6.1.4 Second Overtone $N(CH_3)_3$ *Trans*

| | Anharmonic factor | | 2 | 0 | -2 | | | |
|---|---|---|---|---|---|---|---|---|
| #1 | 5415 | 1459 | 1103 | 7979 | -24 | 8003 | | |
| | | | | 65 | | 62 | | |
| #2 | 7914 | 0 | 0 | 7914 | -27 | 7941 | 7935 | 6 |
| | | | | -14 | | 86 | | |
| #3 | 5415 | 1444 | 1043 | 7900 | 45 | 7855 | | |

| Details Number | Band | PED | Description | Notes |
|---|---|---|---|---|
| #1 | 5415 | \|0,0>\|2> | | Calculated Value |
| | | | | |
| | 1459 | 81 S5 | Me asym def' | This combination is observed for the |
| | | 13 S4 | Me sym def | fundamental region |
| | | | | |
| | | | | |
| | 1103 | 88 S19 | Me rock' | |
| | | | | |
| | | | | |
| | | | | |
| #2 | 7914 | 0,0>\|3> | | Calculated Value |
| | | | | |
| | | | | |
| | | | | |
| | | | | |
| | | | | |
| | | | | |
| | | | | |
| | | | | |
| #3 | 5415 | \|0,0>\|2> | | Calculated value |
| | | | | |
| | 1444 | 95 S17 | Me asym def' | |
| | | | | |
| | | | | |
| | | | | This combination is observed for the |
| | 1043 | 55 S15 | asym NC str | fundamental region |
| | | 36 S20 | Me rock" | |
| | | | | |
| | | | | |

## 6.1.5 Second Overtone $N(CH_3)_3$ *Trans*

| | Anharmonic factor | | -3 | 0 | -10 | | | |
|---|---|---|---|---|---|---|---|---|
| #1 | 5789 | 1409 | 1186 | 8381 | 13 | 8368 | | |
| | | | | -74 | | -76 | | |
| #2 | 8455 | 0 | 0 | 8455 | 11 | 8444 | 8448 | -4 |
| | | | | 8 | | -39 | | |
| #3 | 5789 | 1409 | 1275 | 8463 | -20 | 8483 | | |

| Details Number | Band | PED | Description | Notes |
|---|---|---|---|---|
| #1 | 5789 | \|2,0>0> | | |
| | | | | |
| | 1409 | 106 S16 | Me sym def | |
| | | | | |
| | | | | |
| | | | | Not observed combination in |
| | 1186 | 80 S6 | Me rock' | fundamental region |
| | | | | |
| | | | | |
| | | | | |
| #2 | 8455 | \|3,0>0> | | Calculated Value |
| | | | | |
| | | | | |
| | | | | |
| | | | | |
| | | | | |
| | | | | |
| | | | | |
| | | | | |
| #3 | 5789 | \|2,0>0> | | |
| | | | | |
| | 1409 | 106 S16 | Me sym def | |
| | | | | |
| | | | | |
| | | | | Not observed combination in |
| | 1275 | 43 S15 | asym NC str | fundamental region |
| | | 41 S20 | Me rock" | |
| | | 12 S21 | asym NC3 def | |
| | | | | |

## 6.1.6 Second Overtone $N(CH_3)_2(CD_3)$ *Trans*

| | Anharmonic factor | | -1 | 0 | 0 | | | |
|---|---|---|---|---|---|---|---|---|
| #1 | 5415 | 1463 | 1120 | 7997 | -5 | 8002 | | |
| | | | | 83 | | 61 | | |
| #2 | 7914 | 0 | 0 | 7914 | -27 | 7941 | 7951 | -10 |
| | | | | -6 | | 75 | | |
| #3 | 5415 | 1436 | 1057 | 7908 | 42 | 7866 | | |

| Details Number | Band | PED | Description | Notes |
|---|---|---|---|---|
| #1 | 5415 | \|0,0>\|2> | | Calculated Value |
| | | | | |
| | 1463 | 60 S5 | Me asym def' | |
| | | 28 S17 | Me asym def' | |
| | | | | |
| | | | | This combination is observed for the |
| | 1120 | 57 S16 | Me asym def" | fundamental region |
| | | 20 S15 | asym NC str | |
| | | 20 S4 | Me sym def | |
| | | 15 S20 | Me rock" | |
| #2 | 7914 | \|0,0>3> | | |
| | | | | |
| | | | | |
| | | | | |
| | | | | |
| | | | | |
| | | | | |
| | | | | |
| | | | | |
| #3 | 5914 | \|0,0>2> | | |
| | | | | |
| | 1436 | 71 S4 | Me sym def | |
| | | 28 S16 | Me sym def | |
| | | | | |
| | | | | This combination is observed for the |
| | 1057 | 68 S17 | Me asym def" | fundamental region |
| | | 32 S5 | Me asym def' | |
| | | | | |
| | | | | |

## 6.1.7 Second Overtone $N(CH_3)_2(CD_3)$ *Gauche*

| | | | | | | | | |
|---|---|---|---|---|---|---|---|---|
| | Anharmonic factor | | 0 | 0 | 0 | | | |
| #1 | 5785 | 1436 | 1168 | 8389 | 15 | 8374 | | |
| | | | | -66 | | -70 | | |
| #2 | 8455 | 0 | 0 | 8455 | 11 | 8444 | 8449 | -5 |
| | | | | 12 | | -44 | | |
| #3 | 5785 | 1436 | 1246 | 8467 | -21 | 8488 | | |

| Details Number | Band | PED | Description | Notes |
|---|---|---|---|---|
| #1 | 5785 | \|2,0>0> | | |
| | | | | |
| | 1436 | 71 S4 | Me sym def | |
| | | 28 S16 | Me sym def | |
| | | | | |
| | | | | This combination is observed for the |
| | 1168 | 68 S6 | Me rock' | fundamental region |
| | | 14 S19 | Me rock' | |
| | | | | |
| | | | | |
| #2 | 8455 | \|3,0>0> | | Calculated Value |
| | | | | |
| | | | | |
| | | | | |
| | | | | |
| | | | | |
| | | | | |
| | | | | |
| | | | | |
| | | | | |
| #3 | 5785 | \|2,0>0> | | |
| | | | | |
| | 1436 | 71 S4 | Me sym def | |
| | | 28 S16 | Me sym def | |
| | | | | |
| | | | | Not observed combination in |
| | 1246 | 64 S26 | asym NC str | fundamental region |
| | | 28 S31 | Me rock" | |
| | | 12 S32 | asym NC3 def | |
| | | | | |

## 6.1.8 Second Overtone $N(CD_3)_2(CH_3)$ *Trans*

| | Anharmonic factor | | -2 | 0 | -4 | | | |
|---|---|---|---|---|---|---|---|---|
| #1 | 5415 | 1453 | 1060 | 7926 | -49 | 7975 | | |
| | | | | 12 | | 77 | | |
| #2 | 7914 | 0 | 0 | 7914 | 16 | 7898 | 7906 | -8 |
| | | | | -20 | | 45 | | |
| #3 | 5415 | 1423 | 1060 | 7894 | 41 | 7853 | | |

| Details Number | Band | PED | Description | Notes |
|---|---|---|---|---|
| #1 | 5415 | \|0,0>2> | | Calculated Value |
| | | | | |
| | 1453 | 60 S17 | Me asym def'' | |
| | | 32 S5 | Me asym def' | |
| | | | | |
| | | | | This combination is observed for the |
| | 1060 | 65 S5 | Me asym def' | fundamental region |
| | | 34 S17 | Me asym def' | |
| | | | | |
| | | | | |
| #2 | 7914 | \|0,0>3> | | Calculated Value |
| | | | | |
| | | | | |
| | | | | |
| | | | | |
| | | | | |
| | | | | |
| | | | | |
| | | | | |
| | | | | |
| #3 | 5415 | \|0,0>2> | | |
| | | | | |
| | 1423 | 63 S16 | Me sym def | |
| | | 40 S4 | Me sym def | |
| | | | | |
| | | | | This combination is observed for the |
| | 1060 | 65 S5 | Me asym def' | fundamental region |
| | | 34 S17 | Me asym def' | |
| | | | | |
| | | | | |

## 6.1.9 Second Overtone $N(CD_3)_2(CH_3)$ *Gauche*

| | Anharmonic factor | | -1 | 0 | -8 | | | |
|---|---|---|---|---|---|---|---|---|
| #1 | 5791 | 1453 | 1144 | 8387 | 31 | 8356 | | |
| | | | | -68 | | -92 | | |
| #2 | 8455 | 0 | 0 | 8455 | 7 | 8448 | 8451 | -3 |
| | | | | 14 | | -56 | | |
| #3 | 5791 | 1423 | 1263 | 8469 | -35 | 8504 | | |

| Details Number | Band | PED | Description | Notes |
|---|---|---|---|---|
| #1 | 5791 | \|2,0>0> | | |
| | | | | |
| | 1453 | 60 S17 | Me asym def' | |
| | | 32 S5 | Me asym def' | |
| | | | | |
| | | | | This combination is observed for the |
| | 1144 | 48 S6 | Me rock' | fundamental region |
| | | 35 S19 | Me rock' | |
| | | | | |
| | | | | |
| #2 | 8455 | \|3,0>0> | | Calculated Value |
| | | | | |
| | | | | |
| | | | | |
| | | | | |
| | | | | |
| | | | | |
| | | | | |
| | | | | |
| | | | | |
| #3 | 5791 | \|2,0>0> | | |
| | | | | |
| | 1423 | 63 S16 | Me sym def | |
| | | 40 S4 | Me sym def | |
| | | | | |
| | | | | Not observed combination in |
| | 1263 | 57 S26 | asym NC str | fundamental region |
| | | 33 S31 | Me rock" | |
| | | 11 S32 | asym NC3 def | |
| | | | | |

# 7 Appendix 2

## 7.1 Wiring

The connections to the computer are defined. The format used to define the connections to the computer is as follows: the channel of the National Instruments PCI-6052E data acquisition card will be given first, number of the connector on the national Instruments SCB-68 connector is the number in parenthesis followed by what it is connected to.

Analog Channel 1 (33)-PFI0/Trigger1 (11)

Analog Channel 9 (66)-Digital ground (44)

Analog Channel 2 (65)-PFI1/Trigger1 (10)

Analog Channel 10 (31)-Digital ground (9)

Analog Channel 3 (30)-Positive terminal of the power meter

Analog Channel 11 (63)-Negative terminal of the power meter

Analog Channel 6 (25)-output of microphone preamplifier and analog ground (24) via a 100 kΩ resistor.

Analog Channel 14 (58)-ground of microphone preamplifier and analog ground (24) via a 100 kΩ resistor.

Analog output ground (54)- negative side of tungsten wire

Analog output 1 (21)-positive side of tungsten wire

Analog output ground (55)- negative terminal of the optical chopper signal in

Analog output 0 (22)- positive terminal of the optical chopper signal in

Digital ground (9)-Analog output ground (55)

PFI1/Trigger 2 (10)-Analog output 0 (22)

Digital ground (44)-ground of photo diode preamplifier

PFI1/Trigger 2 (11)-output of photo diode preamplifier

Note that all of the wires enter SCB-68 connector block via a ribbon cable which leads to the microphone preamplifier. Inside the microphone preamplifier all of the wires are connected to the ribbon cable.

## 7.2 Preamplifiers

Both the preamplifiers are essentially the same, save for some variation in the resistor sizes. Since the size of the resistors are unimportant (the ratio of the two different resistors defines the amplification, for example if the ratio is 10 the amplification will be ten times) only the microphone preamplifier will be shown.

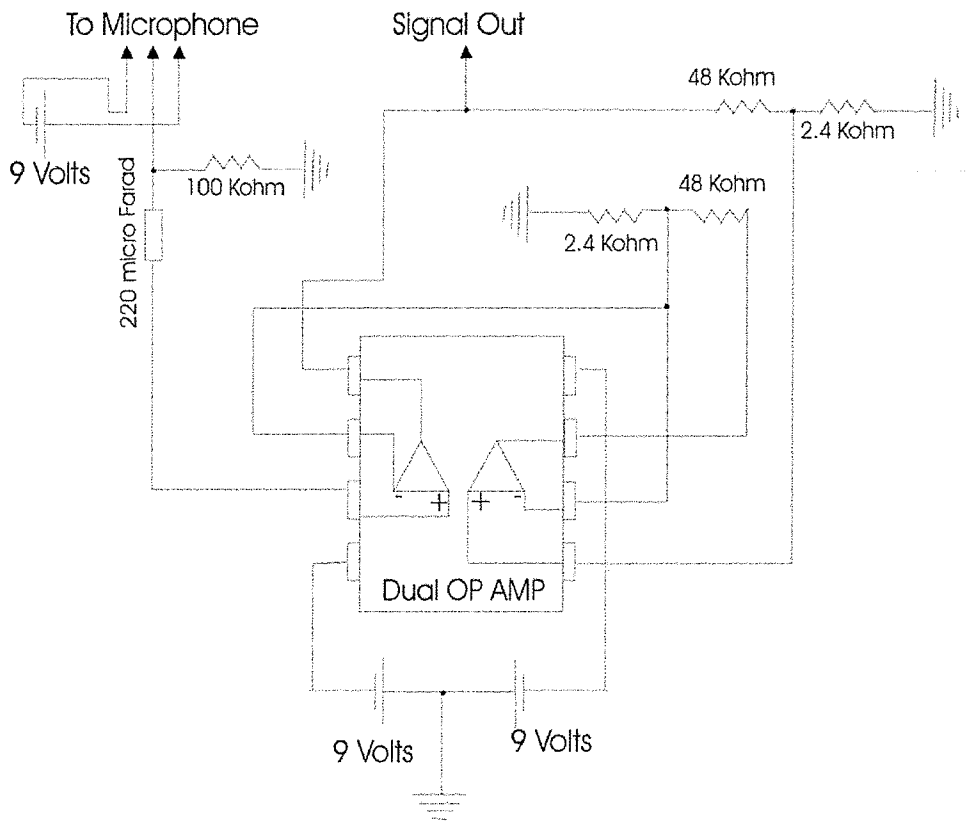


**Figure 7-1.** Diagram of Microphone preamplifier. Black dots indicate where wires that cross each other are connected.

# 8 Appendix 3

## 8.1 ICL-PARPS Program

The ICL-PARPS programs was made using LabView 6.1 which is a visual programing language. Therefore this section will be in the form of a number of figures. At times parts of a figure will be circled. When a part is circled it means that icon refers to another section of programing, which is displayed in another figure. None of the internal functions that come with LabView are expanded in this ways, (for information on these, the reader should consult either the LabView manual or help menus). Also in some parts of the program there are different features depending on the settings or on the time during the operation of the program. In these cases, a figure is shown for each possibility.

There are three major parts to the ICL-PARPS program:

1. The output of control pulses.

2. The Synchronization check.

3. Data acquisition.

For convenience these will be considered separately.

## 8.1.1 Output of control pulses

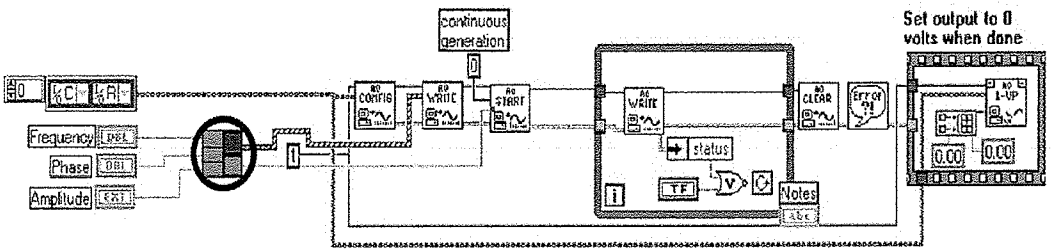


**Figure 8-1.** Out generation portion of the ICL-PARPS program, the circled section is separate program that defines the out parameters, (see Figure 8-2)

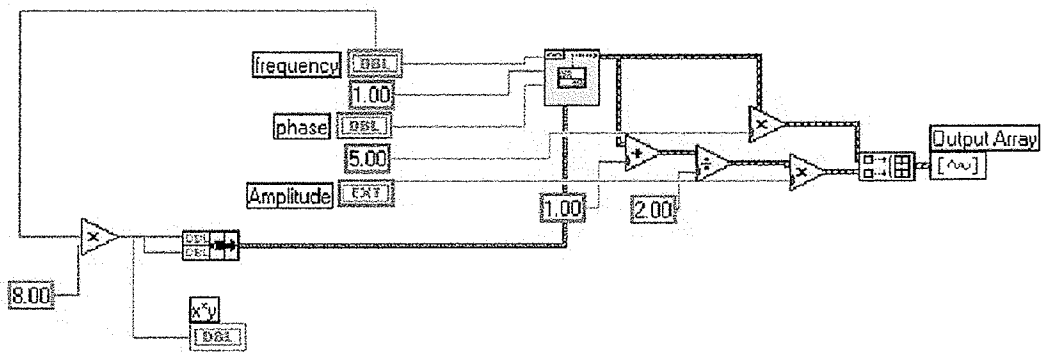


**Figure 8-2.** LabView program for defining the parameters of the output signals.

## 8.1.2 Synchronization Check

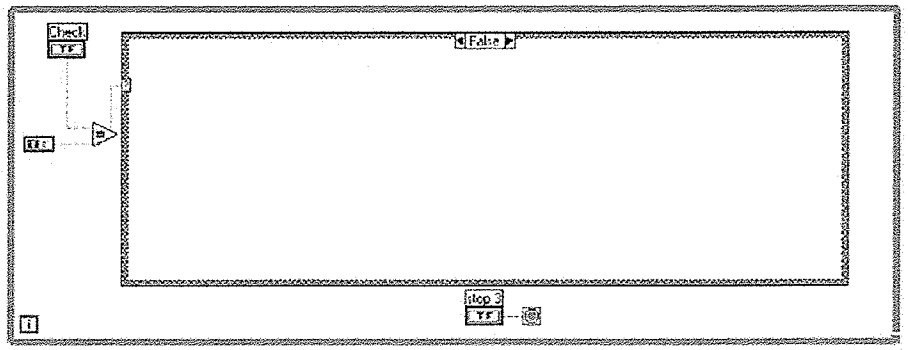


**Figure 8-3.** Synchronization check portion of the ICL-PARPS program prior to activation.

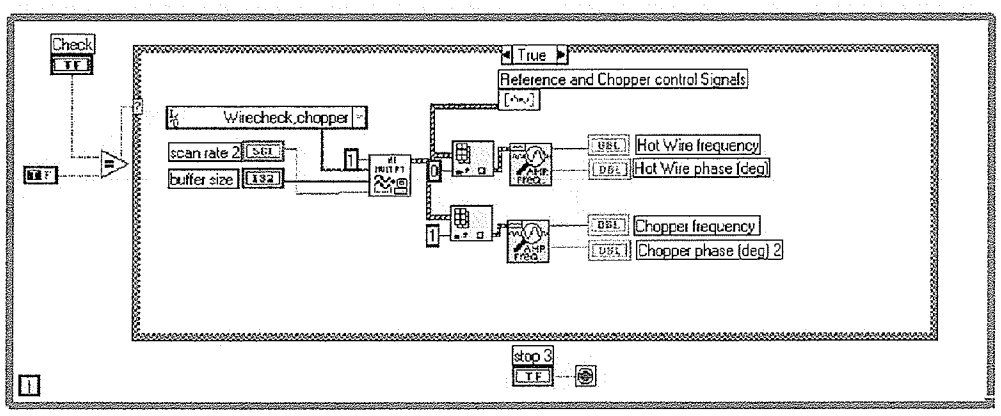


**Figure 8-4.** Synchronization check portion of the ICL-PARPS program after activation.

## 8.1.3 Data Acquisition

The data acquisition portion of the ICL-PARPS program has three modes; test hot-wire, test laser and experiment. For simplicity these are shown separately.

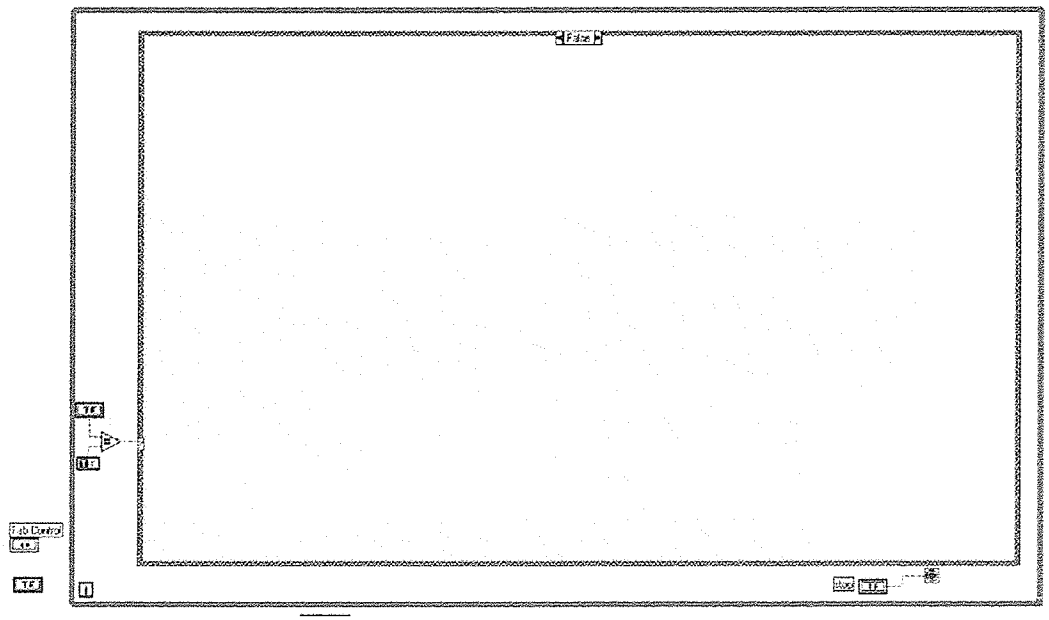


**Figure 8-5.** Data acquisition portion of the ICL-PARPS program prior to activation.

### 8.1.3.1 Test hot-wire mode

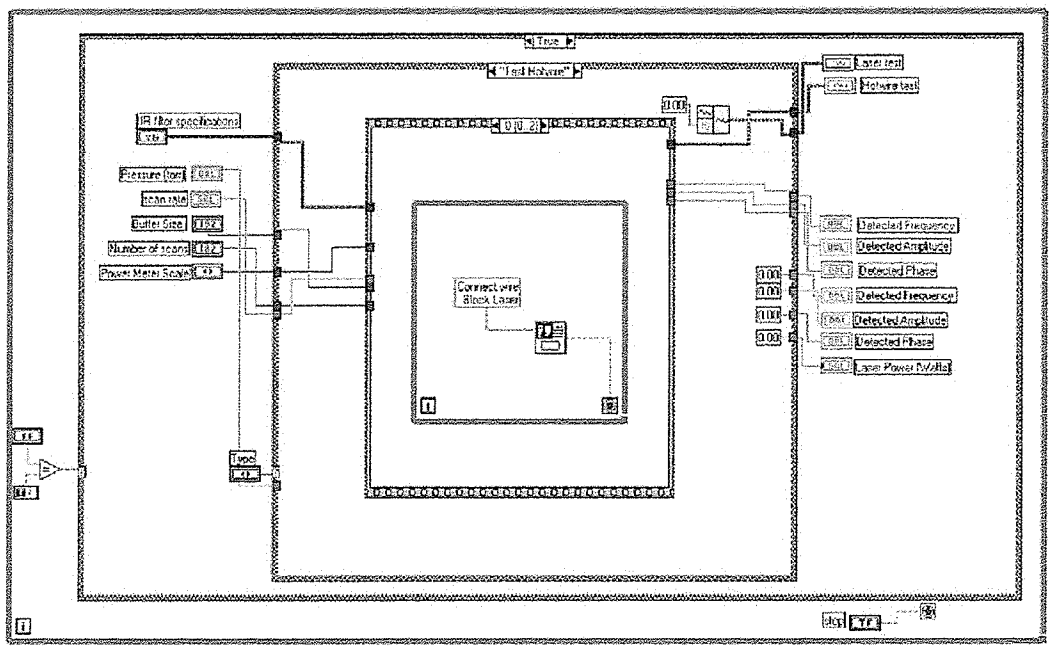


**Figure 8-6.** First step in the data acquisition, for the test hot-wire mode of the ICL-PARPS program. This part simply prompts the user to block the laser and connect the wire.

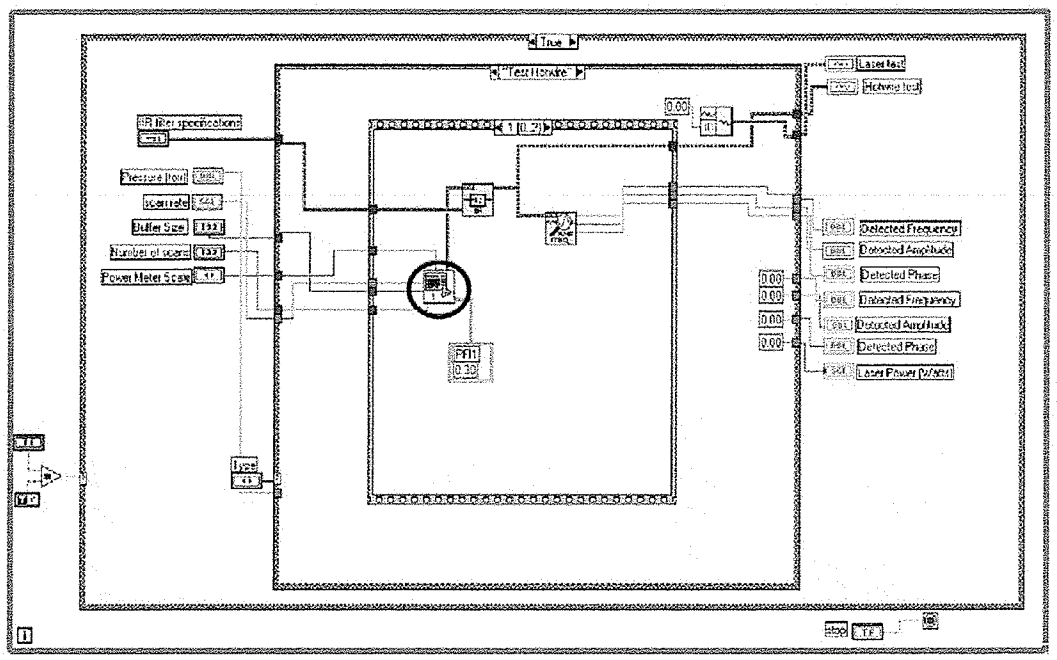


**Figure 8-7.** Second step in the test hot-wire mode, where the actual acquisition of data is done. The circled part is the data collection program (see Figure 8-8 and Figure 8-9).

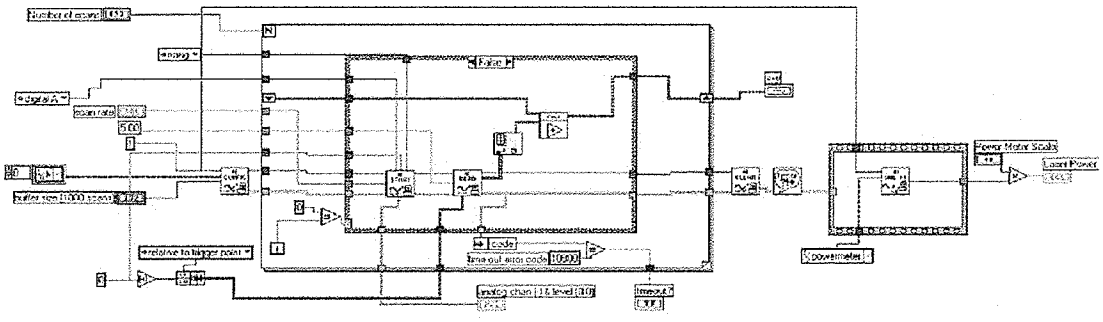

**Figure 8-8.** Data collection for the hot wire portion of ICL-PARPS program. This portion of the program is for before the requested number of scans have been collected.

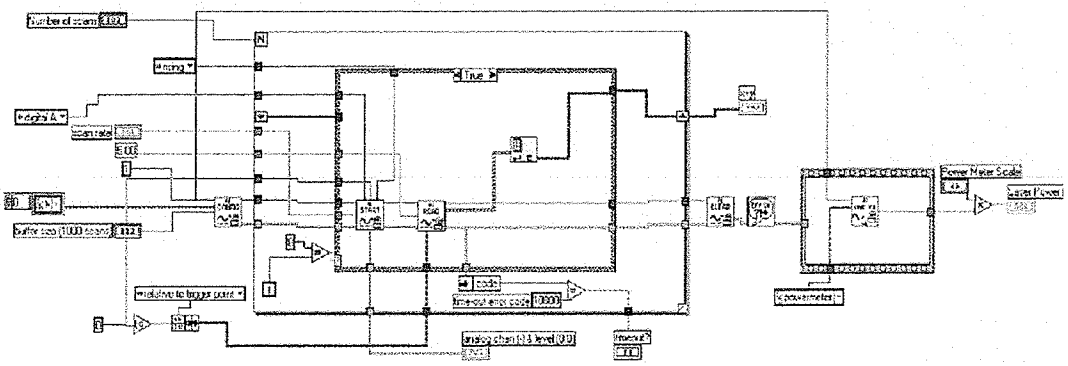

**Figure 8-9.** Data collection for the hot wire portion of ICL-PARPS program. This portion of the program is for after the requested number of scans have been collected.

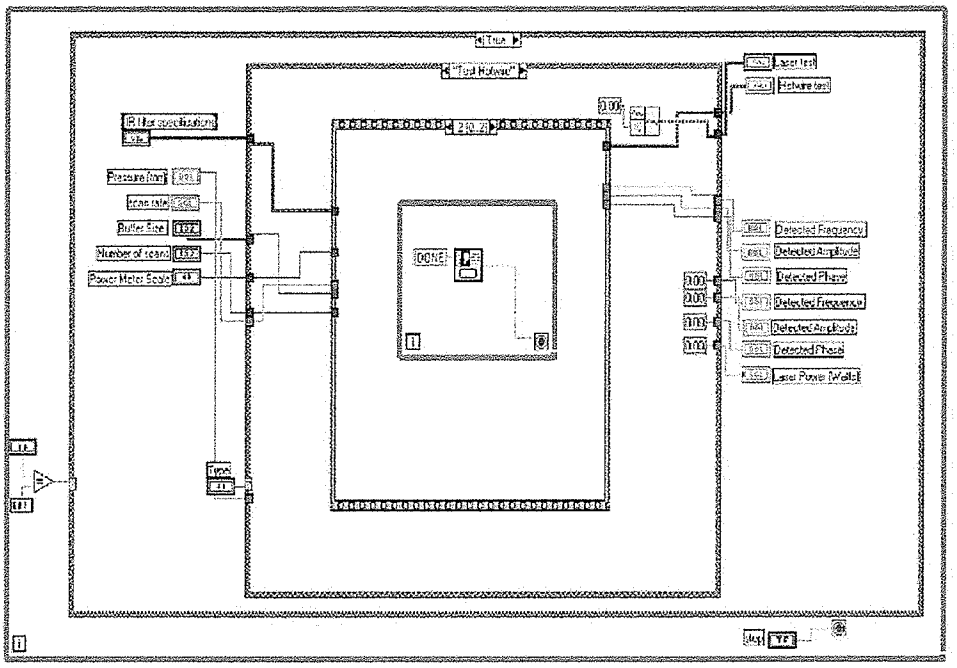


**Figure 8-10.** Final part of the test hot wire part of the ICL-PARPS program, returns a prompt informing the user that data collection is done.

### 8.1.3.2 Test laser mode

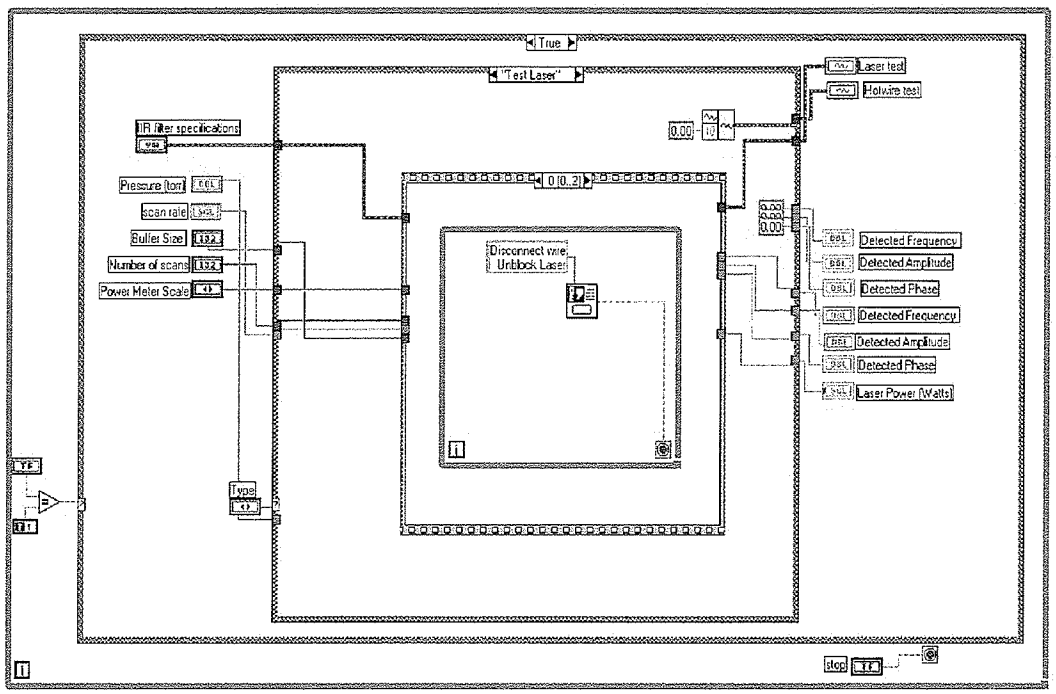


**Figure 8-11.** First step in the data acquisition, for the test laser mode of the ICL-PARPS program. This part simply prompts the user to unblock the laser and disconnect the wire.

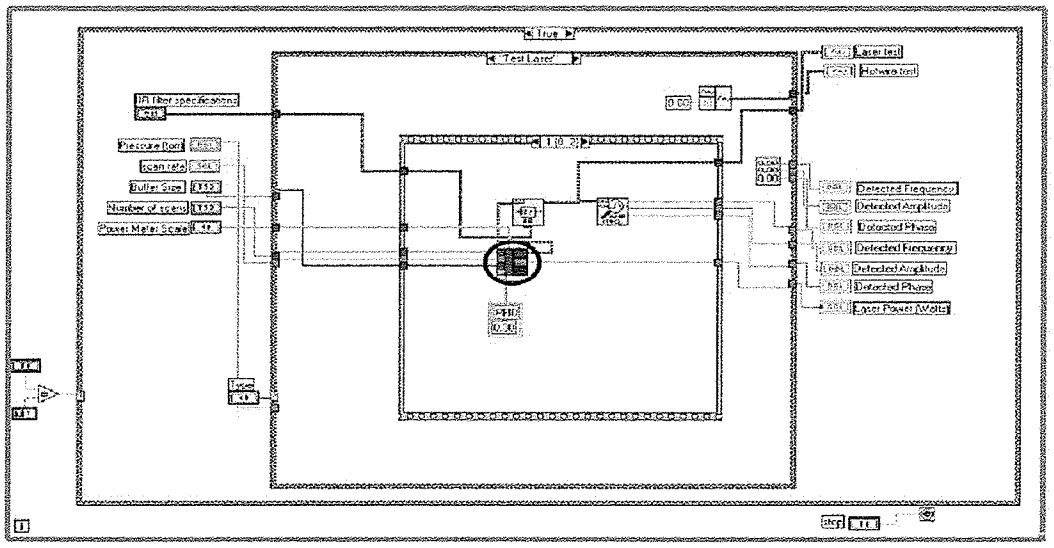


**Figure 8-12.** Second step in the test laser mode, where the actual acquisition of data is done. The circled part is the data collection program (see Figure 8-13 and Figure 8-14).

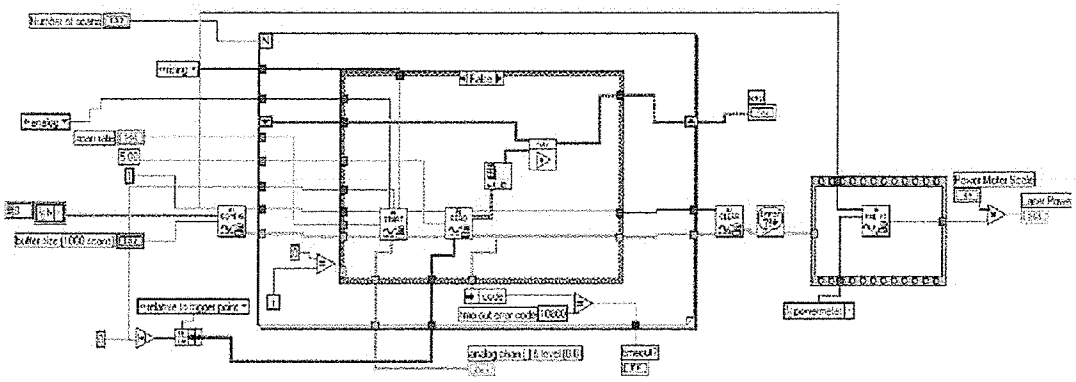

**Figure 8-13.** Data collection for the laser portion of ICL-PARPS program. This portion of the program is for before the requested number of scans have been collected

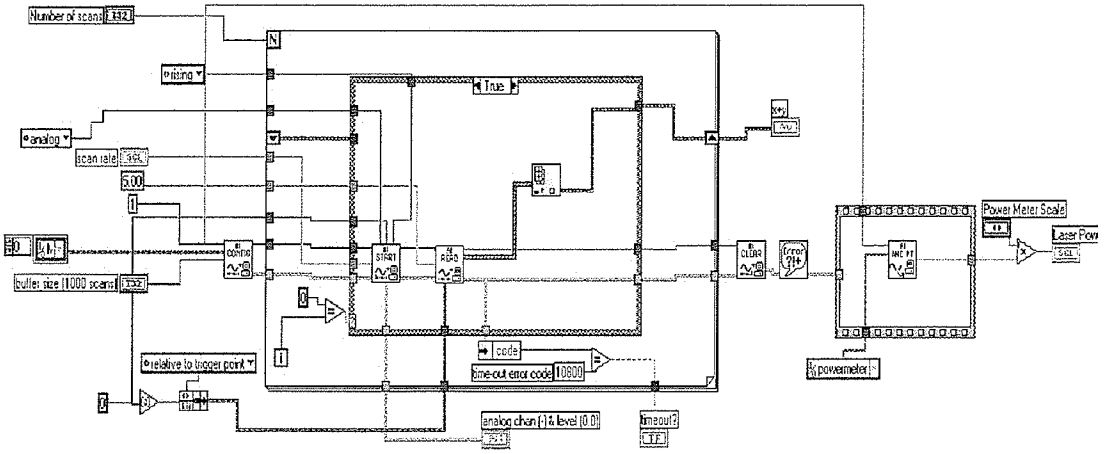


**Figure 8-14.** Data collection for the laser portion of ICL-PARPS program. This portion of the program is for after the requested number of scans have been collected.

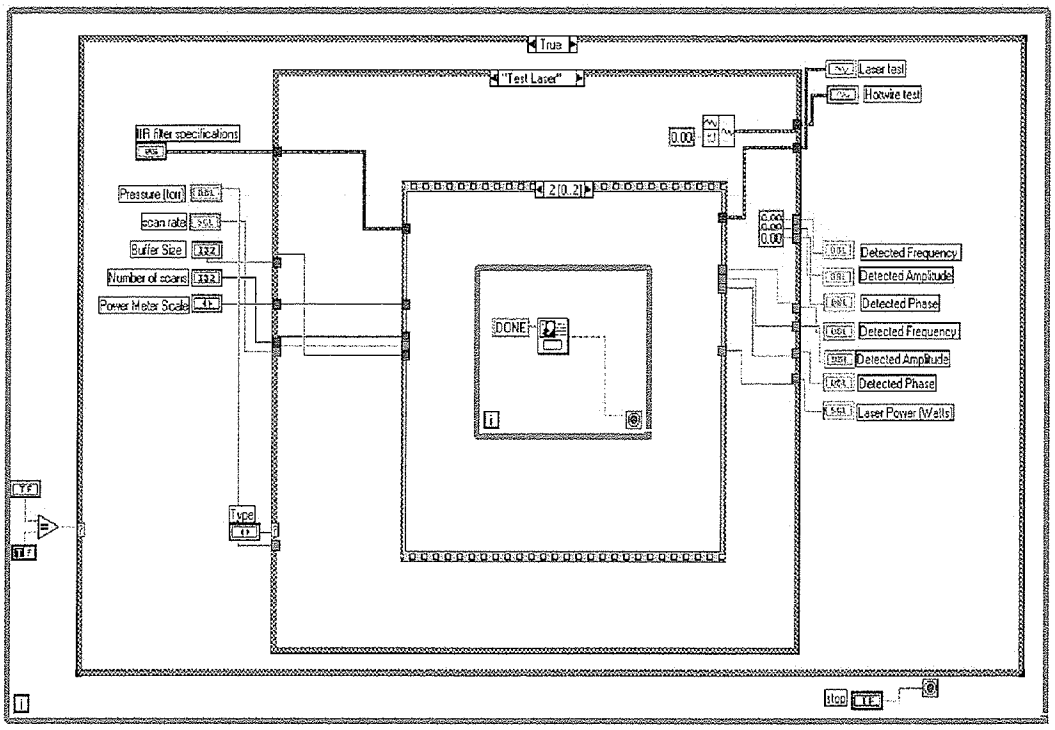


**Figure 8-15.** Final part of the test laser part of the ICL-PARPS program, returns a prompt informing the user that data collection is done.

### 8.1.3.3 Experiment mode

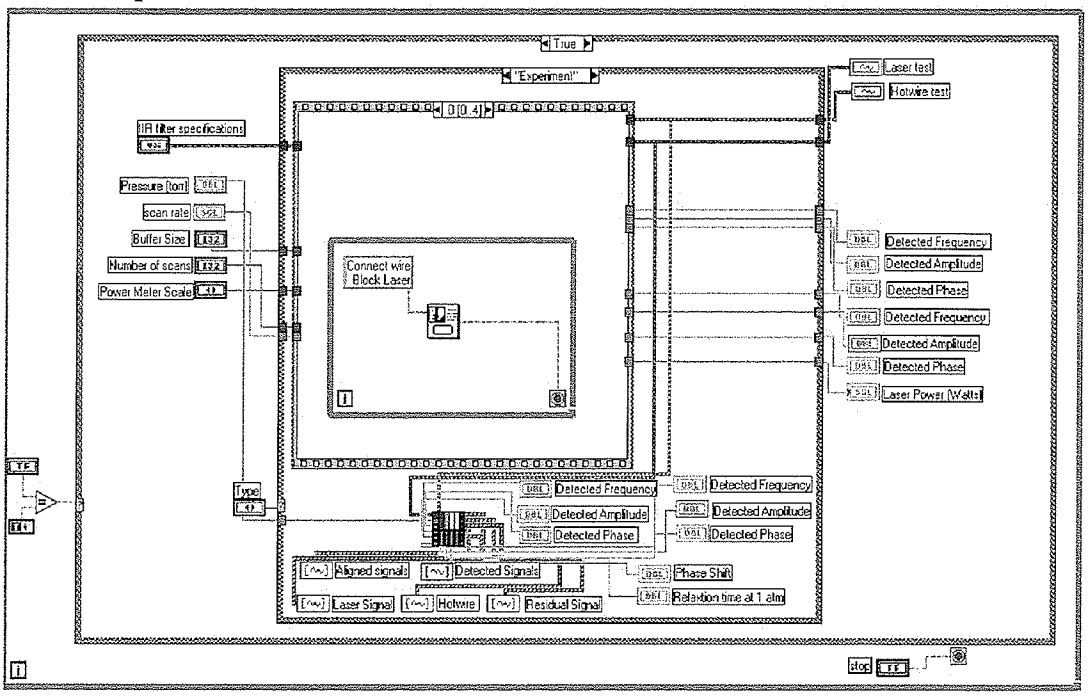


**Figure 8-16.** First step in the data acquisition, for the experiment mode of the ICL-PARPS program. This part simply prompts the user to block the laser and connect the wire.

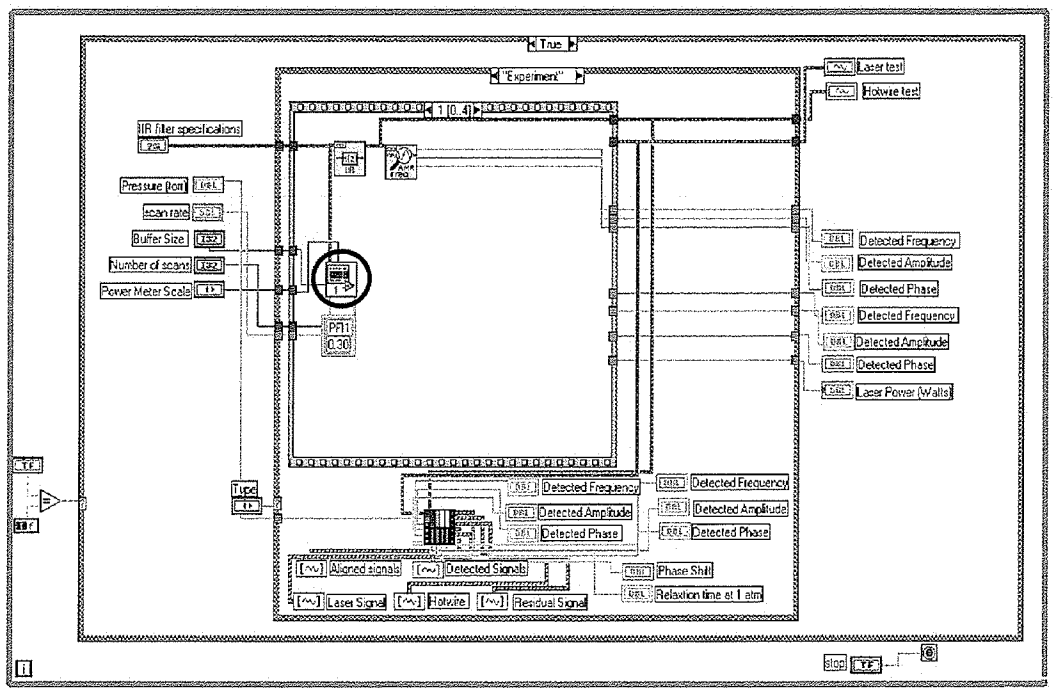


**Figure 8-17.** Second step in the experiment mode, where the actual acquisition of heated wire reference data is done. The circled part is the data collection program (see Figure 8-8 and Figure 8-9).

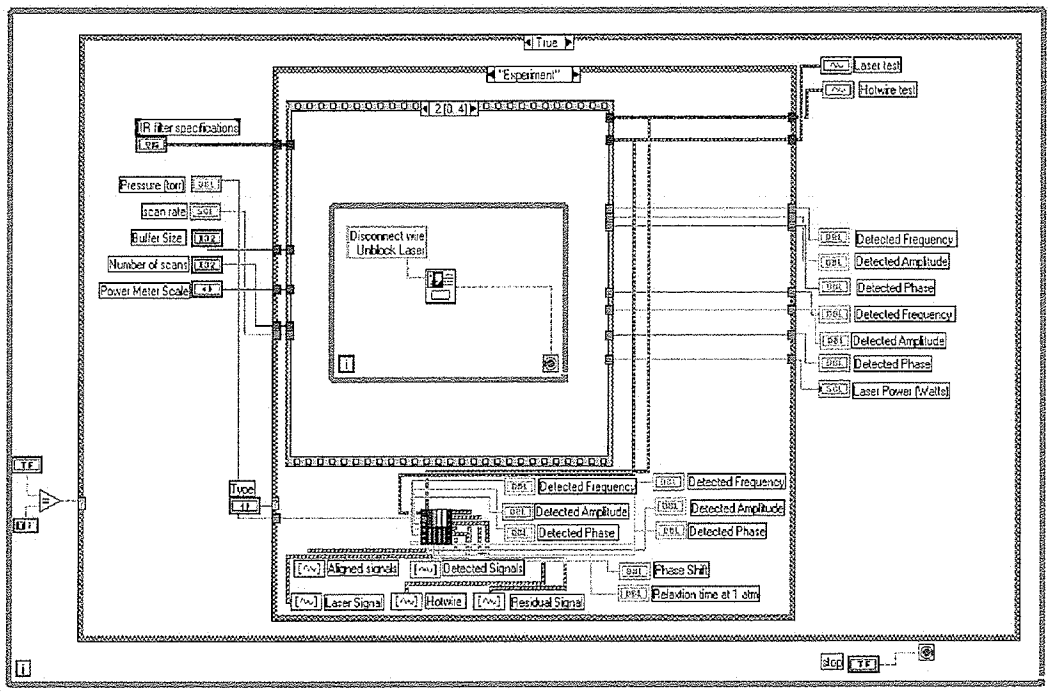


**Figure 8-18.** Third step in the data acquisition, for the experiment mode of the ICL-PARPS program. This part simply prompts the user to unblock the laser and disconnect the wire.

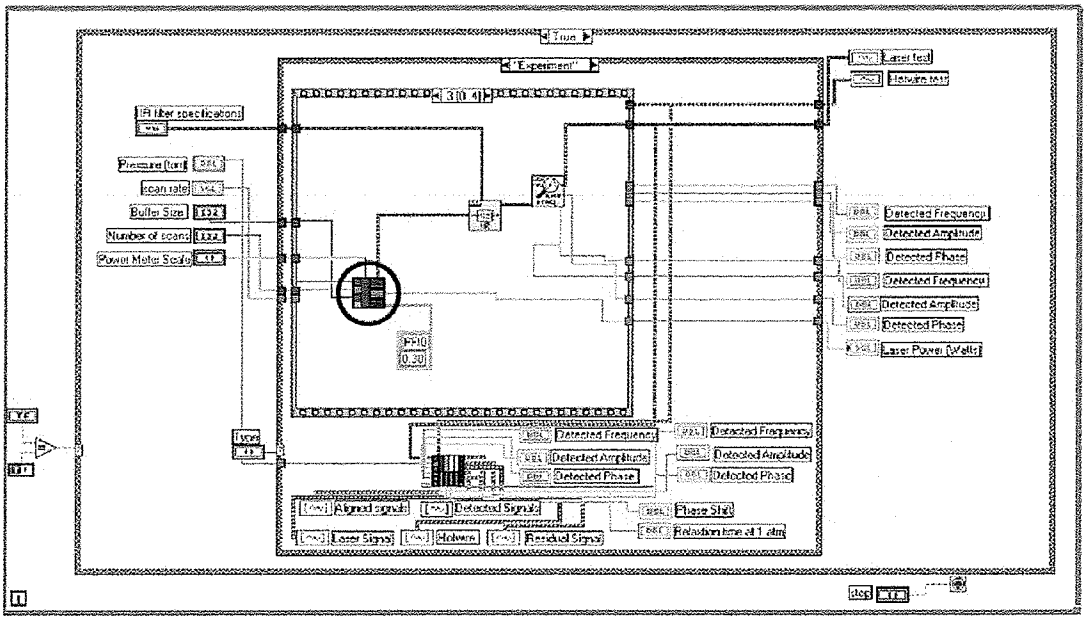


**Figure 8-19.** Fourth step in the experiment mode, where the acquisition of data for the laser induced signal is done. The circled part is the data collection program (see Figure 8-13 and Figure 8-14).

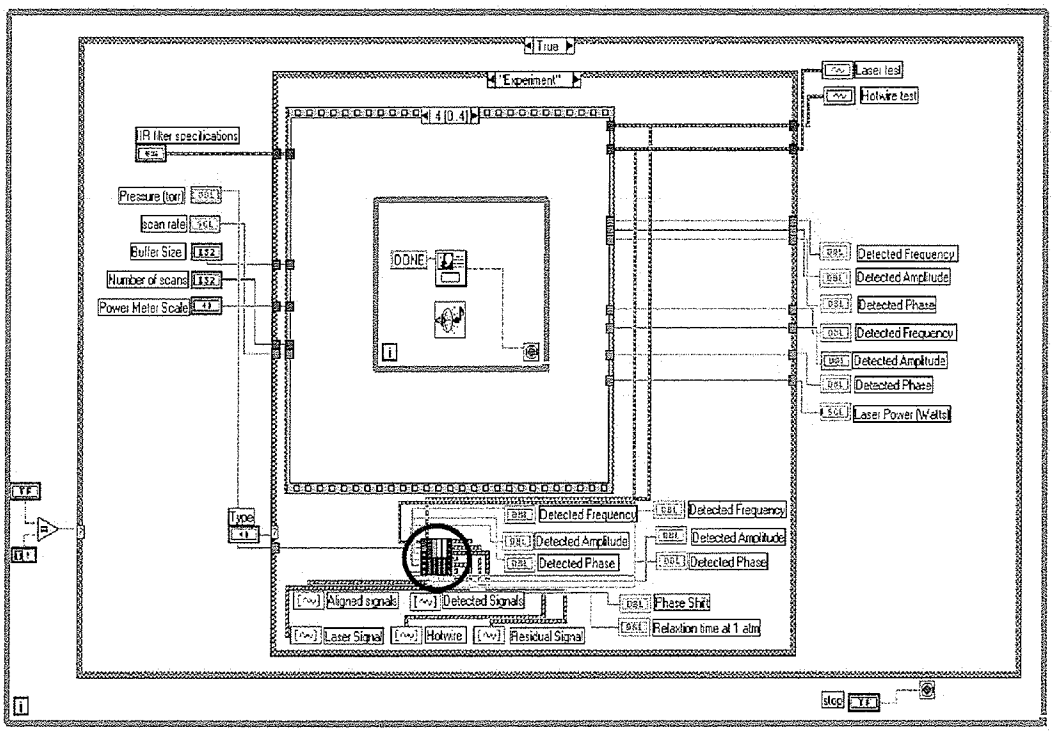


**Figure 8-20.** The last step in the experiment mode, the user is prompted that data acquisition is done, and analysis is preformed by the circled part of the program (see Figure 8-21)

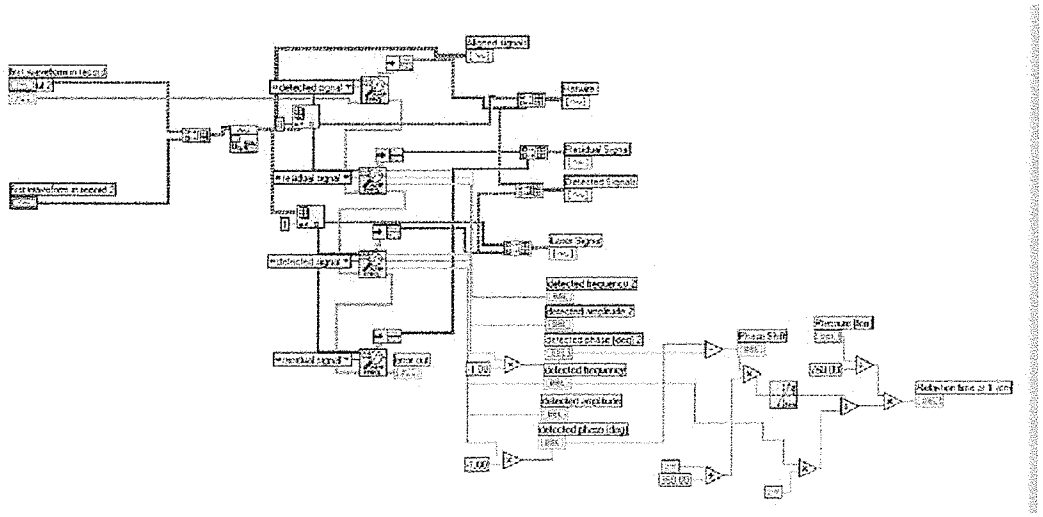

**Figure 8-21.** This part of the program calculates the observed phase lag between the heated wire signal and the laser induced signal and from that calculates an apparent V-T relaxation time at one atmosphere of pressure.

# 9 Appendix 4

## 9.1 ICL-PARPS User Manual

A brief user manual for the ICL-PARPS system is presented here to permit further study on this system.

### 9.1.1 Setup

Before the ICL-PARPS system can be used a certain amount of setup is required. It is assumed that the user of the instrument is familiar with the operation of dye lasers so the alignment of the dye laser is not discussed, here. However, the dye laser must be aligned and the birefringent filter set to the wavelength of the band that is to be studied.

#### 9.1.1.1 ICL-PARPS Cell

For a description of the cell refer to Section 4.2.1.2 on page 185 of this thesis.A picture of the cell is shown in Figure 9-1. Before the cell is setup there will be 6 holes in the cell (not including the vacuum line connection. Four of the holes are at the ends of the two channels and are beveled at the brewster angles. The two holes that are on top of the channels and have female screw fittings. The microphone mounts are white plastic screws with microphones inset into the bottom and 3 prong electrical connectors on top. These screws should be screwed into the holes on top of the channels.

To mount the tungsten wire into the cell, take a length of narrow diameter tungsten wire about twice the length of the cell (25 cm) and pass it through the cell. Then find the two wire mounts. These are white plastic parts with metal dowels and 5 screws which

match the position of the screw holes that surround the holes at the ends of the channels. Place o-rings in the circular indentation on the backs of the wire mounts. String the tungsten wire.

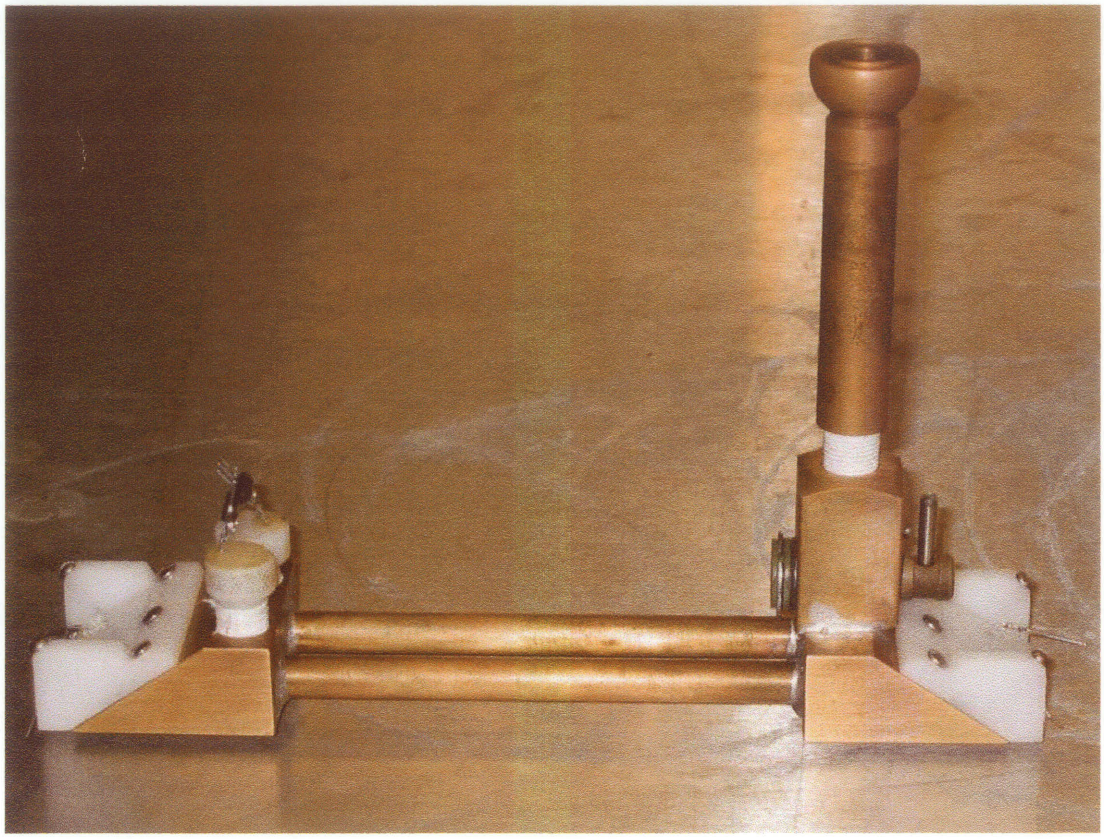

**Figure 9-1.** Picture of Helmholtz cell for the ICL-PARPS system, with double wire mounts attached.

through the tiny holes in the middle if the mount. Carefully place the mounts against the faces of the cell, so the screws line up with the screw holes in the faces of the cell (be sure that the wire is free to move back and forth). Carefully tighten all of the screws, note that on the side of the cell were the valve is, the stop-cock may have to be pushed back to access the top screw. Be sure to return this to its normal position when done. Solder the tungsten

wire carefully to the metal dowels on each side. Be careful not to let the dowels get too hot as this may melt the plastic. Loosen the screws that stop the dowels from turning. Turn one of the dowels three times so the tungsten wire is wrapped around it and tighten the screw to lock this dowels in place. Turn the other dowels until the tungsten wire is tight, care is needed as wire is not very strong and snaps easily. Once the wire is tight, tighten the screw to lock the dowels in place. Fill the holes which the wire passes through with epoxy to seal them. A five minute epoxy is suggested, since it is soft enough to be drilled out of the hole if the wire needs to be changed. On the other side of the cell, epoxy clean fused silica windows over the remaining holes so that the laser may pass through the cell.

The cell may now be evacuated and filled with the desired gas. Note that the valve handle pointing up parallel to the connection to the vac-line is the closed position and at 90 degrees to the connection to the vac-line connection is closed.

### 9.1.2 System set-up

Once the cell is set-up and filled, it is placed within the cavity of the laser, such that the laser lases through the windows of the cell. After it is ensured the laser is lasing through the cell it is best to block the pump beam until it is needed.

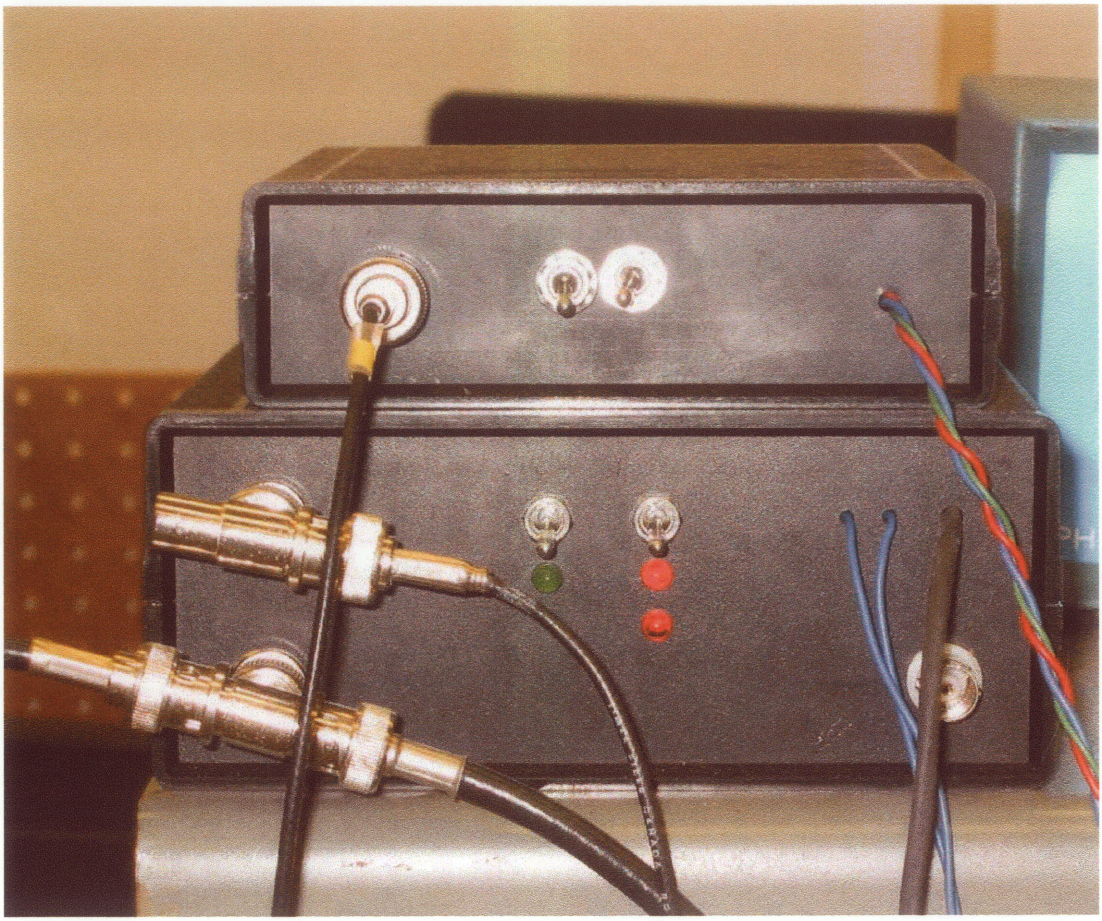

**Figure 9-2.** Top preamplifier for the photo-diode. Bottom preamplifier for the microphone.

There are two black boxes, which are the preamplifiers. One has one wire coming out of the front a BNC connector and two switches on the front. The wire out the front has a female connector on the end. This connects to the photo diode. The photo diode should be placed in front of the dye laser output. The second preamplifier has a connection for a ribbon cable on the back. This should be connected to the ribbon cable that comes out of

the computer connector block. On the front there are three BNC connectors (two on one side one on the other), The single BNC connector goes to the output of the power meter. On the other side the bottom BNC connectors go to the chopper control, the top to the photo diode preamplifier. The two blue wires coming out of this box carry the pulse for the heated wire. They should be connect to metal dowels which hold the tungsten wire via alligator clips. All of the switches on both of the preamplifiers should be in the up position (on).

## 9.2 Running the ICL-PARPS experiment

Once the setup is complete open Lab View and the ICL-PARPS 8.1 program. Notice that the ICL-PARPS program has a number of tabs. Each tab leads to a function of the program.

## 9.2.1 Parameters

The first tab is parameters (see Figure 9-3).

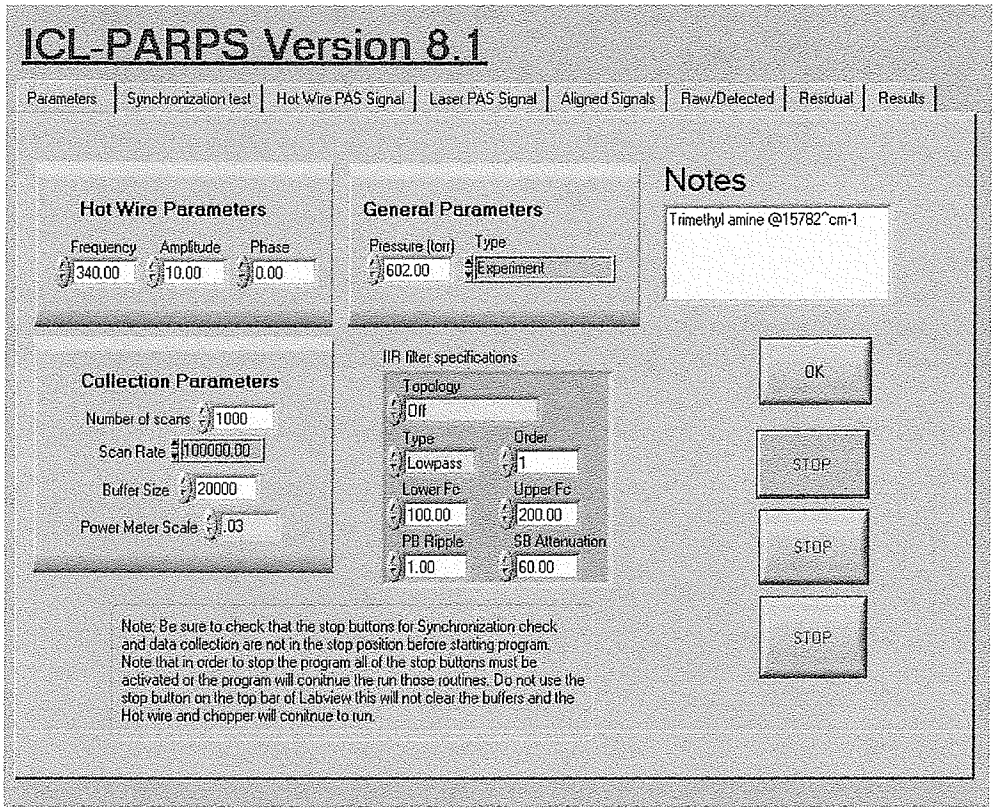


**Figure 9-3.** Screen capture of the Parameters page of the ICL-PARPS program.

It is on this page that all the settings that control the instrument are entered. Each set of parameters will be explained in the following sections.

### 9.2.1.1 Hotwire Parameters

- Frequency: This is the frequency in Hz which both the pulses through the heated wire and the chopper will be at. This should be set at the resonance frequency for the cell. Since this will change based on pressure and the nature of the gas, it is best to find this experimentally. The easiest way to accomplish this is to vary the frequency while using the test hotwire experiment mode (see Section 9.2.1.4) untill the highest amplitude signal is observed.
- Amplitude: This defines the voltage of the pulses through the hotwire. This parameter can be varied between 0 and 10 volts. Unless one is attempting to match the amplitude of the laser induced signal a setting of 10 volts is preferred.

- Phase: This defines the phase shift of the pulses through the wire. In this version of the ICL-PARPS system the phase parameter doesn't really do anything. Though the phase of the heated wire pulses will be shifted so will the optical chopper and the trigger signals, resulting in the observations being the same as if a zero phase shift was used.

#### 9.2.1.2 Collection Parameters

- Number of Scans: This defines how many scans of the signal will be co-added by the program. More scans will increase the signal to noise ratio but will also take more time. For strong signals 100 scans is enough and for weaker signals 1000 scans is good. Generally if a acceptable signal to noise ratio is not achieved with 1000 scans, the signal is not strong enough for reliable results to be obtained even with a higher number of scans.
- Scan rate: This is the number of points measured per second. Within the operating range of the ICL-PARPS system 100 000 is acceptable. It is not advisable to run the instrument at a lower scan rate then this. If very high modulation frequencies are used this can be increased up to 330 000, but system resources often run out prior to the completion of the experiment if the scan rate is set this high.
- Buffer: This is the number of points measured per scan or how long each scan is. For example setting the buffer to 50 000 would mean each scan collected half a second of data. The buffer should be set so that a large number of cycles are collected. The higher the buffer setting the more accurate the results will be. However, higher buffer settings do take more time to collect and use up more system resources. Generally a buffer between 2000 and 3000 is acceptable.
- Power meter scale: This parameter is not relevant to the current incarnation of the ICL-PARPS system as the power meter has been replaced by a photo diode. However, if in the future the power meter is reintroduced this should be set to the same scale as the power meter.

#### 9.2.1.3 IIR Filter conditions

The setting of the filter should always remain off. The filters may cause phase errors. If the signal is very noisy the filters may be used to help diagnose the problem.

#### 9.2.1.4 General Parameters and Notes

- Pressure: The pressure of the gas in the cell should be entered.
- Type: There are three modes in which the ICL-PARPS system operates. Test hotwire and Test laser, collect data for only the heated wire signal or laser induced signal respectively. These modes are useful for determining the resonance frequency and ensuring all of the components of the system are operating properly before the experiment is run. The third mode is the experiment mode. In this mode both the heated wire signal and laser induced signal are collected sequentially and all be necessary calculations are done.

- Notes: Here any note about the experiment can be entered. For example the wavelength of the laser radiation used and the name of the compound being studied.

#### 9.2.1.5 Operation

Once all the parameters have been set, click the run button on the LabView function bar (see the LabView manual). This will activate the program. Then press the OK button.

What happens next will depend on the Type setting.

Type=Test Hotwire:

- A prompt will appear which reads "Connect wire, Block Laser".
- Connect the blue wires (from the preamplifier with lights) to the metal dowels on the cell (the ones holding the tungsten wire). Connect the black wire (from the same preamplifier) to the microphone on the side of the cell containing the wire and make sure the pump laser is blocked from entering the dye laser.
- Press OK.
- When the data acquisition is done a prompt to that effect will appear.
- Press all three stop buttons in order.
- The results will be shown in the Hotwire Signal Tab.

Type=Test Laser:

- A prompt will appear which reads "disconnect wire, unblock Laser".
- Disconnect the blue wires (from the preamplifier with lights) from the metal dowels on the cell (the ones holding the tungsten wire). Connect the black wire (from the same preamplifier) to the microphone on the side of the cell which the laser passes through and make sure the dye laser is lasing through the cell.
- Press OK.
- When the data acquisition is done a prompt to that effect will appear.
- Press all three stop buttons in order.
- The results will be shown in the laser Signal Tab.

Type=Experiment:

- A prompt will appear which reads "Connect wire, Block Laser".

- Connect the blue wires (from the preamplifier with lights) to the metal dowels on the cell (the ones holding the tungsten wire). Connect the black wire (from the same preamplifier) to the microphone on the side of the cell containing the wire and make sure the pump laser is blocked from entering the dye laser.
- Press OK.
- A prompt will appear which reads "disconnect wire, unblock Laser".
- Disconnect the blue wires (from the preamplifier with lights) from the metal dowels on the cell (the ones holding the tungsten wire). Connect the black wire (from the same preamplifier) to the microphone on the side of the cell which the laser passes through.And make sure the dye laser is lasing through the cell.
- Press OK.
- When the data acquisition is done a prompt to that effect will appear.
- Press all three stop buttons in order.

The data can be saved by going to the operations menu on the LabView function bar and choosing Data logging and Log. Data can be retrieved by going to the same menu and choosing retrieve. (see LabView Manual).

The results are shown in the rest of the tabs.

## 9.2.2 Synchronization Check

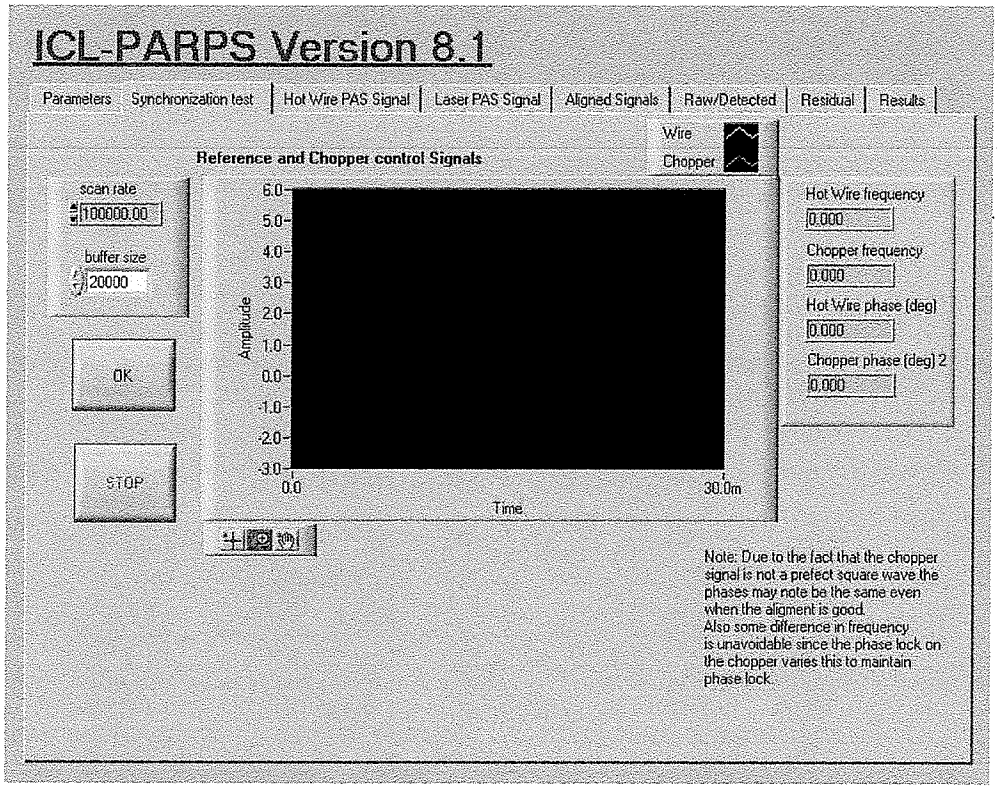


**Figure 9-4.** Screen capture of the synchronization check page of the ICL-PARPS program.

This tab is a separate function of the ICL-PARPS system. It can be used to test the trigger signals of the system. They need not be exactly in sync, but two square wave should appear. The Hotwire square wave should have an amplitude approximately equal to the amplitude setting on the parameters page. The laser square wave should have a amplitude of at least 1. Note that this must be run with the laser passing through the cell and the photo diode in place. The heated wire and the microphone do not need to be connected.

### 9.2.3 Hotwire PAS signal

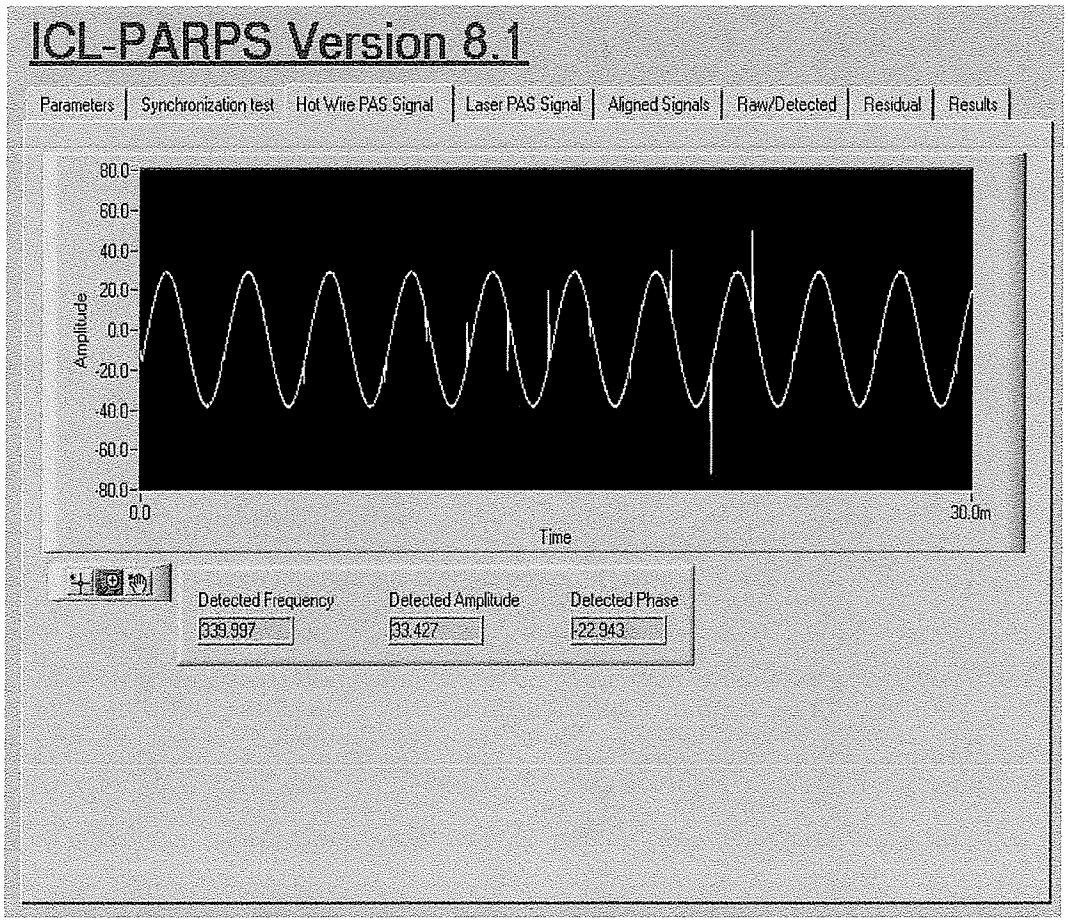


**Figure 9-5.** Screen capture of the Hotwire PAS signal page of the ICL-PARPS program.

This page shows the unmodified photoacoustic signal from the heated wire. The frequency, amplitude and phase are reported along on the bottom. The function bar at the bottom left corner, can be used to zoom in on sections of the wave. This is the only tab in which data will be displayed in the test hotwire mode.

### 9.2.4 Laser PAS Signal

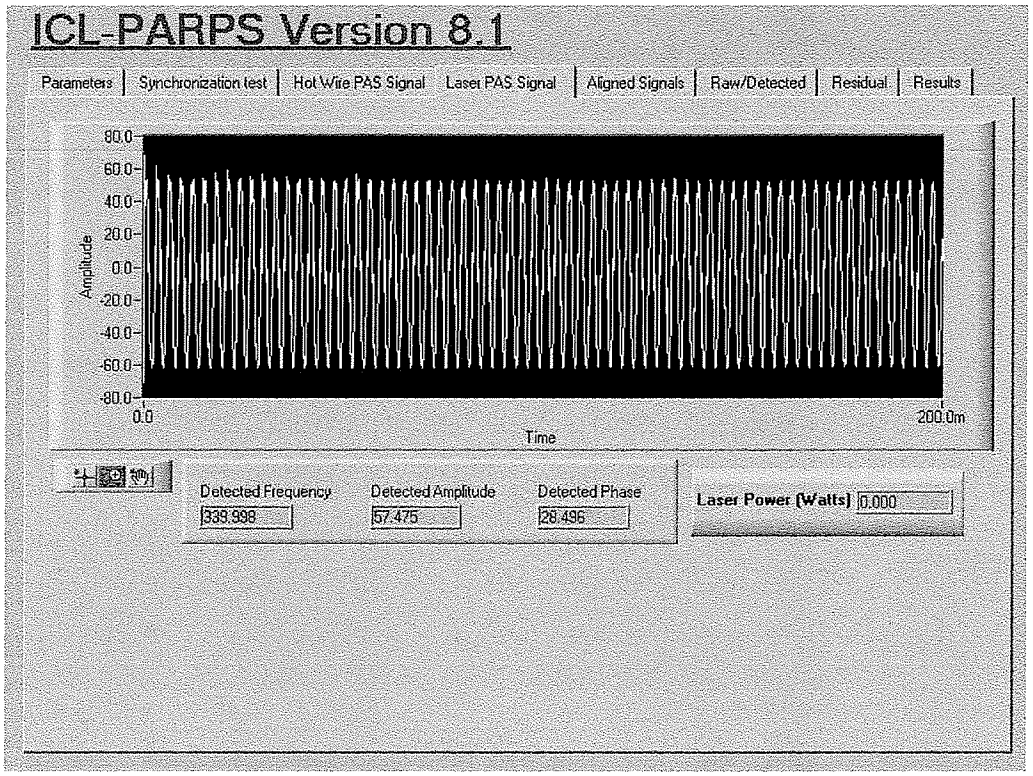


**Figure 9-6.** Screen capture of the Laser PAS signal page of the ICL-PARPS program.

This page shows the unmodified photo acoustic signal from induced by the laser. The frequency, amplitude and phase are reported along on the bottom. The function bar at the bottom left corner, can be used to zoom in on sections of the wave. This is the only tab in which data will be displayed in the test laser mode. Note that the Laser power will always read as 0.00.

## 9.2.5 Aligned Signals

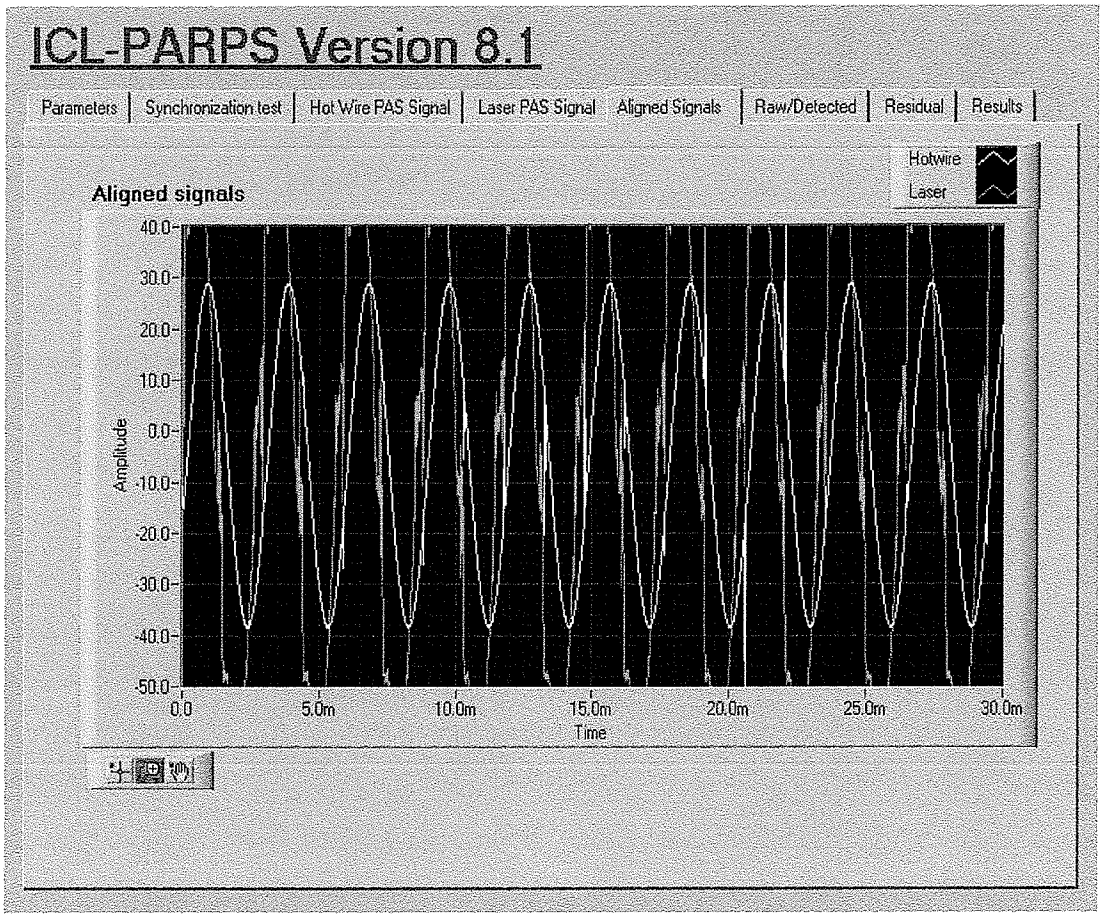


**Figure 9-7.** Screen capture of the Laser PAS signal page of the ICL-PARPS program.

Both the laser induced and heated wire unmodified signals are shown with the trigger point set to time=0. The function bar at the bottom left corner, can be used to zoom in on sections of the wave.

### 9.2.6 Raw/Detected

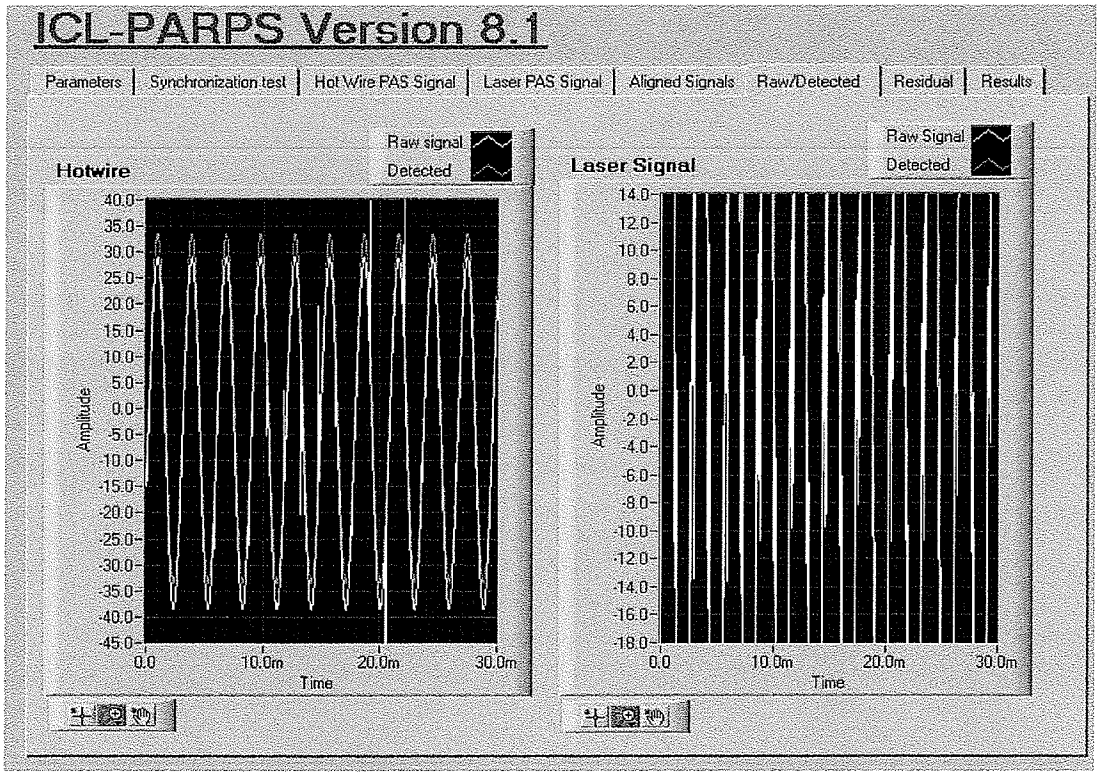


**Figure 9-8.** Screen capture of the Raw/Detected page of the ICL-PARPS program.

This tab shows the sine waves to which the detected signals were fit in order to get the frequency, amplitude and phase information, and the real signals. This page should always be checked to insure that the fit is appropriate.

### 9.2.7 Residual

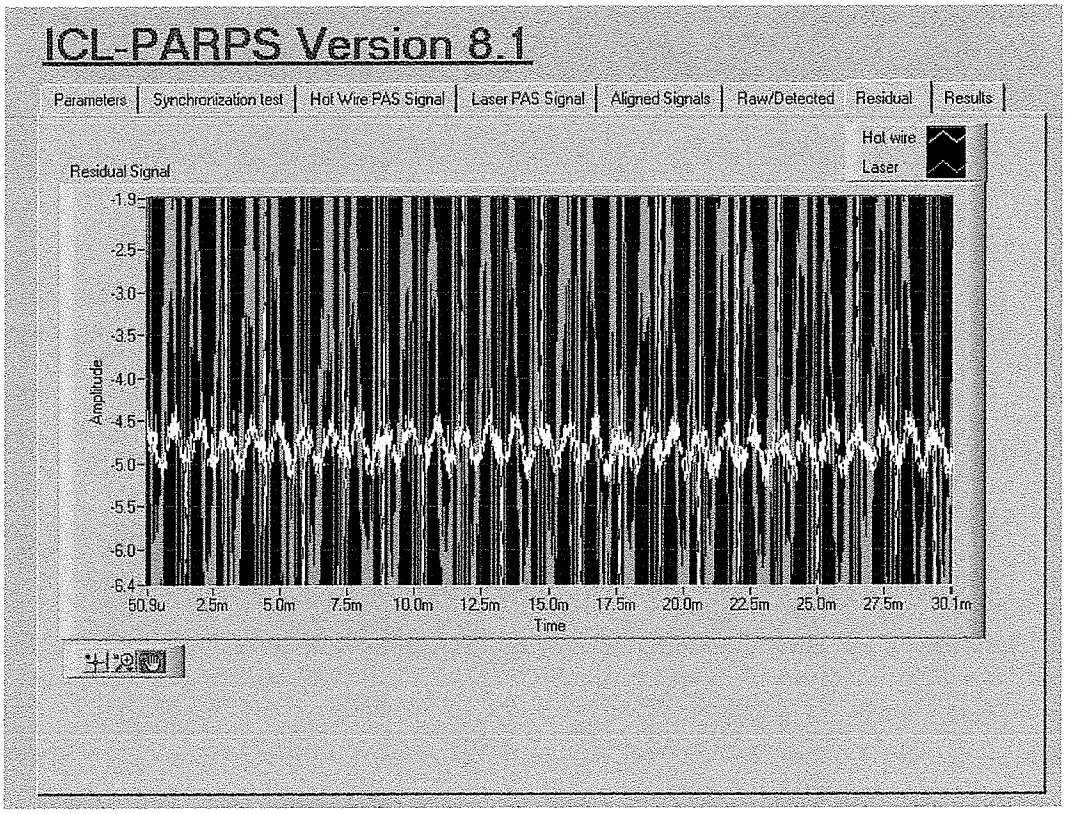


**Figure 9-9.** Screen capture of the Residual page of the ICL-PARPS program.

This page displays the residual from the fit.

## 9.2.8 Results

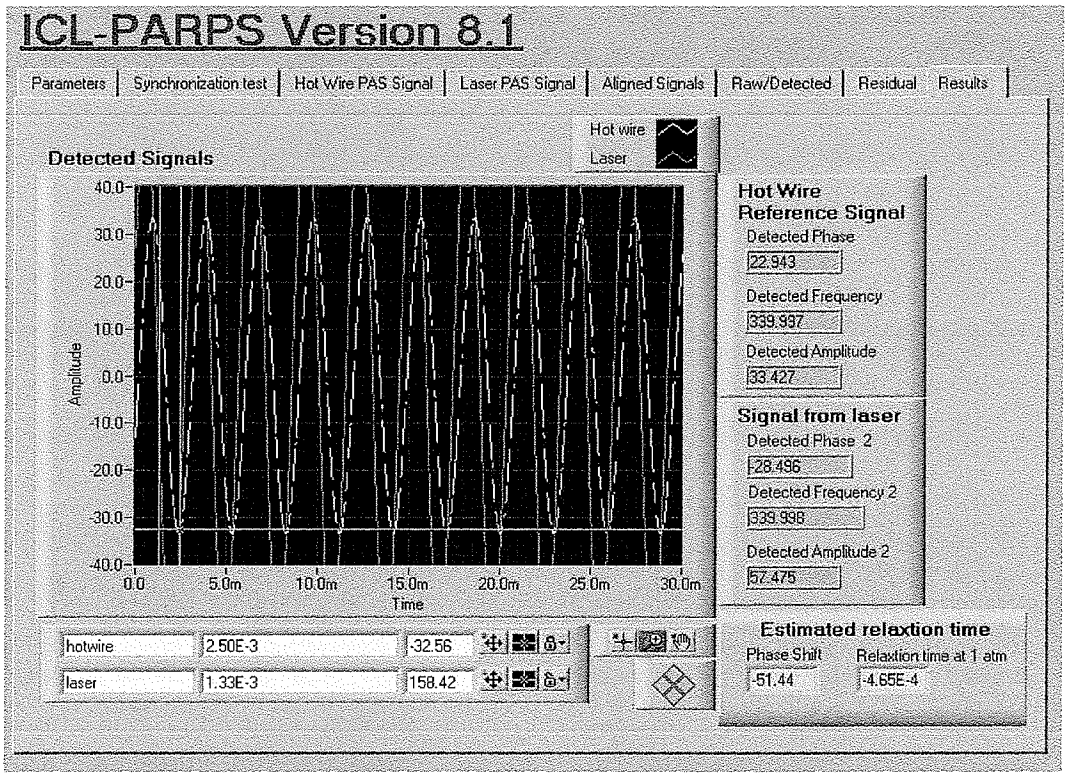


**Figure 9-10.** Screen capture of the Results page of the ICL-PARPS program.

This page displays the results of the experiment. The wave graphed are the detected wave (*i.e.*, the sine waves to which the data was fit). The controls along the bottom allow the coordinates of points along either wave to be found. (see LabView manual for details). Along the right hand side all of the detected parameters are shown. Notice that the phase values have the opposite sign as what was shown in the Hotwire and Laser PAS signal tabs. This is because these values refer to phase lag rather than phase. Also note that it is likely to be inappropriate for this sign change to occur (see Section 4.4.3 on page 215). The phase

shift is simply the difference between the phase lags and the relaxation time at one atmosphere. It is calculated assuming the phase shift stated and correcting for pressure.

# Bibliography


[1] G. Herzberg, "Infrared and Raman Spectra", (Van Nostrand Rienhold Co. New York, 1945).

[2] E.B. Wilson, J.C. Decius, and P.C. Cross, "Molecular Vibrations", (McGraw-Hill Book Co., N.Y. 1955).

[3] J. M. Hollas, "Modern Spectroscopy, Third Edition", (John Wiley & Sons, N.Y. 1996).

[4] S. F. A. Kettle," Symmetry and Structure", (Wiley, New York, 1995).

[5] Puccianti, Nuovo Cimento, 11, 241 (1900) as reported in [6]

[6] J. W. Ellis, Trans. Farad. Soc. 25, 888 (1929). and references therein.

[7] Birge and Spöner, Physical Rev., 28, 259, 1926.

[8] R. Freymann, Ann. de Phys. $10^{e}$ serie, t. XX, 243 (1933)

[9] H. Kempter, Zeitschrift f. Physik. Chem. B50, 23 (1941)

[10] R. Surhrmann and P. Klein, Zeitschrift f. Physik, Bd 116, 1 (1940)

[11] R. Suhrmann, Angew. Chem. 62, 507 (1950).

[12] B. Timm and R. Mecke, Zeitschrift f. Physik, 98, 363 (1935).

[13] P. Ganswein and R. Mecke, Zeitschrift f. Physik, 99, 189 (1936).

[14] V. Otto and R. Mecke, Zeitschrift f. Physik, 99, 204 (1936).

[15] R. Mecke, Zeitschrift f. Physik, 99, 217 (1936).

[16] W. Siebrand, J. Chem. Phys. 46, 440 (1967).

[17] W. Siebrand, J. Chem. Phys. 47, 2411 (1967).

[18] W. Siebrand and D. F. Williiams, J. Chem. Phys. 49, 1860 (1968).

[19] T. E. Martin and A. H. Kalantar, J. Chem. Phys. 49, 235 (1968).

[20] B. R. Henry and W. Siebrand, J. Chem. Phys. 49, 5369 (1968).

[21] R. J. Hayward, B. R. Henry and W. Siebrand, J. Mol. Spect. 46 207 (1973).

[22] R. J. Hayward and B. R. Henry, J. Mol. Spect. 50, 58 (1974).

[23] R. J. Hayward and B. R. Henry, J. Mol. Spect. 57, 221 (1975).

[24] R. J. Hayward and B. R. Henry, Chem. Phys. 12, 387 (1975).

[25] B. R. Henry, Acc. Chem. Res. 10, 207, (1977).

[26] R. Wallace, Chem. Phys. 11, 189 (1975)

[27] R. Wallace, Chem. Phys. Let. 37, 115 (1976).

[28] R. L. Swofford, M. E. Long and A. C. Albercht, J. Chem. Phys. 65, 179 (1976).

[29] W. R. A. Greenlay and Bryan Henry, J. Chem. Phys. 69, 82 (1978).

[30] B. R. Henry, M. A. Mohammadi and J. A. Thomson, J. Chem. Phys. 75, 3165 (1981).

[31] B. R. Henry and R. J. D. Miller, Chem. Phys. Lett. 60, 81 (1978).

[32] W. R. A. Greenlay and B. R. Henry, Chem. Phys. Lett. 53, 325 (1978).

[33] H. S. Moller and O.S. Mortensen, Chem. Phys. Lett. 66, 539 (1979).

[34] O. S. Mortensen, B. R. Henry and M. A. Mahammadi, J. Chem. Phys. 75, 4800 (1981).

[35] B. R. Henry and I. F. Hung, Chem. Phys. 29, 465 (1978).

[36] H. L. Fang and R. L. Swofford, J. Chem. Phys. 72, 6382 (1980).

[37] H. L. Fang and R. L. Swofford, J. Chem. Phys. 73, 2607 (1980)

[38] B. R. Henry and M. A. Mohammadi, Chem. Phys. 55, 385 (1981).

[39] C. L. Dykstra, " Introduction to Quantum Chemistry" (Prentice Hall, New Jersy, 1994).

[40] S. Peryerimyoff, M. Lewerenz and M. Quack, Chem. Phys. Lett., 109, 563 (1984).

[41] H. Dübal and M. Quack, J. Chem. Phys. 81, 3779 (1984).

[42] J. L. Duncan and A. M. Ferguson, J. Chem. Phys. 89, 4216 (1988).

[43] J. L. Duncan, Spectrochimica Acta, 45A, 1067 (1989).

[44] M. S. Burberry and A. C. Albrecht, J. Chem. Phys. 70, 147, (1979).

[45] I. Schek, J. Jortner and M. L. Sage, Chem. Phys. Lett. 64, 209, (1979).

[46] M. S. Burberry and A. C. Albrecht, J. Chem. Phys. 71, 4631, (1979).

[47] P. R. Stannard, M. L. Elert and W. M. Gelbart, J. Chem. Phys. 74, 6050, (1981).

[48] K. Tamagake, S. Hyodo, and T. Fugiyama, Bull. Chem. Soc. Jpn. 55, 1267, (1982).

[49] S. Hyodo, K. Tamagake, and T. Fugiyama, Bull. Chem. Soc. Jpn. 55, 1272, (1982).

[50] K. Tamagake, S. Hyodo, and T. Fugiyama, Bull. Chem. Soc. Jpn. 55, 1277, (1982)

[51] O. S. Mortensen, M. K. Ahmed, B. R. Henry and A. W. Tarr, J. Chem. Phys. 82, 3903, (1985).

[52] A. W. Tarr, D. J. Swanton and B. R. Henry, J. Chem. Phys. 85, 3463, (1986).

[53] K. K. Lehmann and A. M. Smith, J. Chem. Phys. 93, 6140, (1990).

[54] W. F. Murphy, F. Zerbetto, J. L. Duncan, and D. C. McKean, J. Phys. Chem. 97, 581, (1993).

[55] H. B. Henbert, G. D. Meakins, B. Nicholis and A. A. Wagland, J. Chem. Soc. 1462, (1957).

[56] H. B. Braunholtz, E. A. V. Ebsworth, F. G. Mann, and N. Sheppard, J. Chem. Soc. 2780 (1958).

[57] R. D. Hill and G. D. Meakins, J. Chem. Soc. 760 (1958).

[58] H. P. Hamlow, S. Okuda, and N. Nakagawa, Tetrahedron Lett. 2553 (1964).

[59] J. A. Pople, Tetrahedron, 30, 1605, (1974).

[60] A. Allan, D.C. McKean, J. P. Perchad and M. L. Josein, Spectrochim. Acta, Part A, 27, 1409, (1971).

[61] D.C. McKean, Chem. Comm., 1373, (1961).

[62] D.C. McKean, J. L. Duncan and L. Batt, Spectrochim. Acta, Part A, 29, 1037, (1973)

[63] L. J. Bellamy and D. W. Mayo, J . Phys. Chem., 80, 1217, (1976).

[64] K. M. Gough and B. R. Henry, J. Am. Chem. Soc., 106, 2781, (1984).

[65] H. G. Kjaergaard, H. Yu, B. J. Schattka, B. R. Henry and A. W. Tarr, J. Chem. Phys., 93, 6239, (1990).

[66] H. G. Kjaergaard, B. R. Henry and A. W. Tarr, J. Chem. Phys., 94, 5844, (1991).

[67] B. I. Niefer, H. G. Kjaergaard,and B. R. Henry, J. Chem. Phys., 99, 5682, (1993).

[68] H. L. Fang, D. M. Meister, and R. L. Swofford, J. Phys. Chem., 88, 410, (1984).

[69] B. E. Billinghurst, K. M. Gough, G. R. Low and H. G. Kjaergaard, J. Mol. Struc., 687, (2004).

[70] C. Manzanares I, N. L. S. Yamasaki, E. Weitz, J. Phys. Chem., 91, 3969, (1987).

[71] E. Rinehart, P. Reinjart, and J. Wollrab, J. Mol. Struct., 47, 556, (1973).

[72] J. R. Durig, and M. G. Griffin, J. Chem. Phys., 47, 2220, (1977).

[73] L. Anastasakos, and T. A. Wildman, J. Chem. Phys., 99, 9453, (1993).

[74] Z. Rong, D. L. Howard, and H. G. Kjaergaard, J. Phys. A, 107, 4607, (2003).

[75] Private communication with H. G. Kjaergaard

[76] Donated by D. C. McKean.

[77] P. Bellaiche-Sharpe, K. M. Gough, B. J. Schattka, T. MacDonald, Rustenberg, A. Struyk, and G. McDonnell, Appl. Spectrosc. 50, 1366, (1996).

[78] B. J. Schattaka, K. M. Gough, and B. R. Henry, Can, J. Anal. Sc. and Spec. 42, 35, (1997).

[79] A. M. Smith, U. G. Jorgensen, and K. L. Lehman, J. Chem. Phys. 87, 378, (1989).

[80] Bio-Rad Win-IR for Microsoft Windows Level 2, Galactic Industries, 1991-1994.

[81] Gaussian 94, Revision C.3, M. J. Frisch, G. W. Trucks, H. B. Schlegel, P. M. W. Gill, B. G. Johnson, M. A. Robb, J. R. Cheeseman, T. A. Keith, G. A. Petersson, J. A. Montgomery, K. Ragavachari, M. A. Al_laham, V. G. Zakrzewski, J. V. Ortiz, J. B. Foresman, J. Cioslowski, B. B. Stefanov, A. Nanayakkara, M. Challacombe, C.

Y. Peng, P. Y. Ayala, W. Chen, M. W. Wong, J. L. Andres, E. S. Replogle, R. Gomperts, R. L. Martin, D. J. Fox, J. S. Binkley, D. J. Defrees,J. Baker, J. P. Stewart, M. Head-Gordon, C. Gonzalez, and J. A. Pople, Gaussian, Inc., Pittsburgh PA, 1995.

[82] A. Messiah, "Quantum Mechanics", (Wiley, New York, 1961).

[83] W. F. Edgell, R. E. Moynihan, J. Chem. Phys. 45, 1205 (1966).

[84] J. R. Durig, and M. G. Griffin, J. Chem. Phys. 67, 2220 (1977).

[85] A. V. Fedorov, D. L. Snavely, H. G. Kjaergaard, K. M. Gough and B. Billinghurst, J. Phys. Chem. A, 105, 3458, (2001).

[86] L. J. Long "Metallocenes: An Introduction to sandwich complexes" (Blackwell-Science, Oxford, 1998).

[87] J. L. Duncan, Spectrochim. Acta., 26A, 429 (1970).

[88] H. J. Bernstein, Spectrochim. Acta. 18, 161 (1962).

[89] R. M. Badger, J. Chem. Phys. 2, 128 (1934).

[90] R. M. Badger, J. Chem. Phys. 3, 710 (1935).

[91] D. C. McKean, Chem. Soc. Rev., 7, 399 (1978).

[92] D. C. McKean, I. Torto and A. R. Morrisson, J. Mol. Struct. 99, 101 (1983).

[93] D. F. Evans, P. H. Missen and M. W. Upton, J. Mol. Struct., 82, 147 (1982).

[94] D. C. McKean, J. Mol. Struct., 113, 251 (1984).

[95] Y. Mizugai, and M. Katayama, Chem. Phys. Lett., 73, 240 (1980).

[96] J. S. Wong and C. B. Moore, J. Chem. Phys., 77, 603 (1982).

[97] L. N. Lewis, J. Organomet. Chem., 234, 335 (1982).

[98] F. L. Blackburn, D. L. Snavely and I. Oref, Chem. Phys. Lett. 178, 538 (1991).

[99] T. VanMarter, C. Olsen and D. L. Snavely, J. Phys. Chem. 98, 5404 (1994).

[100] A. V. Fedorov, and D. L. Snavely, J. Phys. Chem. 103, 7795 (1999).

[101] A. V. Fedorov, and D. L. Snavely, J. Phys. Chem. 98, 5404 (1997).

[102] A. V. Fedorov, and D. L. Snavely, J. Phys. Chem. A, 102, 6234 (1998).

[103] P. Bellaiche-Sharpe, K. M. Gough, B. J. Schattka, G. R. Low and H. G. Kjaergaard, J. Phys. Chem. A, 102, 10230 (1998).

[104] G. L. Henderson, M. A. Roehrig, P. Wikrent, S. G. Kukolich, J. Phys. Chem., 96, 8303 (1992).

[105] W. Tam, D. F. Eaton, J. C. Calabrese, I. D. Williams, Y. Wang and A. G. Anderson, Chem. Mater., 1, 128 (1989).

[106] S. S. Butcher, J. Chem. Phys., 42, 1830 (1965).

[107] N. Matsuzawa, J. Seto, and D. A. Dixon, J. Phys. Chem., 88, 1298 (1984).

[108] C. Glidewell, J. Organomet. Chem., 102, 339 (1975).

[109] P. W. Atkins, "Molecular Quantum Mechanics" 2nd edition, ( University Press, Oxford, 1983).

[110] H. G. Kjaergaard, R. J. Proos, D. M. Turnbull and B. R. Henry, J. Phys. Chem., 100, 19273 (1997).

[111] G. R. Low and H. G. Kjaergaard, J. Chem. Phys., 110, 9104 (1999).

[112] D. D. Perrin, W. L. F. Armarego, "Purification of Laboratory Chemical" 3rd ed. (Perigamon Press, New York, 1988).

[113] A. V. Fedorov, D. L. Snavely, J. Phys. Chem. A, 101, 9042 (1997)

[114] J. D. Dunitz, L. E. Orgel, and A. Rich, Acta. Crystallogr. 9, 373 (1956).

[115] A. K. Hedberg, L. Hedberg, and K. Hedberg, J. Chem. Phys., 63, 1262 (1975).

[116] P. Seiler, and J. D. Dunnitz, Acta. Crystallogr., B36, 2255 (1980).

[117] P. Seiler, and J. D. Dunnitz, Acta. Crystallogr., B36, 2946 (1980).

[118] L. Hedberg, and K. Hedberg, J. Chem. Phys., 53, 1228 (1980).

[119] A. Rosencwaig, " Photoacoustics and Photoacoustic Spectroscopy" (Wiley-Interscience, 1980, New York).

[120] P. Atkins, " Physical Chemistry" ( W.H Freeman and Company, 1994, New York).

[121] L. Landau and E. Teller, Phys. Z. Sowjetunion, 10, 34 (1934).

[122] R. L. Taylor and S. Bitterman, Rev. Mod. Phys., 41, 26, (1969).

[123] G. M. Jursich, D. R. Ritter, and F. F. Crim, J. Chem. Phys., 80, 4097, (1984).

[124] J. R. Airey, and I. W. M. Smith, J. Chem. Phys., 57, 1669, (1972).

[125] H. Chen, R. L. Taylor, J. Wilson, P. Lewis, and W. Fyfe, J. Chem. Phys., 61, 306, (1974).

[126] V. Zenianari, B.A Tikhomirov, Yu. N. Ponomarev and D. Courtois ,J. Chem. Phys., 122, 2, (2000).

[127] D. L. Drapcho, R. Curbelo, E. Y. Jiang,. R. A. Crocombe, W. J. McCarthy, Applied Spectroscopy, 51, 4, 453 (1997).

[128] T. L. Cottrell, I. M. MacFarlane A. W. Read and A. H. Young, Trans. Faraday. Soc., 62, 2655, (1966).

[129] J. T. Yardley, M. N. Fertig, and C. B. Moore, J. Chem. Phys., 52, 1450, (1970).

[130] F. Barocchi and R. Vallauri, J. Chem. Phys., 51, 10, (1969).

[131] M. H. De Vasconcllos, F. Cannemeijer and A. E. De Vries, Chem. Phys. Lett., 12, 154, (1971).

[132] T. L. Cottrell, and J. C. McCoubrey, " Molecular Energy Transfer in Gases" (Butterworths, 1961, London).

[133] M. E. Jacox and S. H. Bauer, J. Phys. Chem. 61, 833, (1957).

[134] J. A. Barnes, T. E. Gough, T. Q. Murdock and M. Stoer, Rev. Sci. Instrum., 67, 371, (1996).

[135] B. J. Schattka, K. M. Gough and B. R. Henry, Can. J. Anal. Sci. and Spec., 42, 35, (1997).

[136] R. S. Quimby, P. M. Selzer and W. M. Yen, Applied Optics, 16, 2630, (1977).

[137] W. A. McClenny, C. A. Bennett, Jr., G. M. Russwurm, and R. Richmond, Applied Optics, 20, 650, (1981).

[138] P. Hess and C. B. Moore, J. Chem. Phys.,65, 2339, (1976).

[139] E. Avramides and T. F. Hunter, Chem. Phys., 57, 441, (1981).